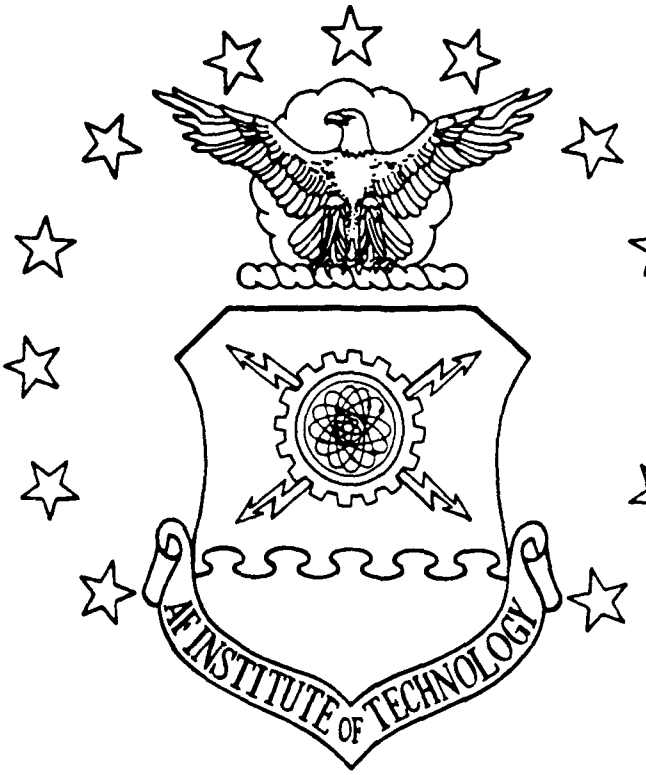

EVALUATION OF DOPED PHTHALOCYANINES AND A CHEMICALLY-SENSITIVE FIELD-EFFECT TRANSISTOR FOR DETECTING NITROGEN DIOXIDE

THESIS

Thomas J. Jenkins
Captain, USAF
AFIT/GE/ENG/89D-18

DEPARTMENT OF THE AIR FORCE
AIR UNIVERSITY
AIR FORCE INSTITUTE OF TECHNOLOGY
Wright-Patterson Air Force Base, Ohio

AFIT/GE/ENG/89D-18

EVALUATION OF DOPED PHTHALOCYANINES AND A CHEMICALLY-SENSITIVE FIELD-EFFECT TRANSISTOR FOR DETECTING NITROGEN DIOXIDE

THESIS

Thomas J. Jenkins
Captain, USAF
AFIT/GE/ENG/89D-18

Approved for public release; distribution unlimited

AFIT/GE/ENG/89D-18

EVALUATION OF DOPED PHTHALOCYANINES AND A CHEMICALLY-SENSITIVE FIELD-EFFECT TRANSISTOR FOR DETECTING NITROGEN DIOXIDE

THESIS

Presented to the Faculty of the School of Engineering
of the Air Force Institute of Technology
Air University
In Fulfillment of the
Requirements for the Degree of
Master of Science in Electrical Engineering

Thomas J. Jenkins, B.S.E.E.
Captain, USAF

4 December, 1989

Acknowledgements

I can not fully express my appreciation of the invaluable assistance provided by many individuals during this research effort. The guidance of my thesis advisor, Maj E. Kolesar, extended beyond mere office visits to the thorough review of my work. His helpful suggestions were not cookbook solutions to be blindly followed, but rather, they offered the opportunity for discovery and insight. Also, the assistance of Don Smith and Bill Trop of the AFIT Electronics and Materials Cooperative Laboratory proved to be indispensable.

I must express my appreciation of the assistance provided by the many individuals of the Avionics Laboratory. Larry Callahan's expertise in packaging the microsensor was invaluable. In addition, Robert Neidhard and Rick Worley of the Avionics Laboratory provided instrumentation and computer support.

I also must thank the EG&G Mound Applied Technology Laboratory for their support and interest in the application of organic semiconductors.

Of course, I would be remiss if I failed to mention my family, Sharon, Laura, and Nathan. Any accomplishments that I have made were gained by their sacrifices.

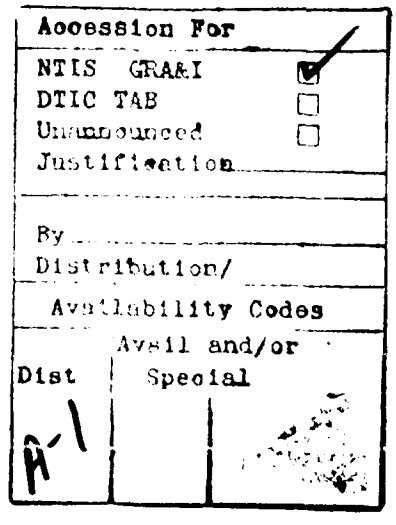

Table of Contents

List of Figures

List of Tables

Abstract

This study involved the design and fabrication of an integrated circuit microsensor for the detection of nitrogen dioxide; metal-doped phthalocyanine compounds were evaluated as a candidate chemically-sensitive membrane, and their performance was compared with respect to sensitivity, reversibility, and specificity. The microsensor consisted of the integration of an array of nine sensing elements with amplifiers, a reference amplifier, and an analog multiplexer. The nine individual sensing elements used an interdigitated gate electrode field-effect transistor (IGEFET) coupled to a serially-connected pair of inverting amplifiers using metal-oxide-semiconductor field-effect transistors (MOSFETs). The interdigitated gate electrodes were coated with thin films of cobalt (II) phthalocyanine (CoPc), copper phthalocyanine (CuPc), lead phthalocyanine (PbPc), nickel (II) phthalocyanine (NiPc), and (undoped) phthalocyanine (Pc). An excitation signal was applied to the integrated circuit, and the multiplexed electrical response was measured in the time-domain and the frequency-domain. The electrical response was evaluated upon exposure to 20-, 80-, and 320-ppb of nitrogen dioxide (NO_2) and diisopropyl methylphosphonate (DIMP) using filtered room air (less than 5% relative humidity) as the diluent. The electrical response was evaluated for film thicknesses of approximately 1500 Å and 500 Å. The microsensor's operating temperature was thermostatically controlled at 30°C and 120°C for the evaluation. The rank ordering of the sensitivity of the materials to nitrogen dioxide from most to least sensitive was: CoPc, NiPc, CuPc, PbPc, and then (undoped) Pc. The materials were found to be reversible by heating the microsensor to 70°C while purging with the diluent gas. The rank ordering of the specificity towards NO_2 was (from most to least selective):

CoPc, NiPc, PbPc, (undoped) Pc, and then CuPc. For the test parameters studied, the 1500 Å film thickness and the 30°C operating temperature yielded optimum microsensor electrical response.

Evaluation of Doped Phthalocyanines and a Chemically-Sensitive Field-Effect Transistor for Detecting Nitrogen Dioxide

I. Introduction

Background

The development of solid state chemical sensors is an active area of research that has immediate military potential. This case is easily demonstrated. Within just the narrow field of electronic devices, the last I.E.E.E. International Electron Devices Meeting in 1988 had a session specifically dedicated to chemical sensors. The papers addressed topics concerning biosensors, ion-sensitive field-effect transistors, and thin-film gas detectors (1; 2; 3). The military potential of this research area can best be demonstrated by citing two relevant examples.

A military application of chemical sensors can be envisaged in the production of high performance aircraft and other modern weapon systems. Their manufacture involves, to some extent, the polymerization of epoxy resins and composite materials. Since the chemical reactions that occur during polymerization proceed in a variable manner, a closed-loop process control scheme could be effectively utilized to ensure the quality of the final product (4). A miniaturized solid state sensor would be ideally suited for this type of control scheme since the sensor could provide an *in-situ* measurement of the cure process.

Another example of the military potential of these sensors is the detection and measurement of toxic or corrosive vapors that pose a threat to personnel and electronic equipment. An example of a hazardous gas is nitrogen dioxide (NO_2), which is used as an oxidizer in hydrazine propulsion systems. The traditional, industrial hygiene methods for monitoring NO_2 vapors involve schemes utilizing gas chromatography and mass spectrometry (5:42). These instruments are representative of large and expensive systems that are unacceptable under battlefield conditions. A possible solution is the development of a chemical microsensor (5:42-43).

The development of a miniaturized solid state sensor for monitoring hazardous chemical species would have several advantages. An adequately packaged solid state microsensor would also be rugged. Additionally, its small physical size would allow it to be incorporated as a subsystem within a complete weapon system.

In particular, the monitoring of the oxides of nitrogen has been identified as a valuable application of a chemical sensor (6). Detonation materials are known to out-gas nitrogen dioxide, which causes the corrosion of the detonator's electrical firing mechanism. Therefore, a microsensor has immediate application as a rugged, light-weight system for detecting this corrosive compound. In addition, the sensor has application for monitoring the state of stockpiled munitions and their electrical systems as the detonation material ages.

A potential sensor for the applications discussed above is the interdigitated gate electrode variant of the chemically-sensitive

field-effect transistor (CHEMFET). This variant of the CHEMFET consists of a metal-oxide-semiconductor field-effect transistor (MOSFET) which has an interdigitated gate electrode structure substituted for the conventional gate contact. Therefore, this variant of the CHEMFET is referred to as an interdigitated gate electrode field-effect transistor (IGEFET) (7). When the interdigitated gate electrode is coated with a chemically-sensitive membrane, the CHEMFET becomes the integration of a miniaturized chemical sensor and a MOSFET amplifier. This device has been investigated for use as a solid state sensor for environmentally-sensitive compounds (7).

The interdigitated gate electrode structure consists of a metallized driven electrode which is physically and electrically isolated from a floating electrode that connects directly to the transistor's gate oxide. An illustration of the CHEMFET is given in Figure I-1.

In operation, the interdigitated portion of the electrode is coated with an organic polymer. When a pulse excitation is applied to the driven gate electrode, the characteristic response of the CHEMFET is found to change as a function of the challenge gases and the material used to coat the electrode. Sensors based upon metal-doped phthalocyanine [M(Pc)] polymers have been found to be extremely sensitive to nitrogen dioxide (7; 8). For example, metal dopants of cobalt, copper, lead, magnesium, nickel, and zinc in M(Pc) have demonstrated electronic sensitivities to nitrogen dioxide concentrations on the order of 1 part-per-billion to 10 parts-per-million (7; 8; 9).

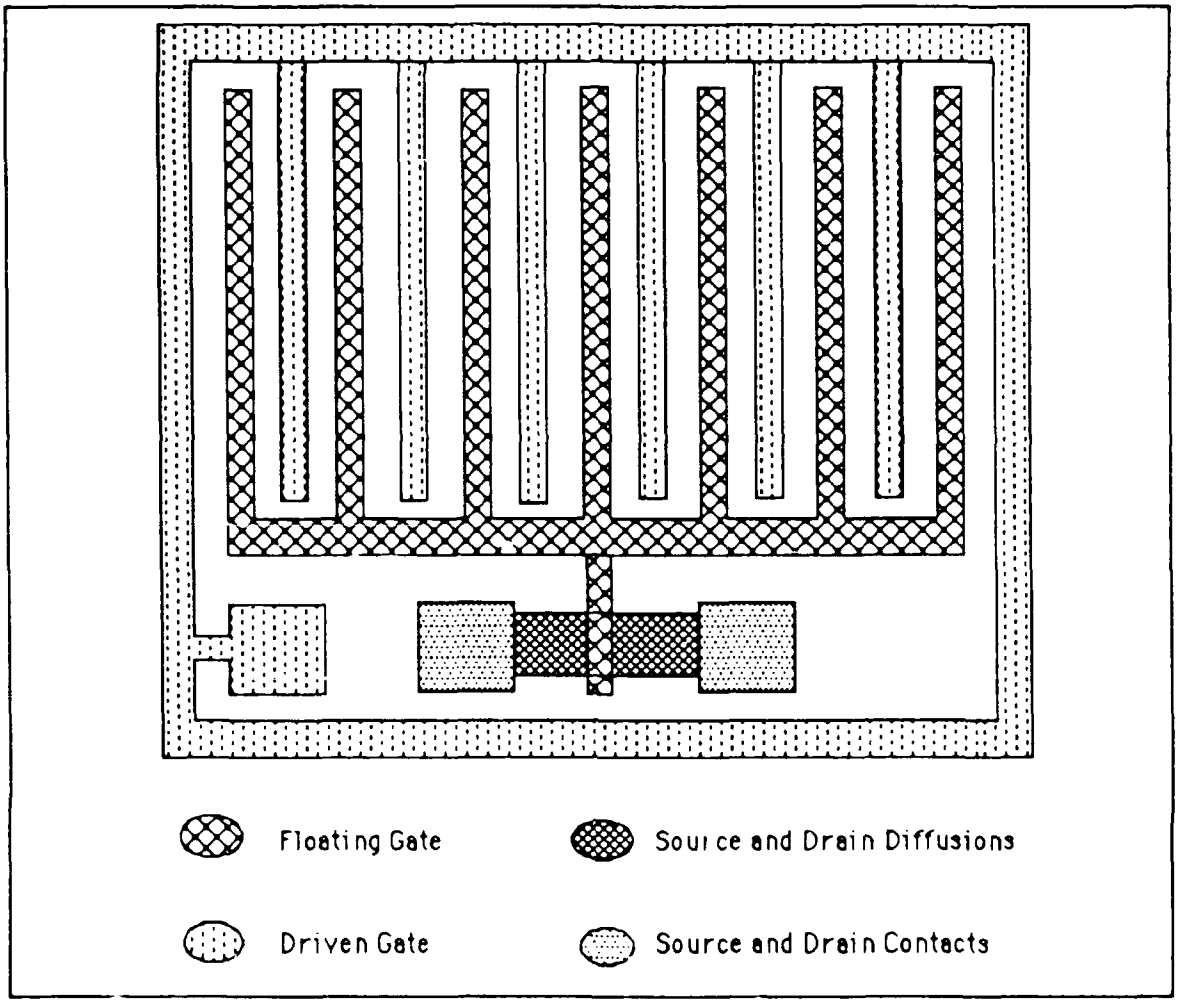

Figure I-1. Illustration of the IGEFET (7).

Problem Statement

The desired result of this thesis evaluation is a rank ordering of the sensitivity, specificity, and reversibility performance characteristics of representative M(Pc) samples with respect to temperature, humidity, and polymer thickness. Metal-doped

phthalocyanine polymers containing cobalt, copper, lead, and nickel are evaluated, in addition to an undoped phthalocyanine polymer.

Scope

A more comprehensive examination of M(Pc) based sensors is warranted based upon the preliminary performance results reported in the literature (7). Similar to all solid-state electronic devices, the reasons for further investigation of these sensors involved two critical issues, material properties and geometries.

The issue of material properties concerned impedance and doping mechanisms. The earlier investigation of Cu(Pc) by Capt John Wiseman (7) identified an anomalous change in the impedance of the electrode structure when challenged with a high concentration of nitrogen dioxide, as well as a sensitivity to extremely low concentrations of the gas. Also, the work by Khanna, et al., indicated that sensor performance parameters (such as sensitivity, response time, and reversibility) may depend upon the doping mechanism involved with the various M(Pc) polymers (8). A closer examination of the reported impedance changes due to large challenge concentrations (greater than 100 parts-per-billion) may reveal more detail about the doping mechanisms of M(Pc).

A fundamental geometrical issue concerns the thickness of the M(Pc) polymer. The work by Lee (10) indicated that one of the critical parameters in developing a lumped-element circuit model of an interdigitated gate electrode is the thickness of the material coating the electrode's fingers. Also, the work by Khanna, et al., (8)

indicated that the thickness of the various M(Pc) polymers affected a sensor's performance.

In addition to the material and geometrical issues, further development of the existing CHEMFET architecture (depicted in Figure I-1) is also warranted. To enhance its potential application as a microsensor, the CHEMFET was incorporated to form a two-dimensional array of sensing elements. This concept is illustrated in Figure I-2. By coating the individual elements with different M(Pc) polymers, the specificity of the microsensor was anticipated to be improved. A specificity enhancement was anticipated if the microsensor generated a unique response from two or more of the elements in the array with respect to a chemical specie's presence.

The response of the sensor could have been determined by several techniques. However, the specificity must be accounted for in the overall response since a practical microsensor must be selective, as well as sensitive. Additionally, the method should also make effective use of the proposed CHEMFET array. Consequently, the proposed method involves generating a matrix of responses. The implicit assumption involved with this method is that *appropriate* M(Pc) polymers for the sensing elements have been selected. *Appropriate* was defined as exhibiting some measurable response that was a function of the detectant and the detector species.

The generation of the matrix is a multi-step process. The method initially contrasts the response of individual elements within the array with respect to the response of a reference element.

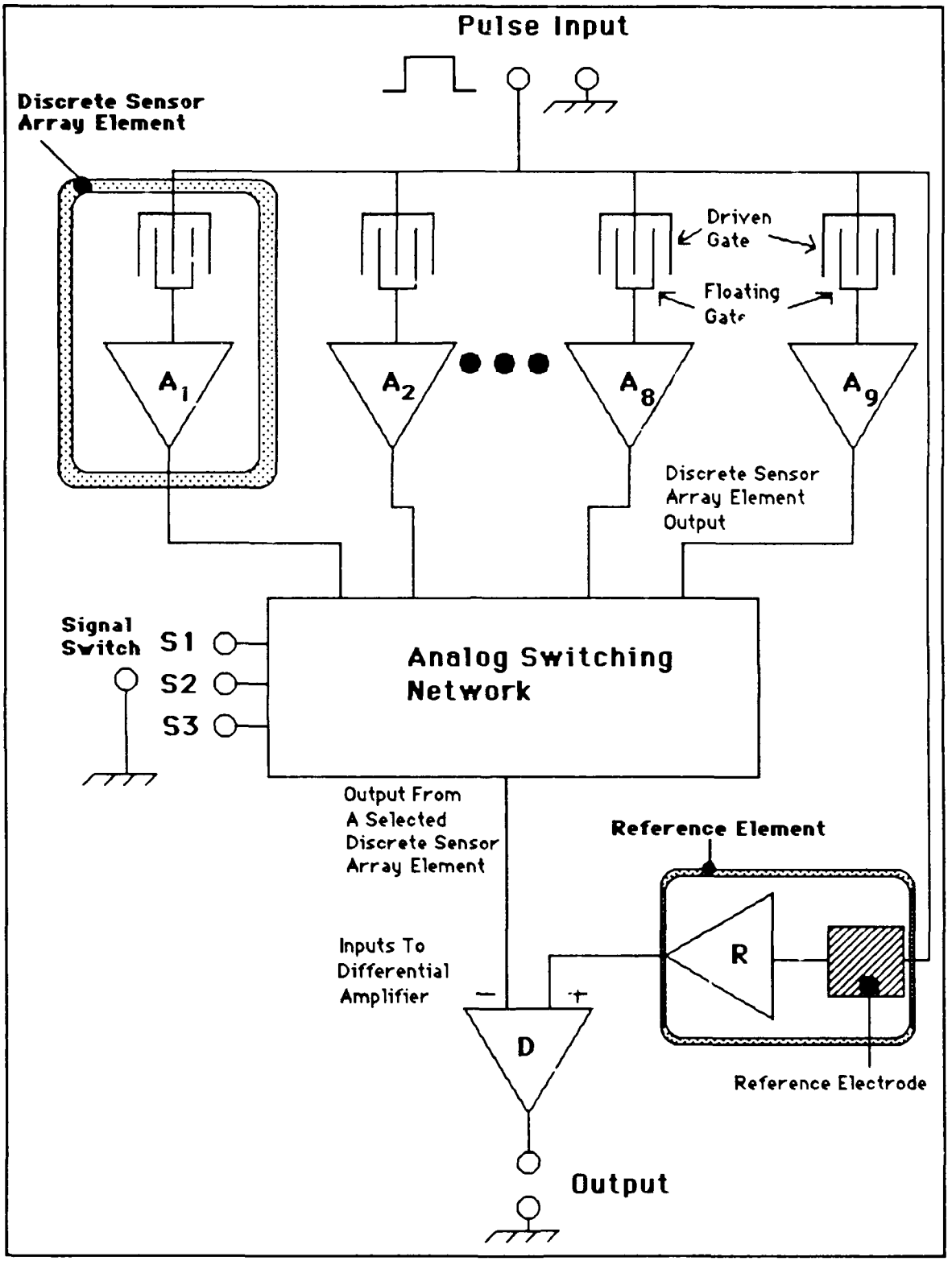

Figure I-2. Architectural Schematic of the CHEMFET Array.

Electrical circuitry is used to scan the elements of the array to sample their individual response. This feature is depicted in Figure I-2 as the analog switching network.

The reference element is composed of an uncoated, solid electrode plate with an area equal to that of the overall interdigitated electrode gate structure. The reference device electrode's plate area was scaled to partially compensate for the parasitic capacitance between the CHEMFET electrodes and the substrate. Additionally, this reference element is used to provide temperature compensation for the amplifiers. The contrasting mechanism was implemented as a simple, arithmetic difference of the response of an array element and the reference. As an alternative, the contrasting mechanism was also implemented by using a differential amplifier. Hence, the sensor response was pre-amplified prior to any subsequent signal processing. While generating this response data set, a "difference matrix" was constructed.

The difference matrix is a three-dimensional entity. The first dimension corresponds to the type of M(Pc) polymer or its location in the two-dimensional electrode array. The second dimension in the difference matrix corresponds to either frequency or time. For example, frequency was used in the case of the spectral, gain, and phase responses; whereas, time was used for the DC impedance responses. Additionally, frequency was used for the AC impedance (real and imaginary parts, as well as magnitude and phase). The characteristic response time of an AC impedance component (such as

the imaginary part) with respect to a detectant would be revealed by using a dimension of time. The third dimension corresponds to the value of the different response of an element in the array with respect to the reference element at a particular value of frequency or time.

It was anticipated that this difference matrix could provide a *characteristic response. The matrix represented a unique surface in* a three-dimensional response-space. A "response-surface" is illustrated in Figure I-3. In essence, a response-surface or difference matrix is anticipated to provide a fingerprint that could be used to identify a specific specie and its concentration through additional processing techniques, such as well established pattern recognition algorithms.

Therefore, by modifying the CHEMFET's architecture, by selecting the appropriate polymer coatings, and by selecting an advantageous data-reduction scheme, the microsensor could function as the input section of a rudimentary, solid-state, chemical analyzer; or a precise detector of a specific chemical compound. Although a fully-functional prototype of this microsensor concept was not the goal of the thesis, a verification of the concepts was demonstrated. Hence, this study could potentially lead to improved solid state sensors for military applications.

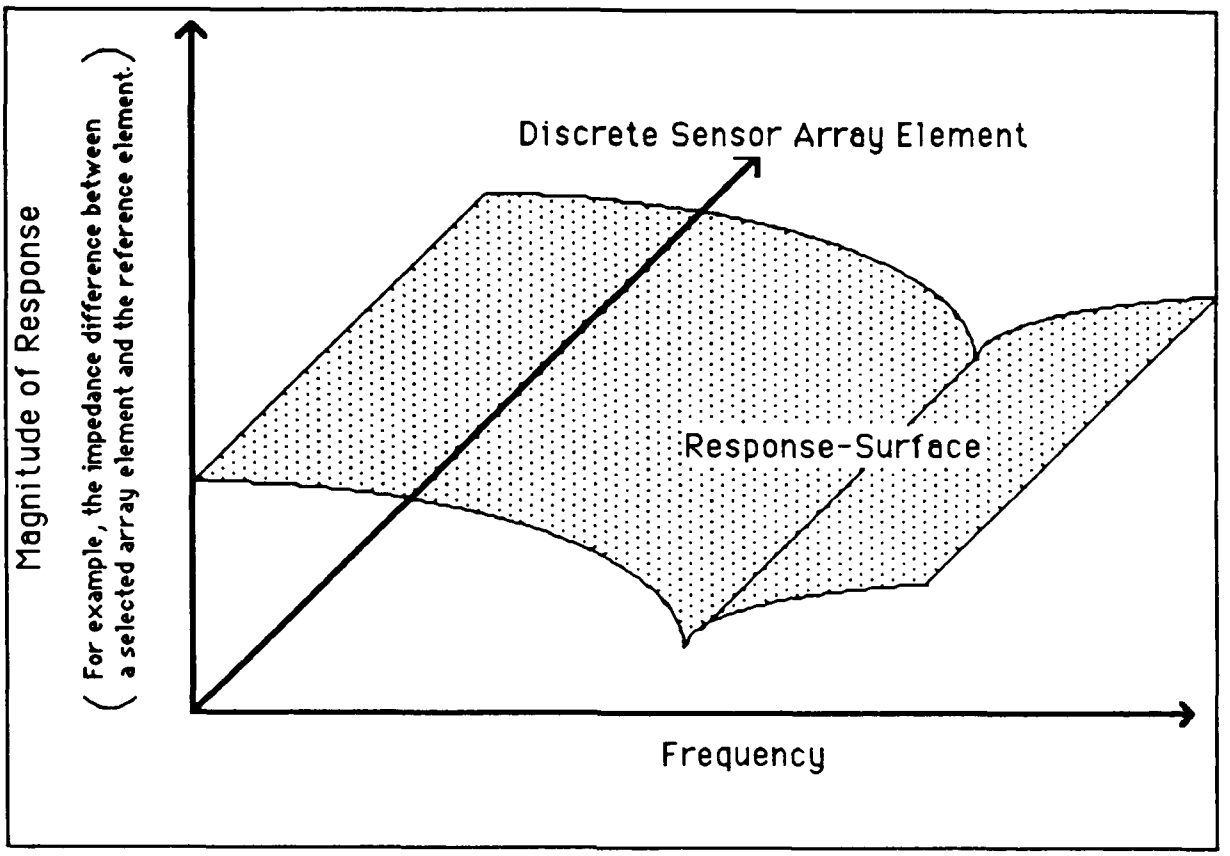

Figure I-3. Illustration of a Sensor Response-Surface.

Definitions

For the purpose of this thesis, a few key words need to be defined. Sensitivity, specificity, and reversibility will be defined in terms of the CHEMFET's performance, and the CHEMFET was viewed as a general system function. This function consists of an entity with dependent outputs and independent inputs. Inputs to this system were the concentrations and type of detectant species. Outputs from this system include the measured electrical characteristics, such as the spectral content, gain, phase, and impedance response-surfaces.

Sensitivity is defined as the ratio of the change in the output to the change in the concentration of a detectant specie. The change in the output was computed as the arithmetic difference of the sensor's final response-surface and the initial response-surface. The change in concentration was computed as the arithmetic difference between the final concentration and the initial concentration of the detectant.

Specificity is defined as the ability to unambiguously associate a class of response-surfaces with a specific type of detectant. For example, it was anticipated that a particular detectant, such as nitrogen dioxide, would produce a characteristic spectral response-surface that could be translated in the response-space as a function of concentration. However, the particular shape or form of the response-surface would be unique to the detectant (nitrogen dioxide in this example). In other words, the translation may affect the location of a unique surface, but the translation may not affect the shape of the unique response-surface. This behavior would be representative of the class of equivalent response-surfaces. Specificity may also be manifested with a class of response-surfaces that contain multiple surfaces which are not equivalent. In this case, a single surface in the class is associated with just one combination of type and concentration of a detectant. This behavior is more complex than the previous description of specificity since a second detectant at some arbitrary concentration may produce the same surface as the one characteristic of the class belonging to the first detectant. In this research effort, specificity was quantified by using a normalized, arithmetic difference between classes.

Reversibility is defined as the ability to reproduce an initial response-surface after varying the concentration of a detectant relative to some reference concentration level. The reversibility property was manifested in the following process: (1) the initial response-surface was at some equilibrium for a given initial concentration level of the detectant, (2) the concentration was changed and the response-surface attained a new equilibrium state, (3) the concentration was changed back to the initial value and the response-surface attained a final equilibrium state that would, ideally, be identical with the initial equilibrium state [step (1)] after some finite period of time. Reversibility was quantified in this research effort by an arithmetic difference of the initial and final response-surfaces. In the definition of reversibility and sensitivity, the initial concentration *does not have to equal zero.*

Approach

The approach of this investigation was divided into seven major processing steps: microsensor design, M(Pc) calibration, test cell fabrication, microsensor qualification, M(Pc) deposition, microsensor performance data collection, and data reduction. An overview of these major steps follows.

Microsensor Design.

During this step of the process, a microsensor and a polymer deposition mask was designed. The design of the microsensor was based upon the earlier configuration of the CHEMFET (7). The principal features of the design consisted of:

(1) a two-dimensional array of nine sensing elements utilizing an interdigitated gate electrode field-effect transistor (IGEFET),
(2) MOSFET amplifiers to provide signal gain,
(3) a reference element with a MOSFET amplifier to provide temperature compensation, and
(4) an electronic multiplexing circuit for interrogating specific elements in the array.

In addition, throughout the entire layout of the microsensor, an abundant supply of bond pads and physical links were provided. These features permitted the isolation of defective components.

The microsensor design step also included the design of a deposition mask that was used when depositing the chemically-active polymers on the CHEMFET sensor's electrodes. The design of this particular mask, as well as the microsensor, was generated using the AFIT very large scale integration (VLSI) design tools. The microsensor, *sans* polymer, was fabricated using the Metal-Oxide-Semiconductor Implementation Service (MOSIS) facilities (University of California, Berkeley, CA).

M(Pc) Calibration.

Once the microsensor design was completed and submitted to MOSIS for fabrication, the next processing step began. During this step, a technique was developed to deposit and measure the thickness of the cobalt, copper, lead, and nickel substituted phthalocyanine polymers, in addition to the undoped phthalocyanine material. The polymer deposition mask was fabricated using the

facilities in the AFIT Cooperative Electronics and Materials Processing Laboratory. The deposition process was accomplished by thermal sublimation under vacuum onto blank oxidized wafers. The thickness measurement was accomplished by contact profilometry after sputtering a thin film of gold over the samples.

Test Cell Fabrication.

This step involved fabricating the test cell and establishing the integrity of the gas generation and delivery system. This action was taken concurrently with the M(Pc) calibration step. The test cell provided temperature control, a humidity sensor, the multiplexer, wiring harness, and a signal output. Establishing the integrity of the gas generation and delivery system involved providing a regulated gas flow and a humidity control system. The test cell was able to maintain stable temperatures of 30, 70, and 120 degrees Celsius, while simultaneously maintaining a stable relative humidity level of 2%, 50%, and 100%.

Microsensor Qualification.

This step commenced when the fabricated microsensors were received, and the focus was now shifted to the task of qualifying of the MOSIS produced integrated circuits. Random samples of the devices were checked to ensure electrical isolation of the floating- and driven-gate electrodes. In addition, a visual inspection of the interdigitated structure was accomplished. The proper operation of the multiplexer and amplifiers was also verified. The verification of the design of the microsensor was simplified by having one-third of the microsensors mounted and bonded by MOSIS. Faulty

components within a microsensor were by-passed and/or isolated by wire-bonding and trimming the metallized signal line that was fabricated by MOSIS. After the design was verified, three of the microsensors were selected to continue the process.

M(Pc) Deposition.

This subprocess began after qualifying three samples of the microsensors, and it involved the deposition of the test polymers on the array of the interdigitated gate electrode structures. The test polymers consisted of cobalt-, copper-, lead-, and nickel-doped phthalocyanine, as well as an undoped phthalocyanine thin film.

Two thicknesses (approximately 500- and 1500-Å) of each of the metal-doped phthalocyanines were deposited, and a single thickness (approximately 1500-Å) of the undoped phthalocyanine. The first microsensor consisted of the five 1500-Å thick polymers. The second and third microsensors consisted of the four 500-Å thick metal-doped polymers.

After the polymers were deposited, the microsensor die were bonded in a dual in-line package (DIP). The completed microsensor package was then placed in the test cell.

Microsensor Performance Data Collection.

Once the polymers were deposited, the devices were tested under gas flow conditions. The microsensor devices were challenged with two test gases. These gases were nitrogen dioxide (NO_2) and diisopropyl methylphosphonate (DIMP). Filtered room air was used as the carrier (diluent) gas for the test gases and as the purge gas. The challenge gas concentrations were maintained at 20-, 80-, and

320-ppb for nitrogen dioxide and DIMP. The same challenge concentrations were used for both test gases to facilitate the comparison of sensor performance.

The experimental procedure used to challenge the microsensors consisted of several steps. Initially, the first microsensor (polymer thickness of approximately 1500-Å) was exposed to filtered room air whose relative humidity was 10%, 50%, and 100% while the microsensor's temperature was maintained at 25°C, 70°C, and 110°C. The DC resistance of the interdigitated electrode was measured during this exposure.

The first microsensor was initially thermostated at 30°C, and then at 120°C, during which the device was challenged with the two test gases at the three gas concentrations. The relative humidity was held at less than 5%. The second microsensor (polymer thickness of approximately 500-Å) was maintained at 30°C while being challenged with NO_2 at the three gas concentrations. Again, the relative humidity was held at less than 3%. In all cases, the challenge gas exposure was preceded and followed by a purge with filtered room air. These independent test variables and their respective values are summarized in Table I-1.

While challenging the microsensor, several electrical parameters were measured. These parameters served as the dependent test variables during the experimental procedure. The output values of the tests consisted of the DC resistance of the polymers measured with respect to time and applied bias, the AC impedance of the polymers (real part, imaginary part, magnitude,

Table I-1. Independent Test Variables (Including Filtered Room Air) and Their Respective Values.

Temperature (°C)	Relative Humidity (%)	Test Gas Type	Test Gas Concentration (ppb)	Polymer Type	Polymer Thickness (Å)
25	5	Air	20	H_2(Pc)	500
30	10	NO_2	80	Co(Pc)	1500
70	50	DIMP	320	Cu(Pc)	
100	100			Ni(Pc)	
120				Pb(Pc)	

and phase) measured with respect to frequency, the transfer function (gain and phase) measured with respect to frequency, the response to a voltage pulse excitation in the time-domain, and the spectral response to the voltage pulse excitation. The dependent test variables are summarized in Table I-2.

Data Reduction.

Once the test data was gathered, data reduction was accomplished. This process consisted of rank ordering the sensitivity, specificity, and reversibility of the unsubstituted-phthalocyanine, as well as the cobalt-, copper-, lead-, and nickel-substituted phthalocyanine polymers with respect to temperature and polymer thickness relative to a dry environment (less than 5% relative humidity). This evaluation was based upon the response-surfaces generated from combinations of the independent and dependent test variables.

Table I-2. Dependent Test Variables.

DC Resistance	
With Respect to Time	Resistance, Time (0 - 60 min)
With Respect to Applied Bias	Resistance, Voltage (1 - 10 V)
AC Impedance	
With Respect to Frequency	Magnitude and Phase Real and Imaginary Components Frequency (1 KHz - 1 MHz)
Transfer Function	
Frequency-Domain	Gain and Phase Frequency (1 - 200 KHz)
Voltage Pulse Response	
Time-Domain	Voltage Magnitude Time (10^{-3} second period)
Frequency-Domain	Power Magnitude Value (dBm) Frequency (1 - 200 KHz)

Plan of Development

A review of the current literature concerning microsensors is presented in Chapter II. Chapter III presents the theories of electrical transport in phthalocyanine and organic semiconductors in general, as well as, its importance in microsensors. Chapter IV provides a detailed description of the microsensor design and experimental approach. Chapter V summarizes the test and performance evaluation results. This thesis concludes in Chapter VI with a presentation of the conclusions and recommendations.

II. Literature Review Concerning Chemically-Sensitive Electronic Devices and the Phthalocyanine Polymer

Introduction

This literature review addresses the significance, theory, and operation of several electrical devices that are chemically-sensitive. Devices particularly sensitive to oxides of nitrogen and organic compounds are emphasized. The general significance of these devices was presented in Chapter I. The theory and operation of these devices are reviewed in this chapter by examining the important aspects of individual sensor elements, as well as arrays of these sensor elements. In addition, the incorporation of an organic semiconductor in the sensor scheme is reviewed. This objective is accomplished with a brief review of some general properties of phthalocyanine, a significant organic semiconductor for chemically-sensitive devices. Two primary methods of depositing the material are also reviewed. The applicable properties of the challenge gases used in this thesis effort are reviewed, as well. The literature review concludes with a brief summary of the significant findings and the implication of these findings on the design of the microsensor developed in this thesis effort.

Chemically-Sensitive Electronic Devices

The review of the types of chemically-sensitive devices is arbitrarily divided into three major sections. The first section deals

with structures not based on a familiar transistor architecture. The second section addresses transistor-based structures while the third presents a review concerning arrays of sensor elements.

Non-Transistor Based Structures.

Examples of chemically-sensitive devices based upon a piezoelectric device, a surface acoustic wave device, a notch filter, a resistive structure, and a capacitive structure are presented in this section.

Piezoelectric Devices. The piezoelectric effect can be used to fabricate a class of sensors. This class of sensors harnesses the same effect that drives most electronic wrist watches. The piezoelectric effect is manifested by a crystal that mechanically deforms (a bulk wave) when an electric potential is applied. In addition, the crystal will mechanically oscillate at a characteristic frequency when an oscillatory electric field is applied (11:323).

To make use of this effect, the piezoelectric crystal is coated with a chemically-sensitive material (12:1764-1768). In this case, the coating will "react" with the environment by either adsorbing (accumulation of material on the surface) or absorbing (accumulation of material within the bulk) the chemical species in the environment.

In several ways, this situation is somewhat analogous to a sponge in water. The surface of the sponge will rapidly become wet when immersed in water. The center of the sponge takes more time

to become wet. Similarly, adsorption on a coated crystal occurs more rapidly than absorption. Therefore, a piezoelectric effect based sensor has a faster response time when adsorption is the predominant interaction mechanism.

Extending the analogy, the mass of the coated crystal increases when adsorption and absorption occur. This effect is similar to the sponge becoming heavier when immersed in water. In fact, the change in mass is the principle by which the piezoelectric based sensor detects a chemical specie (12:1764-1768). The change in mass is related to the change in the natural frequency of oscillation by (12:1764-1768):

$$\delta F = (-2.3 \times 10^6 F^2)(\delta m/A) \qquad (2.1)$$

where

δF = change in the natural (resonant) frequency (Hz)

F = natural (resonant) frequency (MHz)

δm = change in mass (grams)

A = surface area of the detector (cm^2).

This class of sensors has an estimated sensitivity in the range of picograms. As an example, this sensor technology could detect concentrations of organophosphorus compounds that were on the order of parts-per-billion (ppb) (13:2057-2060).

While a piezoelectric effect based sensor may be quite sensitive, there is a major problem. This problem can be explained again by using the water-sponge analogy. Just as a sponge will

absorb practically any liquid, a very broad range of "contaminants" can "stick" to the crystal's coating. For example, dust or moisture in the environment can affect the mass of the detector. This situation may manifest itself when the dust or moisture is more massive than the intended detectant. Hence, the contaminant's equivalent response noise may swamp the detector's sensitivity.

Surface Acoustic Wave Devices. Another class of sensors can be fabricated using the principle of surface acoustic waves. Wohltjen and Snow developed a sensor based upon this principle (14:66-70). They fabricated a sensor consisting of dual-SAW delay-lines. It is illustrated in Figure II-1.

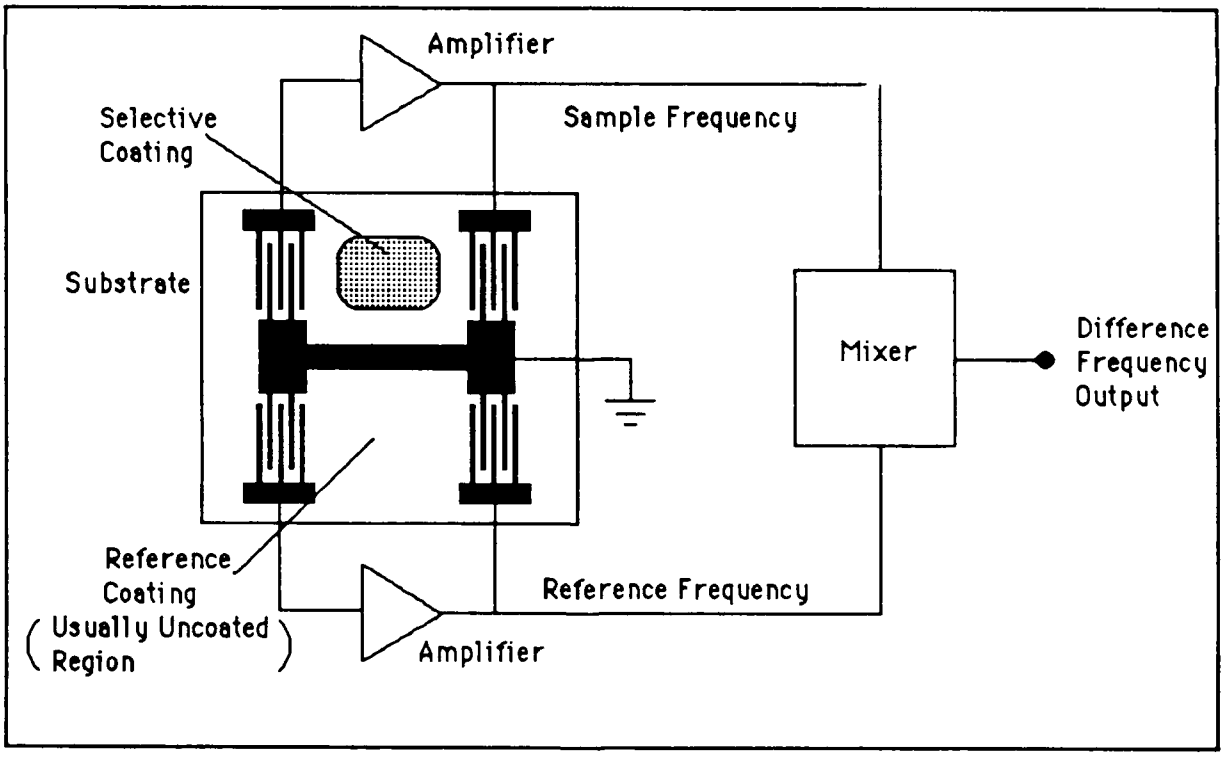

Figure II-1. Dual-SAW Delay-Line Chemical Vapor Sensor (14:66).

The method of vapor detection is very similar to that of a piezoelectric effect (bulk wave) based sensor. When vapors alter the mass or mechanical properties of the films, the oscillation frequency shifts. Since the two delay lines are coated with different materials, the frequency shifts differ. This difference is obtained with the mixer circuit connected to the sensor's output. Wohltjen and Snow reported sensitivities at the parts-per-million (ppm) level (14:70). However, this class of devices has problems similar to piezoelectric devices, since it is also a mass detector.

Notch Filter. Another class of sensors can be fabricated using the principle of a notch filter. A chemically-sensitive notch filter was developed by Kolesar (15). This sensor is realized by establishing a frequency dependent electrical network in which a component's value in the network is sensitive to the presence of a chemical specie. Upon exposure to the chemical specie, or detectant, the conductivity of an element in the filter changes. When this occurs, the notch characteristic of the filter shifts with respect to frequency, as well as its depth.

The notch filter is constructed from a highly conductive ground-plane electrode, a dielectric layer and a resistive thin film surface electrode. This configuration forms a distributed RC network. For the detection of organophosphorus compounds, the resistive layer is realized from a discontinuous copper and cuprous oxide film. In operation, the notch filter adsorbs the detectant; the chemical kinetics were found to be a surface effect.

The fundamental principle concerning the detector's operation is the modulation of the resistive thin film's conductivity upon exposure to a chemical environment. This detection mechanism is different than the modulation of mass that is utilized in the piezoelectric based sensors. The sensor fabricated by Kolesar was able to detect an organophosphorus compound at concentrations less than 10 parts-per-million. In addition, unlike the piezoelectric based sensors, the notch filter presents two dimensions of information (notch depth and frequency shift). Hence, a notch filter based sensor should be able to discriminate between chemical species or interferants.

Resistive Structure. A chemically-sensitive device based upon a resistive structure is known as a chemiresistor (16:1170-1174). A schematic of a typical device is depicted in Figure II-2. In the fabrication of this device, an interdigitated electrode is patterned on an insulating substrate. Also, the electrodes are coated with a chemically-sensitive material, such as an organic semiconductor. During operation, the conductivity of the material is monitored while exposing the coated interdigitated electrode structure to a chemical species.

The principle of operation for a chemiresistor is similar to that of the notch filter to the extent that both classes of sensors rely upon conductivity modulation. Chemiresistors have been fabricated using doped phthalocyanine polymers as the chemically-sensitive material coating the electrodes.

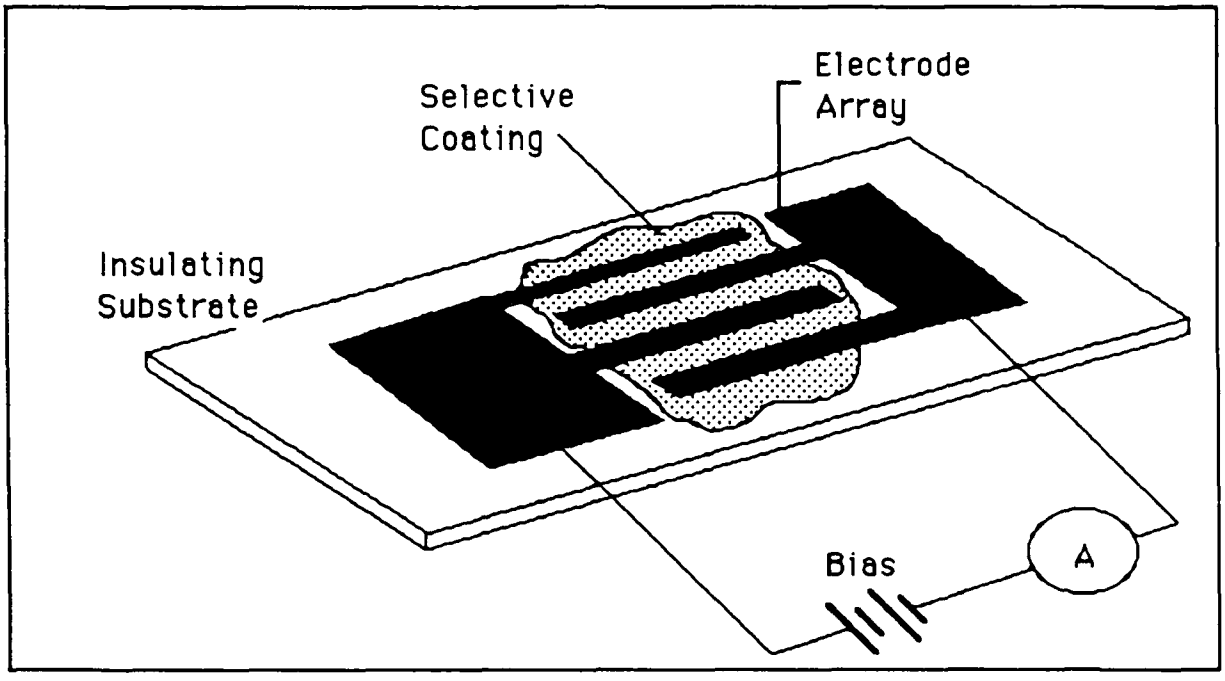

Figure II-2. Schematic of the Chemiresistor Structure (16:1170).

Using phthalocyanine polymers, Jones and Bott (9:27-37) reported the development of chemiresistors with a sensitivity of 44 parts-per-billion of nitrogen dioxide. In the case of a lead-doped phthalocyanine polymer, they reported a 185 percent change in the conductivity of the polymer upon exposure to 44 parts-per-billion of nitrogen dioxide with the sensor operating at 170°C. However, this device also has a potential problem with interferants.

Another type of sensor that can be classified as a resistive structure is the tin oxide (SnO_2) microsensor. This sensor variant derives its name from the coating material. This device is

fundamentally a chemiresistor (17:1; 18:235). This type of sensor has also been investigated for its sensitivity to NO_2, as well as alcohol vapors (17; 18). One widely accepted principle explaining its operation is straightforward. Fundamentally, the change in conductivity is perceived as the modulation of the depletion layer width in SnO_2 due to chemisorption of the detectant molecule (17:4). The typical test arrangement for tin oxide sensors is similar to that of the chemiresistor. The arrangement is depicted in Figure II-3.

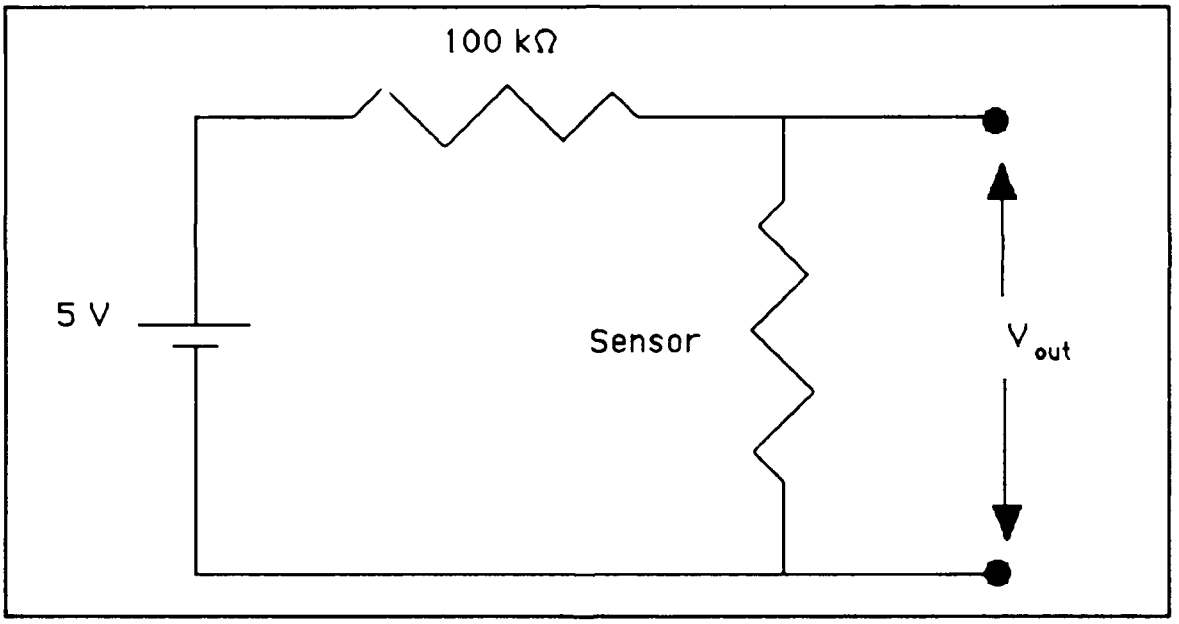

Figure II-3. A Tin Oxide Sensor Test Configuration (17:12).

To enhance the alcohol's sensitivity, the tin oxide film was coated with palladium/gold alloy films (17). Similarly, to enhance sensitivity to NO_2, the tin oxide film was alloyed with indium oxide (18). The palladium/gold alloy films affect alcohol detection by

catalyzing the dissociative adsorption of alcohol (17:5). The palladium/gold alloy film covering the tin oxide manifested a sensitivity to 200 ppm of alcohol (C_2H_5OH) (17:4). Uncoated, the tin oxide sensors were sensitive to concentrations of NO_2 at the 50 ppm level (17:4).

Sberveglieri, et al., chose indium-tin oxide as the chemiresistor material instead of lead phthalocyanine for two major reasons. The first reason was to improve the sensor's response time, and the second was the ease of preparation (18:241). The sensor material reached 90% of its final resistance value in less than 0.7 seconds in an environment of 200 ppm of NO_2 (18:239). In addition, the material could be deposited using radio-frequency magnetron sputtering, a conventional semiconductor process (18:236-237).

Capacitive Structure. Khanna, et al., (8) developed an extension of the chemiresistor. In their device, they sandwiched the chemically-sensitive material between two metals, and, in so doing, they created a lossy metal-insulator-metal (MIM) structure. In the fabrication of this device, they deposited a 200 - 300Å thick layer of a cobalt-doped phthalocyanine polymer. Using this device, they were able to detect a change in current flowing through the device within one minute of exposure to only one part per billion of nitrogen dioxide (mixed with a dry nitrogen carrier gas).

They also examined the harmonic response of the structure. To do so, they excited the structure with a 10 Hz signal. They noted that the change in current flow, relative to the initial value, was

dependent upon the harmonic examined. Upon exposure to the challenge gas, the current component for the first harmonic increased; whereas, the current component for the second harmonic decreased. In addition, they found that the magnitude of the response was dependent upon the concentration of the gas. Also, the response time was on the order of one minute. Hence, this structure may provide clues to several desirable sensor properties, such as sensitivity and specificity. A rational extension of this structure is to couple it with a transistor. This type of "hybrid" structure would synergistically provide for amplification of the harmonics in conjunction with a small solid state device.

Transistor-Based Structures.

This section discusses chemically-sensitive devices based upon a metal-oxide-semiconductor field-effect transistor (MOSFET) structure. The importance of the MOSFET structure in the development of chemically-sensitive devices was noted by P. Bergveld (19:142-143). Upon examination, the equation for the device's drain current presents a number of methods by which the environment may affect an observable quantity. Using the conventional nonsaturated drain current (I_D) equation (20:22):

$$I_D = (\mu C_{ox})\left(\frac{W}{L}\right)\int_0^{V_{ds}} (V_{gs} - V_t - V)\, dV \qquad (2.2)$$

where μ = carrier mobility

C_{ox} = oxide capacitance per unit area

W = gate width

L = gate length

V_{ds} = drain-to-source voltage

V_{gs} = gate-to-source voltage

V_t = threshold voltage

and noting that V_t can be found from (19:142):

$$V_t = \phi_{ms} - (Q_{it} + Q_f + Q_B)/ C_{ox} + 2\phi_f \quad (2.3)$$

where ϕ_{ms} = contact potential

Q_{it} = inversion layer charge density

Q_f = oxide and surface state charge density

Q_B = bulk depletion charge

ϕ_f = bulk Fermi potential

the environmental effects are more evident. For example, the carrier mobility and the contact potential may be significantly affected by the environment (19:142). These effects manifest themselves by altering the drain current.

As noted by Bergveld, small changes associated with the MOSFET structure motivate many variants of the class of chemically-sensitive devices (19:142). For example, an ion-sensitive FET is created by inserting a conducting electrolyte and a half-cell between the gate metal and gate oxide. Additionally, the charge-flow transistor (CFT) and the interdigitated gate electrode field-effect transistor (IGEFET) are viewed as significant variants of a chemically-sensitive field-effect transistor (CHEMFET) which utilizes a MOSFET structure.

Charge-Flow Transistor. The development of a miniaturized solid state sensor for monitoring chemical species would have several advantages. A miniaturized solid state sensor would be rugged. Additionally, a small physical size would make it feasible to incorporate a small, light-weight chemical sensor into other systems, such as *in-situ* prooes.

In the mid-70's, just such a device was developed (10). The device was named the charge-flow transistor (CFT), and it is illustrated in Figure II-4. The device is an extension of a conventional metal-oxide-semiconductor field-effect transistor (MOSFET). The primary distinctions are that the metallized gate electrode is split into two fingers that extend over the channel region, and a thin film is deposited between the split electrode fingers.

The operation of the CFT is similar to that of a MOSFET. However, to explain the operation of the CFT, the metal electrode is assumed to respond to an electrical potential more rapidly than the thin film. In a MOSFET structure, a conductive channel in an enhancement device will not completely form until the potential across the entire gate surface is sufficient to produce the inversion layer. Therefore, the turn-on time is controlled by the slower responding thin film.

This behavior results in a characteristic delay from the time an input voltage signal is applied at the gate pad, until the time an output signal is affected. The developers of this device were able to correlate the chemical state of an epoxy cure to the response of a CFT

by applying the epoxy as the thin film. The response characteristics of the CFT are a function of the conductive properties of the thin film. Consequently, as the conductive properties of the epoxy changed, the response of the CFT changed. However, they noted a limitation in the operation of the CFT.

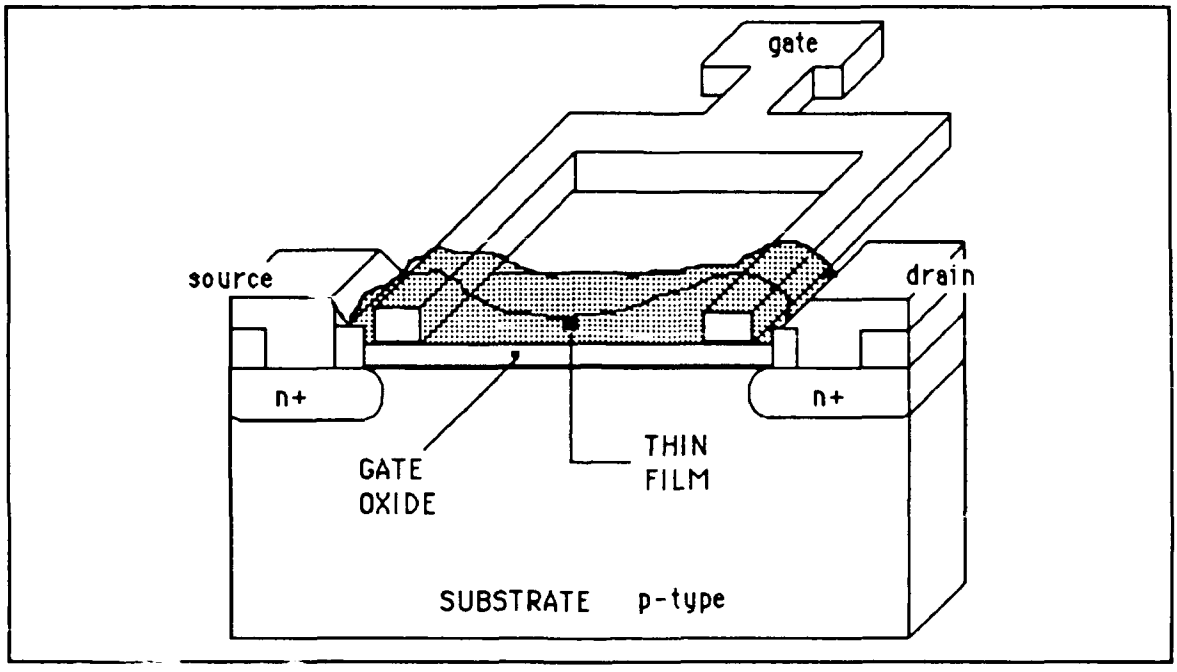

Figure II-4. Illustration of the CFT (10).

This limitation is an asymmetric response in the performance of the device. This feature can be explained using a simple analogy to a water hose. Water will stop flowing through a hose if the hose is pinched-off at any point along its length. Referring to Figure II-4, when the applied gate potential is removed (driven to ground), the

metal portion of the gate electrode's potential rapidly drops. Since the metal portion of the gate electrode is in the channel, the inversion layer in the channel is lost under those regions. Lacking a continuous inversion layer, the device turns-off, irrespective of the potential in the region of the thin film. The metal portion of the electrode that extends over the channel corresponds to the kink in a water hose. Thus, the turn-off time is a function of the faster responding metal, and it is not a function of the slower responding thin film.

As a result of this performance limitation, the metal electrodes were moved to a position over the source and drain diffusions. With this modification, the channel formation in the CFT is a function of the thin film's potential and not that of the metal electrode. Therefore, the new device switched symmetrically.

Another modification was made in the early 80's to improve the linearity of the device (10). This improvement involved moving the coated electrode away from the MOSFET's conductive channel. This modification also reduced the troublesome parasitic impedances. Thus, the linearity of the sensor was improved. In 1983, a commercial system incorporating this device variant became available. The device was designed as a microdielectrometer (10). Using a set of calibration curves, the complex dielectric constant of a material coating the electrodes could be extracted. This detector had now assumed the structure of an interdigitated gate electrode chemically-sensitive field-effect transistor.

Interdigitated Gate Electrode Field-Effect Transistor. Another potential sensor for the applications discussed above is the interdigitated gate electrode field-effect transistor (IGEFET) which is a significant variant of the chemically-sensitive field-effect transistor (CHEMFET). This device is a rational extension of the CFT. An IGEFET is a MOSFET with an interdigitated, chemically-sensitive electrode substituted for the conventional gate electrode of a MOSFET. In essence, the IGEFET can be conceptualized as the integration of a miniaturized chemical sensor and a MOSFET amplifier. This device has been investigated for use as a solid state sensor for environmentally-sensitive compounds (7).

The interdigitated gate electrode configuration in a IGEFET consists of a metallized driven-electrode which is physically and electrically isolated from a floating-electrode that connects directly to the transistor's gate oxide. An illustration of the IGEFET is depicted in Figure II-5.

In operation, the interdigitated portion of the gate electrode structure is coated with an organic polymer. When a voltage pulse is applied to the driven gate electrode, the characteristic response of the IGEFET is found to change as a function of the challenge gases and the material used to coat the electrode.

The IGEFET's operation is very much an extension of the lossy, capacitive structure of Khanna, et al., that was reviewed in the section concerning capacitive structures. The conductive properties of the organic polymer can be affected upon exposure to specific chemical species, and the MOSFET amplifier provides a level of gain

sufficient to ensure a proper signal-to-noise ratio for processing the output signal. Similar to Khanna, et al., the spectral response of the device is one of its important response features. Hence, the time- and frequency-domains of the electrical performance of the IGEFET are analyzed, such as the gain and phase of the system, as well as the real and imaginary components of the impedance of the interdigitated gate electrode structure.

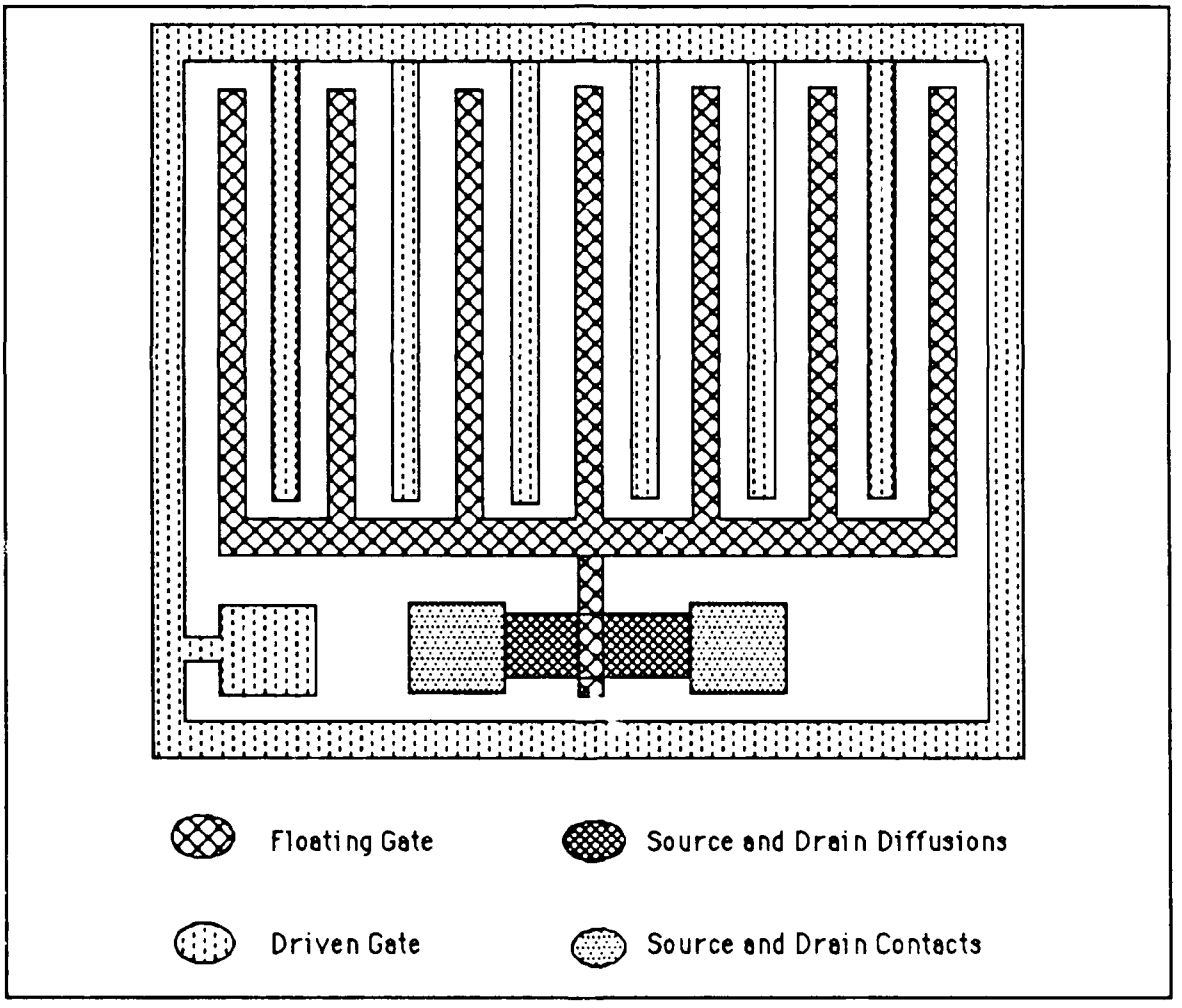

Figure II-5. Illustration of the AFIT IGEFET (6).

Since several components of the response of the thin film coating can be monitored with the IGEFET, it may be possible to enhance the sensitivity and the specificity with this solid-state, chemically-sensitive device (7). An IGEFET that was fabricated by Wiseman was found to be sensitive to a gaseous contaminant (NO_2) whose concentration was 20 parts-per-billion (7). In addition, the response of the IGEFET differed for a different chemical species. A further extension of the IGEFET technology is the proper selection of the thin film material and its geometry, *vis-a-vis*, the interdigitated electrode configuration and film thickness (7).

Sensor Arrays.

As explained in Chapter I, the microsensor developed in this thesis consisted of an array of individual detectors. The literature review found that several other researchers have recognized the value of using multiple detector elements within a sensor.

Bott and Jones investigated a sensor that consisted of six individual elements (21:128-131). They demonstrated that multisensor systems could detect the gaseous products from a fire such as carbon monoxide (CO), methane (CH_4), nitrogen dioxide (NO_2), and nitrogen oxide (NO). Of the six sensors, three different types of thin films were used. One type was lead phthalocyanine [Pb(Pc)]. Another type was zinc oxide (ZnO), while the third type consisted of a catalytic device used to detect the flammable gases. The operation of the first two types of thin film sensors were based upon modulating the conductivity of the detecting material.

They selected materials to detect particular gaseous components in the environment. They selected the Pb(Pc) material since it has demonstrated sensitivities to concentrations of NO_2 below 10 ppb. In addition, the Pb(Pc) would be sensitive to other strongly electrophilic gases such as NO, chlorine, and fluorine, but it would be insensitive to CH_4 (21:129). The ZnO was selected to detect CO, while the catalytic device measured CH_4.

An important feature of their method was the fact that they selected sensor materials and devices that were optimized to detect a particular gaseous component. Therefore, a disadvantage of their method is that the number of elements in their multisensor increases as the number of detectant types increase. Additionally, their selection of a detector material was also based upon the fact that the different materials were sensitive to different concentrations of the same gaseous vapor (21:128). This methodology yielded a large dynamic sensitivity to a particular vapor than what might have been expected with a single detector material. An additional disadvantage is the non-quantitative nature of some of the measurements (21:130). However, an advantage is the inherent specificity of the sensor since the materials are selected for their high sensitivity to particular classes of detectants.

Muller, et al., developed a multidimensional array of sensors for gas analysis (22:81-84). The individual elements in their array were MOS diodes utilizing palladium. To make the diodes chemically-sensitive, they coated the palladium with zeolite

crystallites. The principle of detection involves a change in the capacitance due to contaminant exposure.

Muller, et al., attempted to correct a problem with their simple arrays. With a simple array, each individual detector within the array would be sensitive to one detectant comprising a gas mixture. Therefore, the concentration of a detectant would be found by determining the response of the single element that was sensitive to the detectant. This explanation assumes perfect selectivity for a sensor element. In addition, to detect n-number of gases and interferants, an array of n-number of detectors would be required. However, in actuality, perfect selectivity does not exist. While a sensor may be more sensitive to a particular detectant, it will also be sensitive to other detectants to some degree. Muller, et al., called this "cross sensitivity" (22:81).

Muller, et al., demonstrated that "cross sensitivity" would be an advantage in a chemically-sensitive device that was realized from an array of detectors (22:81-82). Their method required two assumptions. First, they assumed "cross sensitivity" did exist. Second, they assumed the sensitivity of each element was different for any given detectant. Using these assumptions, they then constructed a matrix of the responses of the detector elements and the collection of detectants. This concept is depicted in Figure II-6.

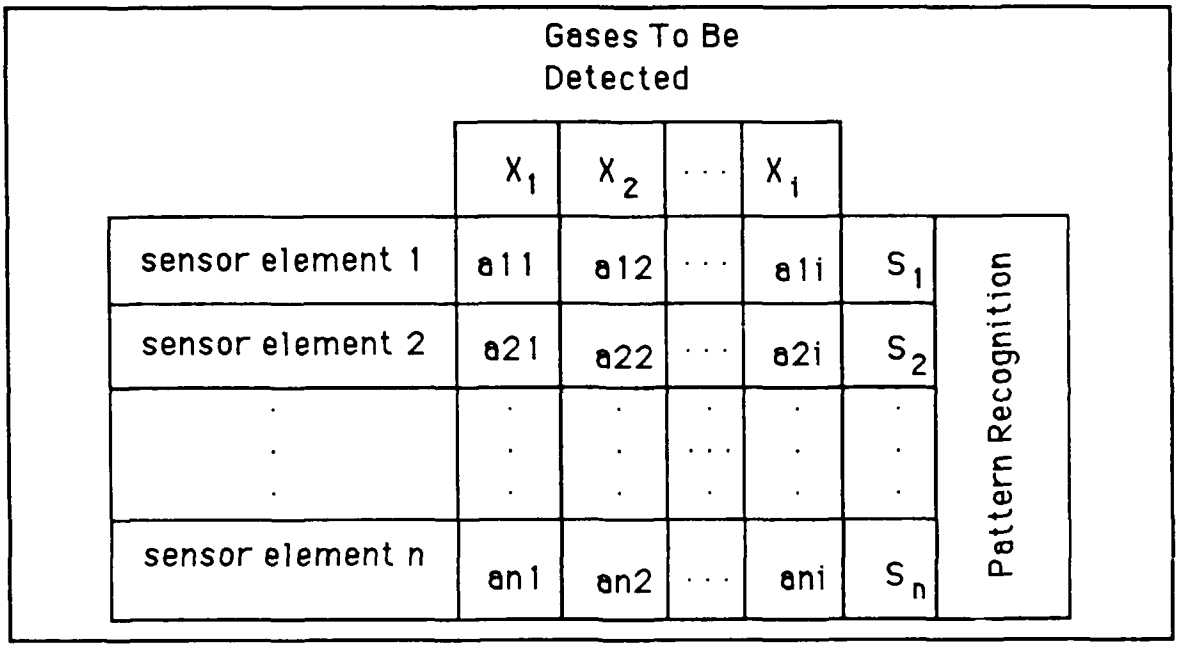

Figure II-6. Schematic of a Multidimensional Sensor (22:82).

From this matrix, a signal spectrum (denoted as S_n) was derived. They proposed that pattern recognition techniques could then be applied to this spectrum to identify the presence of the detectants. To find the concentration of a particular detectant gas, they proposed to correlate the intensity of the signal spectrum with concentration. The spectrum that Muller, et al., defined was not a spectrum in the sense of signal magnitude with respect to frequency, but rather, the collection of responses associated with a particular sensor element. Using the device they fabricated, the spectrum consisted of changes in capacitance.

The advantage of their method was that the number of elements in the array can be less than the number of detectants. Another advantage was that materials for the detectors may have

"cross sensitivity". A disadvantage with their method was that concentration is found only from spectrum intensity. This failed to consider the case where a sensor may become saturated with increasing vapor concentration. As the sensor becomes saturated, the response to an incremental concentration increase may become highly nonlinear (in the extreme, the response intensity may remain constant as the vapor concentration increases). In addition, the spectrum intensity was only a function of the change in capacitance. Another disadvantage with their implementation was the lack of on-chip circuitry to scan the array of diodes.

On June 2, 1987, J. Stetter, S. Zaromb, and R. Penrose received a patent for a sensor array to detect toxic gases (23). One of the important features of their invention was the detection of hazardous components in a gas using the response pattern from a collection of individual sensors. It is illustrated in Figure II-7.

The operation of their invention incorporates a multi-step process (23). The air containing possible hazardous components was drawn into the system across a heated filament. The filament was capable of oxidizing the hazardous component into one or more derivatives. The detectant and its derivatives were then passed through the sensors and exhausted. The individual sensor elements could be electrochemical, semiconductive, or catalytic. The response of the sensors was monitored and compared to patterns stored in the memory portion of the instrument.

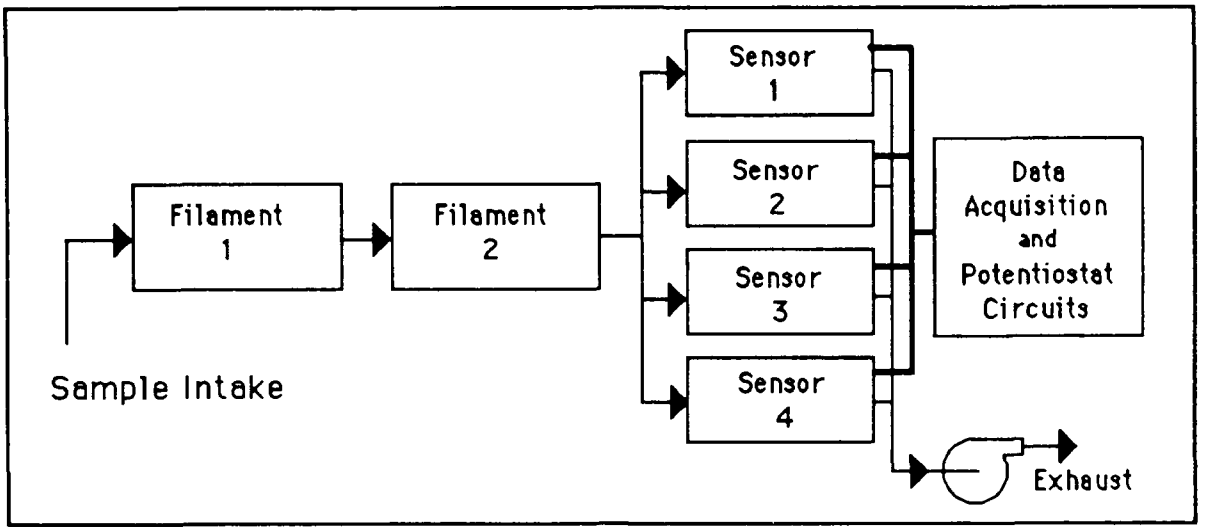

Figure II-7. Schematic of a Patented Sensor Array (23).

The sensor conditions such as vapor flow rate, temperature, and bias voltage were varied to increase the number of potential sensor responses. Stetter, et al.. varied the sensor conditions to increase the number of responses in order to improve the selectivity of the instrument (23). According to Stetter, et al., (23) the number of different components that could be identified was easily determined. The number of identifiable components was proportional to the number of independent parameters (P) that could be found. This value was determined by (23):

$$P = MS \qquad (2.4)$$

where M = number of different operating modes

S = number of selective sensors in the array.

Variations of the operating conditions can be justified by reconsidering the work of Muller, et al., that was discussed previously. By changing the operating conditions, the dimensionality

of the matrix of Muller, et al., is increased. This explanation logically assumes that the sensitivity of the individual sensor elements change with changes in their operating conditions. This condition effectively increases the number of sensors since the higher-dimensional matrix could be mapped back into a new two-dimensional matrix with the number of test gases (X_i) held constant.

The advantage of this sensor scheme is that the total system is self-contained and requires few elements in the sensor array (23). However, relative to a comparable microsensor application, this scheme has several significant disadvantages. Obviously, the device is not contained within an integrated circuit, but rather, it is a collection of mechanical and electrical parts. Another disadvantage is that the power requirement is 2 watts. Additionally, the sensors alone require a space 8 cm by 15 cm by 8 cm (23). Finally, the need for filters and valves (23) hinders the immediate insertion of this technology as a miniaturized, solid state sensor.

Many other researchers have investigated the use of multisensor arrays. For example, Rose-Pehrsson, et al., also researched the application of sensor arrays (24:421-428). In their work, they studied an array of surface acoustic wave devices that were coated with different vapor sensitive coatings. They found that "individually, the sensors lack selectivity; however, an array of the sensors can produce a unique fingerprint for each vapor of interest (24:421)." In their study, Rose-Pehrsson, et al., applied pattern recognition techniques to classify 10 different vapors and 2-component mixtures of those vapors with 85% accuracy using 3

discrete sensors (24:421). The training data consisted of the response values of 4 sensors to 10 test vapors. The response value was the magnitude of the frequency shift produced in the SAW sensors. The detectants were the 10 vapors at two concentrations and a 2-component mixture of every combination of the 10 vapors at one concentration. The resulting data set was a 220 X 4 matrix (24:422). An adaptive least squares algorithm was used to classify the responses (24:423).

An obvious advantage of this system was its selectivity, but the researchers admitted concentration analysis was difficult due to "quantitative differences" in the data (24:427). They attributed the differences to problems with the sensor materials (aging), fluctuations in the vapor sources, and temperature variations (24:425). One source of error they did not consider was the inherent problems associated SAW devices. For example, as previously identified, a SAW device is ultimately a pure mass detector.

Organic Semiconductors

In the initial review of transistor-based structures, the thin films used to coat the electrodes on the transistors were often treated as being the detector and the detectant, simultaneously. For example, the CFT application that monitored epoxy cure used the epoxy as the thin film coating that created the detector structure. In essence, the chemical environment for the sensor was the sensor, itself. In addition, in this type of arrangement, the possible changes

in the material may be dominated by bulk properties. A desirable property of a chemically-sensitive device is a fast response time and reversibility. These two properties could more easily be enhanced in a device based upon surface effects rather than a bulk effect. Hence, as alluded to in the review of the CHEMFET, the proper choice of materials to form the thin film is a critical issue that must be addressed in developing a versatile, chemically-sensitive device; the thin film is the heart of the detector.

A material with semiconductive and organic properties is highly desirable (7). A semiconductor would simplify the fabrication of a solid state device. For example, if the sensor material's conductivity is thermally activated, a match between the material and the sensor's electronics might be simplified. In addition, since gas exposure induced conductivity modulation is a desirable detection mechanism, the material should possess a state where it is not a good insulator, and not a good conductor. In other words, the desirable modulation should be in the vicinity of a point (varies both greater than and less than), rather than only along one direction in some continuum. In addition, a candidate material should be sensitive to organic materials if the sensor is intended to detect organic species.

The compounds classified as organic semiconductors are an excellent candidate for the chemically-sensitive thin film. As the previous examples of chemically-sensitive devices showed, various forms of the phthalocyanine compounds (an organic semiconductive material) are excellent candidates. Therefore, some general

properties of the phthalocyanine compounds are reviewed as examples of organic semiconducting polymers. Then, a review of phthalocyanine deposition methods is presented.

General Properties of the Phthalocyanine Compounds.

Phthalocyanine polymers are an example of organic semiconductors. In 1948, Eley and Vartanyan independently discovered the semiconducting property of phthalocyanine and its metal derivatives (25:205). According to Bolto, their work was probably the earliest report of semiconduction in organic materials (excluding organic photoconductors) (25:205). As previously noted in Chapter I, sensors based upon metal-doped phthalocyanine [M(Pc)] polymers have been found to be extremely sensitive to nitrogen dioxide (7; 8). For example, metal dopants of cobalt, copper, lead, magnesium, nickel, and zinc in M(Pc) have demonstrated electronic sensitivities upon exposure to nitrogen dioxide to concentrations spanning 1 part-per-billion to 10 parts-per-million (7; 8; 9).

In addition to chemical sensors, several uses of the compounds of the phthalocyanines are reported in the literature. Within the chemical industry, phthalocyanine is used as a dye and coloring agent due to its stability (26:113). From an academic perspective, since Eley's and Vartanyan's studies, the material has played a key role in the studies of crystal and molecular structure (26:113). In addition, quasi-one-dimensional conductors fabricated from

phthalocyanine are being investigated for an application involving an organic artificial neural device (27:1428).

The general molecular structure of a metal-doped phthalocyanine is depicted in Figure II-8. The previously mentioned dopants, such as cobalt, are represented by the M in the center of the structure. Nitrogen is represented by the N. Undoped phthalocyanine is usually represented by the structure depicted in Figure II-9 where H denotes hydrogen.

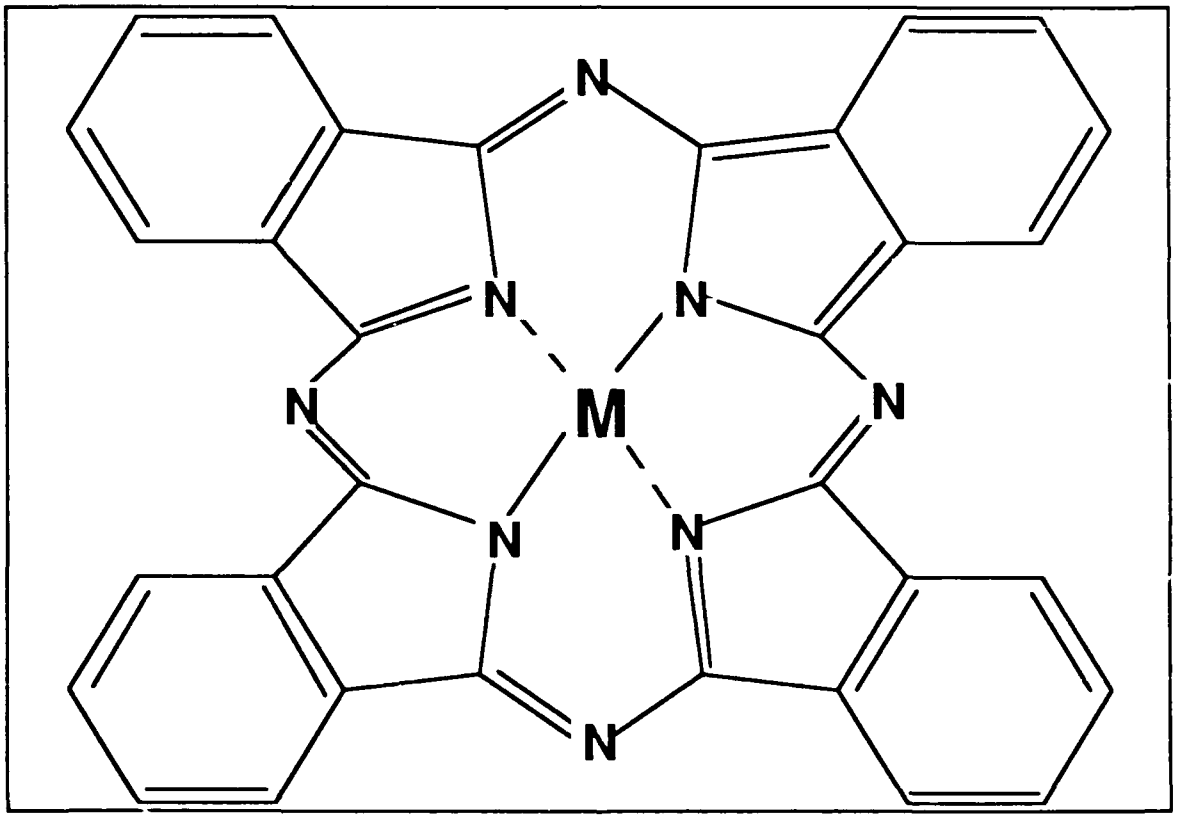

Figure II-8. Chemical Structure of Metal-Doped Phthalocyanine (25:205).

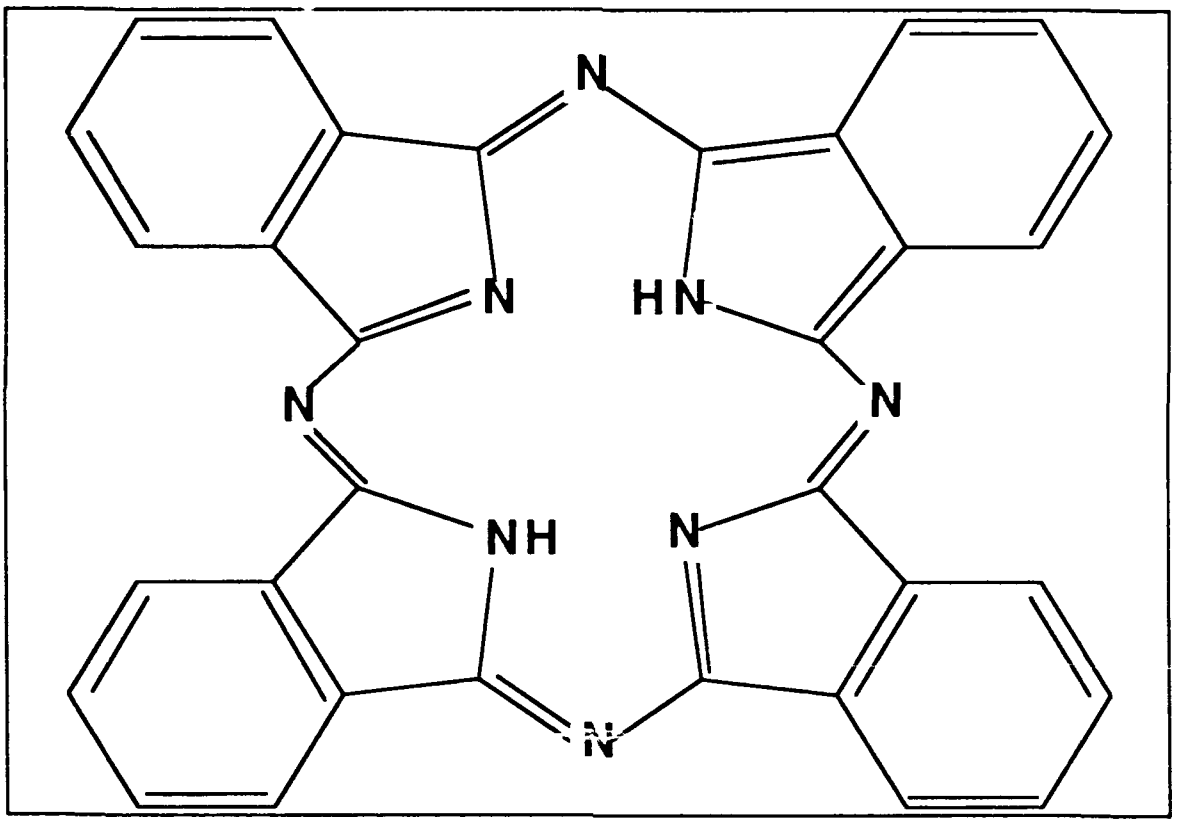

Figure II-9. Chemical Structure of Undoped Phthalocyanine (28:185).

X-ray analysis has shown that the molecule is flat, and that all the carbon-nitrogen bond distances have an equal value of 1.34 Å (28:185). Since the bonds have equal length, there is no true localization of the double bonds depicted in the figures. The affect of this "delocalization" is addressed in Chapter III.

The material is a derivative of tetraazaporphyrin, which is a macrocyclic compound (29:133-134) that belongs to the class of materials known as porphyrins (30:108). Phthalocyanine is classified as tetrabenzotetraazaporphyrin (29:136). The system of alternating carbon-nitrogen bonds is found in several naturally occurring compounds (28:185), and the bonding of the central metal atom is

particularly interesting. For example, both chlorophyll-a and chlorophyll-b are derived from the porphyrin ring structure with magnesium as the centrally coordinated metal atom (31:708). Also, embedded in the cytochrome-*c* protein structure, the heme-group is derived from a porphyrin ring system with iron as the centrally coordinated metal atom (32:156). While the chlorophyll and cytochrome compounds are associated with electron transport in biological systems (32:156,168), it is the electron transport properties of phthalocyanine that have been exploited in many chemically-sensitive devices presented in this review.

Many of the sensors that were reviewed used phthalocyanine compounds in a polymeric form. When the phthalocyanines are polymerized, they may be prepared in either an idealized flat planar structure or a cofacial arrangement (like beads on a necklace) (33:43). Conductivity in this material is probably due to the mechanism known as thermally-activated hopping (which is discussed in Chapter III) (33:43). The value of conductivity varies from approximately 10^{-12} mho/cm to 10 mho/cm. The actual value depends on doping, composition, and the polymeric structure (33:43).

Tne planar structure of this polymer has distinctive properties (33:43). The crosslinked planar structure does not require dopants other than the metal atom which is complexed in each phthalocyanine ring to enhance the material's electrical conductivity. In addition, the electrical conductivity in this type of structure is approximately proportional to the square root of the applied

pressure. Generally, this form of a phthalocyanine polymer is infusible, insoluble, and amorphous.

The cofacial form of the phthalocyanine polymers has several distinctive properties (33:43-44). The conductivity of the cofacially-linked polymers of phthalocyanine depends strongly on doping. Of the various possible dopants, iodine is the most studied, although other organic electron acceptors have been used. In a chemically-sensitive device, the detectant species itself, could serve as the dopant. Hence, the detector's change in conductivity would be due to a doping mechanism.

In the cofacial form of this polymer, it has been found that conduction slowly increases as the mole fraction of the dopant-to-metal ion reaches 1:1. This feature is characteristic of a "molecularly doped" charge transfer system (33:44). In addition, Cotts and Reyes pointed out that the cofacial form of the phthalocyanine polymers is slightly more tractable than the planar, crosslinked phthalocyanine polymers. Also, the cofacial form can be dissolved in H_2SO_4 or sublimed as thin films (33:44). The sublimation technique makes it possible to fabricate the film coating on a CHEMFET or chemiresistor, for example. In fact, the last iteration of the CHEMFET used sublimation to deposit a thin film (about 1000 Å) over the interdigitated gate electrode pattern (7).

Deposition of Phthalocyanines for Sensor Applications.

Primarily, the phthalocyanines have been deposited by two general methods (34; 35; 36; 37). One method utilizes the technique known as sublimation. The other method utilizes the Langmuir-Blodgett technique. This section presents a review of some examples.

In the deposition of lead phthalocyanine, Mockert, et al., used a sublimation technique (34:160). They deposited thin films less than 1000 nm by Knudsen cell evaporation under a vacuum of 10^{-8} mbar. The cell temperature was kept below 670°K to avoid decomposing the material. Also, the substrate's temperature was varied between 250 and 400°K. They used a quartz crystal microbalance to monitor the film thickness during the deposition process. This process produced a sensor sensitive to concentrations of nitrogen dioxide that ranged from 40 ppb to 100 ppb (34:173). Also, they deduced that the interaction was a surface effect (34:173).

Jones, et al., also used a sublimation technique to fabricate a sensor with fast response times (35:467-474). This group of researchers deposited lead phthalocyanine films which are a few microns thick onto alumina substrates with platinum electrodes. Using a preheat treatment (before exposure) of 360 °C for 60 minutes, they measured a response time of less than 10 seconds to nitrogen dioxide.

Baker, et al., prepared a gas detector film of copper phthalocyanine using the Langmuir-Blodgett technique (36:260-263). In the 1930's, Langmuir and Blodgett developed a technique to

deposit organic compounds (37:411). This process requires immersing the sensor's surface into a liquid bath. The material to be deposited on the sensor floats upon the liquid's surface. A monomolecular layer of the material to be deposited is transferred from the liquid to the solid surface with each subsequent immersion (37:411). Baker, et al., found that eight layers of copper phthalocyanine was sensitive to 120 ppm of nitrogen dioxide in nitrogen (36:262).

Properties of Nitrogen Dioxide

A brief literature review was conducted concerning nitrogen dioxide since the gas was the primary detectant used in this thesis. Nitrogen dioxide exists in 3 resonant forms (31:629). The Lewis formulas are depicted in Figure II-10 where the valence electrons are denoted with an "o" or an "x".

At ordinary temperatures, nitrogen dioxide exists in equilibrium with nitrogen tetraoxide. The Lewis structure for nitrogen tetraoxide is depicted in Figure II-11.

As discussed in the previous sections of the literature review, nitrogen dioxide is electrophilic (21:129). This is expected since the molecule possesses an odd number of electrons which results in an unpaired electron. However, nitrogen tetraoxide does not possess an unpaired electron.

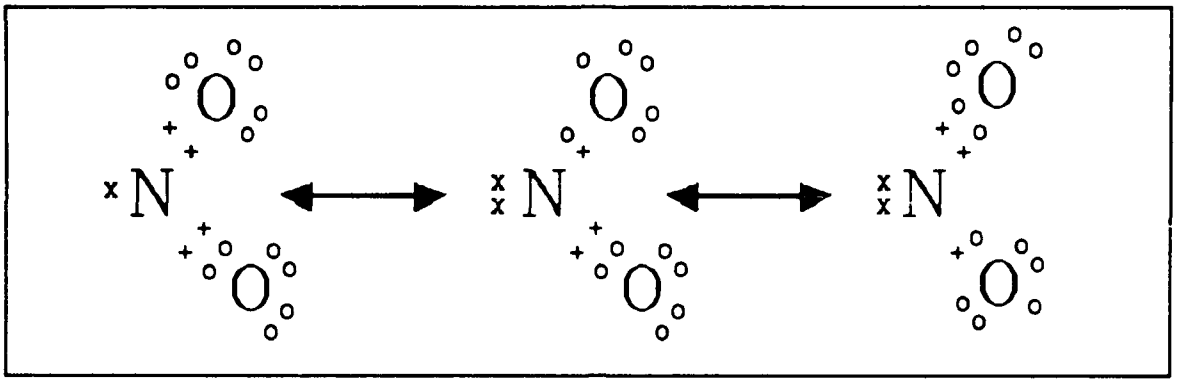

Figure II-10. Resonant Forms of Nitrogen Dioxide (31:629).

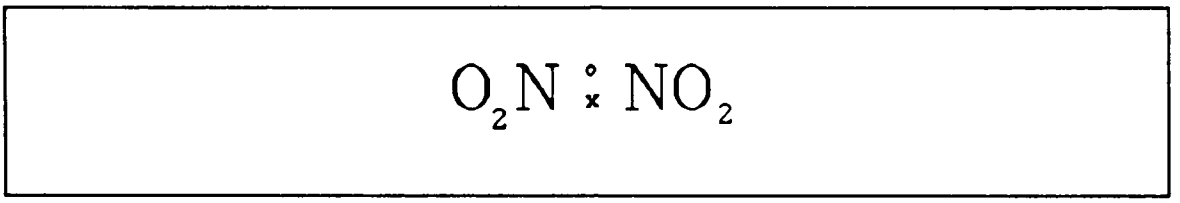

Figure II-11. Lewis Formula for Nitrogen Tetraoxide (31:629).

Properties of Diisopropyl Methylphosphonate

Diisopropyl methylphosphonate (DIMP) was used as a second detectant gas in this thesis effort. A dissimilar challenge gas was required to determine the specificity of the microsensor. DIMP has a different chemical structure than nitrogen dioxide (15:19). The chemical structure of DIMP is illustrated in Figure II-12. Additionally, the detection of DIMP is desirable. Having low toxicity and similar chemical reactivity as other more toxic organophosphorus compounds used as pesticides, DIMP has been used as a simulant (15:17). In addition, structurally related

compounds (for example, the thiophosphoryls) readily oxidize to form phosphoryl compounds. Since oxidized materials lose electrons (31:146), those compounds would be expected to donate electrons during chemisorption. This is the opposite expected reaction of electrophilic compounds (for example nitrogen dioxide). Therefore, the reviewed material would indicate that sensors based upon phthalocyanines would react differently when exposed to organophosphorus compounds and nitrogen dioxide.

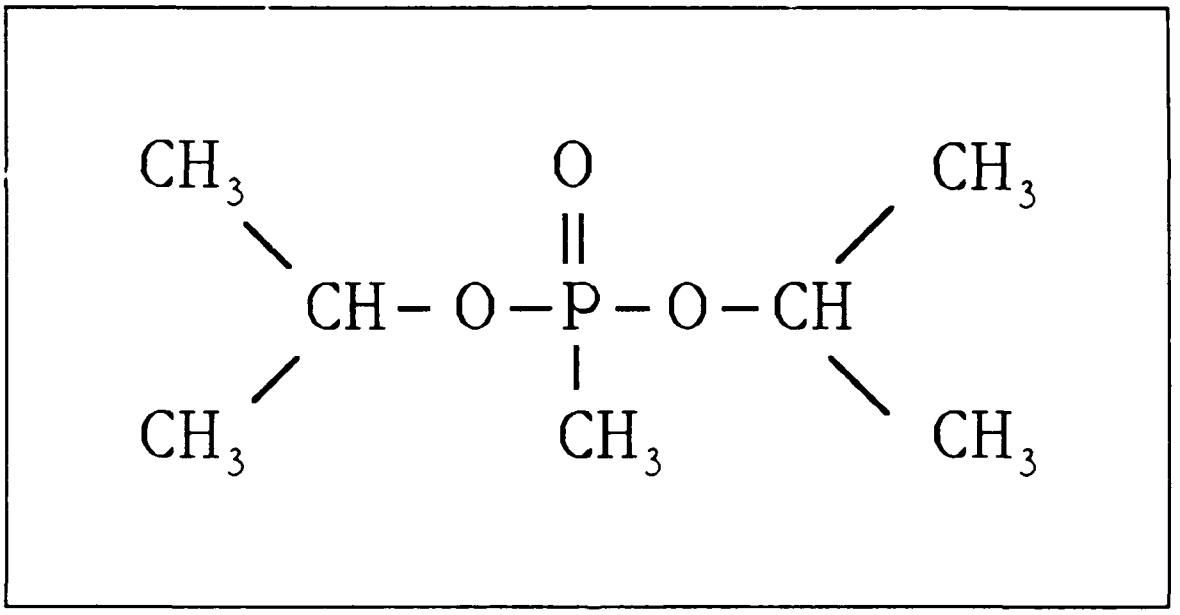

Figure II-12. Chemical Structure of Diisopropyl Methylphosphonate (15:19).

Summary and Conclusions

Examples of chemically-sensitive devices were reviewed. The principles of operation involved change in mass or change in conductivity. For example, sensors based on a piezoelectric structure were found to depend on a change in the mass of the detector's coating. On the other hand, sensors based on a chemiresistor were found to depend on changes in electrical conductivity. The potential problems with a sensor were also dependent upon its mode of operation, as well. For example, the piezoelectric based sensor's performance can be degraded due to its inability to discriminate between species of equal mass that "stick" to its surface.

It was also found that a refinement in a chemically-sensitive device's performance was possible when the sensor element was directly coupled to a MOSFET structure. An example of this class of sensor consisted of the CHEMFET. The CFT and the IGEFET were reviewed as examples of significant variants of the CHEMFET. The IGEFET was found to be a further refinement of the CFT. This type of device provides gain for subsequent signal processing and access to the spectral components of the modulated conductivity.

It was also shown in the review that significant improvements could be expected by combining microsensors into arrays. Specific improvements were found in the microsensor's selectivity and range of detectants.

The concept of incorporating an organic semiconductor into a chemically-sensitive device was also reviewed. The general properties of the phthalocyanine compounds, a significant organic semiconductor for chemically-sensitive devices, were reviewed. In addition, the application of phthalocyanine compounds in chemical sensors was reviewed. The review found that phthalocyanine was sensitive to electrophilic molecules; thus, indicating that sensors using phthalocyanines were sensitive to nitrogen dioxide.

The properties of nitrogen dioxide and diisopropyl methylphosphonate were reviewed, as well. According to the material reviewed concerning their respective properties, sensors fabricated with the phthalocyanines may react differently when exposed to these two gases.

Therefore, based upon the literature review, the microsensor designed in this thesis was significant from two perspectives. From a systems perspective, the microsensor consisted of an array of sensing elements. From a device perspective, the sensing elements consisted of an IGEFET structure employing a hybrid of the chemiresistor and the capacitive structure over-coated with phthalocyanines. The hybrid structure is depicted in Figure II-13.

As a microsensor system, the advantages of applying a collection of sensors were made evident in the course of the literature review concerning arrays. A primary advantage was a possible improvement in sensor selectivity. This feature would yield improved discrimination and chemical signature recognition. A secondary advantage was a possible improvement in the dynamic

sensitivity since materials with sensitivities to different concentrations of the same gas could be integrated within the microsensor.

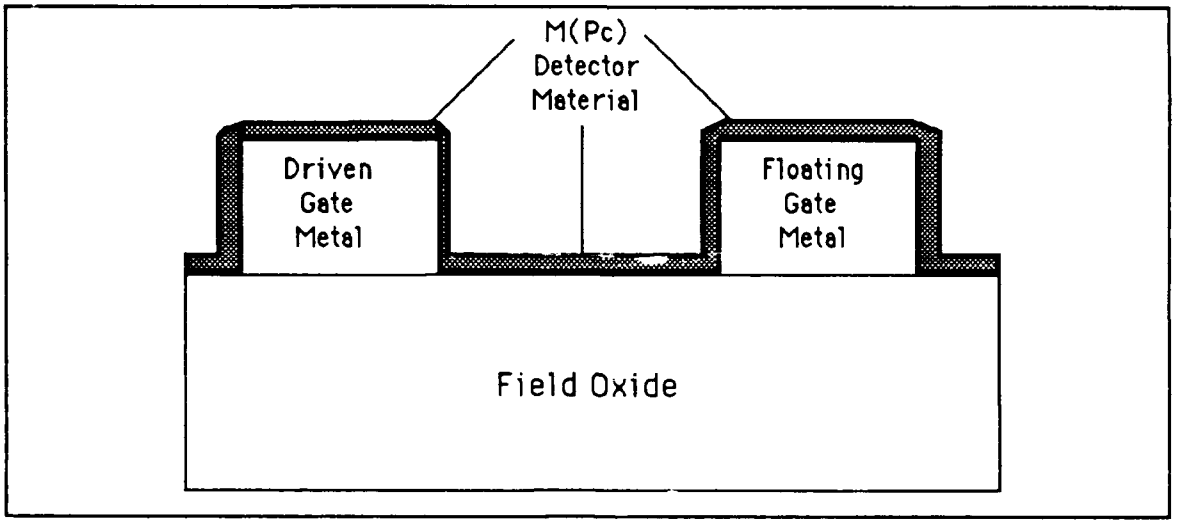

Figure II-13. Hybrid Chemiresistor and Capacitive Structure.

The literature review found a CHEMFET structure employing a hybrid of the chemiresistor and the capacitive structure as an IGEFET. The MOSFET would provide the signal gain for the microsensor electronics to improve the signal-to-noise ratio. At low frequencies, the MOSFET would be coupled to a chemiresistor whose conductivity would be affected by the sorption of detectants. At high frequencies, the MOSFET would be coupled to a complex impedance whose real and imaginary components would be affected by the sorption of detectants. Thus, an advantage would be the production of an enriched response matrix. An additional advantage would be a detection principle based upon the modulation of complex electrical impedance rather than upon the modulation of mass.

III. Theory of CHEMFET Vapor Detection

As previously discussed in Chapter II, the detection principle of the microsensor developed in this thesis effort involves the modulation of the electrical conductivity of phthalocyanine compounds. Therefore, this chapter begins with a brief examination of the conduction mechanisms in organic semiconductors and polymers. Then, within this framework, the next section describes the modulation of the electrical conductivity of phthalocyanine compounds as it pertains to chemical sensors. This chapter concludes with an analysis of complex impedance as it relates to a phthalocyanine-coated interdigitated electrode.

Conduction in Organic Semiconductors and Polymers

The conduction mechanisms in organic semiconductors and polymers are not fully understood (38:106-111). However, according to Cotts and Reyes, the numerous concepts relating to electrical conduction in these materials can be categorized according to chemical structure, carrier type, and the transport mechanism (33:59-74).

From a chemical structural perspective, Cotts and Reyes have found that organic semiconductors appear to fall somewhere between two extremes (33:60). One extreme is the familiar inorganic crystalline lattice. For example, this is the structure associated with

crystalline silicon. The other extreme is the amorphous state. In this latter type of material, it is more appropriate to use mobility gaps rather than energy gaps to characterize the material (33:60). Also, since the energy difference between points in the amorphous material is negligible, the carriers tend to hop from location to location via a weak thermally-activated process (33:60).

According to Cotts and Reyes, several possible charge carriers have been proposed to explain conduction in these materials (33:61-65). They include the following: ionic carriers, localized electronic states, intramolecular excitons, migratory localized ionic states, solitons, and the conventional electron-hole pairs indicative of band theory. For example, ionic carriers are distinct, ionically-charged chemical species, such as hydrogen ions and metallic impurities. The soliton is regarded as a particle that can possess a positive or negative charge. In addition, it can be neutral. Solitons appear to be the result of a defect or kink in the phase of the alternating carbon-carbon double bonds found in polyacetylene, a well-studied conductive polymer (38:106-111).

Since polyacetylene is one of the most intensely studied organic semiconductors and polymers, its doping process can be used as an example. Using the soliton conduction model characteristic of polyacetylene, a fundamental difference between doping organic polymers and doping silicon crystals can be readily illustrated. The doping of silicon crystals typically involves substituting a silicon atom with a dopant atom. As a substituent, the dopant forms a set of covalent bonds as it assumes its position within the crystal lattice.

This is not the case with doping polyacetylene, an organic polymer. The dopant is not a substituent nor does the dopant form a covalent bond, but instead, it removes or adds carriers to the energy band (38:108D). Within polyacetylene, a soliton results from this type of dopant behavior.

The soliton concept is illustrated in Figures III-1 and III-2. Figure III-1 depicts an undoped polyacetylene chain. Initially, the polymer is shown as a long chain of alternating single and double bonds.

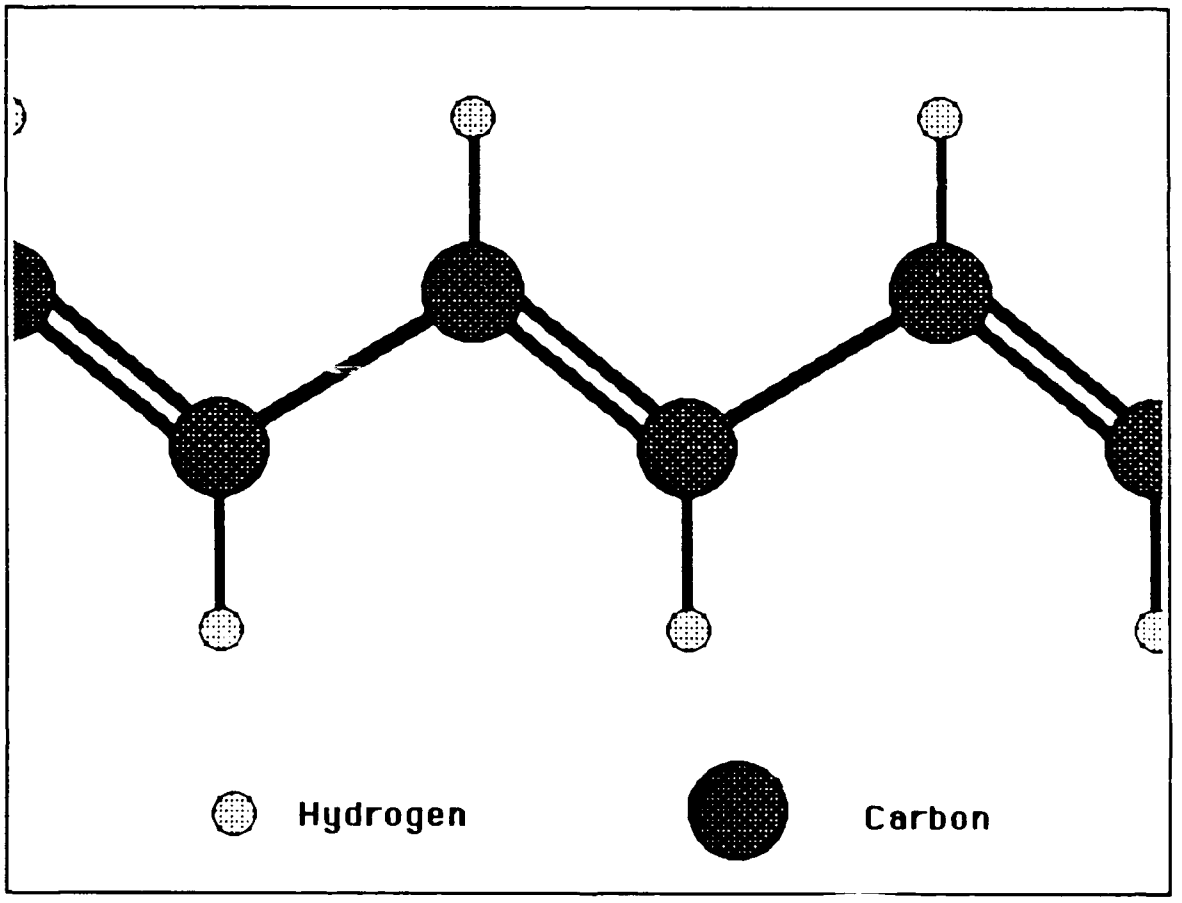

Figure III-1. Illustration of Undoped Polyacetylene (38:108).

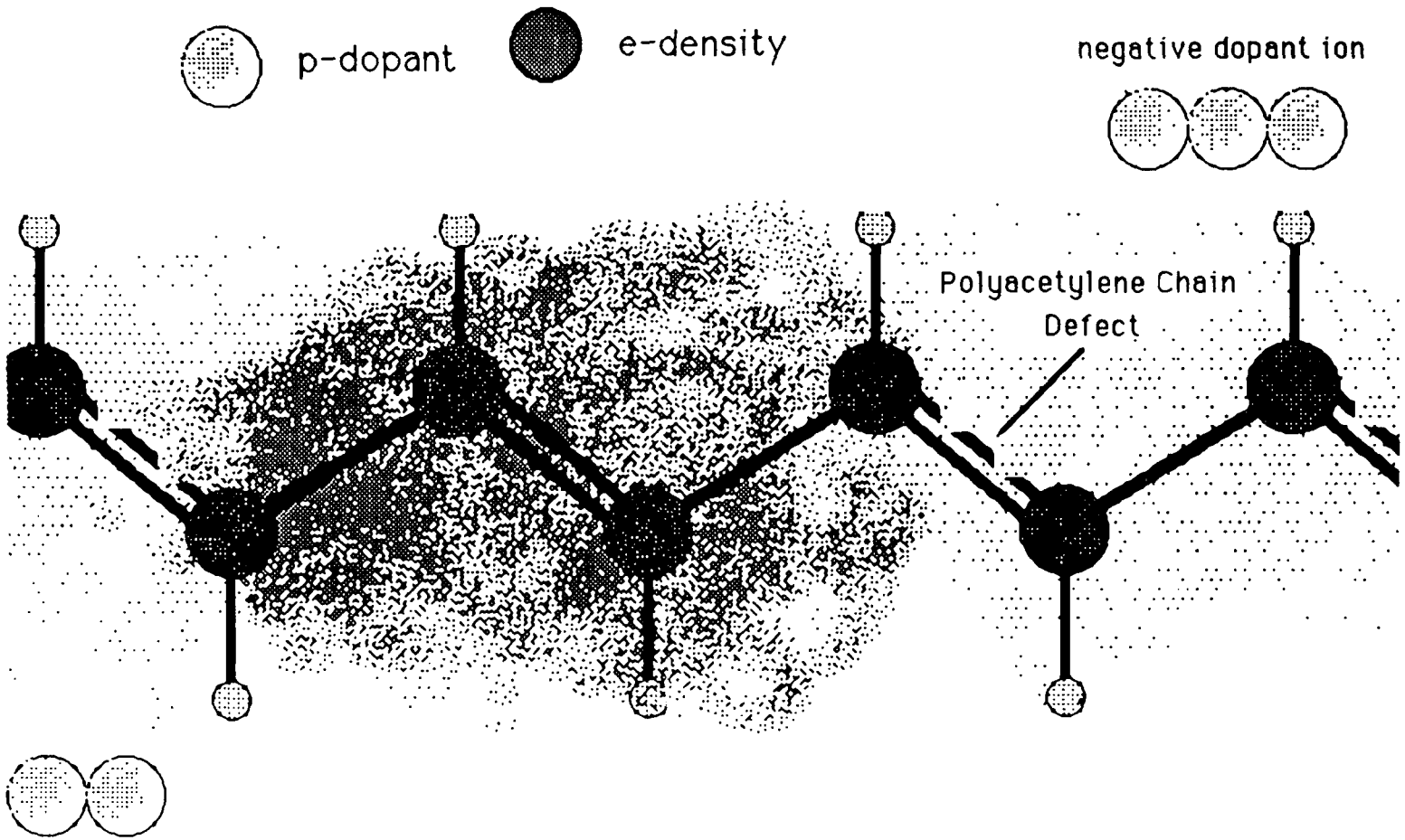

Figure III-2. Illustrative Example of Doped Polyacetylene (38:108D).

Figure III-2 depicts the same chain after doping. As illustrated, the doping process perturbs the chain of alternating bonds between the carbon atoms modeled by way of the adsorption and absorption processes. This perturbation does not break the chemical bonds. Also, the dopant does not react to form a new chemical compound. The perturbation of the uniform electron density is also depicted in Figure III-2.

Several transport mechanisms for the collection of carriers have been proposed, as well (33:65-72). The transport mechanisms are ionic conduction, band-type conduction, hopping (between localized electronic states) conduction, excitonic conduction, and quantum mechanical tunneling conduction (33:65-72). In ionic conduction, mass is actually transported as the ions move through the material. Hence, the ionic transport process is extremely sensitive to the material's stoichiometric variations. Additionally, absorbed water can greatly enhance ionic conductivity, as well. In hopping conduction, the mobility (μ) is a function of temperature (T). Cotts and Reyes report an empirical relationship for hopping mobility as (33:70):

$$\mu = \mu_o \exp\ [-(T_o/T)^{1/4}] \qquad (3.1)$$

where μ_o and T_o are experimentally determined constants.

According to D. Bott, conduction in semiconducting polymers encompasses three broad models (39:1193-1197). The first is a typical band model for crystalline materials. However, when any

disorder is introduced as with amorphous materials, a hopping model is used. The third model involves percolation. Unlike percolation, both the band and hopping models require a homogeneous material (39:1197).

When depositing the various phthalocyanine compounds used in this thesis effort, the material condensed from the gas phase onto unheated die (room temperature). The process is precisely described in Chapter IV. However, for the purposes of this chapter, it is significant to recognize that the deposition surface was cooler than the vapors. Under these deposition conditions, the formation of an amorphous phthalocyanine film that covers the interdigitated electrode structure is thermodynamically favored (40:217). Therefore, models of conduction that employ hopping or percolation may be more appropriate.

Hopping and percolation are less familiar forms of conduction. Hence, a brief review of these two models is in order. Initially, a qualitative description of percolation is presented. This is then followed by a description of the hopping model.

Percolation Model of Conduction.

A simplified two-phase material can be used to illustrate percolation. In this example, one phase is highly conductive while the other phase is not. Therefore, the conductivity is a function of the concentration of the conducting phase. Initially, the material only consists of the nonconductive phase. Hence, the system of the materials is insulating. This situation is shown in Figure III-3.

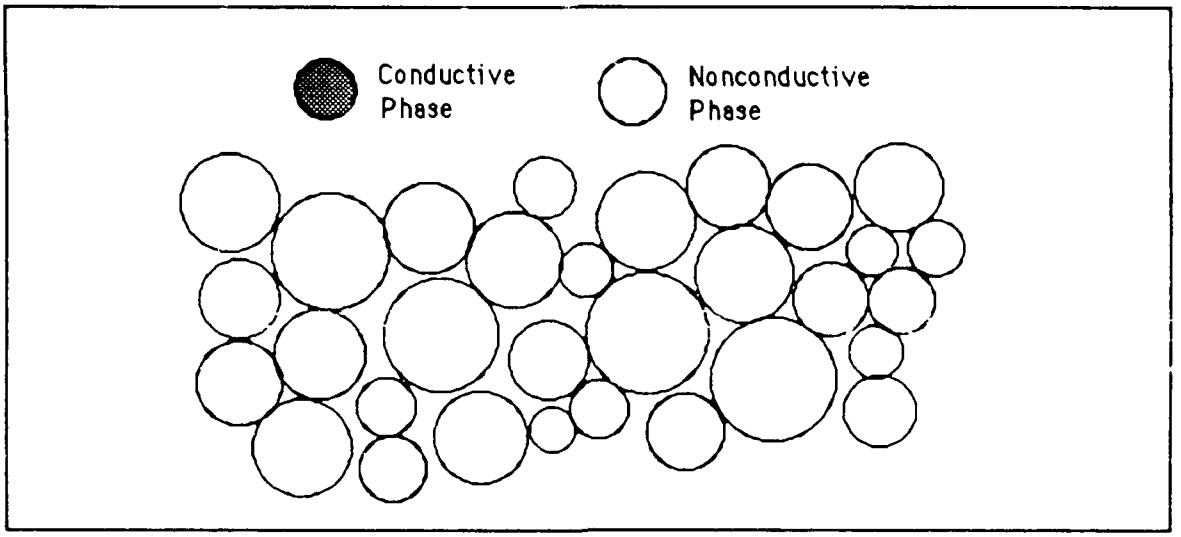

Figure III-3. Totally Insulating Two-Phase System.

With the addition of a low concentration of the first phase, the conductive material is modelled as being isolated (dispersed) within the insulting material. Since no filamentary conductive paths exist, the system of the materials remains insulating, although domains within the system are conductive. This is depicted in Figure III-4.

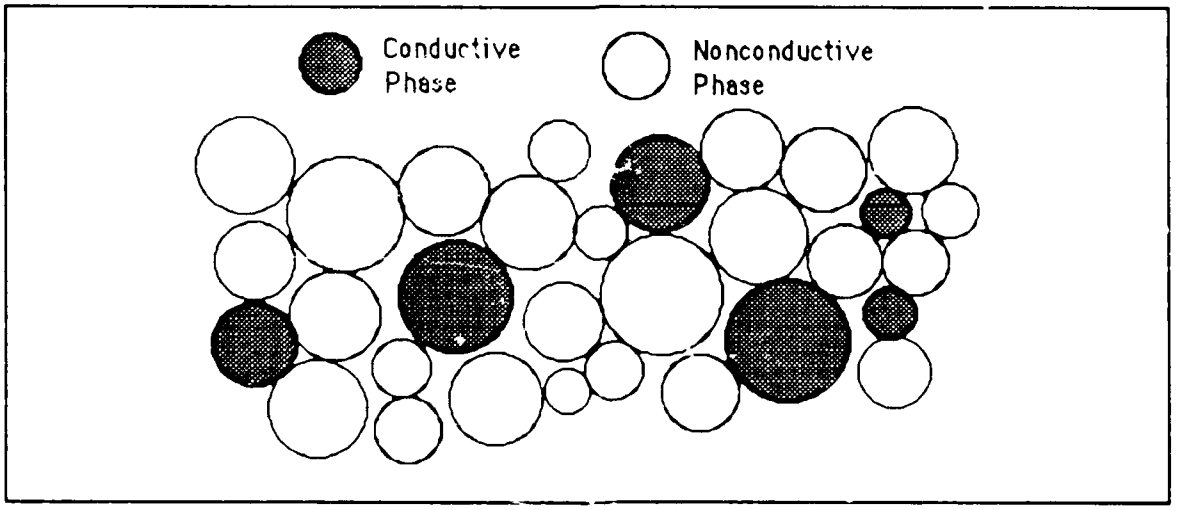

Figure III-4. Nonconductive and Conductive Phases Mixed to form an Insulating Two-Phase System.

As the concentration of the conductive phase increases, a critical density of the conductive phase will occur. Once this critical "threshold" is attained, the conductivity of the system of materials will rapidly increase when filamentary conductive paths are formed (39:1197). This phenomenon is shown in Figure III-5.

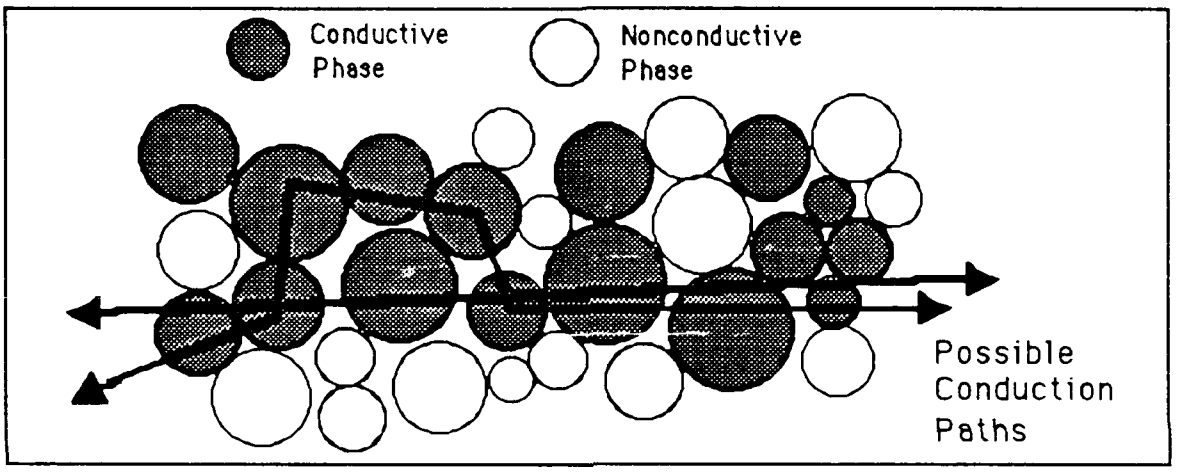

Figure III-5. Percolation Conduction Filaments Formed in a Two-Phase System.

As the concentration of the conductive phase continues to increase, additional conductive paths (filaments) will be formed. Consequently, the system's conductivity will continue to increase and saturate at some characteristic value (bulk conductivity of the conductive phase) when the concentration of the conductive phase becomes 100% (39:1197). Thus, a percolation model of conductivity is appropriate for a material that rapidly switches from a highly nonconductive state to a conductive state with a single or limited

number of intermediate states. The carrier transport mechanism in percolation models has been postulated to be a hopping process (41:137-146).

Hopping Model of Conduction.

To understand the hopping conduction model, the process is examined for the case of amorphous semiconductors which requires the extension of crystalline band theory to noncrystalline solids. The hopping model is based upon the formation of localized states within the solid (42:75). That is, within a crystalline semiconductor, the long-range order results in very sharp conductive valence band edges which are separated by a well-defined forbidden energy gap. In amorphous semiconductors the long-range order is lost, but a short-range order is retained. The result is a distortion of the density of states (N(E)) (43:116). Since the local structure is generally similar to the local structure of a crystal with long-range order, it was considered appropriate to use tight-binding theory to explain some properties of amorphous semiconductors (44:2). Hence, the concept of N(E) is applicable (43:116). In the hopping model of conduction, conductivity is closely related to the distribution of the density of energy states (43:119).

According to Nagels, Mott postulated that the spatial disorder in the potential caused by stoichiometric disorder in a semiconducting material would lead to the formation of localized states (43:117). The localized states are not necessarily distributed continuously within a band. Instead, they may form a tail above and

below the normal band edges associated with ideal crystals. In addition, there is a sharp boundary between the energy ranges of the extended and localized states (43:117). Also, the states are localized since a carrier within a given region will not diffuse to another region having a corresponding energy state at zero temperature (43:117). A model of this extended energy band diagram is shown in Figure III-6 where E_c, E_F, and E_v denote the conduction band, Fermi, and valence band energy levels, respectively. Additionally, E_b and E_a denote the extent to which the localized energy states extend into the forbidden energy gap (the continuum of localized energy states are denoted by shading).

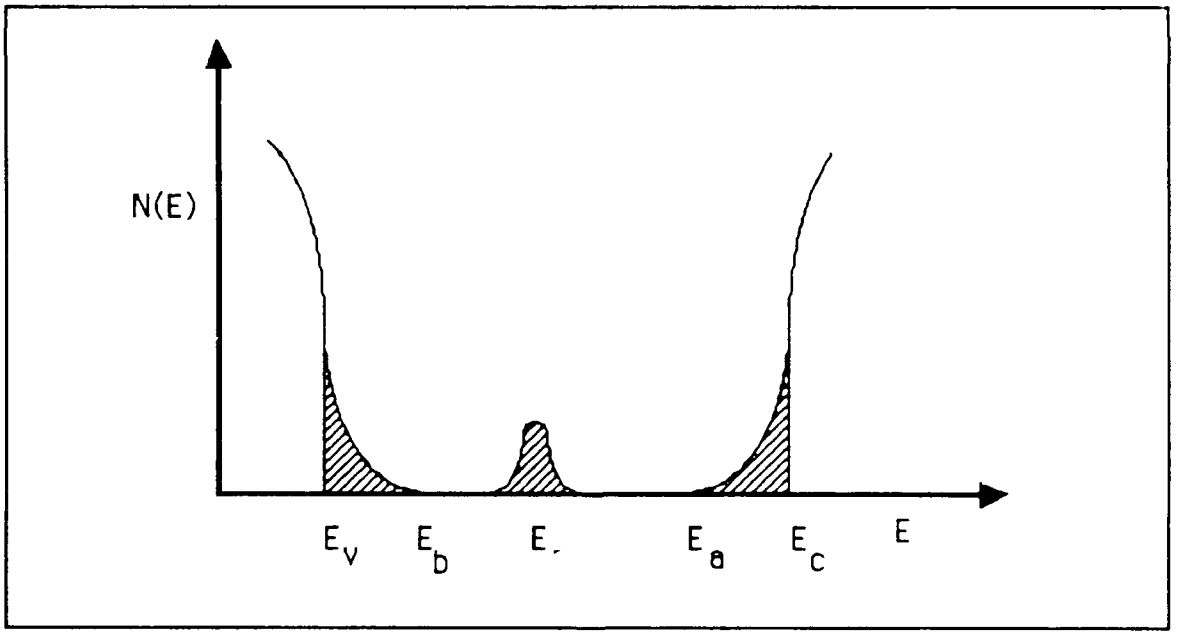

Figure III-6. Davis-Mott Energy Band Model (43:117).

Davis and Mott proposed that an additional energy band would exist near the Fermi energy level (43:118). This additional energy band would exist as a result of the defects in the disordered material, such as dangling bonds. This energy band is depicted in Figure III-6 centered about the Fermi energy level. The interval between E_c and E_v is called a pseudogap, since energy states exist within this region. The pseudogap is defined to be the mobility gap, since the carrier's mobility drops by several orders of magnitude within the localized energy states compared to their mobility within the conventional extended states (43:118).

The Davis-Mott energy band model has been modified to include additional localized states (43:118-119). These additional states account for traps or defect centers that have been found in real materials. For example, impurities in the material may form localized states. In addition, the activation sites in phthalocyanine compounds, upon exposure to specific reactive gases, might be modelled as affecting additional localized states in the pseudogap. This situation is depicted in Figure III-7.

Within the Davis-Mott model, there are three channels of carrier transport (43:120). Carrier transport can occur in the extended states (above E_c or below E_v). Also, carrier transport can occur within the localized energy states by carriers transitioning from one localized state to another by exchanging energy with a phonon (43:124). This process would likely be a thermally-activated process. A third channel exists if the Fermi energy level lies within a band of localized states. If this is the case, carriers may tunnel

between localized states (43:125). The illustration in Figure III-7 depicts the tunneling transport process.

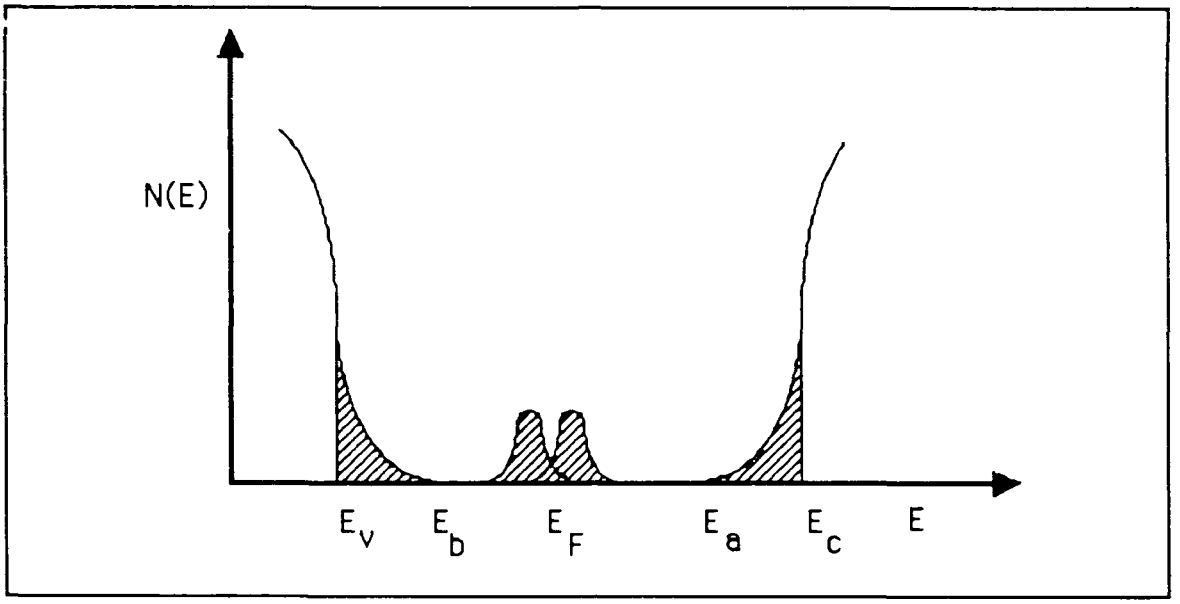

Figure III-7. Davis-Mott Energy Band Model With Defect States (43:117).

Assuming a thermally-activated hopping process, the mobility should have a thermally-activated nature as well (43:124):

$$\mu_{hop} = \mu_0 \exp[\, -W(E)/kT \,] \tag{3.2}$$

where μ_{hop} = mobility associated with hopping

$W(E)$ = work function associated with the localized energy states

k = Boltzmann's constant

T = temperature.

The preexponential constant (μ_0) is found from (43:124):

$$\mu_0 = (1/6)\upsilon_{ph} e R^2/(kT) \tag{3.3}$$

where υ_{ph} = phonon frequency

e = fundamental unit of electronic charge

R = hopping distance.

It should be noted that the expression given by Cotts and Reyes in equation (3.1) corresponds to a hopping model based upon a variable-range localized energy state model. The variable-range condition would likely characterize the situation if there were a distribution of localized energy states (33:70). Nagels uses the following argument to describe variable-range hopping. As the temperature decreases, the number and energy of the phonons will decrease. Hence, for more energetic systems the likelihood of phonon-assisted hops will decrease. Therefore, carriers will tend to hop larger distances to find sites that are more similar in energy as compared to those which exist as nearest neighbors (43:126).

According to Nagels, Mott then derived two functions to describe hopping conductivity (43:124,127). When the carrier transport process involves only the band tails (the regions between E_c and E_a or between E_v and E_b) and a fixed hopping distance, the expression found for electron conduction was (43:124-125):

$$\sigma_{hop} = \sigma_0 \left(\frac{kT}{\Delta E}\right)^s C \exp\left[-(E_a - E_F + W)/kT\right] \tag{3.4}$$

where $\sigma_0 = (1/6)\upsilon_{ph} e^2 R^2/(kT)$

W = energy difference between the localized states

$\Delta E = E_c - E_a$

s = some power s of E that describes the density of states function N(E)

and the constant (C) is given by (43:125):

$$C = s! - (\Delta E/kT)^s \exp(-\Delta E/kT)\left[1 + s(kT/\Delta E) + s(s-1)(kT/\Delta E)^2 + \ldots\right] . \tag{3.5}$$

For the case of variable-range hopping when the Fermi energy level is located within a band of localized states, Mott derived the following expression for hopping conductivity (43:127):

$$\sigma = \sigma_o \exp\left[- A/T^{1/4}\right] \tag{3.6}$$

where σ_o is given by (43:127):

$$\sigma_0 = \frac{e^2}{2(8\pi)^{1/2}} \upsilon_{ph} \left(\frac{N(E_F)}{\alpha kT}\right)^{1/2} \tag{3.7}$$

and A is given by (43:127):

$$A = 2.1 \left[\alpha^3 / \{ kN(E_F) \} \right]^{1/4} \quad (3.8)$$

where α is the rate of decay of the wave function at a hop site. Mott assumed that the density of states was energy independent at the Fermi energy level, there was no correlation in the tunneling effects, there were no multiphonon processes, and that the electron-phonon interactions were negligible (43:127).

A frequency-dependent form of conductivity in a hopping model has been derived, as well. It was found that conductivity is expected to increase with increasing frequency when hopping conduction occurs (42:79; 43:133). Nagels reported that the formula derived by Austin and Mott was (43:133):

$$\sigma(\omega) = (\pi/3)\, e^2 kT\, [N(E_F)]^2\, \alpha^{-5} \omega [\ln(\upsilon_{ph}/\omega)]^4 \quad (3.9)$$

in the case of conduction about the Fermi energy level. A similar frequency dependence was also found for the situation of conduction in the energy band tails (43:134).

To summarize this section concerning the conduction mechanisms, several characteristics were noted. While conduction in organic semiconductors and polymers is not fully understood, several models have been postulated that can provide a qualitative analysis. In addition, the fundamental doping processes would appear to differ from those in crystalline, inorganic semiconductors. Provided the carrier transport can be modelled to some extent, the question remains as to how an absorbed vapor may affect the transport

process. The next section specifically addresses how vapors may affect carrier transport in phthalocyanine compounds.

Modulation of Carrier Transport in Phthalocyanine Compounds

The current state of knowledge concerning conduction in phthalocyanine compounds is similar to that of conduction in organic semiconductors and polymers. This knowledge has been summarized by Pizzini, et al., in the following statement:

> The influence of the adsorption of various gases at the surface of phthalocyanine (Pc) single crystals on their electrical properties in the dark or under illumination is well recognized, although the very nature of the different elementary processes involved is still under discussion. (45:481)

This subsection provides a review of the discussion.

According to Nieuwenhuizen, et al., the interaction of vapors at the chemical interface of phthalocyanine compounds may result in changes of mass, electrical conductivity, or the piezoelectric, dielectric, and elastic properties (46:232). In their work, they reported the possible existence of two types of adsorption sites. One type of site forms a charge-transfer complex between nitrogen dioxide and phthalocyanine, and another type of site provides a condensation or physisorption localized region where gas molecules percolate into the phthalocyanine bulk (46:232).

The adsorption process can occur at two distinct sites (46:233). The large "electron cloud" at the periphery of the phthalocyanine molecule could interact with electronegative compounds. A second site within metal doped phthalocyanine compounds is associated with the positive metal ion in the center of the molecule. This ion may interact with electropositive compounds to form additional coordination complexes. For example, water and ammonia may interact with the metal dopant to form coordination compounds; whereas, nitrogen dioxide may interact with the electron cloud to form a charge-transfer complex. In addition, the percolation of vapors into the phthalocyanine bulk is a function of the physical size of the adsorbing molecule, while the affinity of the vapor towards a phthalocyanine compound determines the extent of physisorption.

Van Ewyk, et al., also studied the interaction of vapors with phthalocyanine compounds (47). They found that mixtures of nitrogen dioxide and dinitrogen tetraoxide was weakly chemisorbed (47:2197). They postulated that strong charge-transfer interactions would result in chemisorption. This situation, in-turn, would yield ionized states and charge carriers. They also postulated that the conduction process involves the migration of positive holes in the phthalocyanine compounds rather than the diffusion of nitrogen dioxide ions (47:2199). In addition, they reported that the effect was confined to a surface conductivity process (47:2196).

Van Ewyk, et al., also found that boron trifluoride produced a smaller enhancement of the electrical conductivity when compared with mixtures of nitrogen dioxide and dinitrogen tetraoxide

(47:2200-2201). Their explanation invokes the localization of charge argument which occurs at a specific site along the alternating bonds of the porphyrin ring structure (previously depicted in Figure II-9). While the nitrogen dioxide and dinitrogen tetraoxide act as π-electron acceptors, boron trifluoride forms a σ-bond with one of the nitrogen atoms in the porphyrin ring. The interaction between a delocalized hole over the porphyrin ring and a π-electron over the nitrogen compounds would be weak (47:2201). With the charge localized within a σ-bond, holes would be strongly held by a localized coulombic field. Therefore, it is less readily available for conduction (47:2201). Hence, the effect of delocalized charge in the porphyrin ring was found to be important in promoting conduction within phthalocyanine compounds.

The studies of Fan and Faulkner have provided information concerning metal/phthalocyanine junctions and bulk conduction in phthalocyanine compounds (48). Their work involved devices fabricated by placing a phthalocyanine compound between two metallic contacts of different metals. They sublimed (under vacuum) a 1000-4000 Å thick layer of undoped and zinc doped phthalocyanine onto a gold layer. The gold electrode provided an ohmic contact. The upper electrode consisted of either aluminum or indium (48:3335). In all the combinations that were studied, a Schottky effect was found (48:3337-3339). With an aluminum contact, they found an open-circuit dark voltage varying from 0.25 volts to 0.45 volts with undoped phthalocyanine (48:3334). With zinc doped phthalocyanine, they found an open-circuit dark voltage

spanning from 0.2 to 0.45 volts (48:3335). In both cases, the negative voltage was measured with respect to the aluminum contact. In their work, a thin aluminum oxide layer was hypothesized. They assumed holes carried most of the current within the phthalocyanine compounds, and electrons carried the current across the aluminum oxide layer (48:3338). In their work, they also mentioned that cells of aluminum/copper-doped-phthalocyanine/gold also showed Schottky emission conduction (48:3334).

The problem of realizing ohmic contacts between a metal and a phthalocyanine compound was also investigated by Gopel, et al.(49:379). They found that catalytic metals such as platinum and gold, might promote the decomposition of lead phthalocyanine (49:379). They characterized the material using X-ray photoemission, high-resolution electron energy loss spectroscopy, Fourier transform infrared spectroscopy, and fast atom bombardment secondary ion mass spectroscopy (49:379). They concluded that platinum and gold should be avoided for making electrical contacts to lead phthalocyanine. The decomposition process may also produce significant carrier depletion in the region of the contacts (49:379).

The work of Archer, et al., addressed the mechanics of the adsorption of nitrogen dioxide into phthalocyanine compounds (50). They postulated that the process of adsorbing nitrogen dioxide involves the displacement of oxygen (50:389). In their adsorption model, phthalocyanine compounds rapidly uptake oxygen from air

after deposition (50:388). However, the adsorption of nitrogen dioxide is a much slower process, and it is confined to the surface (50:388).

According to Archer, et al., nitrogen dioxide must displace oxygen from the surface of the material. Initially, the oxygen displacement occurs most easily at the weakest adsorption sites. However, these sites also have the smallest sticking coefficients. Therefore, the initial rate of adsorption of nitrogen dioxide is slow. As the nitrogen dioxide is adsorbed, a lateral repulsion effect occurs. This effect has two results. One result is that the adsorbed nitrogen dioxide is widely distributed at isolated sites (50:387). The other result is to enhance the displacement of the more strongly bound oxygen. The sites where this additional oxygen is displaced from also has a larger sticking coefficient for nitrogen dioxide. Hence, the rate of adsorption increases as the initial process of adsorption continues (50:388). The adsorption of nitrogen dioxide is accompanied by an increase in electrical conductivity.

When the process is reversed, the more weakly-bound nitrogen dioxide is initially substituted with oxygen (50:388). The conductivity also decreases. Any remaining nitrogen dioxide is located at the strongest adsorption sites. Therefore, when the phthalocyanine compounds are exposed again to nitrogen dioxide, the adsorption process is rapid (50:388). This result is known as the residual nitrogen dioxide enhancement process.

Adsorption Kinetics

Since the cause of the modulation of conductivity in phthalocyanine compounds is presumed to be due to the sorption of the detectant gas, the number of detectant molecules available for sorption is significant. Therefore, this section describes a method found in the literature to estimate this quantity.

If the sorption process is assumed to be confined to the surface of the detectant material (phthalocyanine), the number of detectant molecules can be estimated from the kinetic theory of gas adsorption onto hard surfaces. The kinetic theory concerning gas adsorption was described by Langmuir and deBoer (14:69) The concentration of the detectant molecules was found from (14:69):

$$\sigma = n\tau \tag{3.10}$$

where σ = number of molecules per surface unit area

n = number of molecules striking the surface unit area per unit time

τ = average time a molecule remains stuck to the surface.

Using the kinetic theory of gases, the value of n was found from the following relationship (14:69):

$$n = 3.52 \times 10^{22} \frac{p}{\sqrt{MT}} \tag{3.11}$$

where p = pressure of the detectant vapor in torr

M = molecular weight of the detectant

T = absolute temperature.

The value of τ was estimated using (14:69)

$$\tau = \tau_o \exp(Q/RT) \tag{3.12}$$

where Q = heat of adsorption

R = the ideal gas constant

τ_o = oscillation time of the molecules in the adsorbed state.

As Wohltjen and Snow point out, many of these parameters are not readily available. For example, the value of τ_o was not readily found; therefore, an order of magnitude estimate of 10^{-13} seconds was used in their work (14:69). However, from adsorption kinetics, the material and geometry of a detector and of a vapor can be qualitatively related to the sensor's performance.

Impedance of an Interdigitated Electrode

To effectively fabricate a microsensor, an engineering model (that employs the physical principles discussed in the previous section) must be considered. The impedance of an interdigitated electrode that has been coated with phthalocyanine compounds could be modelled with an electrical network. In Lee's study of a

CHEMFET, a linear equivalent electrical network was developed (10). The exposed interdigitated electrode gap was completely filled with epoxy that underwent a bulk change in permittivity in his study. The fundamental assumptions in Lee's work were that the material in the gap was basically isotropic and homogeneous.

Lee's assumptions are not applicable for phthalocyanine compounds. In this thesis research, the interdigitated electrode gap was incompletely filled with the phthalocyanine compounds. Therefore, the gap medium is inhomogeneous. In addition, as discussed in the previous section, the modulation of the electrical conductivity of the phthalocyanine compounds appears to be a surface effect rather than a bulk effect [for example, (47)]. Hence, the electrical conductivity mechanism of the phthalocyanine material is also inhomogeneous.

While the surface effect and the incompletely filled gap provide a "macroscopic" argument supporting inhomogeneity, a "microscopic" argument can be made as well. The polycrystalline form of phthalocyanine can exist in at least two phases. The phases are denoted as α and β (51:42). In addition, Fielding, found that repeated sublimation does not improve the homogeneity (52:91). Fielding also found a non-uniform density from crystal to crystal for the phthalocyanine compounds (52:91). Also, as found in the previous section, contact between aluminum and phthalocyanine may be nonohmic [for example, (48)] Therefore, Lee's electrical network model will have to be modified to account for these properties of the phthalocyanine films.

Proposed Electrical Model of the Impedance of an Interdigitated Electrode.

It may be possible to approximately model the impedance of a phthalocyanine thin film with the electrical model depicted in Figure III-8 provided that the applied signals levels are small. The proposed model is an extension of the model of an interdigitated capacitor used as a lumped-element (53:1029).

The model's elements correspond to the physical aspects of the coated interdigitated electrode. The C_{ox} parameter is based upon the fringing or parasitic capacitance between the interdigitated electrodes and the diffusion-well in the substrate. The diffusion-well is fabricated during the MOSFET integrated circuit process to provide electrical isolation and to provide a signal ground. This structure creates a voltage-dependent metal-oxide-semiconductor (MOS) capacitor. Also, the interelectrode fields in the gap will fringe through the field oxide.

In addition, since the fingers behave as coupled transmission lines, additional dispersive electrical fields will be established between the metal of the interdigitated electrode and the material below the field oxide as a signal propogates through the interdigitated electrode. The lossy nature of the interdigitated capacitor is expected to contribute towards its natural resonant frequency (53:1029).

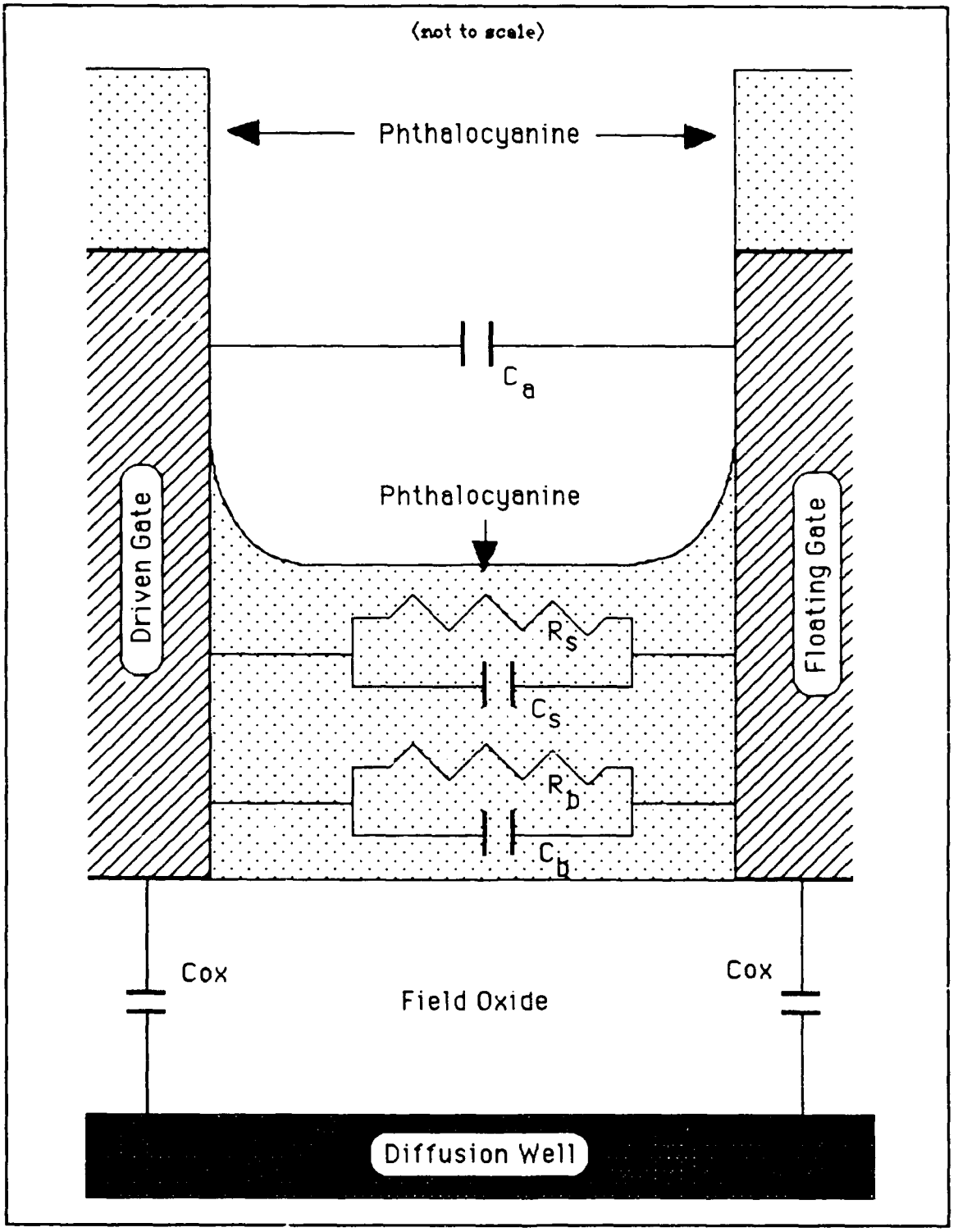

Figure III-8. Proposed Electrical Model of a Phthalocyanine Coated Interdigitated Electrode Structure.

A material parameter for this capacitance, C_{ov}, is the permittivity of the glass used in MOSFET field oxides and of the diffusion layer beneath the field oxide. Another material parameter is the doping density in the diffusion-well since a MOS capacitor exists. The significant geometries affecting this capacitance is the field oxide thickness and the electrode dimensions.

The balance of the gap capacitance is represented by the elements C_a, C_s, and C_b. The capacitance, C_a, represents that portion of gap capacitance for which the significant medium is air. Since the phthalocyanine compounds only partially fill the gap, an electric field will be established in an air dielectric that contains the vapor to be detected. C_a is inversely proportional to the film thickness, and its value diminishes towards zero when the gap is completely filled with the phthalocyanine compound. Hence, the material parameter is the permittivity of air. The geometric parameters are the electrode dimensions, and the difference of the film thickness in the gap relative to the electrode's thickness. If the film thickness in the gap exceeds the electrode's thickness, then C_a is assumed to be negligible. It was assumed that when the gap is completely filled with phthalocyanine, the film thickness on top of the metal is at least as thick as the electrode's thickness. Therefore, any field fringing and coupling between the top surface of the metal electrodes are assumed to be within the phthalocyanine rather than air.

The remaining portion of the electric field within the gap is within the phthalocyanine compound. This medium is further divided to account for the surface effect of vapor detection. This

model assumes that the surface activation sites actually extend some physically finite, but small distance into the bulk of the phthalocyanine film.

The physical basis of C_b is the capacitance associated with the bulk of the phthalocyanine film which fills the gap. The C_s parameter is associated with a surface layer of some finite thickness (δ) that is affected by the mechanism which modulates the electrical conductivity of the phthalocyanine film in the gap. Of the three gap capacitances, C_s is expected to vary; C_b and C_a are expected to remain essentially static. The material parameter associated witn C_s is the permittivity of the exposed phthalocyanine material. Since permittivity is related to conductivity and the conduction carrier current density, and it is also related to conductivity by its dielectric relaxation time (54:639), C_s is expected to be affected by the absorption of a chemically-active gaseous species. The material parameter associated with C_b is the permittivity of the bulk of the phthalocyanine film within the interdigitated electrode gap.

The geometric parameters of C_s consist of the depth (δ) and the electrode spacing. Correspondingly, the geometric parameters of C_b consist of the electrode spacing and the difference between the thickness of the phthalocyanine compound and the depth (δ).

The resistance of the coated interdigitated electrode is approximated by two resistances, R_s and R_b. The assumption is that the shunt path through the field oxide has a much larger resistance value compared to the resistance value of the phthalocyanine compound within the gap. Also, it is assumed that the resistance of

the phthalocyanine compound within the gap is much larger than the series resistance of the metal used for the interdigitated electrode structure.

The physical basis for R_s and R_b is the same argument used to establish C_s and C_b. In essence, the phthalocyanine compound is treated as a lossy capacitor; therefore, the resistive element is considered a shunt path for the respective capacitive element. The material parameter associated with the resistors consists of the conductivity. The geometric parameters of path length and cross-sectional area are the same as those attributed to C_s and C_b. Hence, R_s is expected to vary with absorption of the chemically-active vapor while R_b will likely remain essentially constant.

The nonohmic aspect of the contact between the aluminum and phthalocyanine is not explicitly shown in Figure III-8. However, if a Schottky effect were to be present, it could be included in the model. Any capacitance associated with a Schottky contact between the phthalocyanine compounds and the aluminum metal used in MOSFET fabrication would be in series with the shunt phthalocyanine capacitances. In addition, the resistance of the Schottky contact would be in series with the shunt phthalocyanine resistances. The parameter values of the Schottky capacitance and resistance are material and geometry dependent since they would be functions of the applied DC bias, the appropriate diode equation, the phthalocyanine thickness, and the electrode dimensions.

This model of the complex impedance of the interdigitated electrode structure coated with a phthalocyanine compound is

fundamentally a qualitative model. It is not fully quantitative since the parameters affecting conductivity in the phthalocyanine compounds, that is, percolation, hopping, localization of states, traps, adsorption coefficients, etc., are not readily calculated, nor fully understood [for example, (45)]. However, the electrical model may provide a tool that relates fundamental material and geometrical considerations in the development of a chemically-sensitive microsensor based upon the IGEFET.

Also, since the proposed model relates physical parameters to electrical impedance, the model may provide a qualitative tool for optimizing the design of the sensor. As an example, the model promotes a dynamic R_s, but a static R_b. Therefore, the magnitude of the changes in the film's DC resistance caused by gas exposure can be interpreted in terms of the superposition of R_s and R_b. To improve the signal-to-noise ratio (SNR), the model implies that R_b must be maximized relative to the expected changes in R_s, since these two resistances are in parallel. Thus, the smaller of these two shunt resistors will predominate the measured electrode electrical resistance. To increase R_b, the model would imply that the phthalocyanine film thickness should be made as small as possible (that is, on the order of δ). However, when the film thickness within the gap is decreased, the value of the C_a element will increase. The function used to compute the element value for C_s should remain stable as long as the film thickness in the gap is at least as thick as δ. Thus, the SNR of the dynamic C_s and C_a elements would be expected to decrease since these two capacitances are in parallel. Therefore, in

this simplified example, the process of simultaneously maximizing the SNR of the sensor with respect to both the capacitive elements and the resistive elements might be used to optimize the film thickness and electrode dimensions.

Summary

This chapter discussed the concepts which have been postulated to explain conduction in organic semiconductors and polymers. As demonstrated in this Chapter and Chapter II, these materials have been intensely studied in the past for applications involving the sensing of chemical compounds. The fundamental mechanisms of electrical conduction were found to be not well understood.

Two general models of electrical (transport) were discussed. The first being percolation, and the second being hopping. These two models are significantly different in that hopping conduction assumes homogeneity while percolation conduction may occur in inhomogeneous media.

Percolation was found to be characterized by the sudden on set of conduction, that is, the organic semiconductor "switches" from a low-conductive to a high-conductive state with few intermediate values. The implication for phthalocyanine compounds would be that activation sites with adsorbed nitrogen dioxide would represent a conductive phase, while sites without adsorbed nitrogen dioxide would represent the nonconductive phase. Therefore, when a critical

density of the conductive phase was attained, the phthalocyanine material would suddenly become conductive.

The hopping model of conduction was found to be primarily an "extension" of the energy band theory to disordered systems such as polycrystalline materials. The consequence of the disorder manifested itself as creating localized energy states that could contribute to the electrical conduction process. This additional path is in addition to any conduction that may occur due to extended states (as in conventional energy band theory). The hopping mechanism was characterized as a thermally-activated process. The hopping model of conduction was concluded to be significant because the phthalocyanine material studies in the literature describe the material as being polycrystalline. In addition, the actual carrier transport process in the percolation model may involve a hopping process.

Within the broad framework of electrical conduction in organic semiconductors and polymers, the transport properties of phthalocyanine were presented. The process was found to be intimately related to the concept of activation sites; thus, the activation energy could be used to characterize the process. The process appears to involve a perturbation of the delocalized π-bonds within the phthalocyanine compounds.

A qualitative electrical network model was also presented. This model may provide an qualitative tool for describing the detection mechanism of the IGEFET developed in this thesis effort. This model attempted to relate the material and geometry of the

interdigitated electrode to the modulation of its impedance upon vapor exposure. In doing so, the nonlinear and inhomogeneous nature of the detector was considered in a small signal analysis. An advantage of this model is tnat it has the potential for optimizing the design of the chemically-active film coated interdigitated electrode structure utilized in the CHEMFET microsensor.

IV. Microsensor Design, Experimental Arrangement, and Evaluation Procedures

The design, fabrication, experimental arrangement, and performance evaluation procedures associated with the microsensor are presented in this chapter. The design section describes the rationale, the method, the layout of the integrated circuit, and the preliminary operational characteristics of the microsensor. The fabrication section of this chapter principally describes how the various phthalocyanine compounds were applied to the microsensor and how the gas generation and delivery system in the AFIT Cooperative Electronics and Materials Processing Laboratory was modified. The experimental arrangement and performance evaluation procedures section describes the configuration of the test instrumentation. In addition, the specific electrical parameters and environmental conditions that were monitored, the data collection methods, and the data reduction techniques are described.

Microsensor Design and Characterization

This section begins with a few general comments concerning the microsensor design. These comments are immediately followed with a detailed description of the major subcircuits contained in the microsensor. The section then concludes with a presentation of the preliminary operating characteristics of the microsensor.

General Comments.

The general performance specifications of the microsensor integrated circuit was to have individual sensing elements that had a minimum of 20 dB of voltage gain (20 $\log_{10}$ [V_{out}/V_{in}]) with a 3 dB cut-off frequency of at least 10^6 Hertz. In addition, the anticipated performance of the multiplexer design was to provide at least 20 dB of isolation when a signal line is not selected.

While the design of the microsensor was based upon an earlier configuration of the chemically-sensitive field-effect transistor (CHEMFET) (7), the principal new features of the design for this research effort consisted of:

(1) a two-dimensional array of nine sensing elements utilizing an interdigitated gate electrode field-effect transistor (IGEFET),
(2) MOSFET amplifiers to provide signal gain,
(3) a reference element with a MOSFET amplifier to provide temperature compensation, and
(4) an electronic multiplexing circuit for interrogating specific elements in the array.

In addition, throughout the entire layout of the microsensor, an abundant supply of bond pads and physical links were provided. These features provided ready access to the circuit nodes that linked the major subcircuits in the microsensor. These features permitted

the isolation of defective components since a modular physical layout was used.

The microsensor was designed using the AFIT very large scale integration (VLSI) design tools. The microsensor, *sans* polymer, was fabricated using the Metal-Oxide-Semiconductor Implementation Service (MOSIS) facilities (University of California, Berkeley, CA). The MOSIS scalable 2-micron, double-metal, double-poly silicon, p-well technology was used.

Design of Sensing Elements and Amplifiers.

The individual sensing elements consisted of an IGEFET coupled to a pair of serially connected inverting MOSFET amplifiers. The circuit schematic of a sensing element is depicted in Figure IV-1.

Within the schematic, the IGEFET is denoted by the interdigitated gate electrode and MOSFET M1. The resistor R1 provides the quiescent point for the operation of M1. The serially connected inverting amplifiers consist of MOSFET's M2 and M3, with resistors R2 and R3 providing the respective quiescent points. The source and drain bias nodes are denoted as V_{ss} and V_{dd}, respectively. The electrical stimulus is applied at V_{in}; whereas, the vapor stimulus is applied at the interdigitated gate electrode. The output signal of the sensing element is derived from V_{out}. As is customary, the substrate nodes of the MOSFET's (M1, M2, and M3) are not shown in the schematic. However, the absence of this substrate contact in the schematic does not reflect the contacts' importance. In this research, the substrate connections were used to bias the transistors in their

linear region. This permitted the proper biasing of the transistors without using a gate resistor.

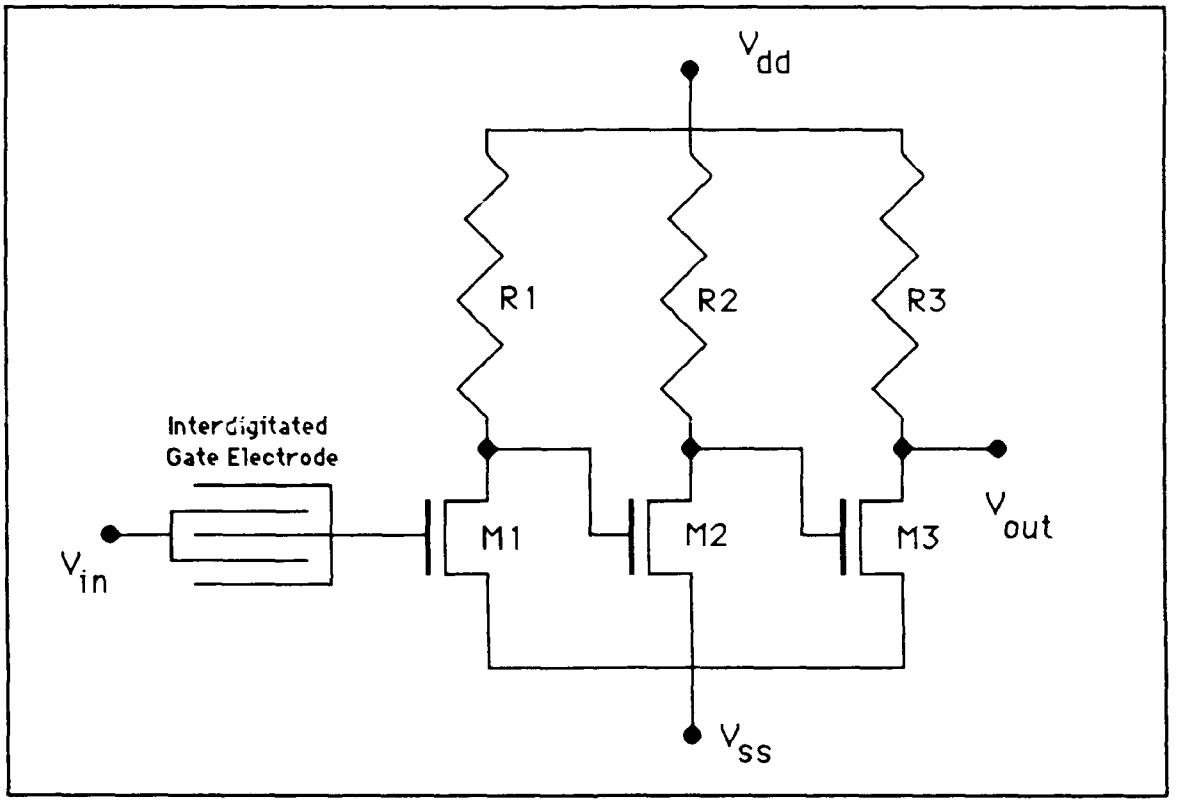

Figure IV-1. Schematic of an Individual Sensing Element and Amplifier.

The design rationale for this biasing scheme and circuit topology involves impedance concepts. In one aspect, the impedance of the interdigitated gate electrode can be approximated as a lossy capacitor with a DC resistance on the order of 10^9 ohms (7). If a gate resistor (nominal values on the order of 10^8 ohms) is used to bias the

IGEFET, the signal may be corrupted (noise) or attenuated (shunt to signal ground). In addition, if the gate bias resistor was fabricated as part of the integrated circuit, a diffusion resistor of sufficient value would consume a large area of silicon.

Another impedance aspect of the design rationale required integrating an amplifier as part of the sensing element. The microsensor elements are switched with on-chip circuitry. Unlike an ideal switch, the fabricated multiplexer was expected to possess some signal loss due to resistance in the on-state (on the order of 10^3 ohms) (20:360-366). Therefore, the electrical signal of the detector was amplified before the switching losses to enhance the signal-to-noise ratio.

Another aspect of the design rationale is one of impedance matching. The impedance of the phthalocyanine coated interdigitated electrode structure is matched to the high impedance of a MOSFET gate, rather than the shunt combination of a gate bias resistor and a MOSFET gate. Another subtle impedance match involves the circuit parasitics.

This aspect also involves the multiplexer, but this case concerns the off-state. When the switch connected to the sensing element is off, there is still a small leakage current (on the order of 10^{-12} amps) in an actual transmission gate (20:513-523). This leakage current can be approximated by the resistance of a reversed biased diode. When compared to the equivalent resistance of the "switched circuits," a larger off-resistance for the switch provides better isolation of the multiplexed elements. From a related perspective,

the time constant of the switch in the off-state should be several orders of magnitude larger than the time constant of the switched circuit. This situation represents the desirable case in this research effort.

Using the designed circuit topology for the sensing elements, the equivalent resistance of the switched circuit, that is, the sensing elements, is the shunt combination of the channel resistance of the linearly biased MOSFET M3 and the resistor R3. Without the circuit topology of the MOSFETs (M1, M2, and M3), the "switched circuit" equivalent resistance would be that of the phthalocyanine coated interdigitated electrode structure (which is several orders of magnitude larger). Hence, the circuit topology enhances the system characteristics by providing a level of input and output impedance matching for the individual sensing elements.

The layout of the circuit is depicted in Figure IV-2, and the electrode pattern is depicted in Figure IV-3. The required element values were derived from circuit simulations using SPICE3 (U.C. Berkeley); whereas, the characteristics of the interdigitated electrode structure were derived from the prior research of Wiseman (7).

The simulation used to design the microsensor is listed in Appendix A. The anticipated model parameters, such as sheet resistance, were derived from prior fabrication runs of a similar MOSIS technology process. The resistors were fabricated with n-type diffusions within a p-well, and the interdigitated gate electrode structure was fabricated with aluminum (second-level metal). A p-well was placed below the interdigitated gate electrode to provide

electrical isolation and voltage bias control of the parasitic MOS capacitance of the structure. MOSFETs M1, M2, and M3 were fabricated as NMOS enhancement-mode devices. The p-well surrounding MOSFETs M1, M2, and M3 was separate from the p-well of the interdigitated gate electrode structure. The designed values of the sensing element components are listed in Table IV-1, and the critical dimensions of the interdigitated gate electrode structure are listed in Table IV-2.

Design of the Reference Element.

A reference element was included in the design of the microsensor. The reference element was designed to mimic the performance of the amplifier characteristics of the individual sensing elements, with one exception. Unlike the sensing elements, the reference element did not have an interdigitated gate electrode. Instead, the input electrode of the reference element was designed as a large metal pad. The layout of the reference element is shown in Figure IV-4.

The critical parameters associated with the reference element's components (with the exception of the "metal pad" of the gate electrode) are the same as those for the individual sensing elements. The solid metal gate electrode was also fabricated using second-level metal over a p-well. The reference element's input electrode measured 2000 microns long and 895 microns wide.

The design rationale for the reference element was twofold. Since the characteristics of the phthalocyanine compounds were to be evaluated with respect to temperature, a method to separate the

effects of temperature relative to the amplifier's electrical performance was desirable. With a reference element using the same configuration of the amplifier as the sensing elements, the temperature effects on the amplifiers could be readily compensated.

Table IV-1. Sensing Element Component Design Values.

Structure	Critical Dimensions		Value
		Number of	
Resistors	Width (μm)	Squares	
R1	3	326	6700 Ω
R2	3	486	10000 Ω
R3	3	364	7500 Ω
MOSFET		Gate Features	
Transistors	Width (μm)	Length (μm)	
M1	9	3	
M2	11	3	
M3	12	3	

Table IV-2. Critical Dimensions of the Interdigitated Gate Electrode.

Parameter	Value
Number of fingers in the floating gate	29
Number of fingers in the driven gate	30
Fingers width (μm)	8
Fingers length (μm)	3758
Finger spacing (μm)	9
Overall array width (μm)	994
Overall array length (μm)	3783

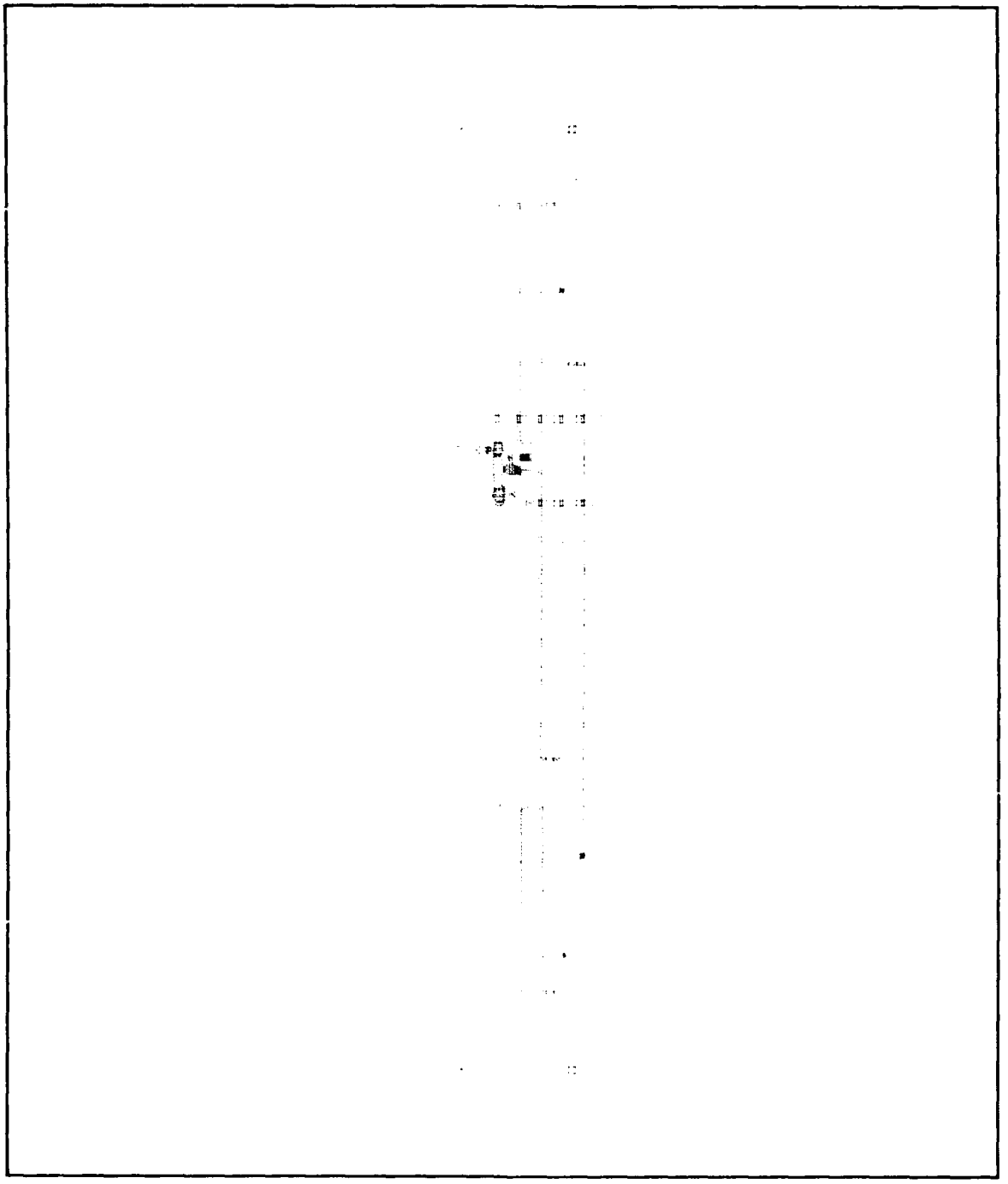

Figure IV-2. Sensing Element (Excluding the Interdigitated Gate Electrode).

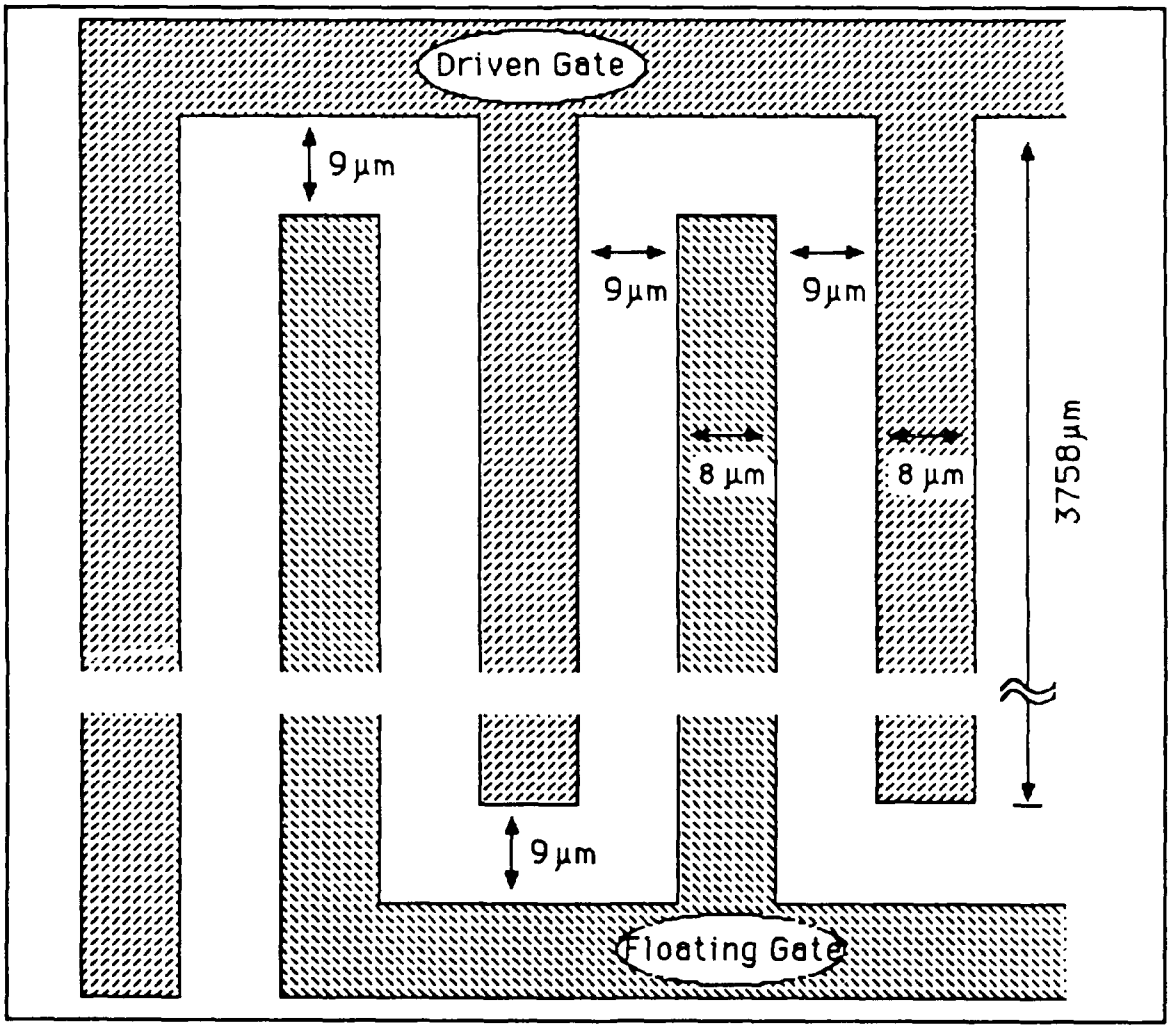

Figure IV-3. Schematic of the Interdigitated Gate Electrode Structure.

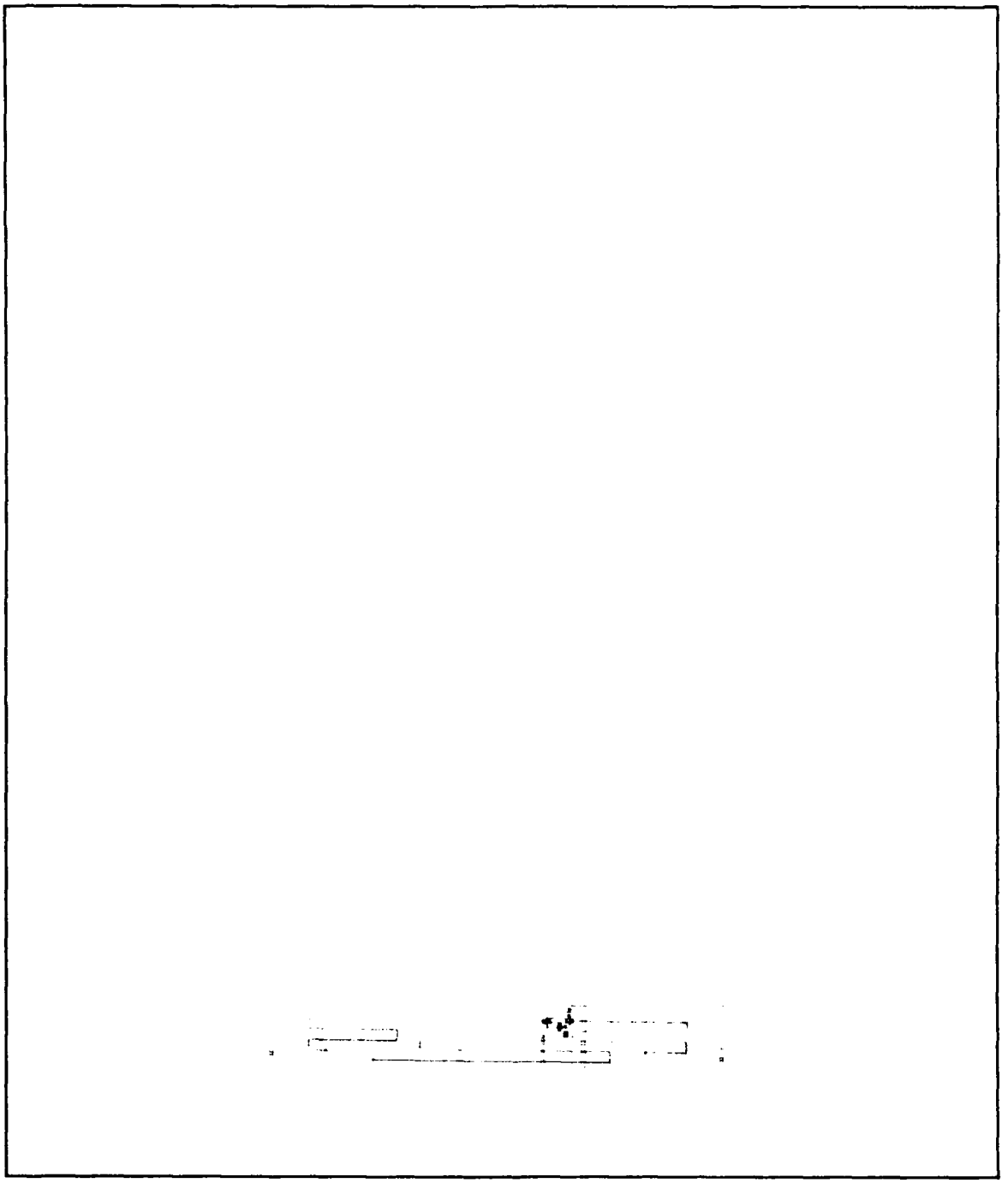

Figure IV-4. Layout of the Microsensor's Reference Element.

In addition, the gate electrode was sized to yield an area equivalent to the total area of the metal used to fabricate the interdigitated gate electrode structures in the sensing elements. The design rationale was to match the parasitic MOS capacitance of the reference electrode to the equivalent parasitic MOS capacitance of the interdigitated gate electrode structures in the sensing elements.

Design of the Multiplexer Circuit.

The multiplexer was designed in a modular manner. The major modules were the digital logic, the switches, and a final output amplifier to drive the microsensor's signal to off-chip circuits. This subsection describes each of these modules.

Digital logic circuitry was used to decode the address of the selected microsensor element to be sensed. Hence, the multiplexer had to address ten lines (nine chemically-sensitive elements and one reference element). The input of the digital logic circuitry consisted of four address lines (designated as A, B, C, and D). The output of the digital logic circuitry (designated as Chem1 through Chem10) was connected to an inverting buffer. This buffer coupled the digital logic to the analog switches that connected the desired microsensor element to the output amplifier.

The digital logic decoder was designed by modifying an existing decoder that was developed by previous AFIT VLSI classes. Hence, the design process for the digital logic was treated as the implementation of a standard cell with modifications. The circuit schematic of the standard cell for one-bit is depicted in Figure IV-5.

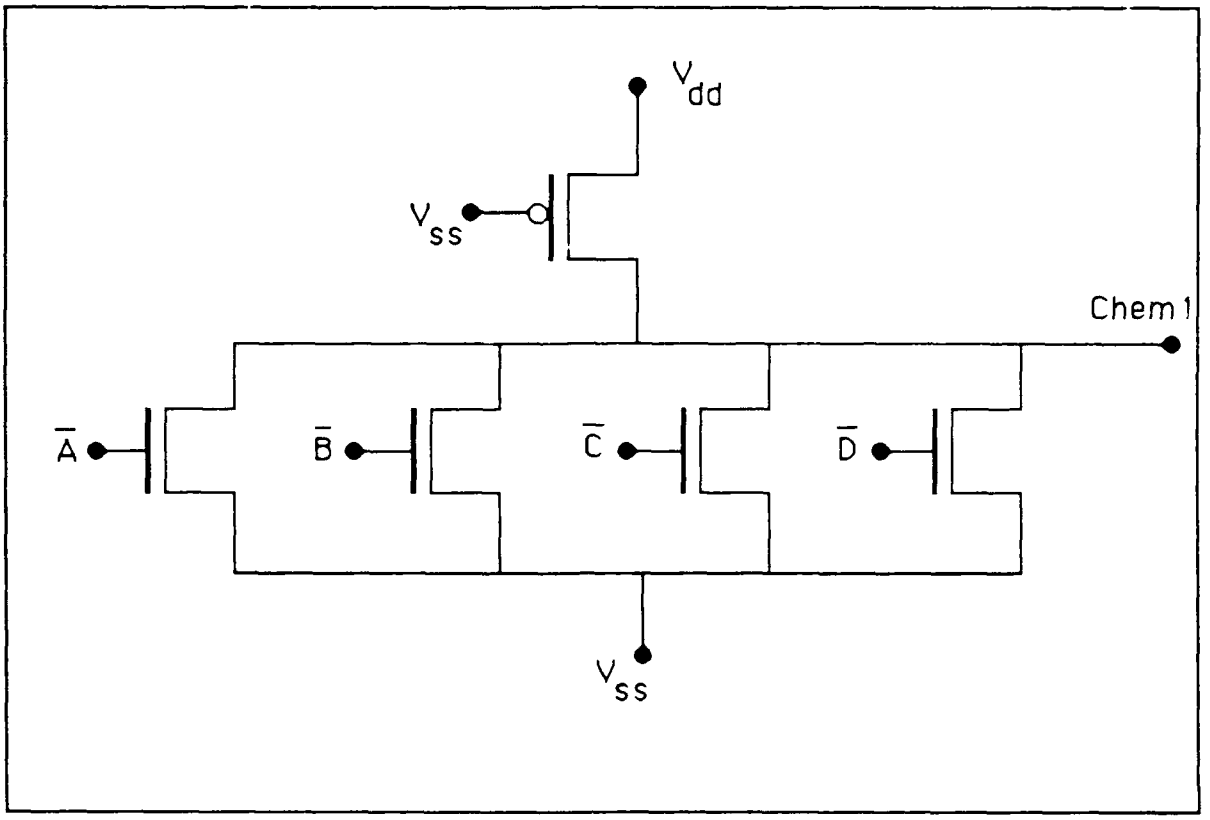

Figure IV-5. Schematic for a One-Bit Slice of the Decoder Logic.

Figure IV-5 provides an example of decoding the address that corresponds to the Chem1 digital logic output. In this example, the overbar on the address lines denotes that the address input word is 0000. With the pull-up transistor always biased "on," and the address lines biased at V_{ss} (corresponding to the logic value 0000), the node designated as Chem1 is driven to nearly V_{dd} (corresponding to the logic value 1). If an address other than 0000 had been provided as the input, at least one of the four NMOS transistors would have been saturated. Therefore, this input would effectively short the Chem1 node to V_{ss} (corresponding to the logic value 0).

The digital logic was simulated to verify that the one-bit standard cells were properly connected in the design for this research effort. Consequently, the performance verification of the decoder design consisted of a logic level simulation. The details of the simulation are provided in Appendix A.

The digital logic output was connected to an inverting buffer. This buffer coupled the digital logic output to the respective analog switch. A schematic of this configuration is depicted for one of the selected lines in Figure IV-6.

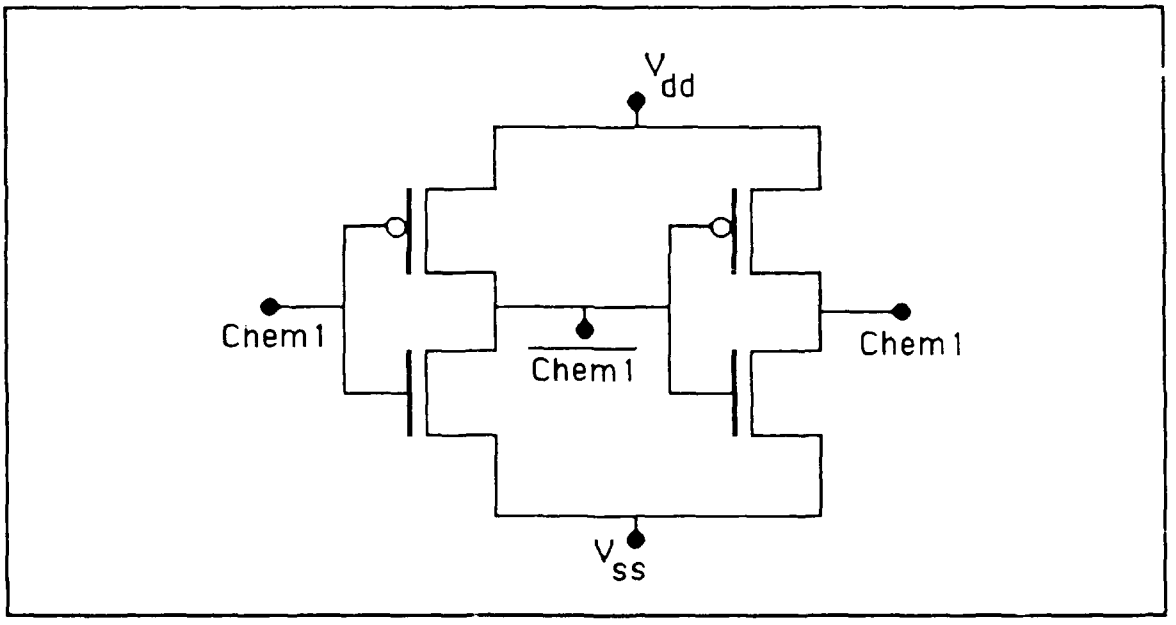

Figure IV-6. Schematic of the Inverting Buffer.

In the example depicted in Figure IV-6, the digital logic output that corresponds to Chem1 is connected to its inverting buffer. The output of the inverting buffer consists of the complemented input and the restored value of the input. The design rationale for this

configuration is to provide for the proper operation of the analog switch that is connected to the outputs of this buffer circuit.

The buffer ensures that the logic levels are fully restored. The restored logic level ensures that the analog switches are driven fully-off or fully-on. Therefore, the inverting buffers couple the nominal transistor sizes in the logic standard cells to the required transistor size of the analog switch.

The design of the analog switch is based upon a transmission gate. The circuit schematic for the switch is depicted in Figure IV-7. As an example, the selection of the microsensor element corresponding to Chem1 is depicted in Figure IV-7. The controlling inputs of this switch consist of Chem1 and its complemented value.

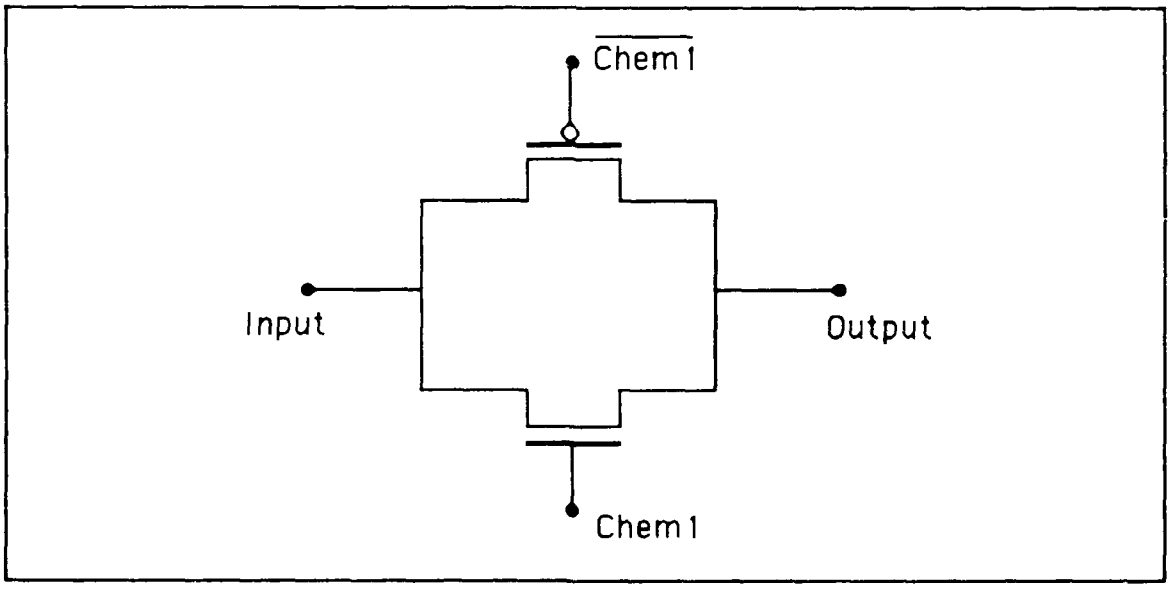

Figure IV-7. Schematic of the Analog Switch Portion of the Multiplexer.

The layout of the digital logic, inverting buffer, and analog switch portion of the multiplexer circuit is shown in Figure IV-8. Due to the design rationale, the critical dimensions associated with these modules in the multiplexer are the transistors' gate lengths and widths in the analog switch. The digital logic is not in the signal path of the microsensor's elements, and the inverting buffers ensure that the logic levels are restored from the quasi-standard cell logic. From the circuit design simulation that is detailed in Appendix A, a suitable PMOS and NMOS transistor size was found to be 3 microns long by 15 microns wide.

The output amplifier module in the multiplexer circuit provides the last stage of amplification before the selected microsensor element's signal is transmitted off-chip. The design rationale was that an output amplifier after the multiplexer would electrically isolate the off-chip electrical environment from the microsensor integrated circuit. The circuit schematic for the output amplifier stage is given in Figure IV-9.

The configuration used for this amplifier is that of an analog voltage follower where the output signal is also routed through a feedback path into the gate of the NMOS transistor designated as M4 in Figure IV-9. The NMOS transistor M5 provides a constant current source for the amplifier circuit. The PMOS transistors M1 and M2 provide the active loads for the current mirrors in the amplifier. The transistor sizing was determined by simulating the circuit, and the details of the simulation input are provided in Appendix A. Additionally, it was determined that the current source could be

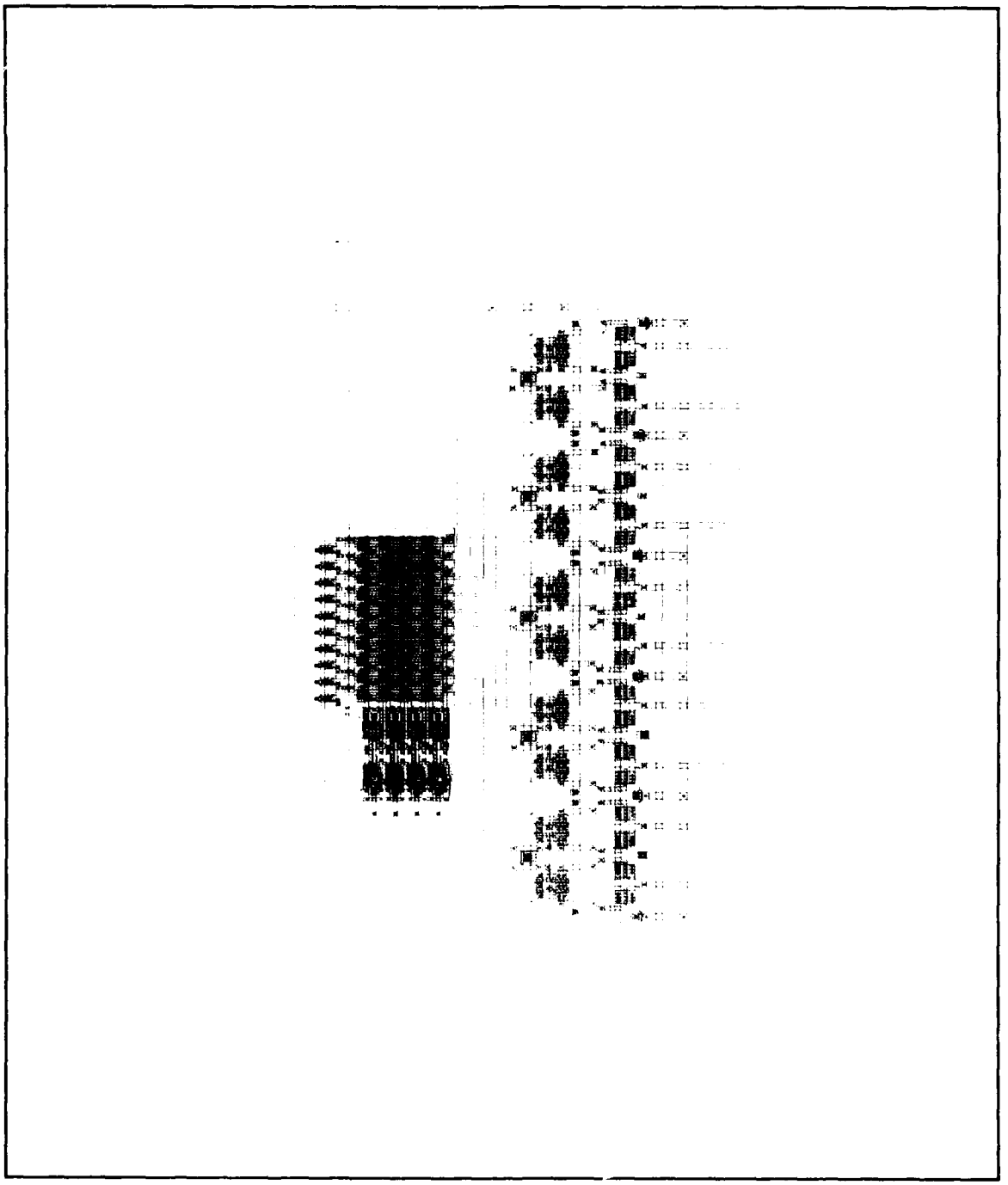

Figure IV-8. Illustration of the Digital Logic, Inverting Buffer, and Analog Switch Portion of the Multiplexer.

sufficiently biased by applying the drain bias voltage to transistor M5.

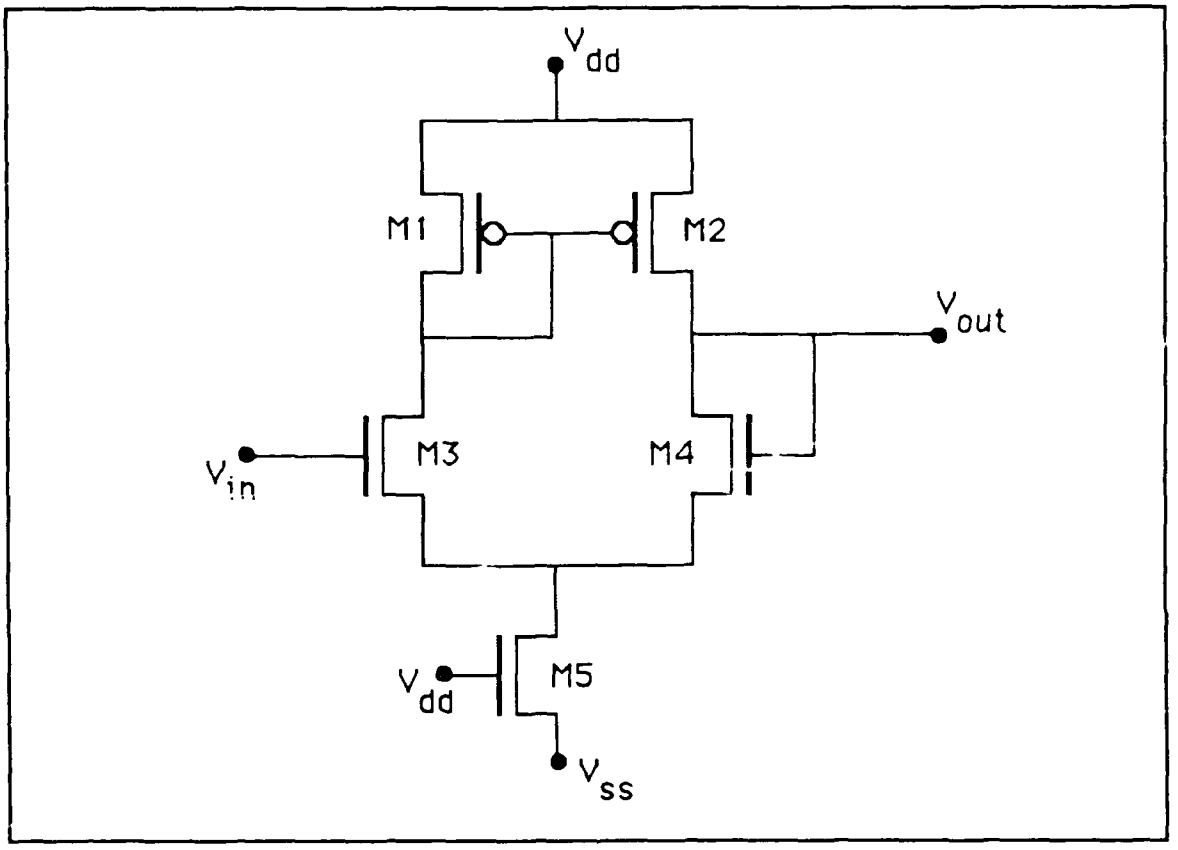

Figure IV-9. Output Amplifier Portion of the Multiplexer Circuit.

The layout of the output amplifier is depicted in Figure IV-10. The critical parameters of the output amplifier configured as a voltage follower are given in Table IV-3.

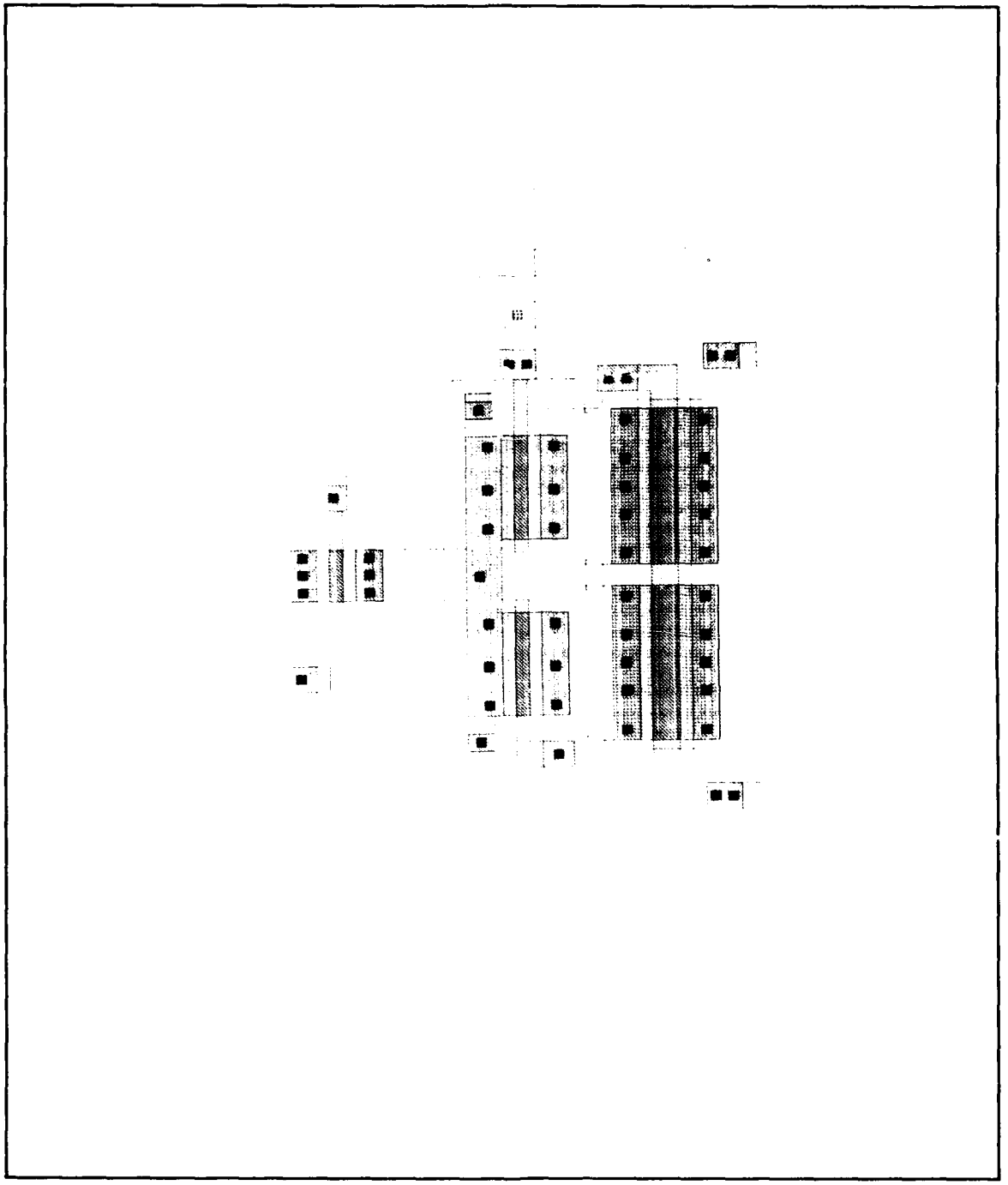

Figure IV-10. Layout of the Output Amplifier Portion of the Multiplexer.

Table IV-3. Critical Parameters of the Output Amplifier.

Parameter	Type	Gate Dimensions	
		Width (μm)	Length (μm)
M1	PMOS	36	6
M2	PMOS	36	6
M3	NMOS	24	3
M4	NMOS	24	3
M5	NMOS	12	3

Operating Characteristics of the Microsensor.

A photomicrograph of the microsensor that was fabricated by MOSIS for this thesis research is presented in Figure IV-11. A diagram of the subcircuits in the photomicrograph is presented in Figure IV-12. The functions associated with the bond pads for the circuit are given in Table IV-4. As previously noted, the MOSIS scalable 2-micron, double-metal, double-poly silicon, p-well technology was used. The specific characteristics of this processing technology are given in Appendix A, and the bond pad diagram is given in Appendix B. Of the 24 circuits delivered by MOSIS, eight of the circuits were packaged and bonded. These circuits were divided into two lots consisting of four packaged and eight unpackaged circuits. One lot was set aside and not used in this research. This lot was treated as an emergency source should the other lot become damaged.

Table IV-4. Bond Pad Identification of the Microsensor Integrated Circuit.

Bond Pad Number	Function
6	Source Voltage Bias (V_{ss})
7	Amplifier Substrate Bias (V_{bias})
8	Drain Voltage Bias (V_{dd})
9	Amplifier Output (Sensing element Chem10)
10	Floating Gate (FG) on Chem10
11	P-Well Bias Under the Interdigitated Gate Electrode (IGE) Structure
12	Amplifier Output of Chem9
13	FG on Chem9
14	P-Well Bias Under the IGE Structure
15	Amplifier Output of Chem8
16	FG on Chem8
17	P-Well Bias Under the IGE Structure
18	Amplifier Output of Chem7
19	FG on Chem7
20	P-Well Bias Under the IGE Structure
21	Amplifier Output of Chem6
22	FG on Chem6
26	V_{dd}
27	V_{bias}
28	V_{ss}
29	V_{ss}
30	V_{dd}
31	Address Bit A
32	Address Bit B
33	Address Bit C
34	Address Bit D
35	Multiplexer Internal Node Between the Chip-Output Amplifier and the Analog Switches
36	V_{ss}
37	Output of the Microsensor Electronics
38	V_{dd}
39	V_{ss}
40	V_{bias}
41	V_{dd}
42	Input Electrode on Chem5 (Reference Element)
43	Amplifier Output of Chem5 (Reference Element)
44	P-Well Bias Under the IGE Structure
45	FG on Chem4
46	Amplifier Output of Chem4
47	P-Well Bias Under the IGE Structure
48	FG on Chem3

49	Amplifier Output of Chem3
50	P-Well Bias Under the IGE Structure
51	FG on Chem2
52	Amplifier Output of Chem2
53	P-Well Bias Under the IGE Structure
54	FG on Chem1
55	Amplifier Output of Chem1
56	V_{dd}
57	V_{bias}
58	V_{ss}
64	Connected to All Driven Gates

When the processing characteristics were received from MOSIS, the level-four SPICE3 models of the MOSFETs were extracted using the program Proc2mod (U. C. Berkeley). Using these models, a simulation of the expected electrical performance of the microsensor was accomplished. The model parameters are listed in Appendix A, as well as the simulation input file used to determine the expected gain and cut-off frequency of the microsensor electronics.

Several modifications, in addition to the changes in the MOSFET models, were made to the simulation network model. Since the sheet resistance of the n-diffusion increased from 20.58 Ω/square to 23.6 Ω/square, the values of the diffusion resistors were proportionally increased. This situation corresponded to a 14.7% increase in the designed resistor values. The gate lengths of the MOSFETs were also changed. The n-channel gate lengths were shortened by 0.5 microns, and the p-channel gate lengths were shortened by 0.17 microns. For a nominal 3 micron long n- or p-channel transistor, this corresponded to a deviation of the gate length of 17% or 6%, respectively.

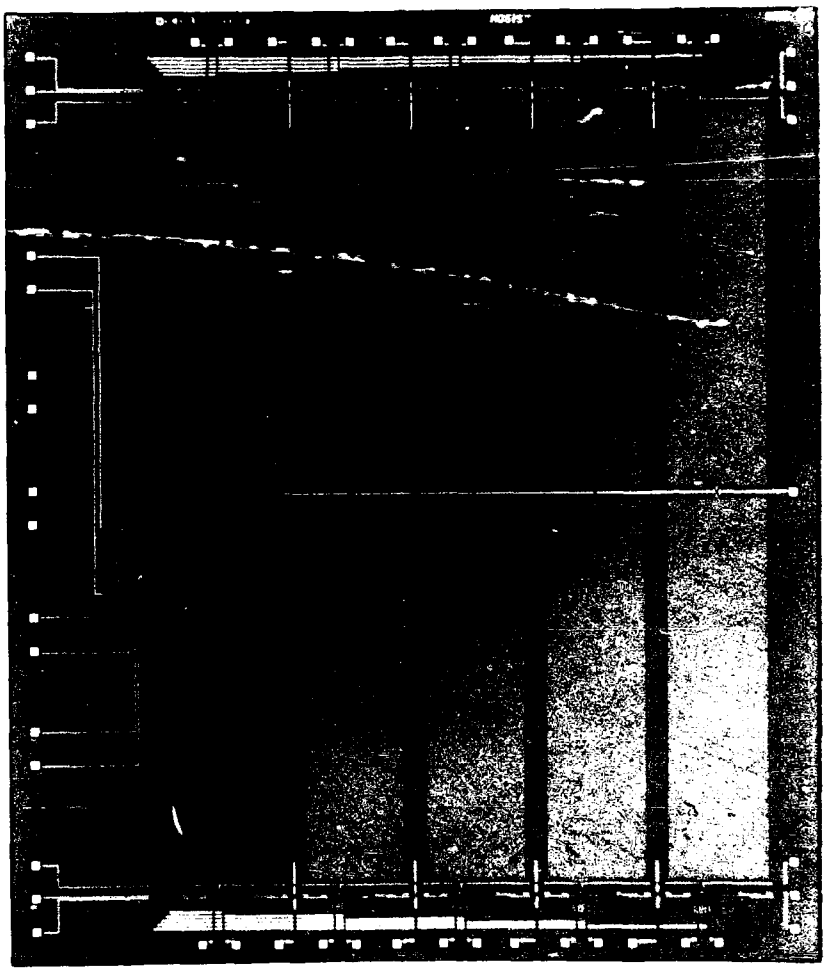

Figure IV-11. Photomicrograph of the Microsensor Integrated Circuit.

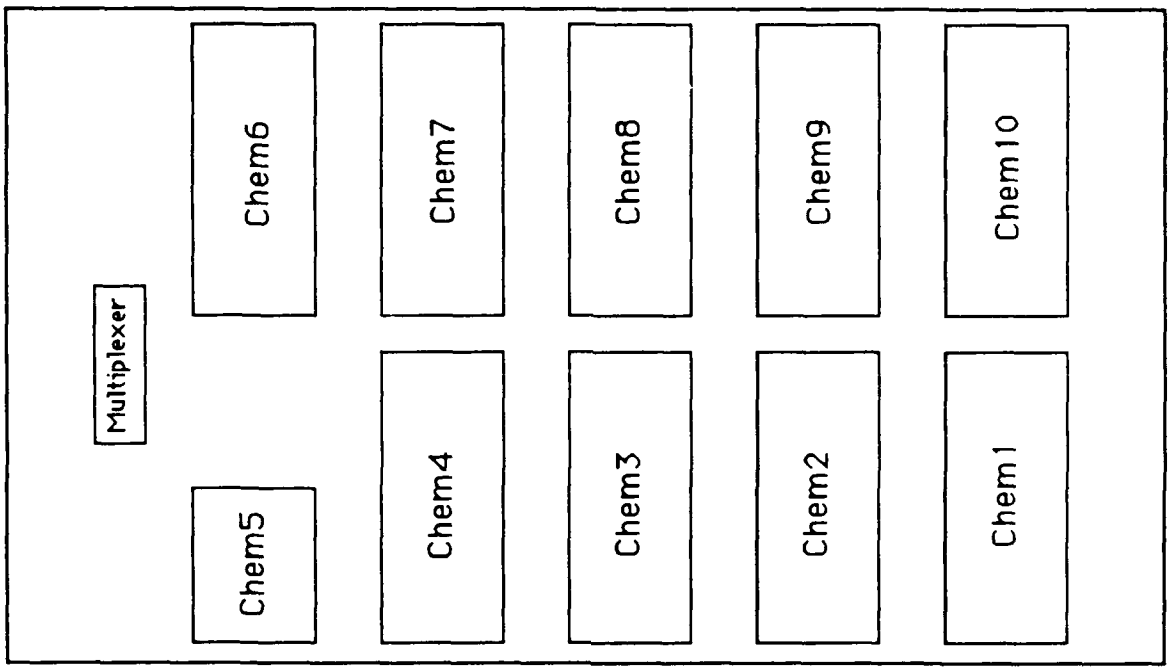

Figure IV-12. Diagram of the Subcircuits in the Microsensor.

The parasitic capacitance of the interdigitated gate electrode was also estimated. From the MOSIS processing data, the second-level metal capacitance was estimated using the metal-2 to substrate area capacitance that was given as 0.024×10^{-15} Farads per μm^2. With a metal area of approximately $1.79 \times 10^6 \mu m^2$, a parasitic capacitance of 43 pF was estimated. The input capacitance is denoted as capara in the network simulation file in Appendix A.

Using this set of simulation values, the expected gain was determined. A plot of the values is given in Figure IV-13. The expected isolation of the switch was also determined; its plot is given in Figure IV-14. From the simulation, the expected signal voltage

gain was 27 dB with a 3 dB cut-off frequency of approximately 3 MHz. The simulated isolation exceeded -340 dB, which is unrealistic. The signal voltage gain was defined as the ratio of the output voltage of the chip (bond pad 37) to the applied signal on the floating gate when that signal line is selected. For example, with a signal applied to bond pad 42, the address 0101 would serve as the input with V_{dd} applied to bond pads 32 and 34, while V_{ss} is applied to bond pads 31 and 33. Hence, the signal voltage gain is the ratio of the voltage at bond pads 37 and 42. The isolation was defined as the same ratio with the signal line not selected.

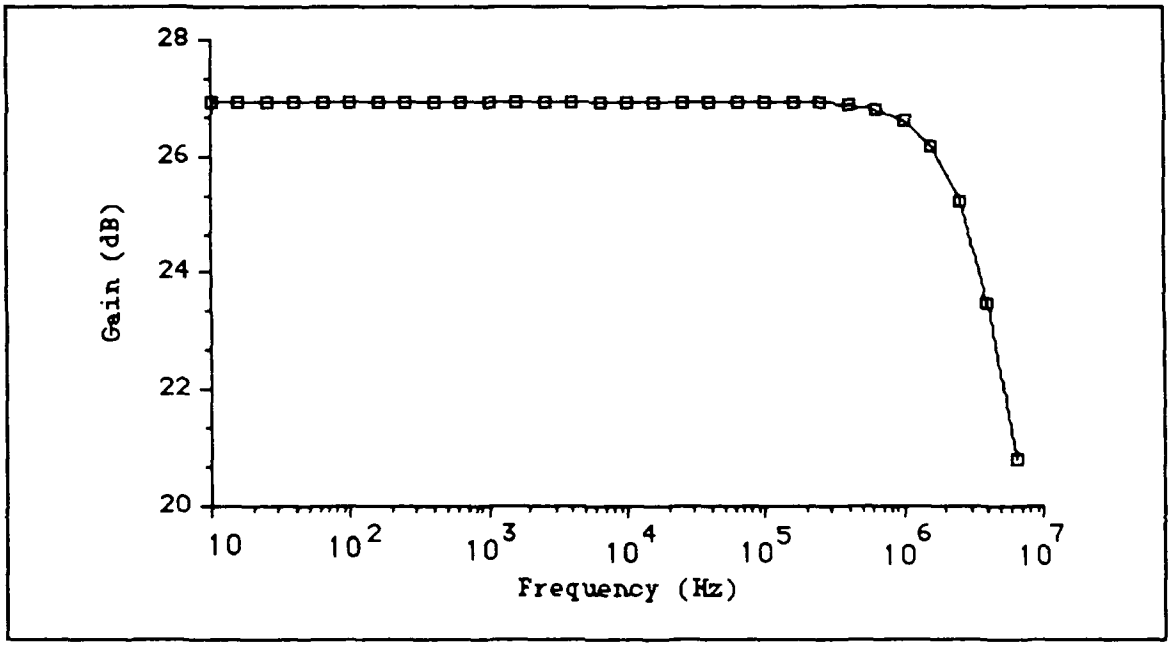

Figure IV-13. Expected Gain of the Microsensor Integrated Circuit.

Once the expected performance of the microsensor electronics was determined, the microsensors were inspected, and their

performance was characterized. This process involved a visual inspection and the measurement of a randomly selected microsensor.

A visual inspection was made of all the circuits in the lot. This inspection consisted of checking for obvious scratches, shorts, or breaks in the interdigitated gate electrode structure. However, the preliminary electrical characterization was done using only packaged circuits to ease the process. This choice assumed that the packaged circuits were representative of all of the circuits.

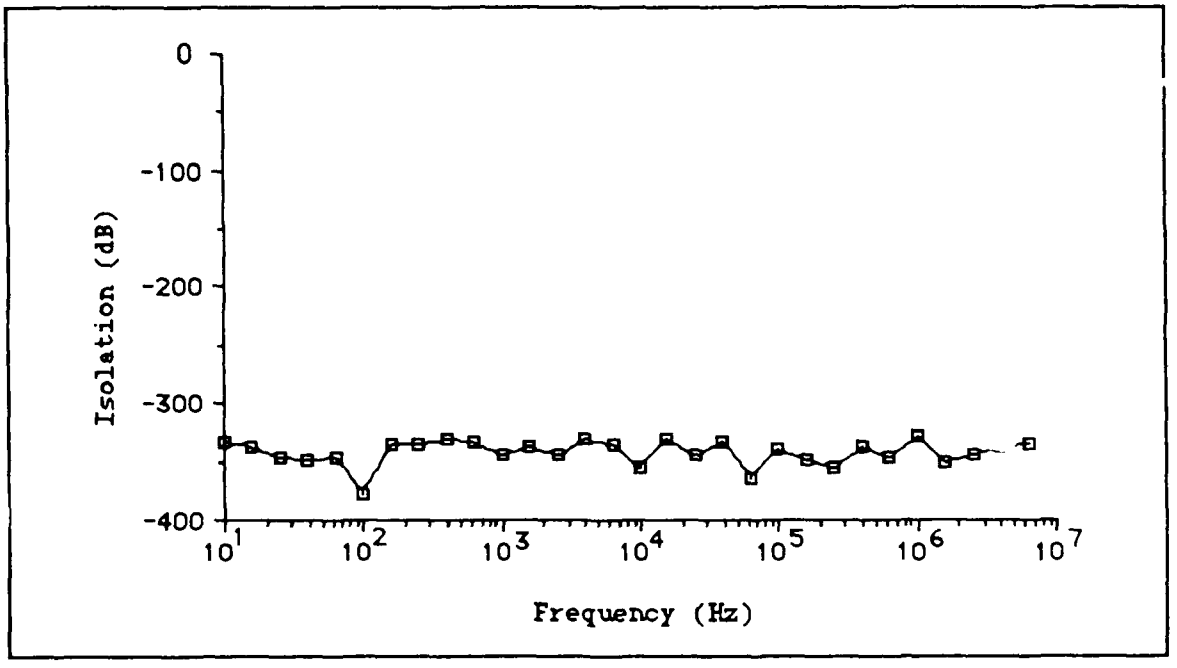

Figure IV-14. Expected Isolation of the Signal Lines.

The visual inspection was done using the microscope on a probe station (The Micromanipulator Company, Model 6200, Carson City, NV). In addition, the resistance of the interdigitated gate electrode structure was checked with a digital multimeter (John

Fluke Mfg. Company, Model 77/AN, Everett, WA). Next, an individual circuit was selected at random to check the DC operation of an amplifier with a semiconductor parameter analyzer (Hewlett Packard, Model HP 4145 B, Palo Alto, CA).

A reference element was biased with a drain and source voltage of +4 volts and -4 volts, respectively. The substrate was biased at ground potential. Using the semiconductor parameter analyzer, the voltage applied at bond pad 42 was swept from -1 volts to +1 volts. The reference element output voltage was monitored at bond pad 43 with the semiconductor parameter analyzer. The resulting DC characteristic is shown in Figure IV-15. From the plot, it was apparent that the fabricated amplifiers possessed a linear region with voltage gain.

All further characterizations of the microsensor were conducted with completed microsensors. For example, the actual voltage gain of the microsensor was determined after the chemically-sensitive coatings were deposited on the interdigitated gate electrode structures. The functionality of the multiplexer was also verified while characterizing the microsensor's frequency response after final fabrication. The test procedure implemented to accomplish this characterization is addressed in the section concerning the experimental test procedures used to measure the transfer function of the microsensor. The results of the characterization are presented in Chapter V.

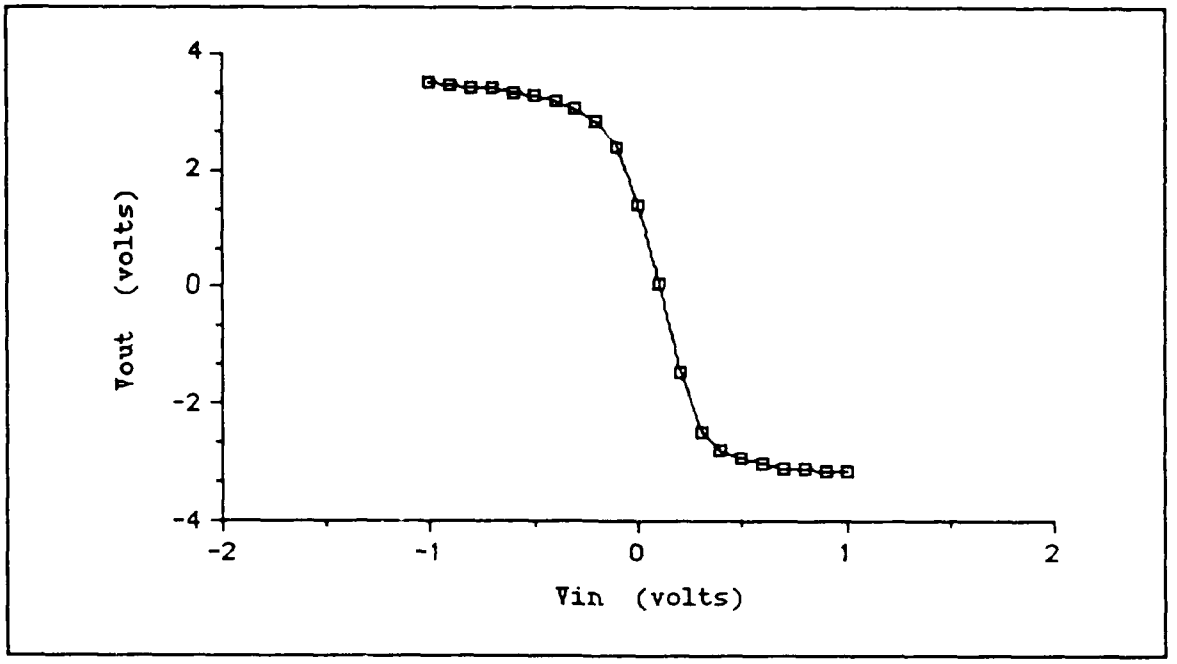

Figure IV-15. DC Operation of the Reference Amplifier Biased with ± 4 Volts.

Final Fabrication

The fabrication section of this chapter principally describes how the various thin films of the phthalocyanine compounds were deposited onto the microsensor, and how the gas generation and delivery system in the AFIT Cooperative Electronics and Materials Processing Laboratory was modified for this research effort.

Deposition of the Phthalocyanine Compounds.

Three unpackaged die were selected from the lot of microsensor integrated circuits for the deposition process. The three dies were designated Die1, Die2, and Die3, respectively. This section

describes the coating configuration and the film thicknesses which were deposited onto the die. The deposition technique developed for this research is described in Appendix C.

The film thicknesses to be studied in this research were 1500 Å and 500 Å. Therefore, the interdigitated gate electrodes on Die1 were selected to be coated with phthalocyanine compounds that were approximately 1500 Å thick. The interdigitated gate electrodes on Die2 were selected to be coated with phthalocyanine compounds that were approximately 500 Å thick. The interdigitated gate electrodes on Die3 were also coated with phthalocyanine compounds that were approximately 500 Å thick. The purpose of Die3 was to provide a die for subsequent analysis in a scanning electron microscope (SEM). The results concerning Die3 are addressed in Appendix C.

The configuration of the phthalocyanine coatings applied to the interdigitated gate electrodes on Die 1 is shown in Figure IV-16. Also, the coating configuration for the interdigitated gate electrodes on Die2 and Die3 is given in Figure IV-17. As depicted in Figure IV-17, the coating configuration for the interdigitated gate electrodes on Die2 and Die3 were identified. The thickness of the various phthalocyanine compounds are summarized in Table IV-5.

The rationale for the coating configuration involved two considerations. The first consideration was to provide a contingency. That is, the voltage sources for the sensing elements were distributed along two sets of power rails which parallel the edges of the integrated circuit. Should one bank of sensing elements fail, the

research could continue using the other functional bank of sensing elements. The second consideration involved the need to evaluate the response of an uncoated interdigitated gate electrode. That is, during data collection using Die1, it became evident that the response of an uncoated interdigitated gate electrode was required. This requirement is further discussed in Chapter V.

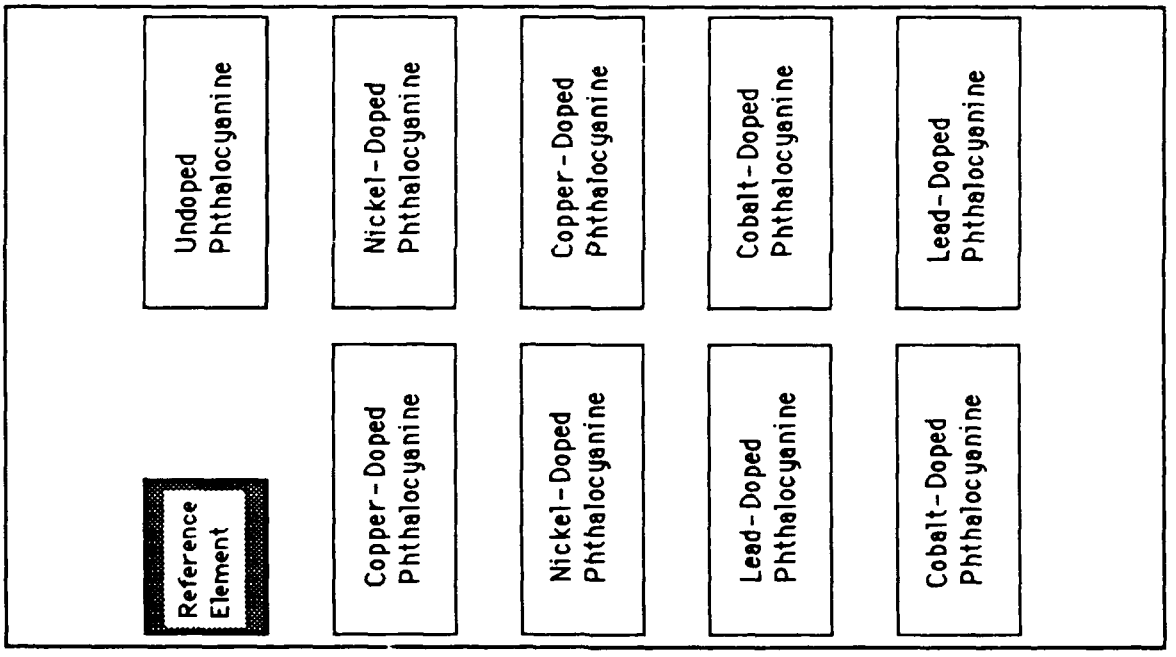

Figure IV-16. Configuration of the Thin Film Phthalocyanine Coatings on Die1.

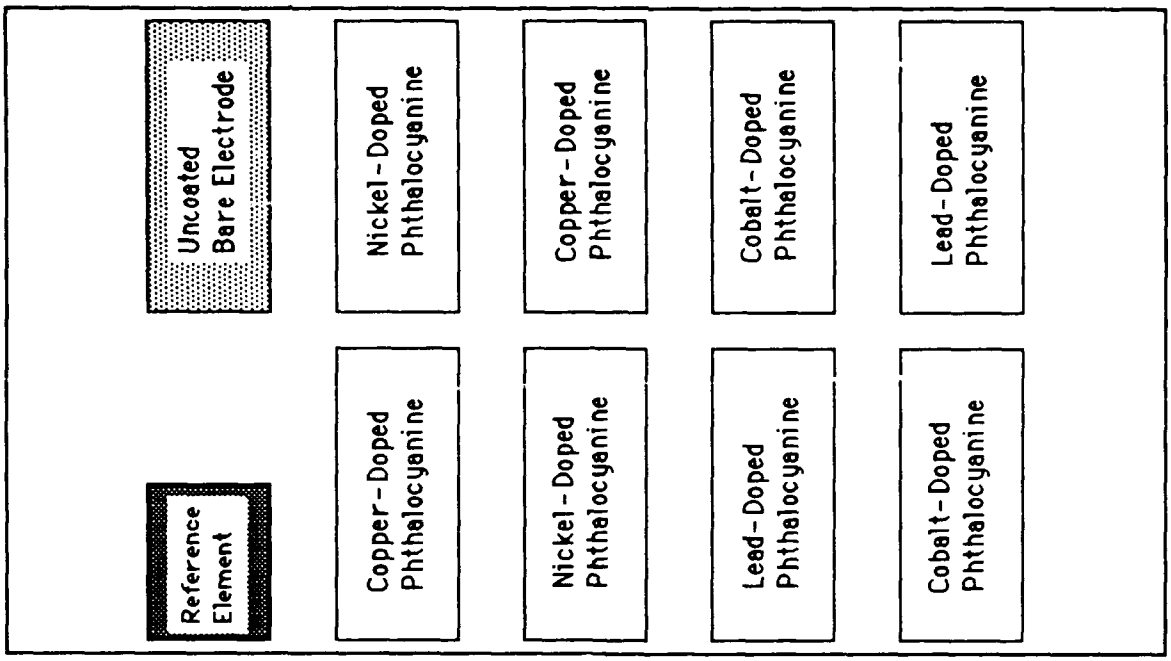

Figure IV-17. Configuration of the Thin Film Phthalocyanine Coatings on Die2 and Die3.

Table IV-5. Thicknesses of the Applied Phthalocyanine Compounds.

	Thickness (Å)		
Material	Die1	Die2	Die3
Cobalt-Doped Phthalocyanine	1300	440	350
Copper-Doped Phthalocyanine	2300	450	560
Lead-Doped Phthalocyanine	1300	460	580
Nickel-Doped Phthalocyanine	1400	400	480
Undoped Phthalocyanine	1600	not used	not used

After the interdigitated gate electrodes were coated with the various phthalocyanine compounds, Die1 and Die2 were mounted in a standard 64-pin dual-in-line (DIP) package. The standard packages sent by MOSIS were used. Die3 was not mounted in a DIP for its subsequent examination in the SEM analysis.

Modification of Gas Generation and Delivery System.

The gas generation and delivery system in the AFIT Cooperative Electronics and Materials Processing Laboratory was modified for this research effort. The general operation and initial design are discussed by Kolesar (55) and by Wiseman (7); this section describes the modifications implemented to improve its performance and utility.

The primary modifications were made to the test cell that contains the microsensor during the gas exposure trials. A one liter glass vessel (approximately four inches in diameter) was located in the AFIT Cooperative Electronics and Materials Processing Laboratory that had ground-glass surfaces at the interface between the lid and body of the vessel. In addition, the lid had 14 ports. The gas delivery lines, the electrical harness, and a Type-K thermocouple (Omega Engineering Inc., Model SA1-K, Stamford, CT) were fitted through these ports. A test fixture to position the mounted microsensor was placed within the test cell. The test cell is depicted in Figure IV-18.

The gas ports consisted of quarter-inch diameter 316 stainless steel tubing (Williams Co., Roselawn, OH), and the wiring harness consisted of 12 RG-58A/U coaxial cables and 56 solid, 22-AWG wires.

The coaxial cables are used to transmit the microsensor's signals such as the driven-gate signal, the floating-gate signal, and the microsensor's output signal. The other 56 wires provided for temperature control, the microsensor's voltage bias requirements, and the multiplexer inputs, as well as access to other nodes internal to the microsensor integrated circuit.

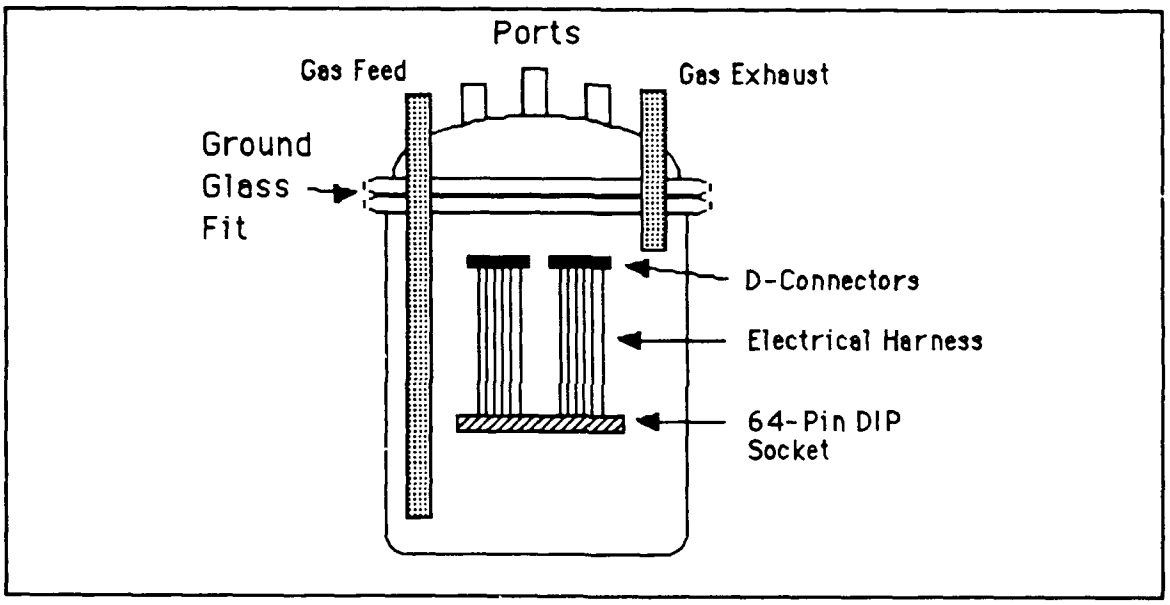

Figure IV-18. Test Cell Used for Gas Exposure.

The D-connectors were used to simplify the insertion and removal of the microsensor. The microsensor was inserted into a DIP socket outside the test cell. The socket and its harness were then inserted inside the test cell. The D-connectors allow a standard electrical interface to remain permanently fitted through the glass lid

of the test cell. The electrical harness between the DIP socket and the D-connectors was "personalized" for a given microsensor design.

The wiring and tubing was tightly wrapped with teflon tape and fitted through the glass ports in the vessel's lid. In addition, large binder clamps were used to secure the lid to the vessel when the microsensor was inserted in the test cell.

To control the operating temperature of the microsensor, a pair of Kapton heater strips (Watlow, Model K005020C5, St. Louis, MO) were secured between the microsensor and the 64-pin DIP socket. The thermocouple was attached to the microsensor's DIP to monitor the operating temperature.

The relative humidity of the test cell was monitored. A hygrometer (Thunder Scientific Corporation, Model HS-1CHDT-2A, Albuquerque, NM) was inserted in the gas exhaust line immediately outside of the test cell. The relative humidity was adjusted using the technique discussed by Kolesar (55).

The challenge gas sources for NO_2 and DIMP were generated by utilizing commercially available gas permeation tubes (GC Industries, Model 23-7502 for NO_2 and Model 23-7392 for DIMP, Chatsworth, CA). A specific gas concentration was established and regulated using filtered room air as the carrier gas in the manner discussed by Kolesar (55) and Wiseman (7) . The permeation tubes were immersed in a thermostatically-controlled water bath (Neslab Corp, Refrigerated Circulating Water Bath, Model RTE-88D, Newington, NH). The precise method used to establish the challenge gas concentration is discussed in Appendix D.

Experimental Arrangement and Performance Evaluation

This section describes the configuration of the test equipment. In addition, the specific electrical parameters and environmental conditions that were monitored, the data collection methods, and the data reduction techniques are discussed.

Test Configuration.

To evaluate the suitability of the phthalocyanine compounds for use with the microsensor, a set of electrical characteristics associated with the interdigitated gate electrode structures (that were coated with the phthalocyanine films) were monitored. These characteristics were monitored before, during, and after exposure to the challenge gases. The set of electrical characteristics and their associated parameters are presented in Table IV-6.

The DC resistance of the interdigitated gate electrodes was measured with an electrometer (Kiethley Instruments, Model 617, Cleveland, OH). The electrometer was operated in its (V/I)-mode to minimize the effects of distributed capacitance in the test instrument configuration. Also, this mode facilitates the measurement of large resistances (up to 10^{16} ohms) (56:2-19).

To measure the DC resistance with respect to time, a 2-volt bias was applied across the driven and floating gate electrodes (positive potential applied to the driven gate). The electrometer's internal voltage source was used to apply the bias. The DC resistance was measured with respect to the applied voltage bias by varying the

electrometer's voltage source from 1 to 10 volts in increments of 1 volt. Before each test session, the electrometer's internal resistance was verified.

Table IV-6. Electrical Characteristics and Associated Parameters.

Characteristic	Parameters
DC Resistance	
With Respect to Time	Resistance, Time (0 - 60 min)
With Respect to Applied Bias	Resistance, Voltage (1 - 10 V)
AC Impedance	
With Respect to Frequency	Magnitude and Phase Real and Imaginary Components Frequency (1 KHz - 1 MHz)
Transfer Function	
Frequency-Domain	Gain and Phase Frequency (1 - 200 KHz)
Voltage Pulse Response	
Time-Domain	Voltage Magnitude Time (10^{-3} second period)
Frequency-Domain	Power Magnitude Value (dBm) Frequency (1 - 200 KHz)

The AC impedance of the interdigitated gate electrodes was measured using the same impedance/gain-phase analyzer that was used to determine the transfer function of the microsensor (Hewlett-Packard Corp., Model HP4194A, Palo Alto, CA). Since this analyzer can be configured to measure both impedance and gain-phase (57), the test instrumentation configuration was simplified. The impedance was measured with a 2-volt bias applied to the

interdigitated gate electrode with the same polarity that was used in the DC measurement. The measurement was made from 1 KHz to 1 MHz. Before each impedance measurement associated with the interdigitated gate electrodes, the HP4194A was calibrated.

As noted above, the resistance and impedance measurements were made by connecting the test intrumentation directly to the interdigitated gate electrode structures. The rationale for this procedure concerns the proposed microsensor's architecture. That is, the microsensor was designed to provide AC voltage signal amplification for subsequent signal processing. While the detected AC signal will be affected by changes in the phthalocyanine compound's resistance or impedance, the actual evaluation of the resistance and impedance changes can also be discerned by direct measurement at the driven and floating gate electrodes.

The transfer function of the microsensor was measured with the HP4194A. To accomplish this measurement, the sinusoidal voltage source of the HP4194A was set to an oscillation magnitude of ±0.01 volts. This was the maximum signal level that could be applied to the driven gate electrode and not overload the HP4194A's input whenever this signal was also amplified by the microsensor. The transfer function was characterized as voltage gain ($20 \log_{10} [V_{out}/V_{in}]$) and phase delay ($\phi_{out} - \phi_{in}$) over the frequency range of 1 to 200 KHz. The excitation signal was applied at the driven gate bond pad (pad 64), and the output was sampled at the chip output pad (pad 37). The multiplexer was used to select the particular

sensing element to be evaluated. Before measuring the microsensor's transfer function, the HP4194A was calibrated.

The voltage pulse response (time-domain) of the microsensor was measured by applying a voltage pulse using a function generator (Hewlett-Packard Corp., Model 3314A, Palo Alto, CA) and sampling the response using a digitizing oscilloscope (Hewlett-Packard Corp., Model 54100 A/D, Palo Alto, CA). The excitation pulse input was applied to pad 64 and the output was sensed at pad 37 using the multiplexer to select the particular sensing element. The excitation pulse input was a square wave with a 1-volt peak amplitude. The pulse's frequency was 1 KHz, and it had a 50% duty cycle.

The voltage pulse response (frequency-domain) of the microsensor was measured by applying a voltage pulse from a pulse generator (Hewlett-Packard Corp., Model 8082A, Palo Alto, CA) and sampling the spectral response using a spectrum analyzer (Hewlett-Packard Corp., Model HP8566B, Palo Alto, CA). A square wave with a 5-volt peak amplitude was used. Also, a pulse width and period of approximately 2 nanoseconds and 1 millisecond, respectively, was used. The selection of the pulse generator, pulse width, and pulse period was determined empirically. That is, the signal source was connected to the reference amplifier, and the spectral response was monitored while adjusting the signal source to yield a maximally flat spectral response from 1 to 200 KHz. The spectrum analyzer was calibrated prior to the measurements.

To determine the transfer function and the spectral response of an interdigitated gate electrode, a linear systems approach was

implemented. A simplified block diagram of the microsensor is shown in Figure IV-19. In the figure, a single sensing element has been selected by the multiplexer. The signals of the other 9 elements of the microsensor array are assumed to be isolated from the system by the multiplexer. In addition, any parasitic affects of the multiplexer are lumped with the amplifier. By assuming a linear system, the response of the interdigitated gate electrode $I(\omega)$ can be determined by (58:261):

$$I(\omega) = r(\omega) / [\, g(\omega)\, A(\omega)\,] \qquad (4.1)$$

where $r(\omega)$ is the measured response of the microsensor, $g(\omega)$ is the pulse generator signal, and $A(\omega)$ is the amplifier's response.

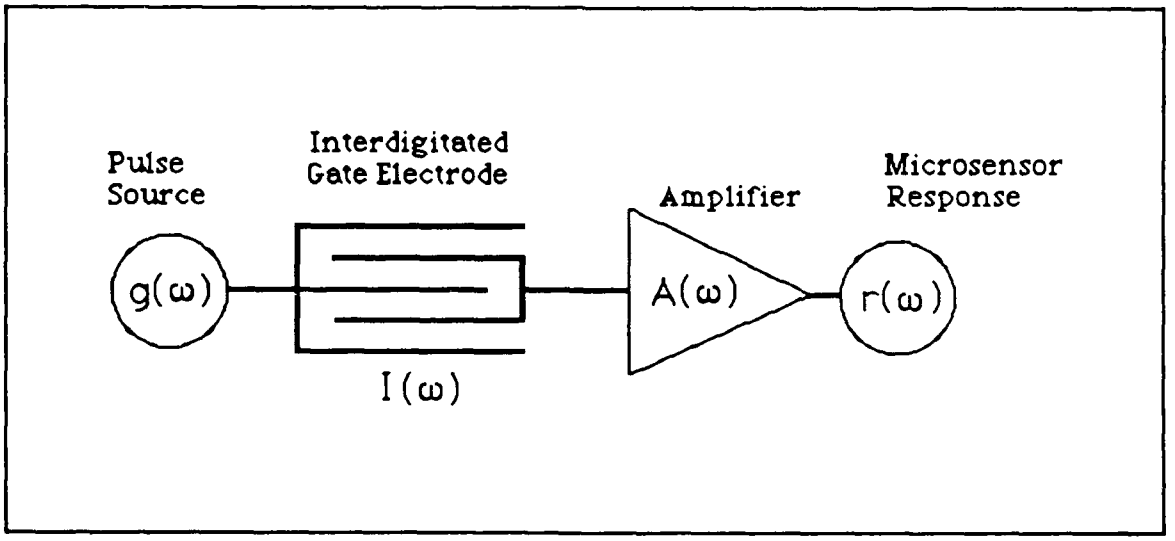

Figure IV-19. Block Diagram of the Microsensor Response.

The product [$g(\omega)\ A(\omega)$] is measured when Chem5 of the microsensor is selected with the multiplexer. This configuration assumes that the Chem5 reference element is representative of the other amplifiers which is a fundamental tenent of the microsensor's architecture. Since the transfer function and the spectral response data are collected in a dB format, the calculation of $I(\omega)$ results from a simple subtraction operation.

The experimental arrangement is summarized in Figure IV-20. A single sensing element is depicted to simplify the diagram. For clarity, only the signal path is shown; the bias and multiplexer control paths are not explicitly shown. In addition, data collection was managed by automating the test instrumentation using a microcomputer (Zenith Data Systems, Model Z-248, St. Joseph, MI) and an IEEE-488 interface card (Capitol Equipment Corp., Model 01000-60300, Burlington, MA). The BASIC computer programs that were written to control the instrumentation are listed in Appendix E. Additionally, the BASIC computer programs written to facilitate the data analysis are listed in Appendix F.

General Test Procedure.

The electrical response of the microsensor was monitored using a three-step procedure. The initial step involved establishing a baseline response for the set of test data discussed in the previous subsection. The microsensor to be tested was placed in the test cell and purged with filtered room air for 24 hours at room temperature.

After this initial purge, a set of test data was collected at the test temperature and humidity to be investigated.

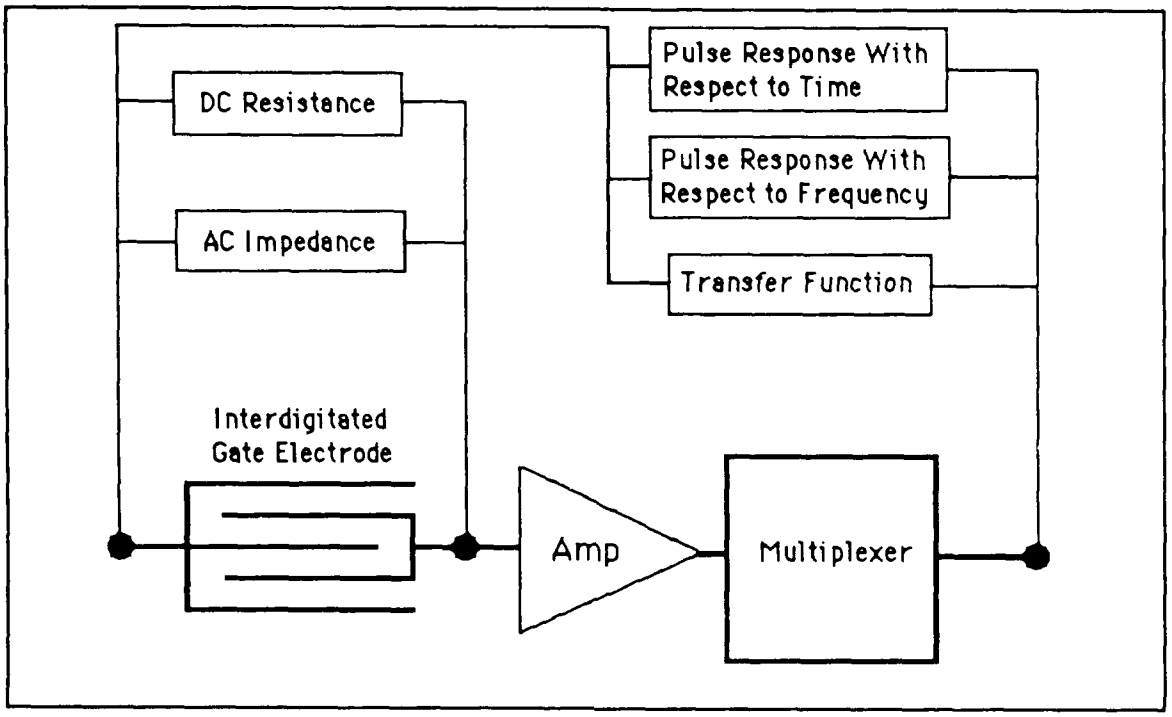

Figure IV-20. Experimental Test Equipment Configuration.

Once the initial state of the microsensor was determined, the microsensor was challenged with the test vapor gas at a specific concentration. The DC resistance with respect to time was measured beginning with the flow of the test gas into the test cell. The array of interdigitated gate electrodes was measured approximately every three minutes for a minimum of 30 minutes. When this time period elapsed or when the microsensor's response appeared to stabilize, the DC resistance with respect to voltage bias was measured with respect to each element in the sensor's array. Once the DC data were collected, the AC impedance of the elements was measured. The

transfer function of the microsensor was then measured. Once these sets of data were collected, the spectral response of the microsensor was determined. This step of the procedure concluded with a measurement of the pulse response (time-domain).

The next step of the data collection procedure involved a purge. The challenge gas flow was terminated, and the test cell was purged with filtered room air. When the purge was started, the microsensor's DC resistance measurement with respect to time was resumed for a time period lasting 30 minutes. At the conclusion of this final 30 minute purge, the pulse response with respect to time was remeasured.

Thus, at the conclusion of the test procedure, a set of test data had been collected that consisted of the initial state (response to filtered room air), the challenged state (response to challenge gas), and the reversed state (response to the final purge with filtered room air). This procedure was repeated for each of the test gas species (NO_2 and DIMP) and challenge concentrations.

Specific Test Procedure.

Initially, Die1 was placed in the test cell. A set of baseline data was collected for the phthalocyanine compounds that consisted of the DC resistance with respect to a specific voltage bias. Each interdigitated gate electrode was measured with filtered room air flowing in the test cell. The response was measured for all combinations of 25°C, 70°C, 100°C, and 10%, 50%, and 100% relative humidity. However, a practical microsensor may minimize the sensor input variations (such as temperature and relative humidity)

relative to the challenge gas. Therefore, all subsequent measurements in the research were completed with the relative humidity maintained at less than 5%.

The complete set of test data was then collected for Die1 using the general procedures discussed in the previous subsection. The challenge gases were nitrogen dioxide (NO_2) and diisopropyl methylphosphonate (DIMP). The challenge gas concentrations were 20 ppb, 80 ppb, and 320 ppb. The operating temperature was maintained at 30°C for the DIMP set of measurements. In the case of NO_2, the measurements were made at 30°C and at 120°C. The complete set of measurements associated with Die2 were made with challenge gas concentrations of 20 ppb, 80 ppb, and 320 ppb of NO_2 at 30°C. These test conditions are summarized in Tables IV-7, -8, and -9, where "Air" represents filtered room air, "Y" (yes) denotes that the test was conducted, "N" (no) denotes that the test was not conducted.

Table IV-7. Initial Environmental Conditions for the DC Resistance Measurement With Respect to Bias for Die1.

Relative Humidity	Microsensor Operating Temperature		
	25°C	70°C	100°C
10%	Air	Air	Air
50%	Air	Air	Air
100%	Air	Air	Air

Table IV-8. Challenge Gases Tested With Die1.

Microsensor Temperature	Gas Concentration (ppb)					
	NO_2			DIMP		
	20	80	320	20	80	320
30°C	Y	Y	Y	Y	Y	Y
120°C	Y	Y	Y	N	N	N

Table IV-9. Challenge Gases Tested With Die2.

Microsensor Temperature	Gas Concentration (ppb)					
	NO_2			DIMP		
	20	80	320	20	80	320
30°C	Y	Y	Y	N	N	N
120°C	N	N	N	N	N	N

Summary

This chapter presented the design of a chemically-sensitive microsensor. The microsensor consists of an array of sensing elements based upon an IGEFET coupled to a serially-connected pair of inverting MOSFET amplifiers. Individual elements of the array are sampled with an on-chip analog multiplexer. The rationale for the various design options were explained, such as the need to amplify the electrical response of the chemically-sensitive phthalocyanine

thin films. In addition to the design of a microsensor, the design of a test cell was described. The test instrumentation configuration and test procedures were also discussed.

V. Results and Discussion

This chapter contains a discussion of the results and analysis of the measured performance responses of the microsensors developed in this thesis. The first section presents the characterization of the microsensor's frequency response. This data constitutes the validation phase of the microsensor integrated circuit design. The second section concerns the experimental results that were obtained with the microsensor that was fabricated using Die1 and Die2.

Characterization of the Microsensor's Frequency Response

To conduct this measurement, the source and drain voltages were connected to the appropriate bond pads and biased with ±5 volts, as required. The gain-phase analyzer was used to determine the AC voltage gain of the discrete microsensor elements. The output of the gain-phase analyzer was connected to the floating gate input of the sensing element being characterized. The input of the analyzer was connected to bond pad 37. The oscillator level of the gain-phase analyzer was set at ±0.01 volts.

The measurement process proceeded in several steps. First, the gain (dB) and phase delay [(ϕ_{out} - ϕ_{in}) in degrees] corresponding to a particular element was measured with the proper address applied to the multiplexer. Next, the analyzer's output was connected to the adjacent sensing element's floating gate input without changing the address supplied to the multiplexer. A

measurement was then taken with this configuration to characterize the isolation of the multiplexer. Next, a new address was loaded into the multiplexer, and the measurement was repeated to characterize the gain and phase delay of the selected microsensor element. This process was repeated until all ten microsensor elements (nine sensing elements and the reference element) were characterized in a selected and unselected mode. The frequency characteristics are given in the following representative plots (Figures V-1 through V-4). The sensing Element Chem2 and the reference element Chem5 are depicted in the selected and unselected states. The additional elements are depicted in Appendix G.

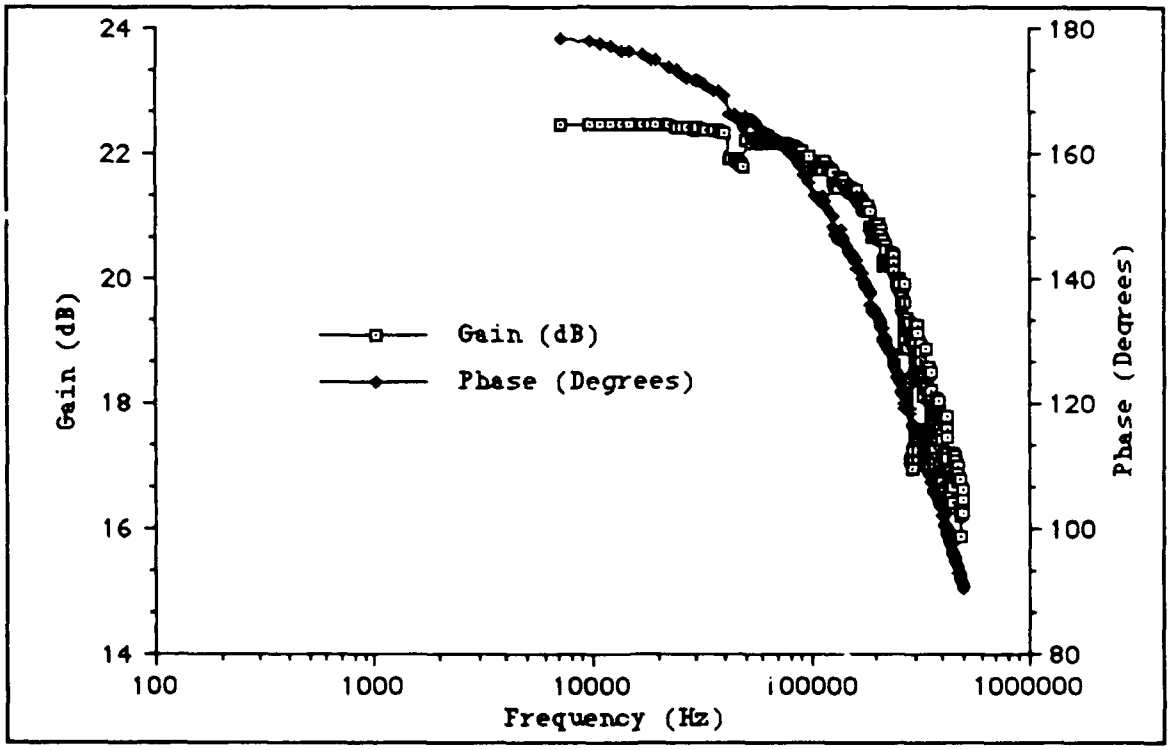

Figure V-1. Sensing Element Chem2 Selected.

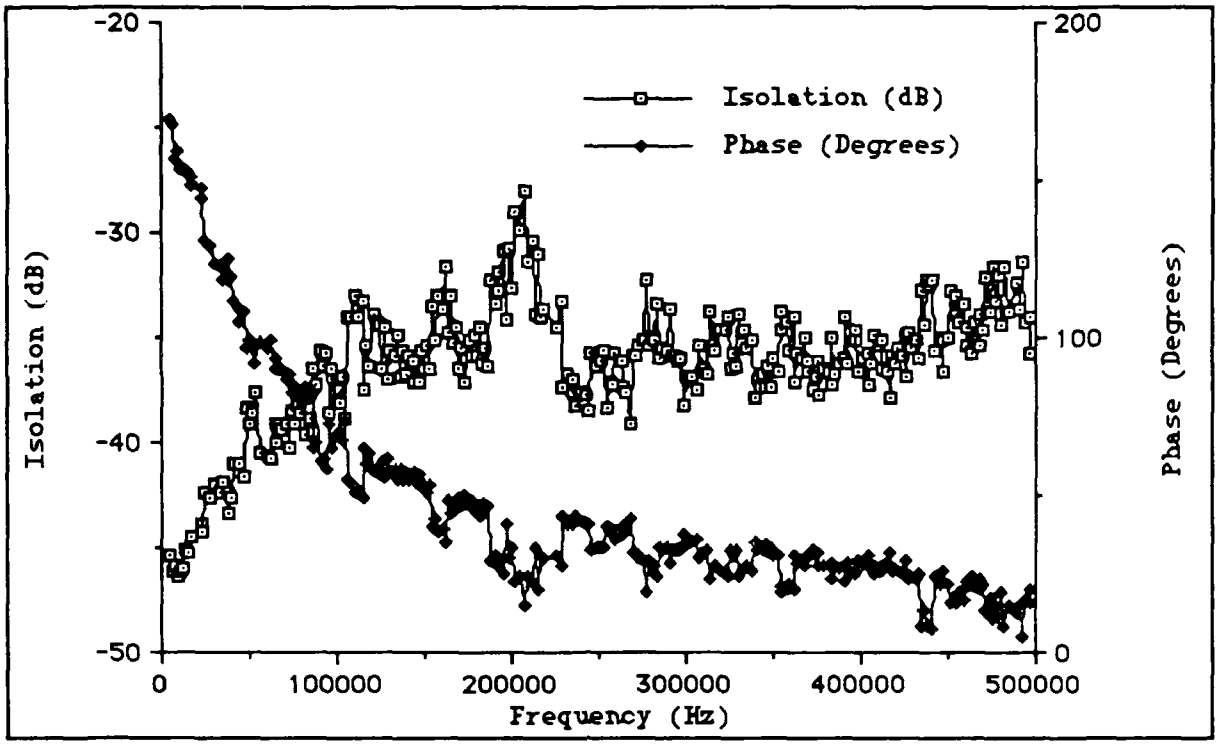

Figure V-2. Sensing Element Chem2 Unselected.

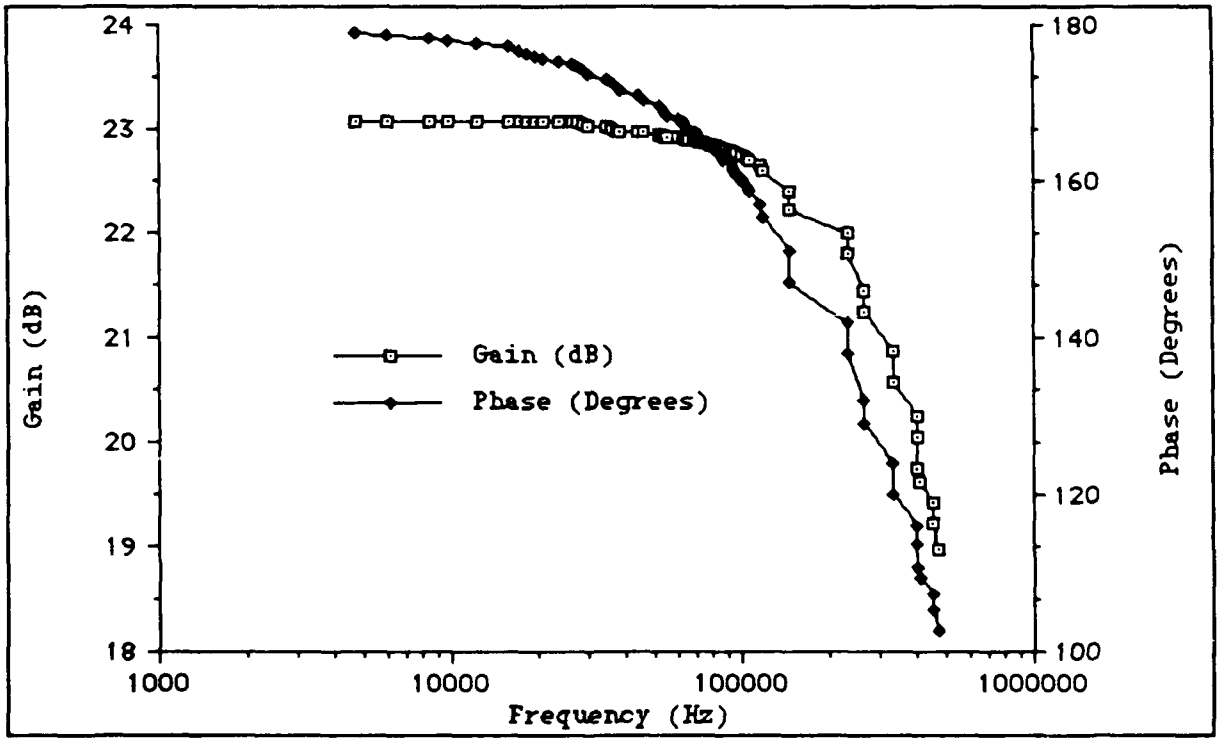

Figure V-3. Reference Element Chem5 Selected.

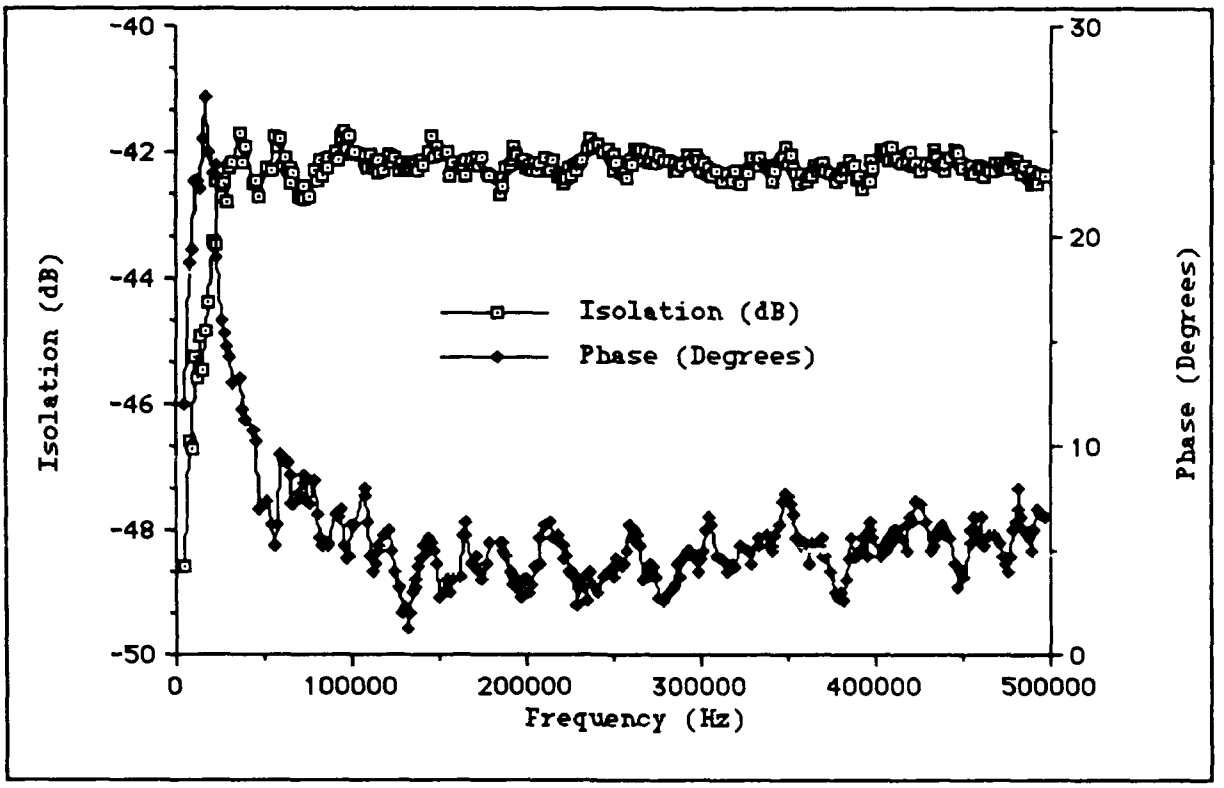

Figure V-4. Reference Element Chem5 Unselected.

For the randomly selected circuit that was characterized, the sensing element designated as Chem1 was not functional. Therefore, only the preliminary frequency characteristics of elements Chem2 through Chem10 are reported as representative of the microsensor circuit. The low frequency gain varied from 24 dB for Chem3 to 21 dB for Chem8, with an average 3-dB cut-off frequency of 450 KHz. Correspondingly, the isolation varied from -42 dB for Chem5 to -22 dB for Chem8.

Microsensor Results

First, the microsensor that was fabricated using Die1 was challenged with nitrogen dioxide (NO_2) and diisopropyl methylphosphonate (DIMP) as the challenge gases. However, before challenging the microsensor with these gases, a set of baseline performance DC resistance responses was collected for exposure to dry laboratory nitrogen gas (N_2) and filtered room air at 10%, 50%, and 100% relative humidity with a die temperature of 25° C, 70° C, and 100° C.

To facilitate the data collection, an attempt was made to use a matrix switch (Wavetek Corp., Model 604, San Diego, CA). The switch was used to connect the measurement instrumentation to a specific interdigitated gate electrode under microcomputer control. As a result, the data collection of the DC resistance of the interdigitated gate electrode structure could be fully automated. The data concerning N_2 and filtered room air at 10%, 50%, and 100% relative humidity with a die temperature of 25° C, 70° C, and 100° C are reported in Appendix H, as well as the electrical characteristics of the matrix switch.

A potential problem was discovered when using the matrix switch to collect the data. The matrix switch was electrically characterized by measuring its open circuit resistance. As depicted in Appendix H, the resistance was variable and on the order of 10^{10} ohms. In addition, the DC resistance of the phthalocyanine coated interdigitated gate electrodes was also very large (on the order of

10^{10} ohms) in some cases. Thus, when using the matrix switch, the measured reading consisted of the shunt combination of the matrix switch's open-circuit leakage resistance and the phthalocyanine-coated interdigitated gate electrode structure's resistance. Therefore, the matrix switch was not considered for use in any additional measurements of the microsensor's characteristics in this thesis research.

The next set of measurements accomplished using Die1 was concerned with the microsensor's response to an NO_2 and DIMP challenge gas concentration of 20 ppb, 80 ppb, and 320 ppb. This set of electrical measurements consisted of the standard measurements discussed in Chapter IV (DC resistance, AC impedance, transfer function, spectral response to a pulse excitation, and the time-domain response to a pulse excitation). For the purposes of this chapter, this set of measurements will be referred to as the "standard set." These measurements were first accomplished with the microsensor operating at 30° C, and then at 120° C. In addition, the test cell's relative humidity was maintained at approximately 5%, unless otherwise indicated.

Room Temperature Operation.

The DC resistance response of the interdigitated gate electrode was examined for each of the phthalocyanine compounds. Figure V-5 depicts the DC resistance change of the cobalt-doped phthalocyanine coated interdigitated gate electrode structure when challenged with a 320 ppb concentration of NO_2. This measurement provides an example of the contrast observed between the

challenged and unchallenged state of the microsensor. In addition, the microsensor is operating at a temperature of 30° C. This is considered to represent the room temperature operation since temperatures below this value can not be reliably thermostated with the heater strips. In addition, as reflected in Figure V-5, the challenge gas begins to flow into the test cell when time equals zero. The corresponding response for the other coatings are shown in Figures V-6 through V-9.

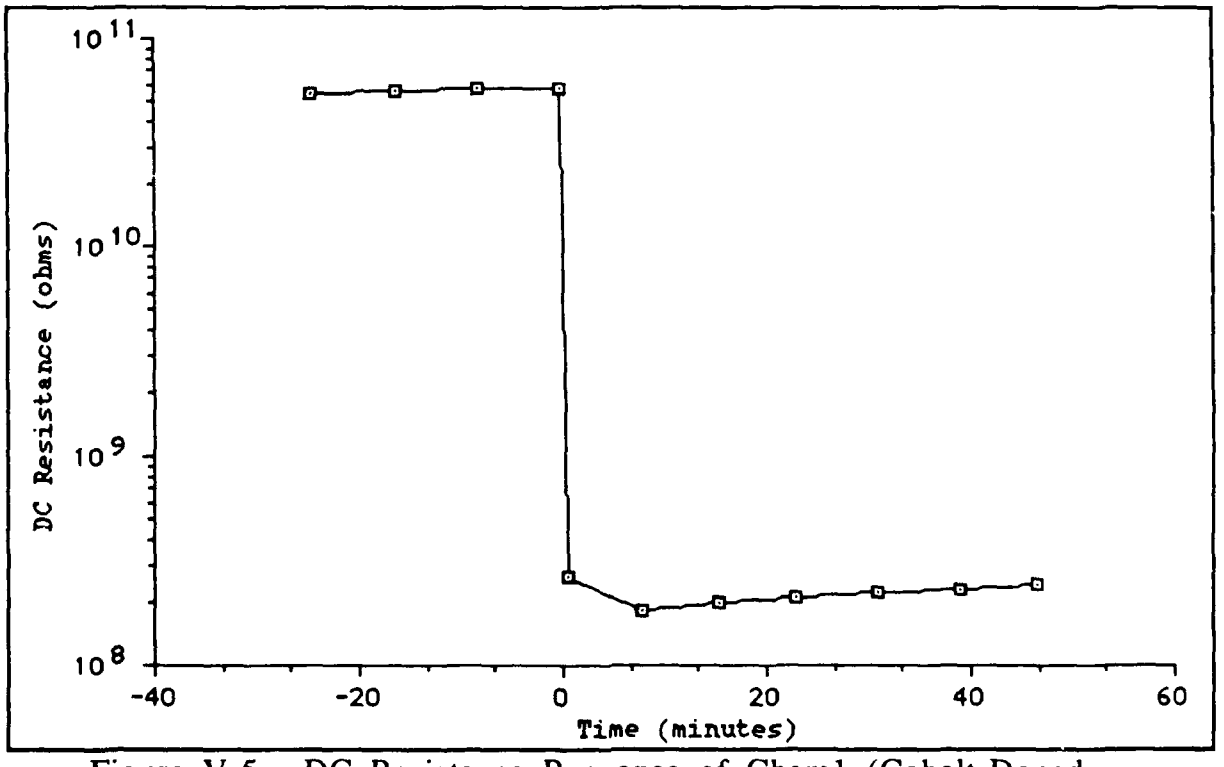

Figure V-5. DC Resistance Response of Chem1 (Cobalt-Doped Phthalocyanine) (320-ppb NO_2; 30° C).

Figure V-6. DC Resistance Response of Chem2 (Lead-Doped Phthalocyanine) (320-ppb NO_2; 30° C).

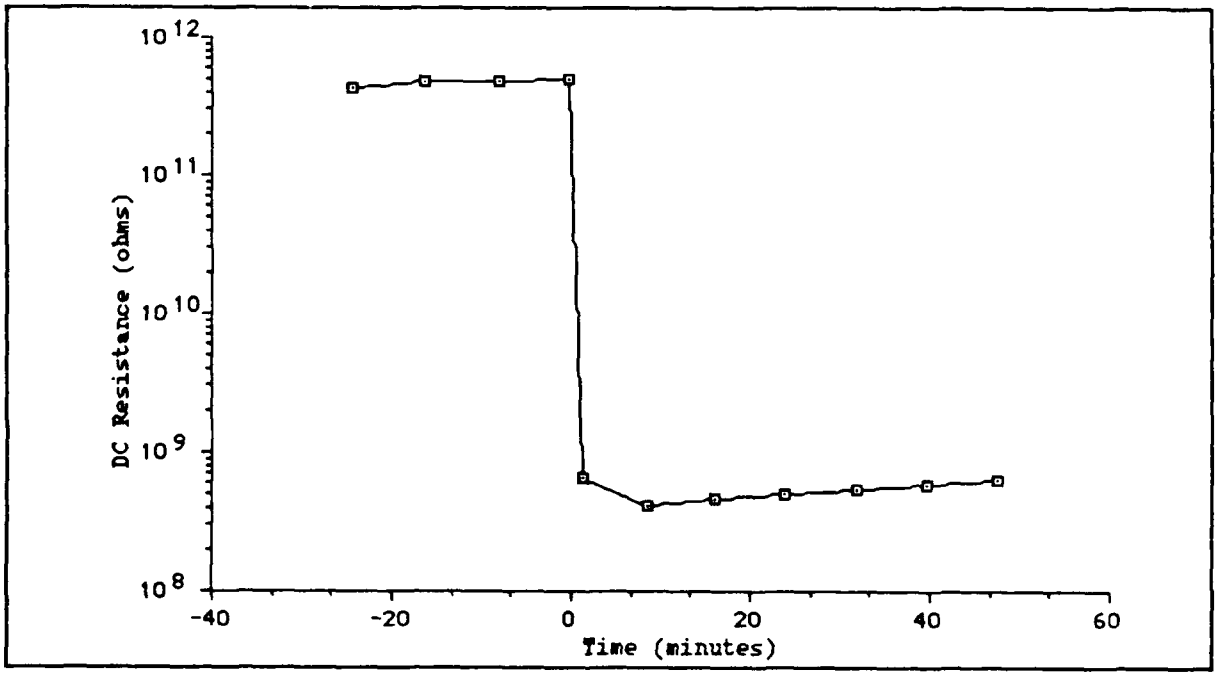

Figure V-7. DC Resistance Response of Chem3 (Nickel-Doped Phthalocyanine) (320-ppb NO_2; 30° C).

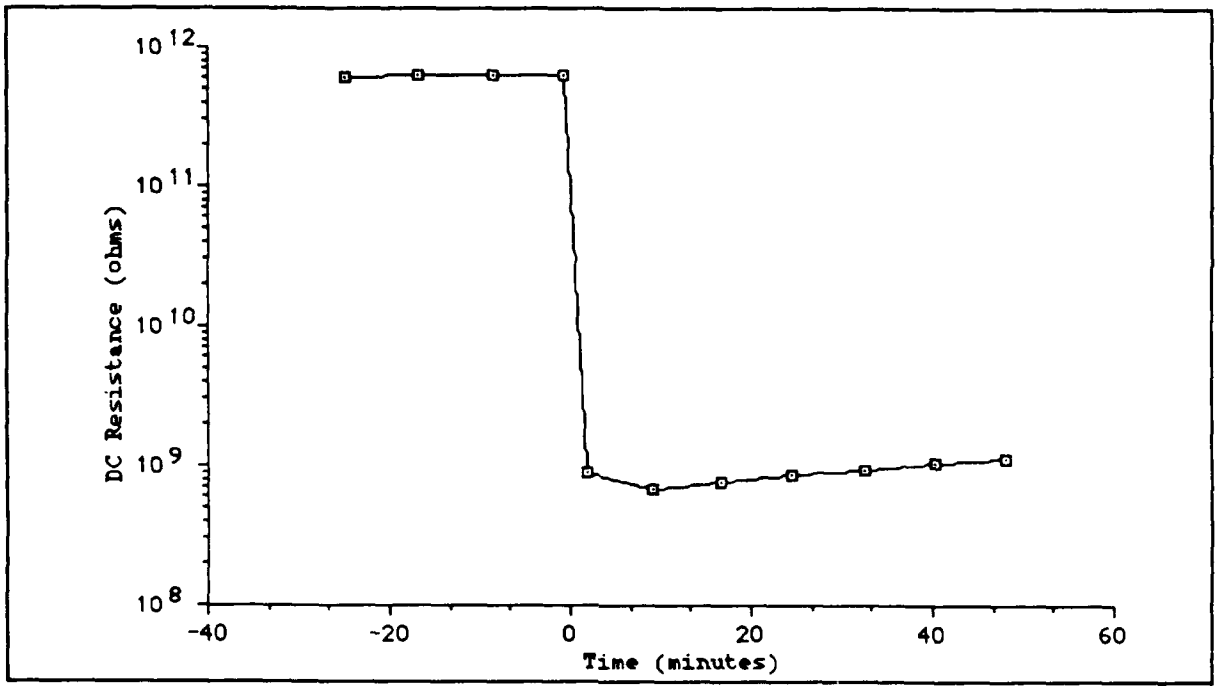

Figure V-8. DC Resistance Response of Chem4 (Copper-Doped Phthalocyanine) (320-ppb NO_2; 30° C).

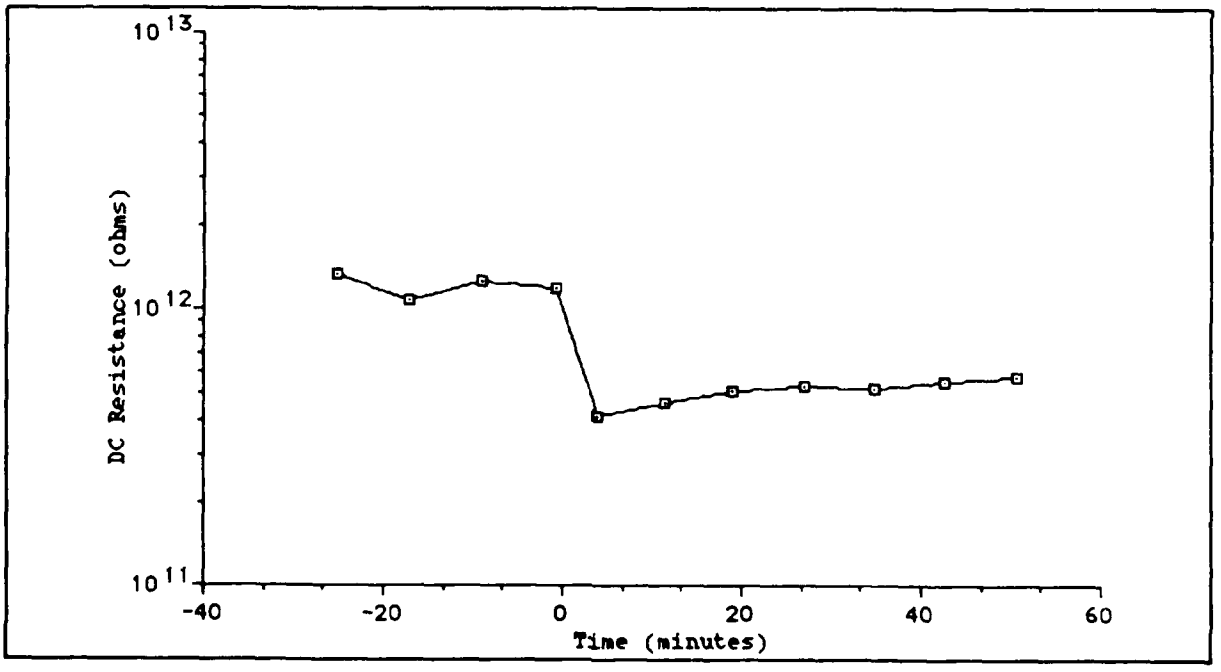

Figure V-9. DC Resistance Response of Chem6 (Undoped Phthalocyanine) (320-ppb NO_2; 30° C).

The DC resistance response with respect to time for exposure of the coated interdigitated gate electrodes is summarized for all three NO_2 challenge concentrations in Figures V-10 through V-14. In these figures, the challenge gas begins to flow into the test cell when time equals zero, and the microsensor is maintained at 30° C.

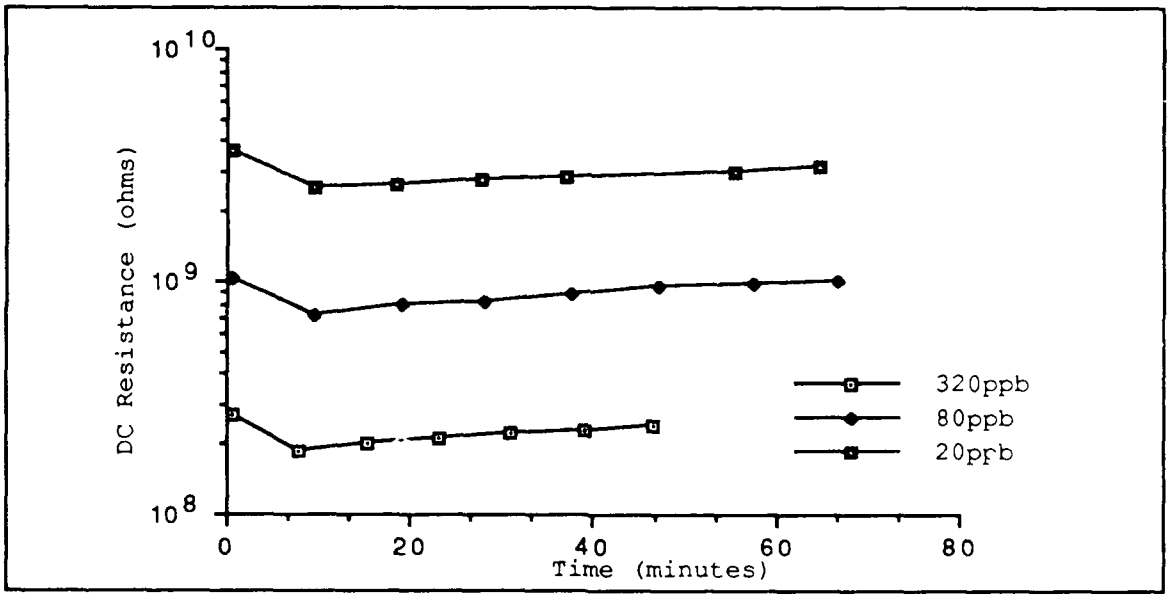

Figure V-10. DC Resistance Response of Chem1 (Cobalt-Doped Phthalocyanine) as a Function of the NO_2 Concentration (30° C).

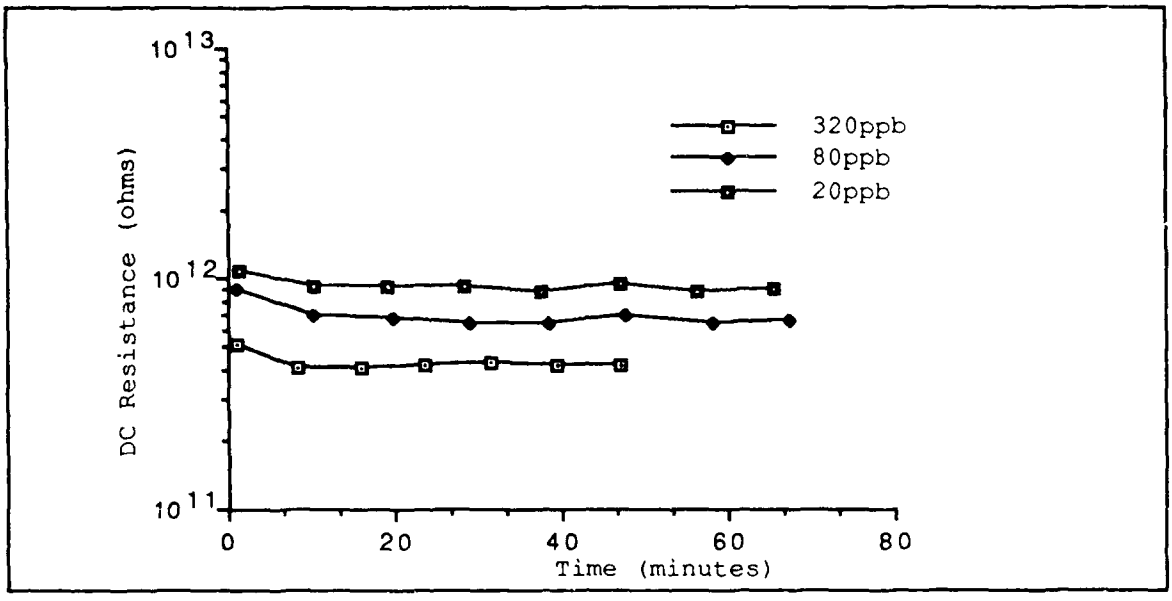

Figure V-11. DC Resistance Response of Chem2 (Lead-Doped Phthalocyanine) as a Function of the NO_2 Concentration (30° C).

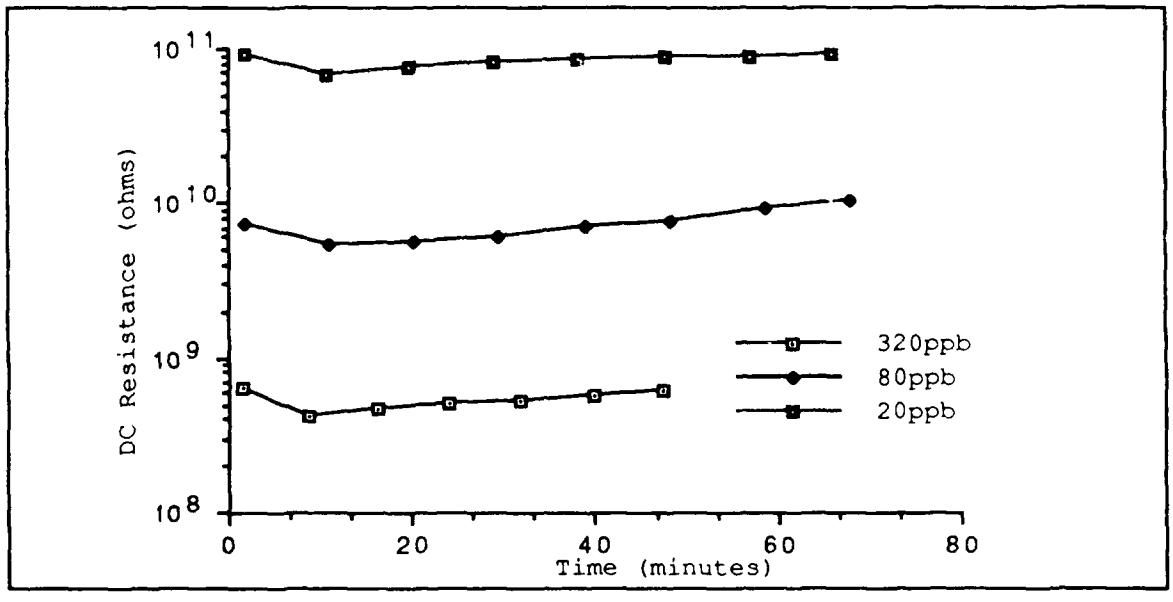

Figure V-12. DC Resistance Response of Chem3 (Nickel-Doped Phthalocyanine) as a Function of the NO_2 Concentration (30° C).

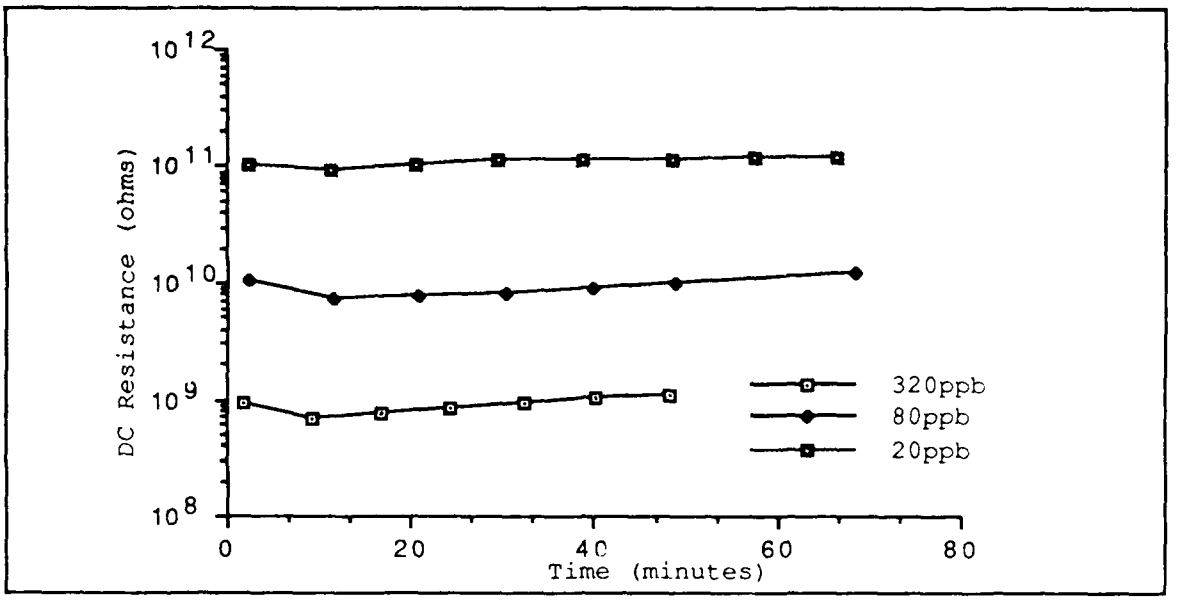

Figure V-13. DC Resistance Response of Chem4 (Copper-Doped Phthalocyanine) as a Function of NO_2 Concentration (30° C).

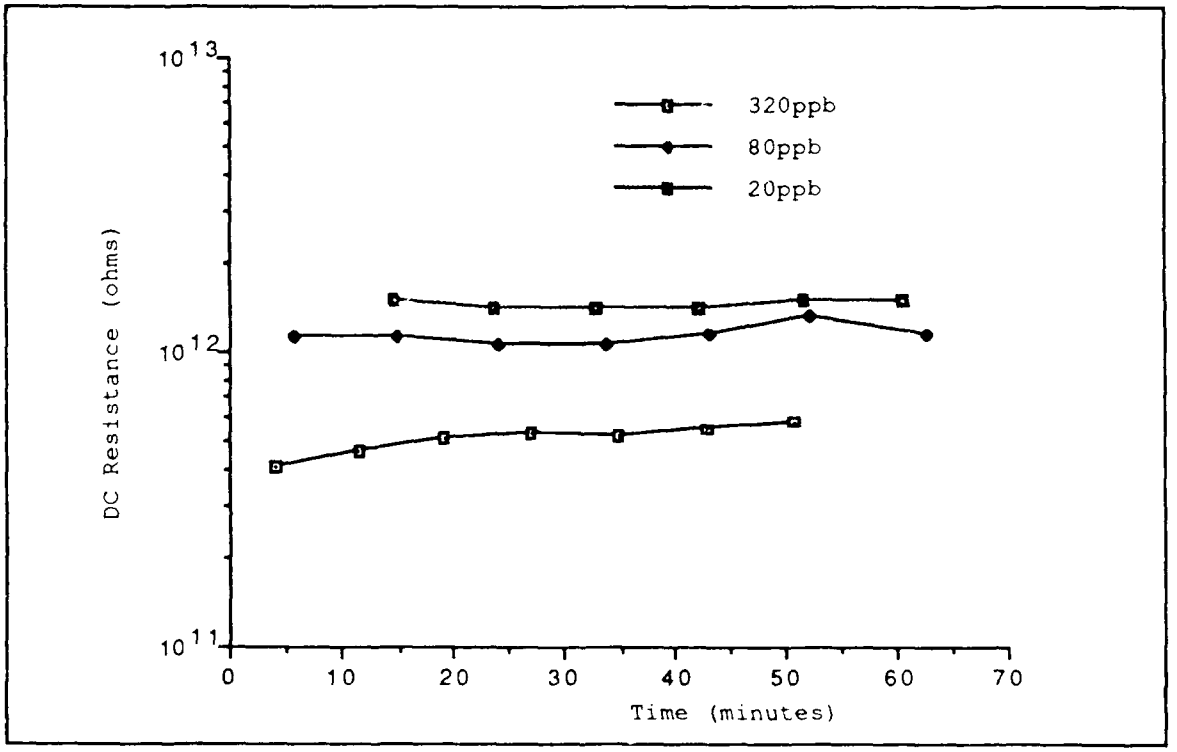

Figure V-14. DC Resistance Response of Chem6 (Undoped Phthalocyanine) as a Function of NO_2 Concentration (30° C).

As previously discussed in Chapter 4, the DC resistance was measured with respect to the applied bias voltage. Examples of the results associated with a 20 ppb challenge concentration of NO_2 are presented in Figures V-15 through V-19 with the microsensor operating at 30° C. As depicted, a measurable response was evident even at the lowest concentration (20 ppb) of NO_2.

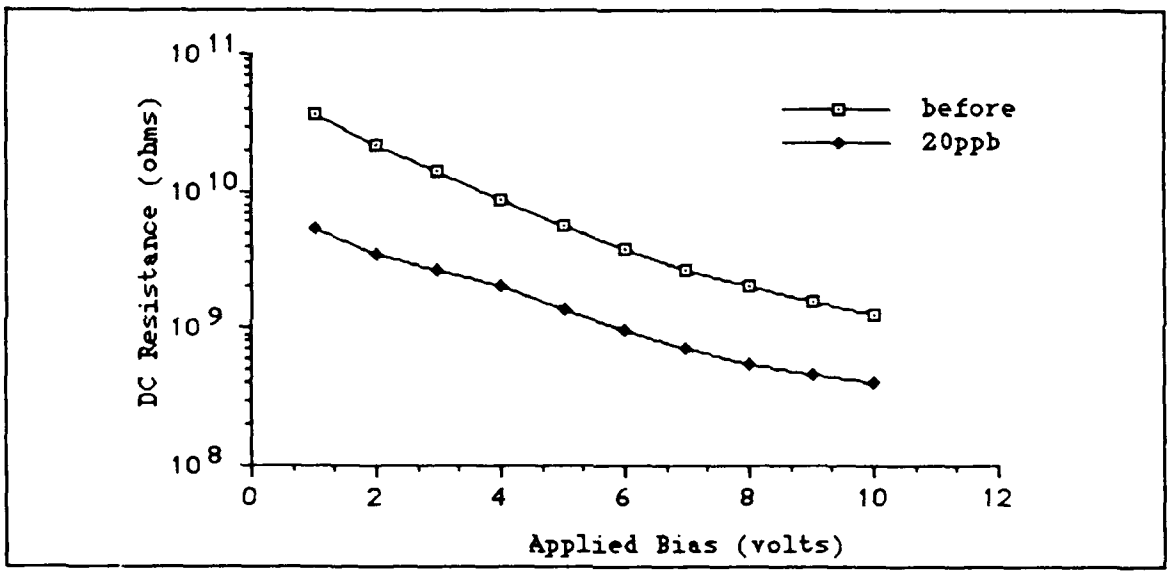

Figure V-15. DC Resistance of Chem1 (Cobalt-Doped Phthalocyanine) with Respect to Applied Bias and Challenge with NO_2 (30° C).

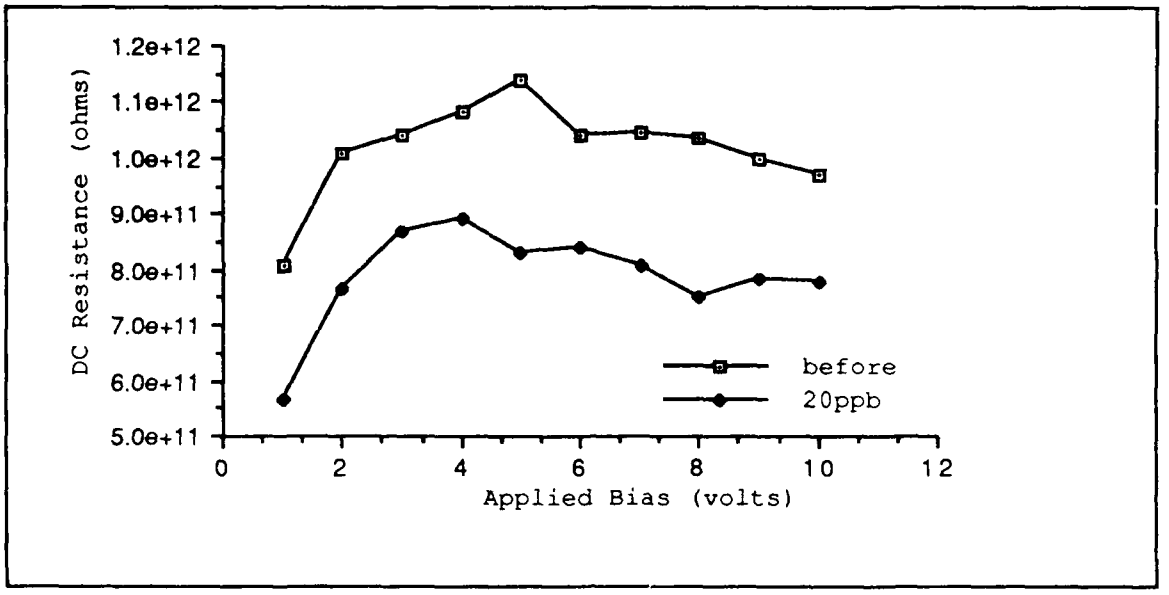

Figure V-16. DC Resistance of Chem2 (Lead-Doped Phthalocyanine) with Respect to Applied Bias and Challenge with NO_2 (30° C).

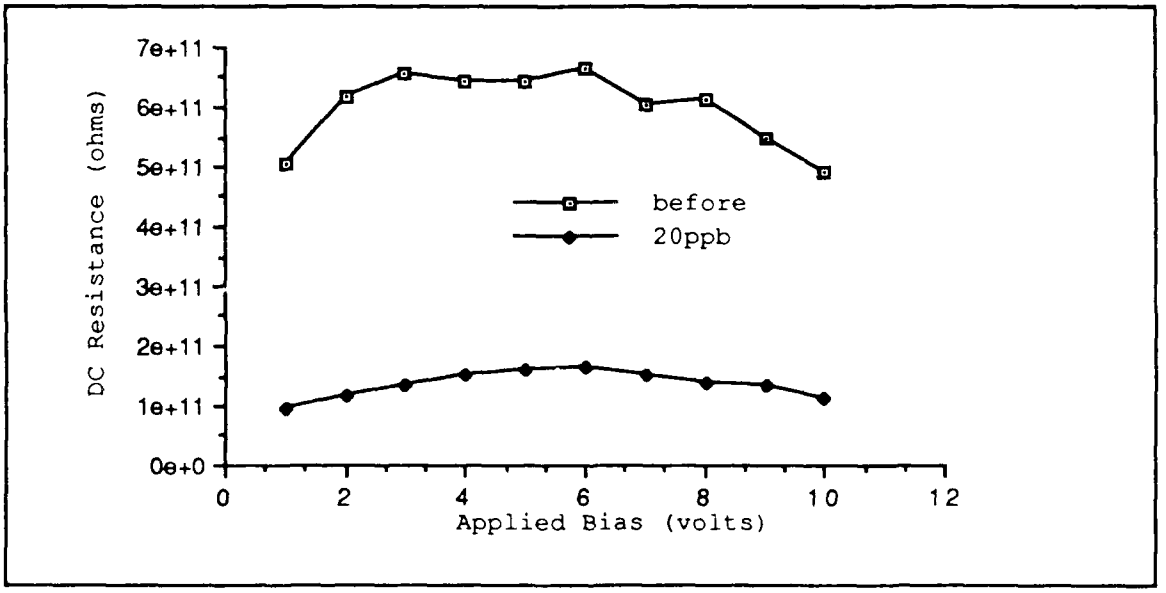

Figure V-17. DC Resistance of Chem3 (Nickel-Doped Phthalocyanine) with Respect to Applied Bias and Challenge with NO_2 (30° C).

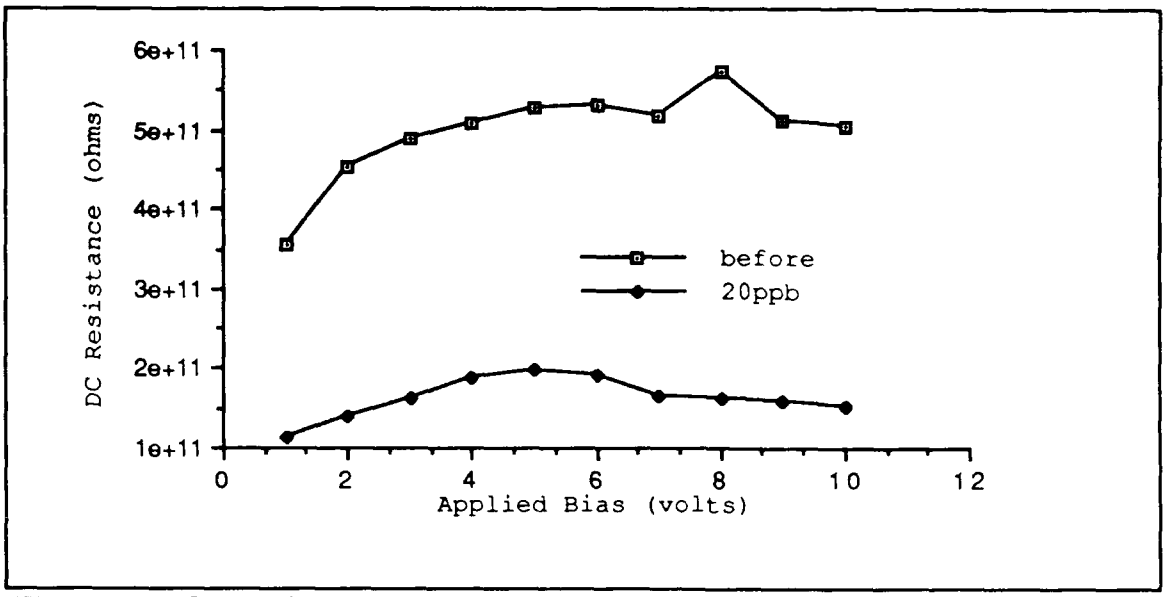

Figure V-18. DC Resistance of Chem4 (Copper-Doped Phthalocyanine) with Respect to Applied Bias and Challenge with NO_2 (30° C).

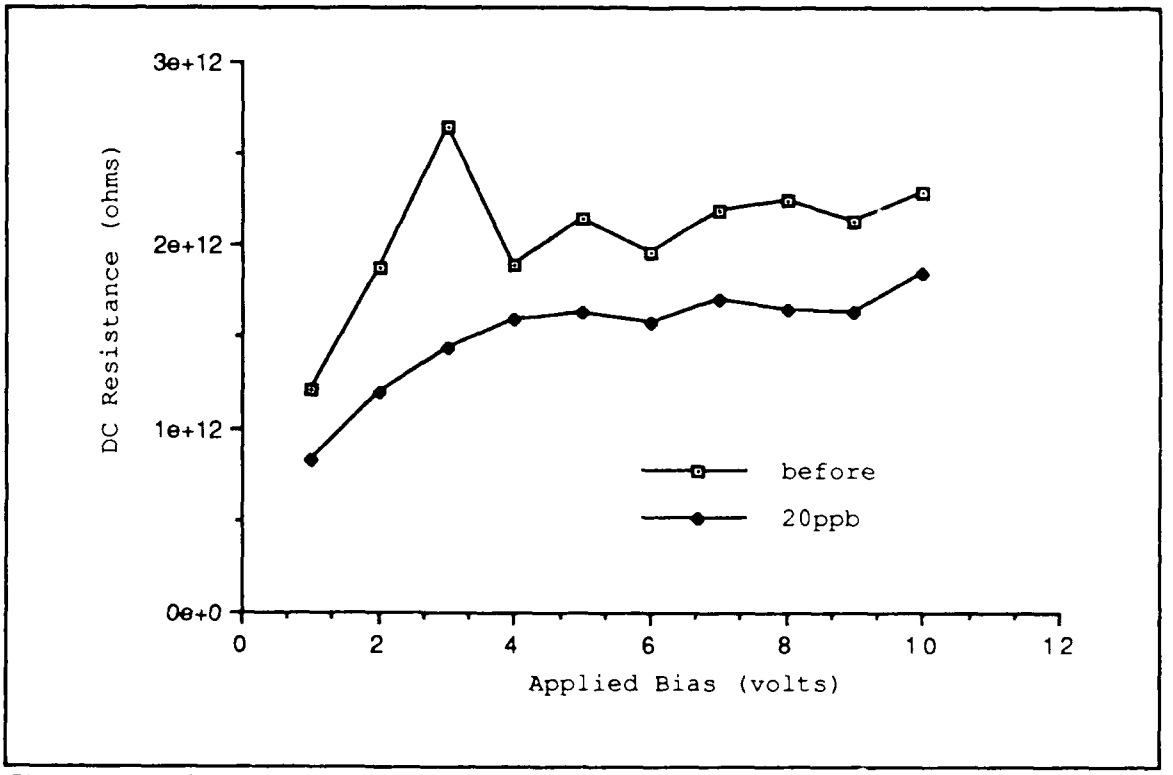

Figure V-19. DC Resistance of Chem6 (Undoped Phthalocyanine) with Respect to Applied Bias and Challenge with NO_2 (30° C).

When the AC impedance of the coated interdigitated electrode structure was measured as a function of the challenge gas concentration, the magnitude and phase were recorded. The real and imaginary values of impedance were then computed. Figures V-20 through V-23 represent examples of the AC impedance for Chem1 (cobalt-doped phthalocyanine) when challenged with 20 ppb of NO_2 (3% relative humidity; 30° C).

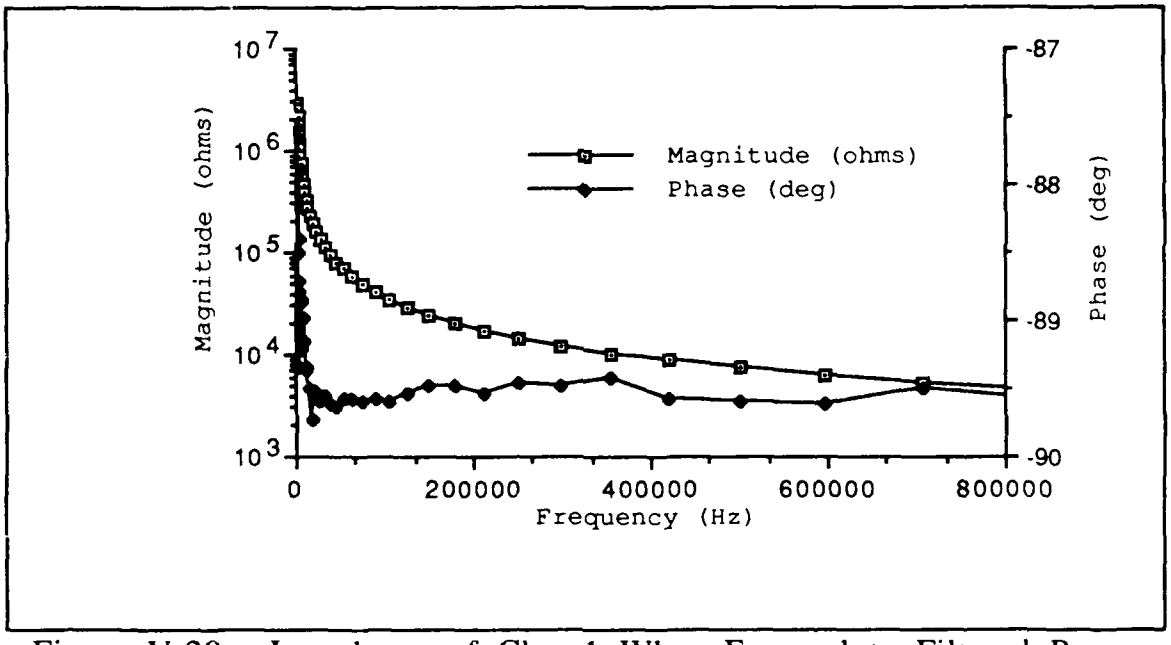

Figure V-20. Impedance of Chem1 When Exposed to Filtered Room Air (3% relative humidity; 30° C).

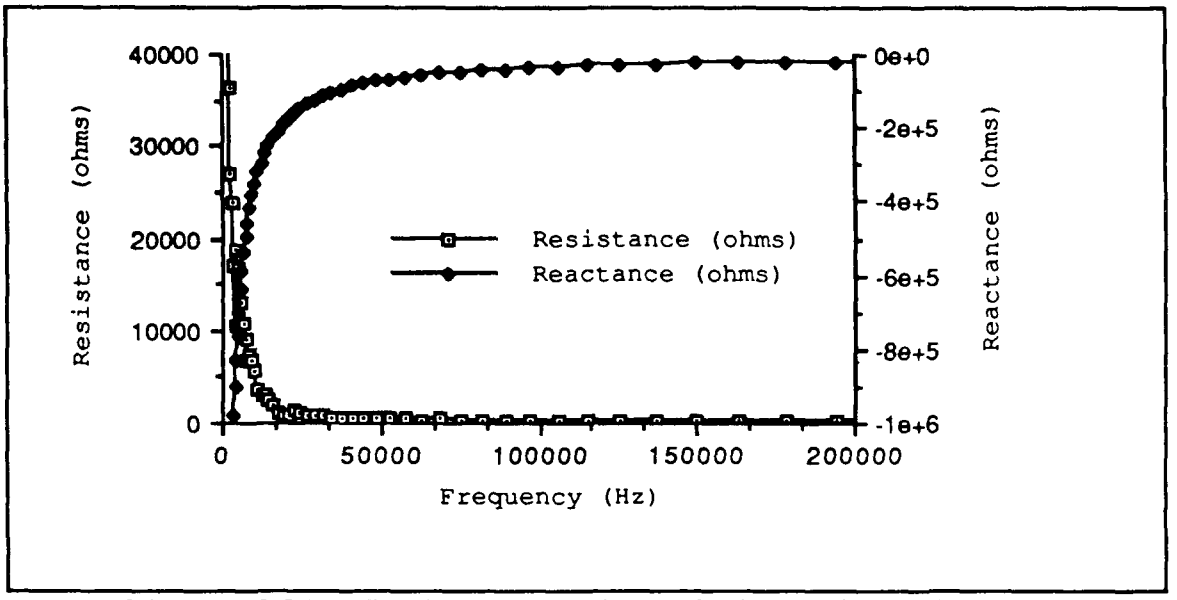

Figure V-21. Real and Imaginary Values of the Impedance of Chem1 When Exposed to Filtered Room Air (3% relative humidity; 30° C).

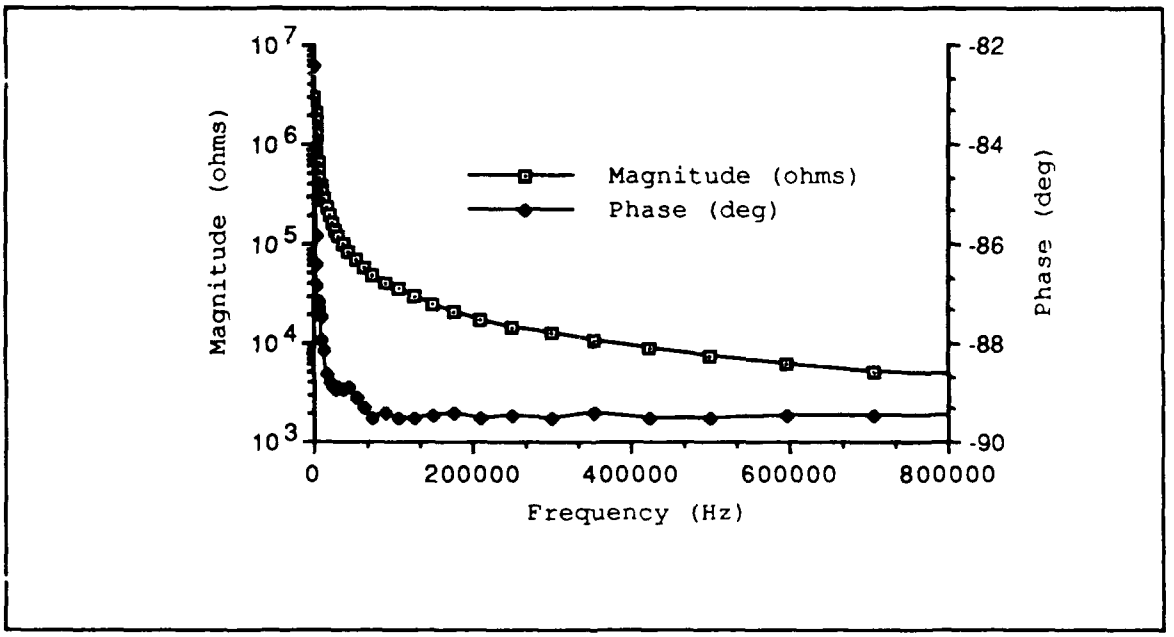

Figure V-22. Impedance of Chem1 When Exposed to 20 ppb of NO_2 (3% relative humidity; 30° C).

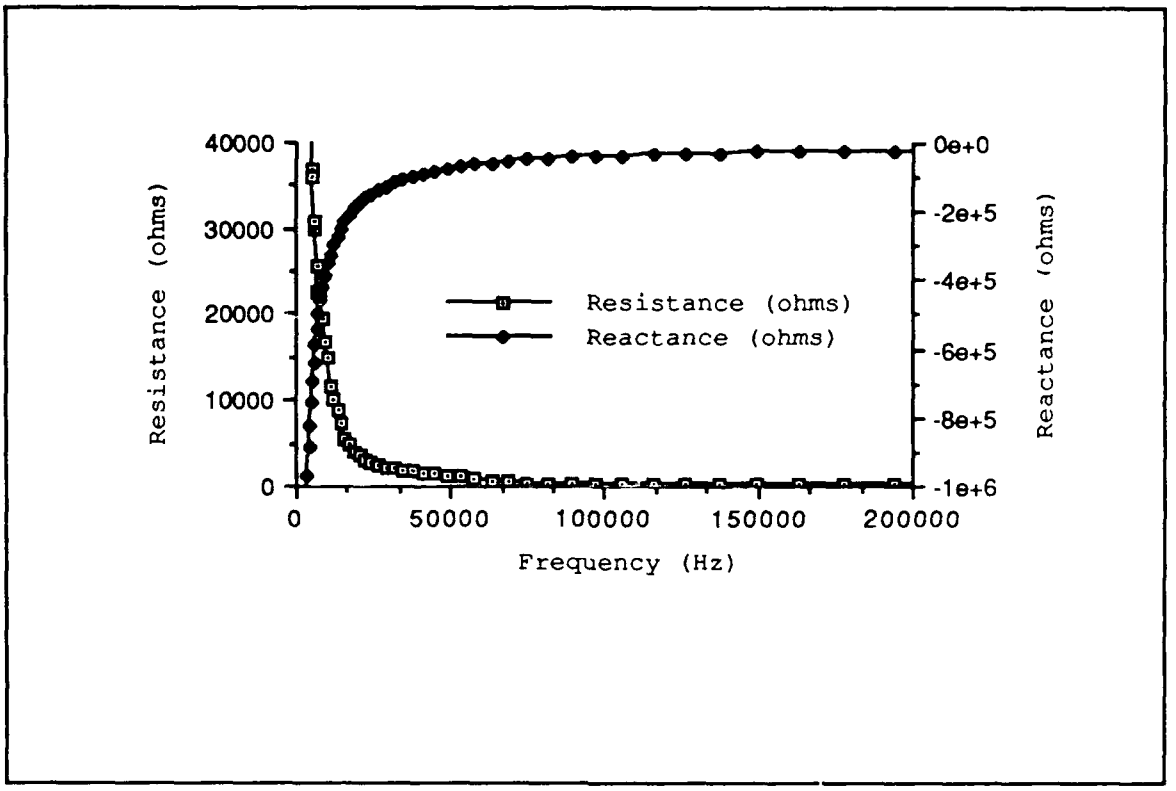

Figure V-23. Real and Imaginary Values of the Impedance of Chem1 When Exposed to 20 ppb of NO_2 (3% relative humidity; 30° C).

To facilitate the analysis of the AC impedance data, Figures V-24 through V-29 were generated where the percent change of the impedance's magnitude and phase is plotted. For example, the percent change of the magnitude of the AC impedance was calculated by subtracting the filtered air response from the challenge gas response and then dividing by the filtered air response. This result was then multiplied by 100.

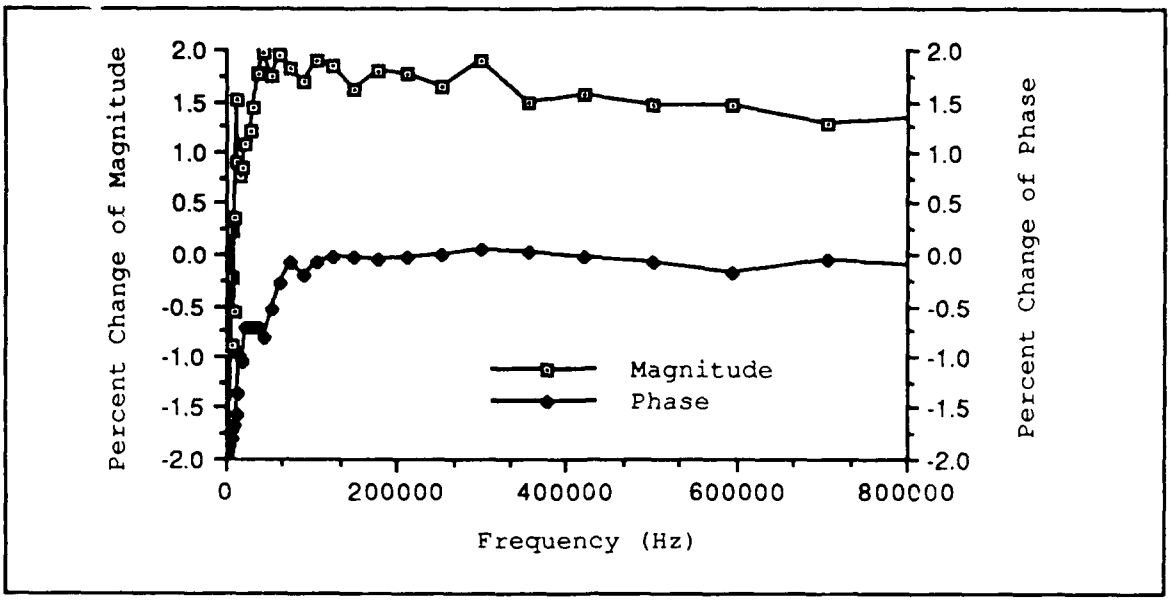

Figure V-24. Percent Change of the Impedance of Chem1 When Exposed to 20 ppb of NO_2 (3% relative humidity; 30° C).

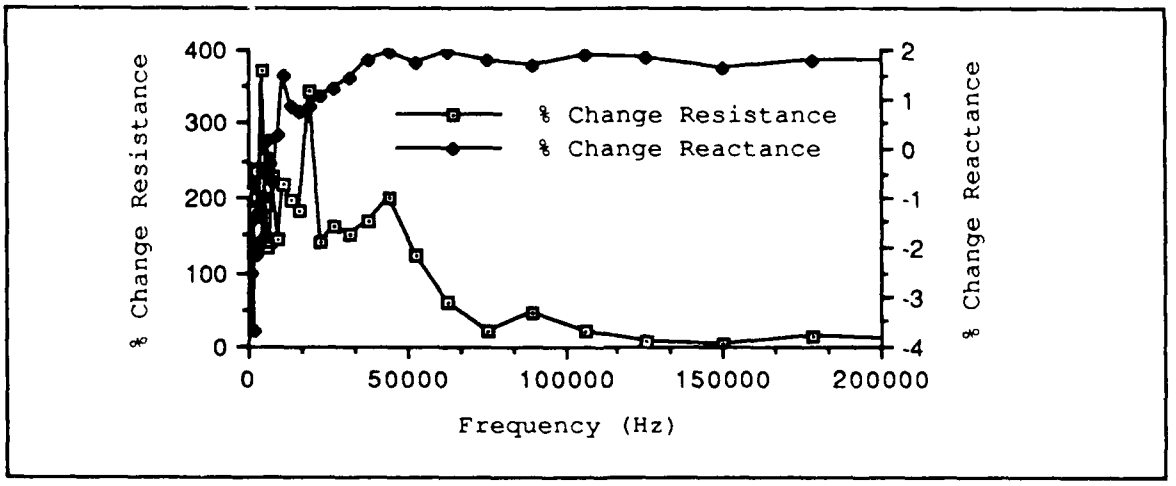

Figure V-25. Percent Change of the Impedance (Real and Imaginary Parts) of Chem1 When Exposed to 20 ppb of NO_2 (3% relative humidity; 30° C).

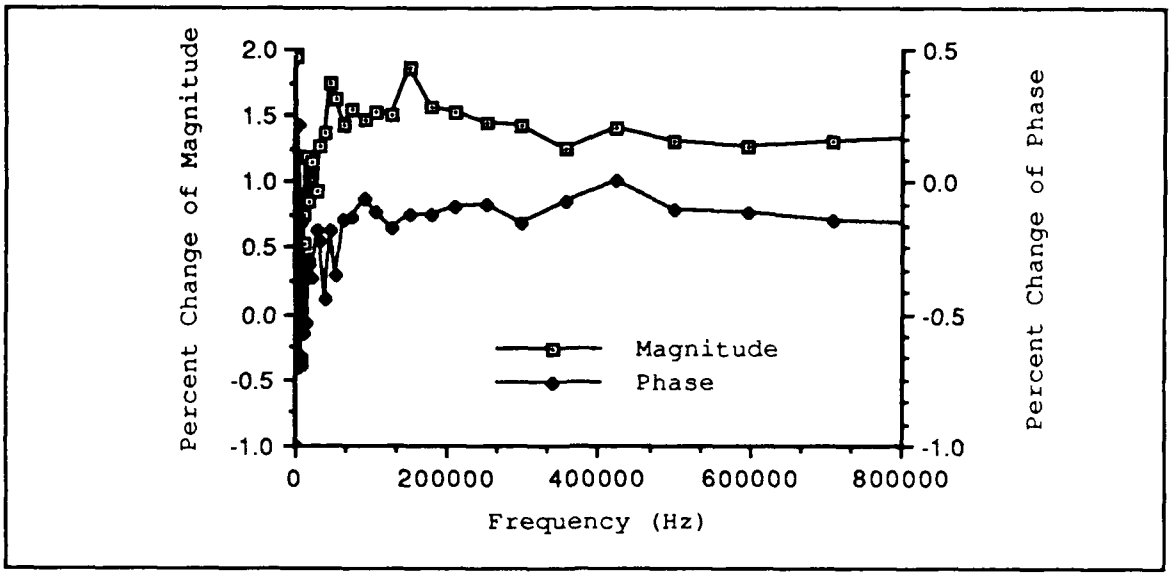

Figure V-26. Percent Change of the Impedance of Chem2 When Exposed to 20 ppb of NO_2 (3% relative humidity; 30° C).

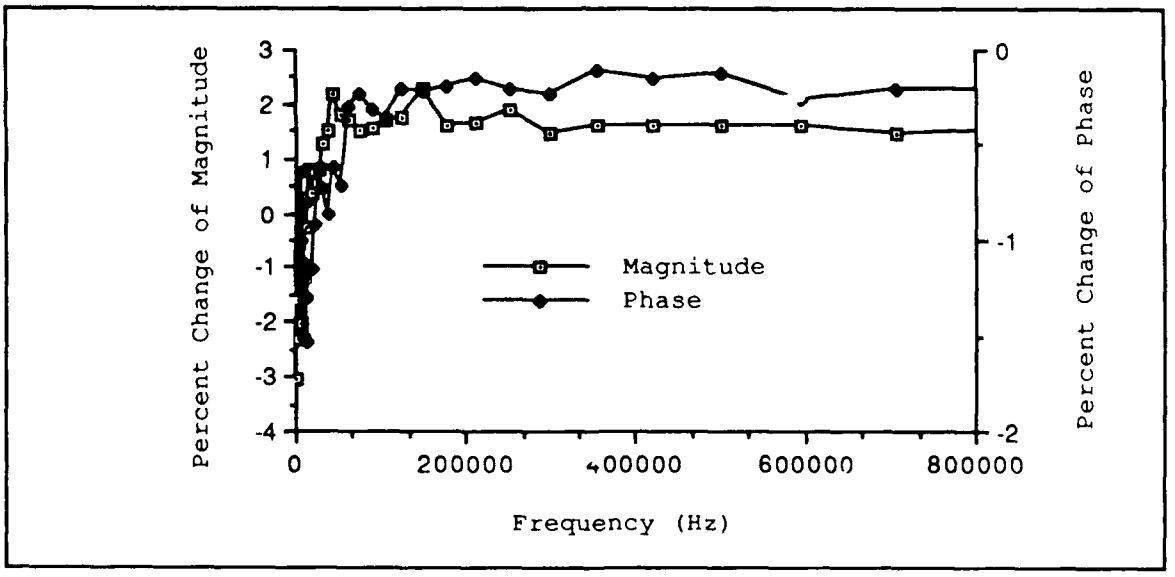

Figure V-27. Percent Change of the Impedance of Chem3 When Exposed to 20 ppb of NO_2 (3% relative humidity; 30° C).

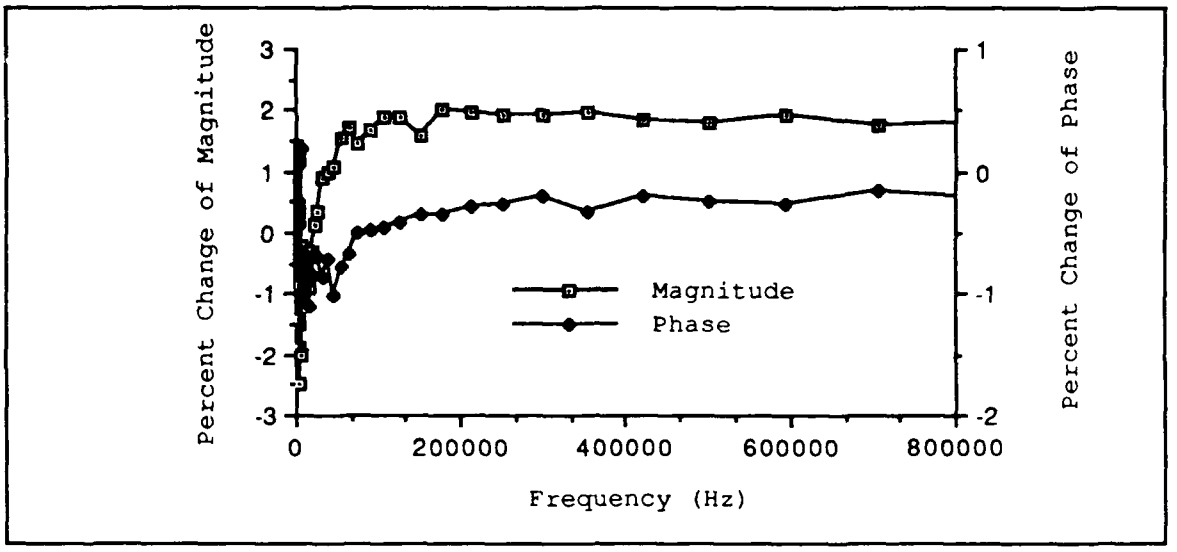

Figure V-28. Percent Change of the Impedance of Chem4 When Exposed to 20 ppb of NO_2 (3% relative humidity; 30° C).

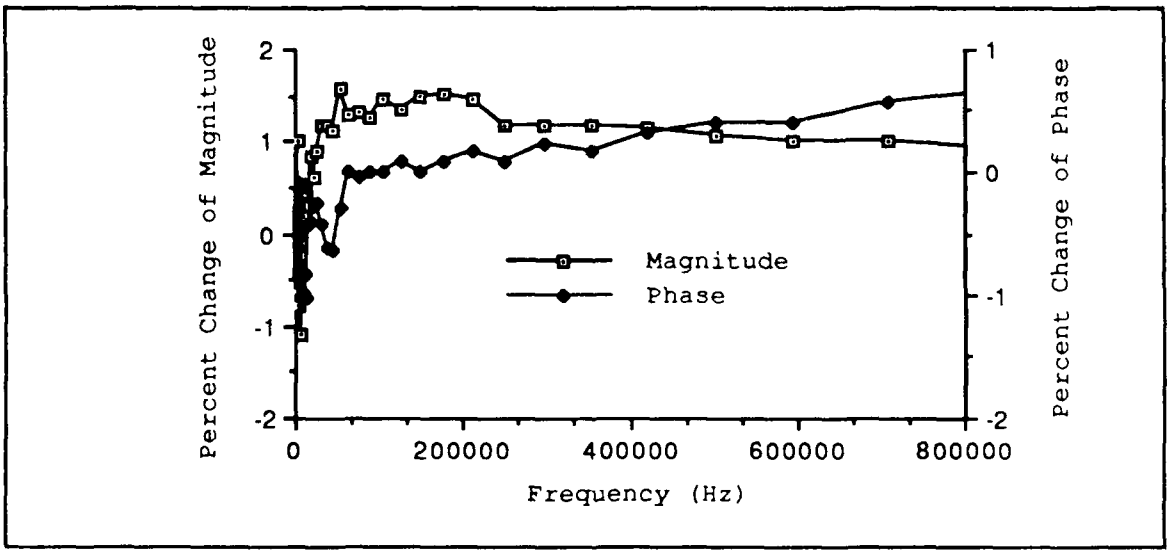

Figure V-29. Percent Change of the Impedance of Chem6 When Exposed to 20 ppb of NO_2 (3% relative humidity; 30° C).

In the next series of plots, Figures V-30 through V-34 summarize the percent change of the AC impedance magnitude associated with the interdigitated gate electrode structures at 30° C as a function of the challenge gas concentration (NO_2).

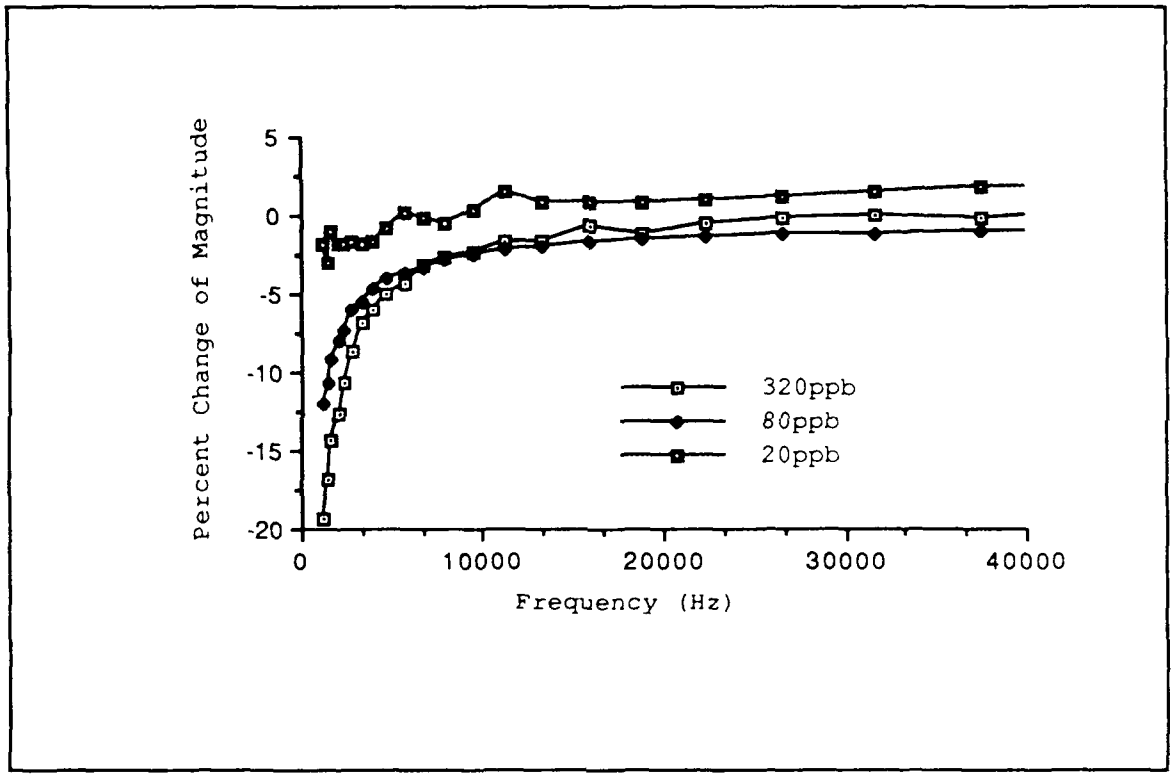

Figure V-30. Percent Change of the AC Impedance of Chem1 With Respect to the NO_2 Challenge Concentration (3% relative humidity; 30° C).

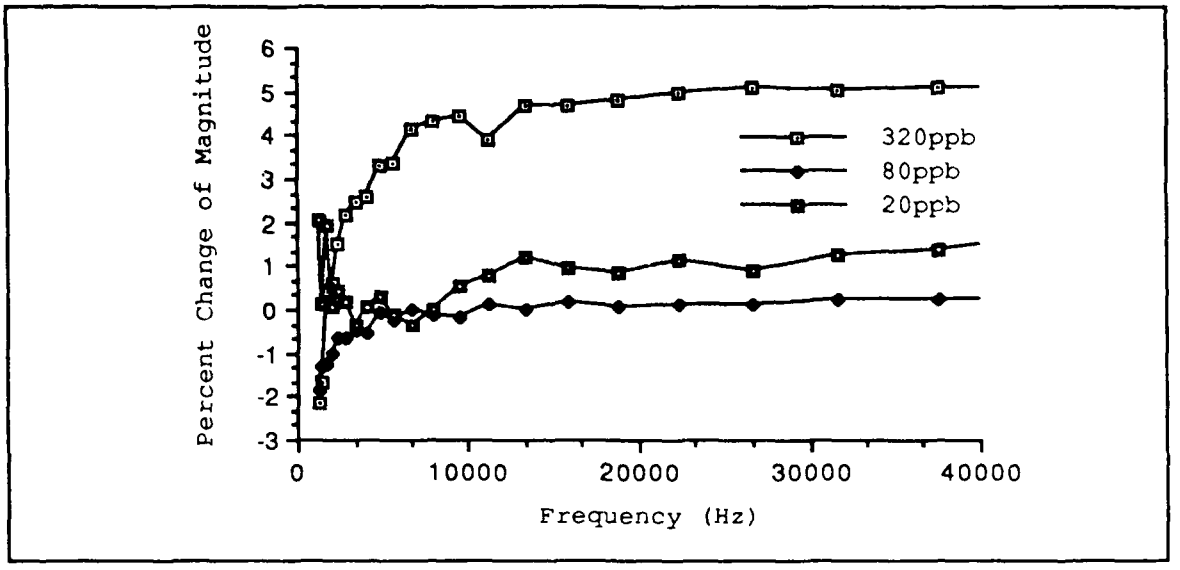

Figure V-31. Percent Change of the AC Impedance of Chem2 With Respect to the NO_2 Challenge Concentration (3% relative humidity; 30° C).

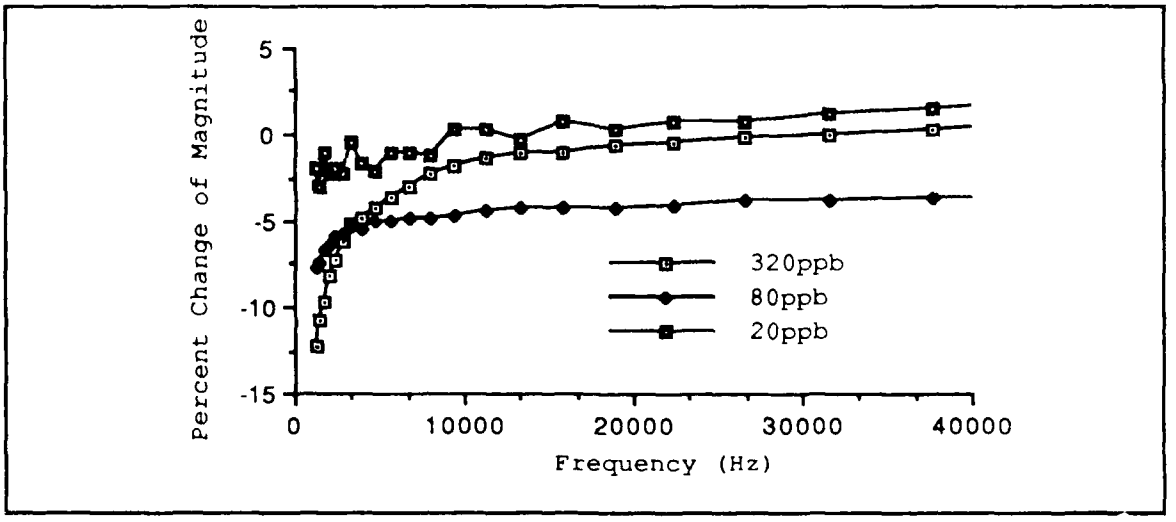

Figure V-32. Percent Change of the AC Impedance of Chem3 With Respect to the NO_2 Challenge Concentration (3% relative humidity; 30° C).

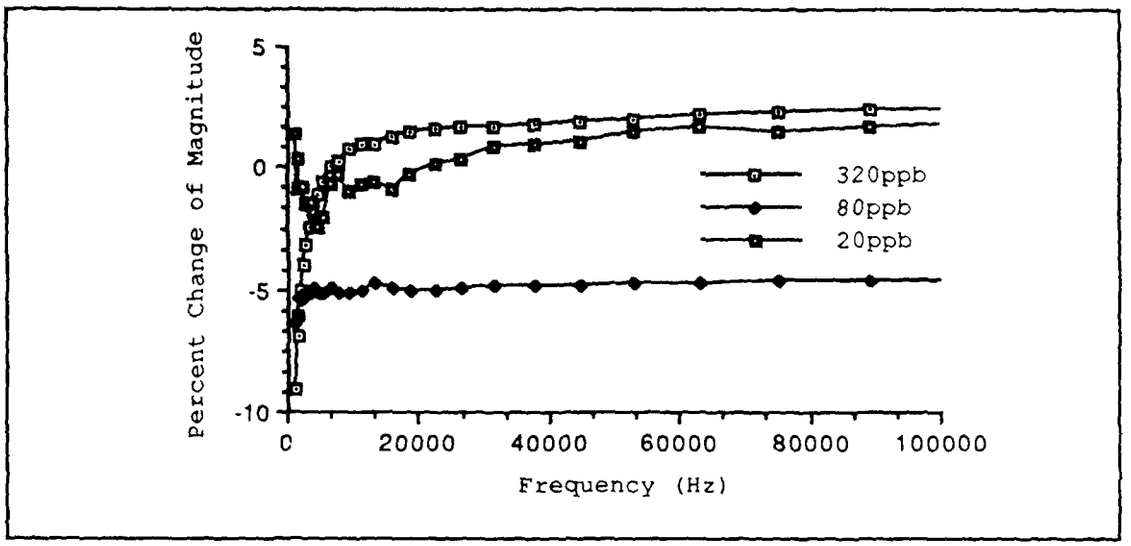

Figure V-33. Percent Change of the AC Impedance of Chem4 With Respect to the NO_2 Challenge Concentration (3% relative humidity; 30° C).

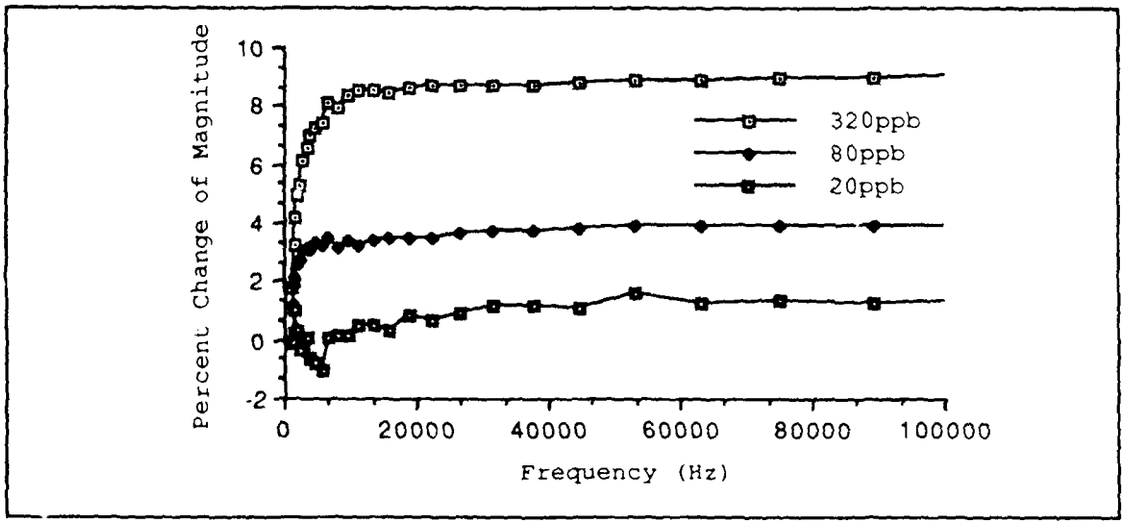

Figure V-34. Percent Change of the AC Impedance of Chem6 With Respect to the NO_2 Challenge Concentration (3% relative humidity; 30° C).

The transfer function of the microsensor was measured for each element of the array, as well. However, when the supply voltages were applied to the microsensor integrated circuit to accomplish this task, the amplifiers failed. Upon inspection, broken bond wires within the DIP cavity were discovered. The extent of the damage was such that some wires were crossed and others had formed bridging faults between V_{ss} and V_{dd}. After rebonding the DIP connections to the microsensor integrated circuit, all the amplifiers and the multiplexer tested as open circuits. Therefore, an instrumentation amplifier (Trig-Tek, Inc., Model 205B, Anaheim, CA) was substituted for the integrated amplifiers. Multiplexing the interdigitated gate electrode structures through the instrumentation amplifier was accomplished by manually connecting the instrumentation amplifier to each interdigitated gate electrode structure, in turn.

As previously discussed in Chapter IV, the transfer function of the interdigitated gate electrode was determined by a multi-step process. This process is not affected by the need to use an off-chip amplifier if the instrumentation amplifier is assumed to be as linear as the on-chip amplifiers. The results associated with the transfer function determination are presented in Figures V-35 through V-38. The relative humidity was less than 3% in all cases. Also, the operating temperature was maintained at 30^{o} C.

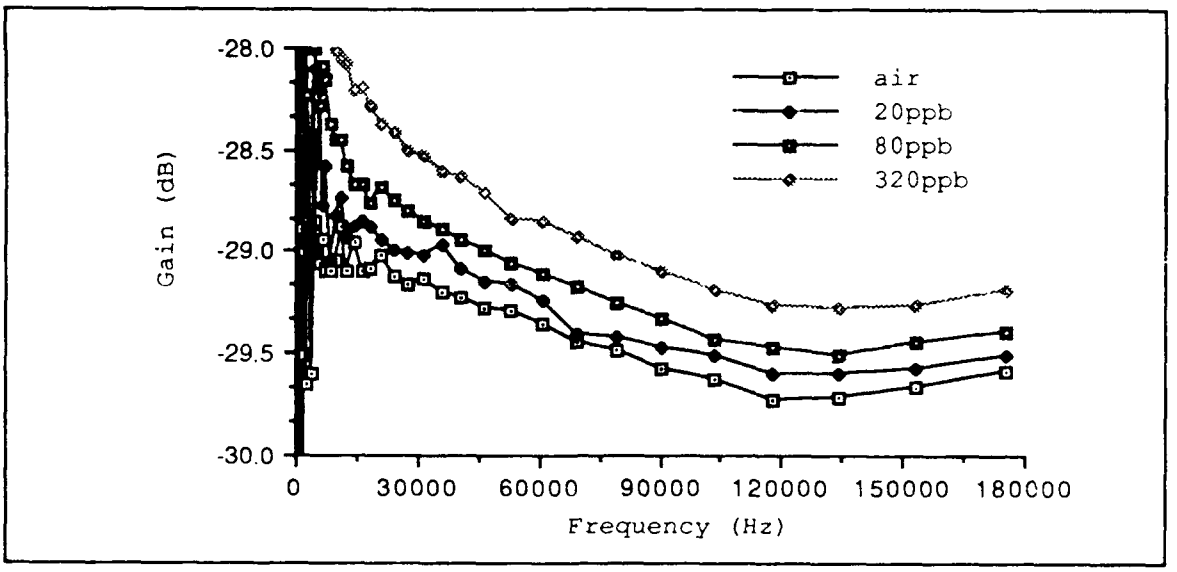

Figure V-35. Magnitude of the Transfer Function for Chem1 as a Function of the NO_2 Gas Concentration.

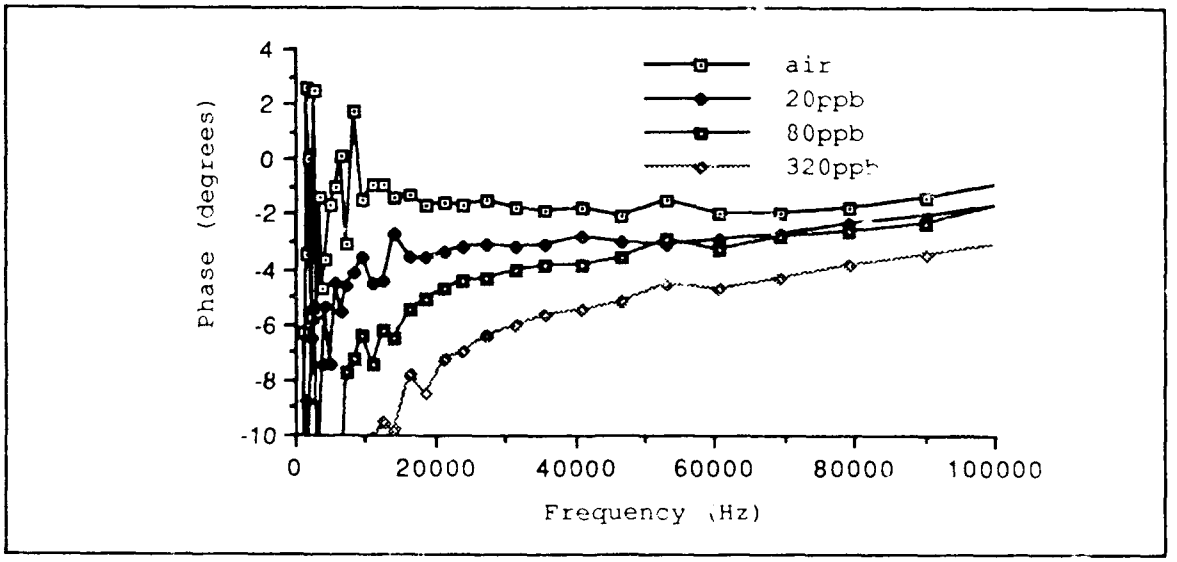

Figure V-36. Phase of the Transfer Function for Chem1 as a Function of the NO_2 Gas Concentration.

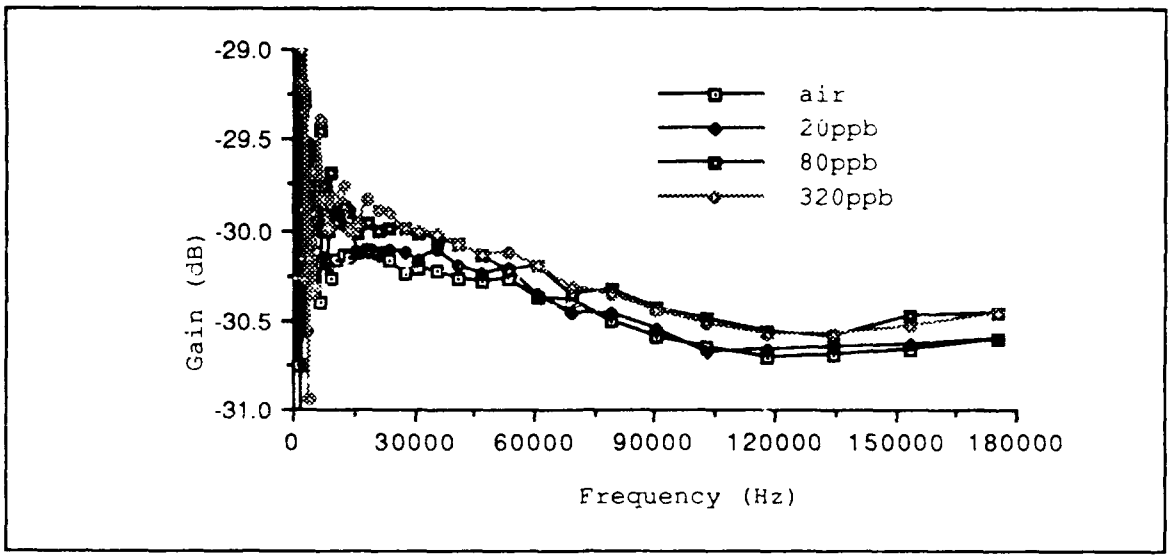

Figure V-37. Magnitude of the Transfer Function for Chem2 as a Function of the NO_2 Gas Concentration.

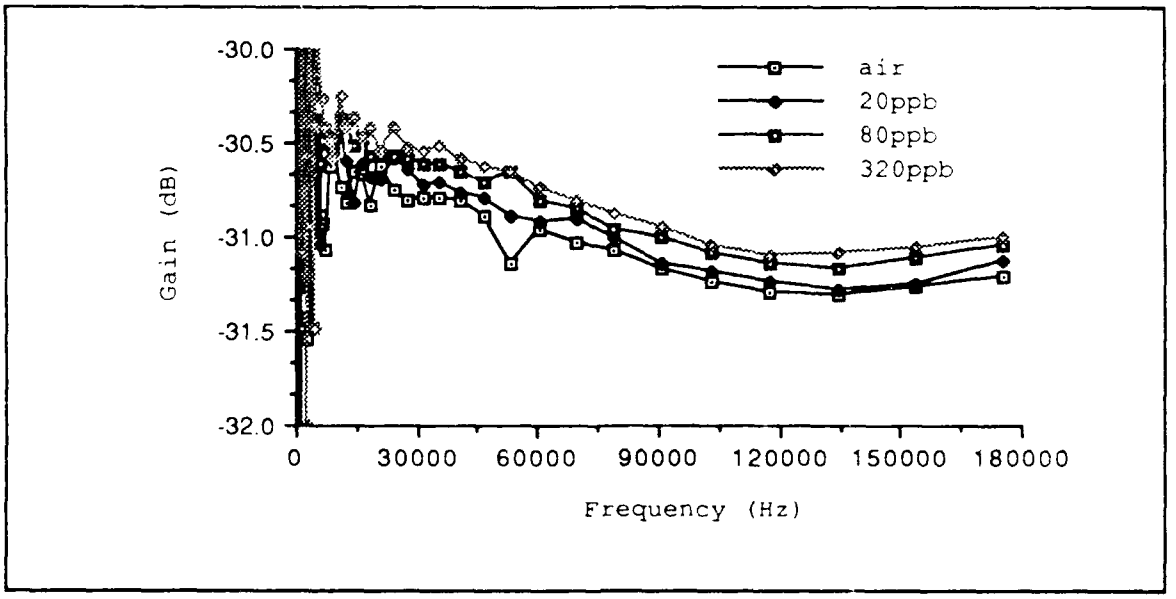

Figure V-38. Magnitude of the Transfer Function for Chem6 as a Function of the NO_2 Gas Concentration.

The response of the microsensor fabricated with Die1 to a pulse excitation was measured in the frequency-domain as a spectral response. The interdigitated electrodes were driven from bond pad 64 with a voltage pulse (2-nanosecond pulse width, 1-millisecond period, and a 5-volt amplitude). The signal that was coupled to the floating gate portion of each interdigitated gate electrode was then amplified with the instrumentation amplifier. Next, the amplified signal was input to the spectrum analyzer.

The parameters of the excitation signal used for this measurement were empirically found by adjusting the amplifier's gain and the pulse generator's output. Since the spectral response of the amplifier and pulse generator are subtracted from the measured spectral response of the microsensor, the most desirable characteristic of the combined amplifier and pulse generator response is a constant power level throughout the measured frequency band. This combined response corresponds to the product $[g(\omega)A(\omega)]$ in equation (4.1) as defined in Figure IV-19. The empirically specified spectrum of the amplified pulse generator signal is depicted in Figure V-39.

The spectral responses of Chem1 in the frequency domain are presented in Figures V-40 through V-44 to demonstrate the data reduction method. In Figure V-40, the spectral response of the amplified Chem1 signal while challenged with filtered room air is presented. This data was then manipulated by the techniques discussed in Chapter IV to remove the product $[g(\omega)A(\omega)]$ to produce Figure V-41. The process is repeated again for Chem1 challenged

with 20 ppb of NO_2 [3% relative humidity (RH); 30° C]. This process is depicted in Figures V-42 and V-43. In Figure V-44, the final normalization of the spectral response is depicted. In this Figure, the challenge gas spectral response is normalized with respect to the equivalent filtered room air response. Hence, this process yields a double normalization of the spectral response in the frequency-domain.

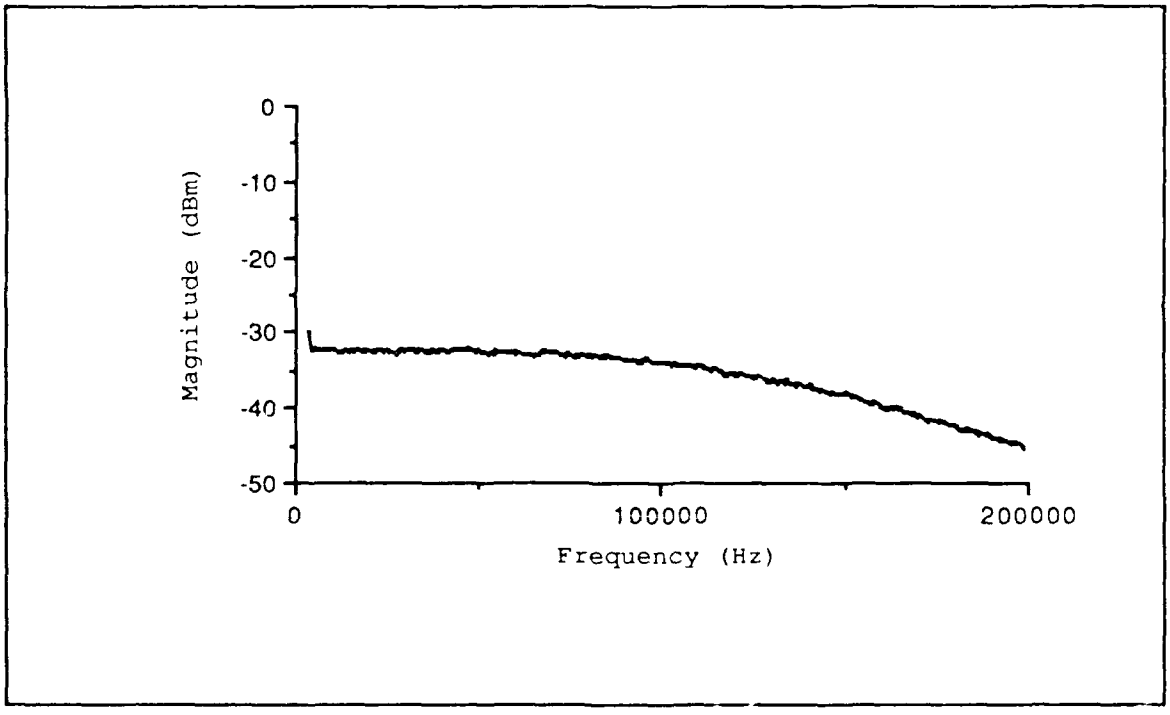

Figure V-39. Spectrum of the Amplified Pulse Generator Signal.

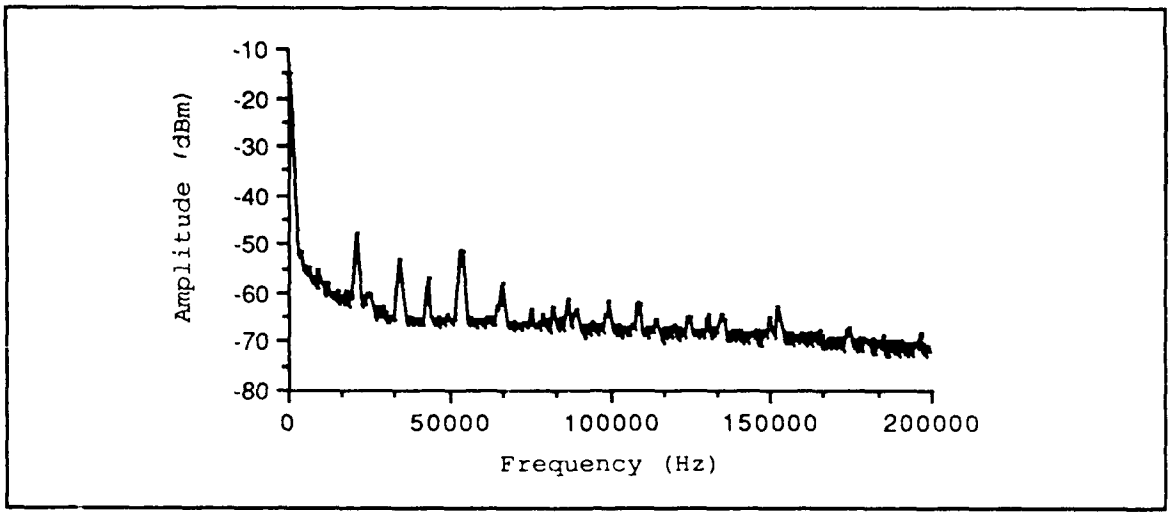

Figure V-40. Spectral Response of Chem1 When Exposed to Filtered Room Air (3% RH; 30° C).

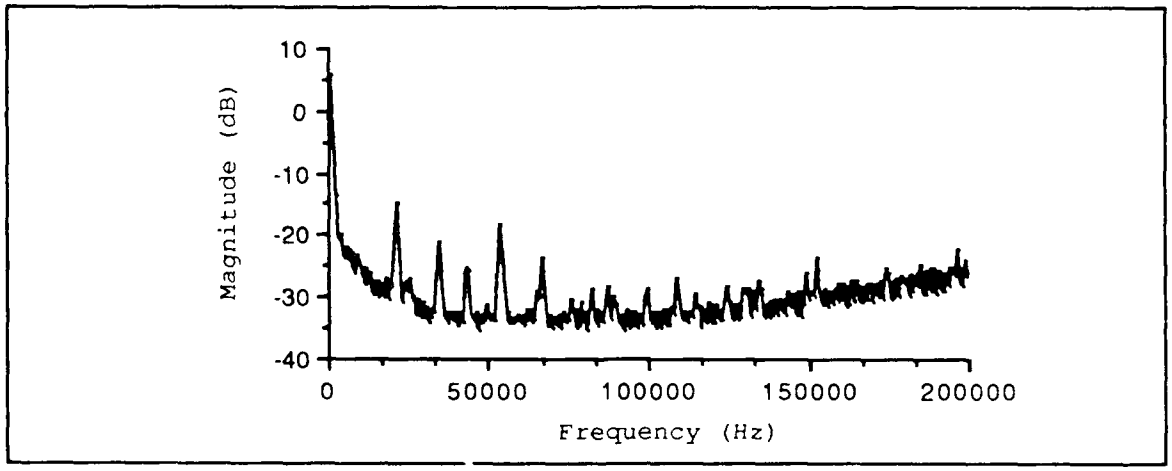

Figure V-41. Normalized Spectral Response of Chem1 When Exposed to Filtered Room Air (3% RH; 30° C).

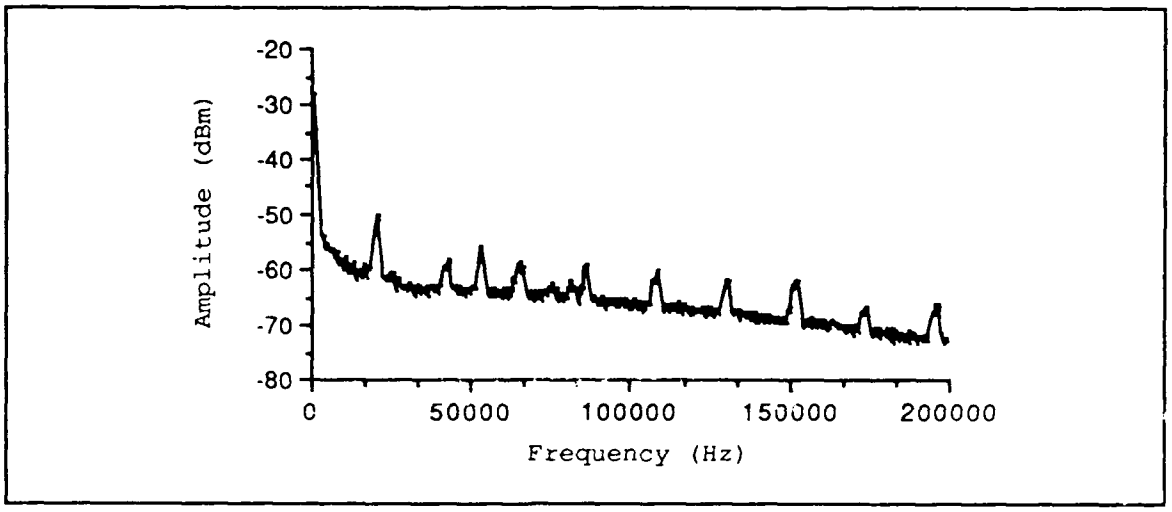

Figure V-42. Spectral Response of Chem1 When Challenged with 20 ppb of NO_2 (3% RH; 30° C).

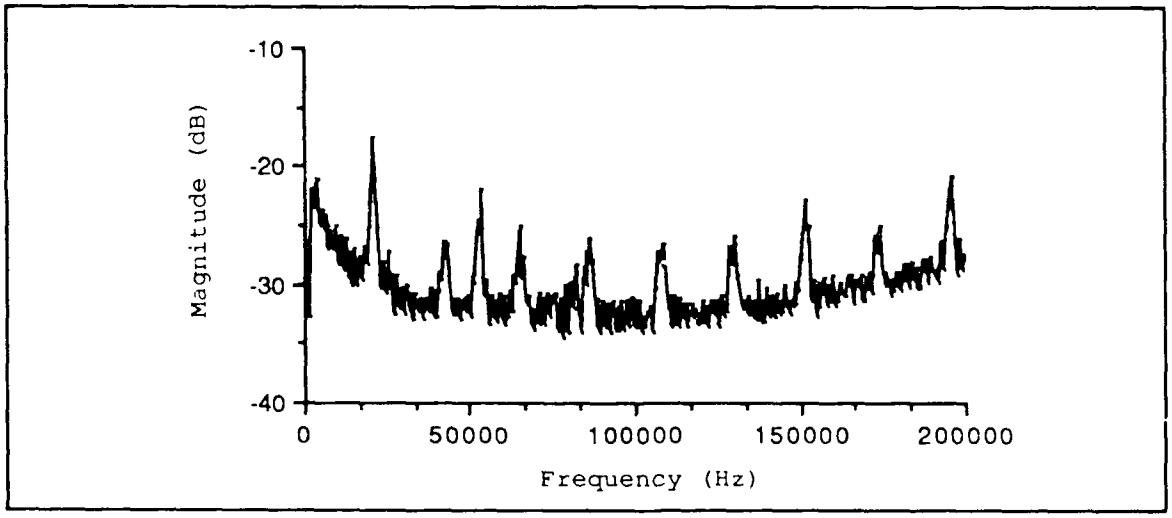

Figure V-43. Normalized Spectral Response of Chem1 When Challenged with 20 ppb of NO_2 (3% RH; 30° C).

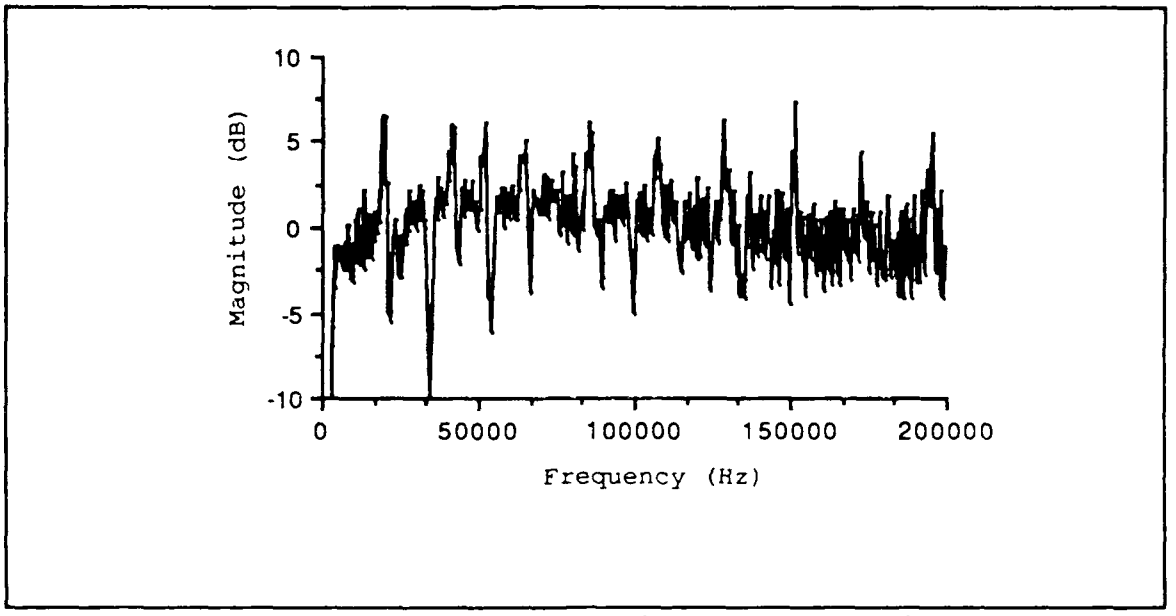

Figure V-44. Double Normalization of Chem1 When Challenged with 20 ppb of NO_2 (3% RH; 30° C).

The spectral response in the frequency-domain of Chem1 while challenged with 80 ppb and 320 ppb of NO_2 (3% RH; 30° C) is depicted in Figures V-45 and V-46. A similar spectral response in the frequency-domain was observed for all the materials that were studied. The spectral peaks appear to shift and diminish. However, additional techniques will have to be developed to correlate the observed response with gas concentration or type. As depicted in Figure V-47, the discrimination of challenge gas concentration may be facilitated with spectral data at the lower frequencies.

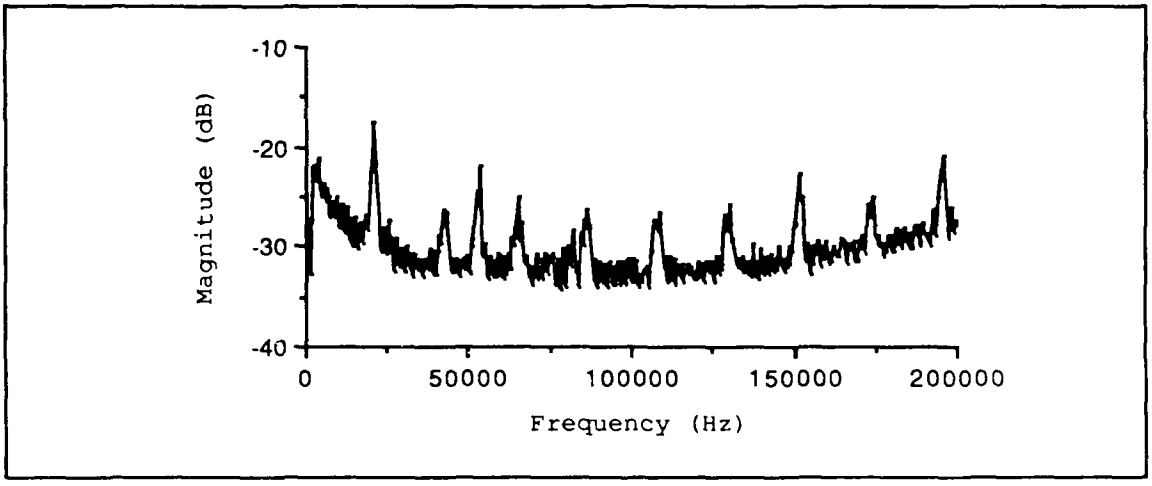

Figure V-45. Normalized Spectral Response of Chem1 When Challenged with 80 ppb of NO_2 (3% RH; 30° C).

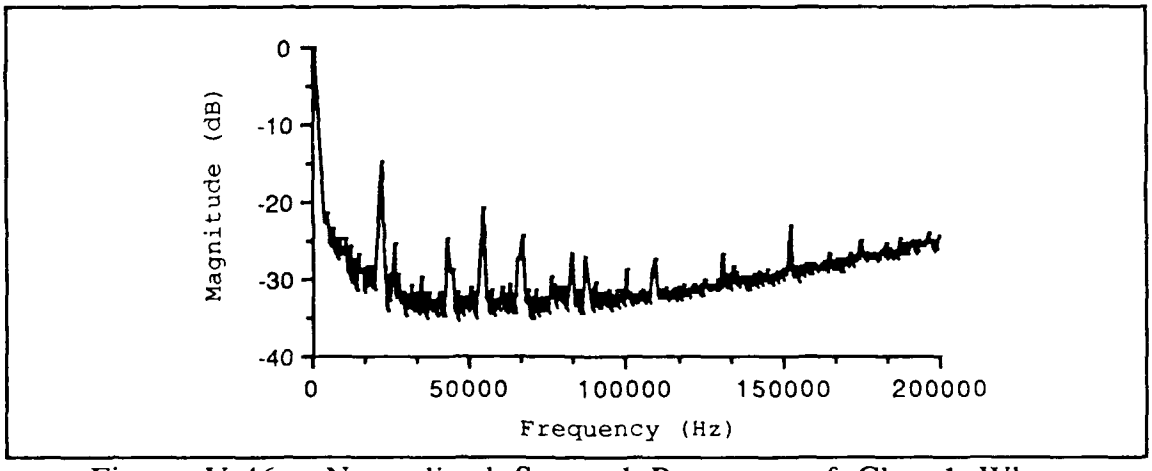

Figure V-46. Normalized Spectral Response of Chem1 When Challenged with 320 ppb of NO_2 (3% RH; 30° C).

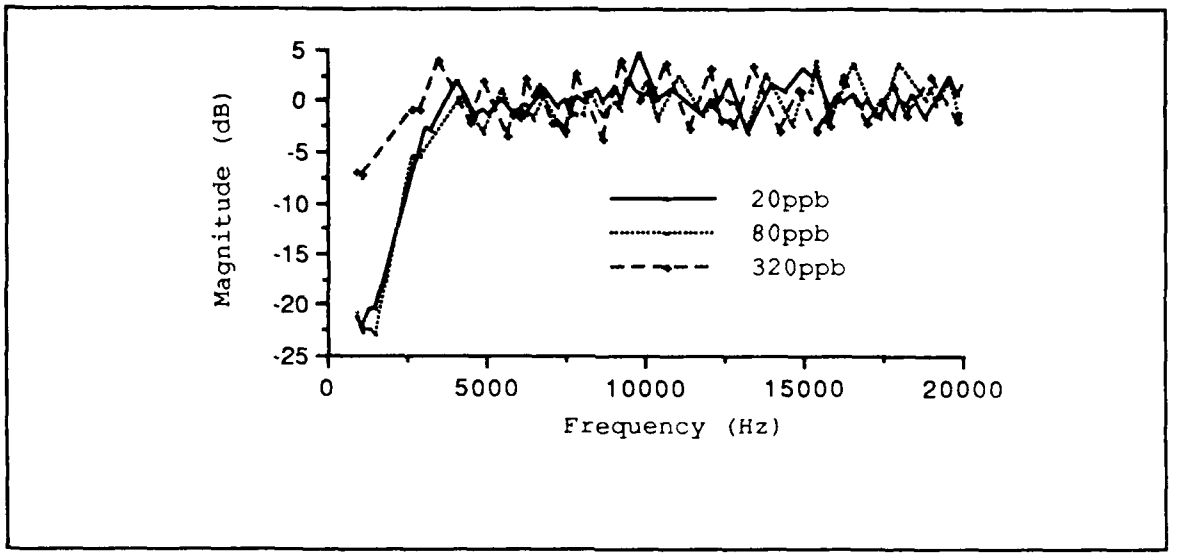

Figure V-47. Double Normalization of Chem4 as a Function of the Concentration of NO_2 (3% RH; 30° C).

The pulse response of the microsensor was measured in the time-domain. A voltage pulse was used to excite the driven gate (bond pad 64) of the microsensor's sensing elements. The electrical response of the individual floating gates were coupled into the instrumentation amplifier. The amplified signal was then measured on the digitizing oscilloscope, as discussed in Chapter IV. The excitation voltage pulse had a ±1 volt peak amplitude, 1 KHz period, and a 50% duty cycle. The instrumentation amplifier was used to amplify the response 20 times (AC gain). The initial electrical response of the sensing elements to filtered room air (3% RH; 30° C) is depicted in Figures V-48 and V-49.

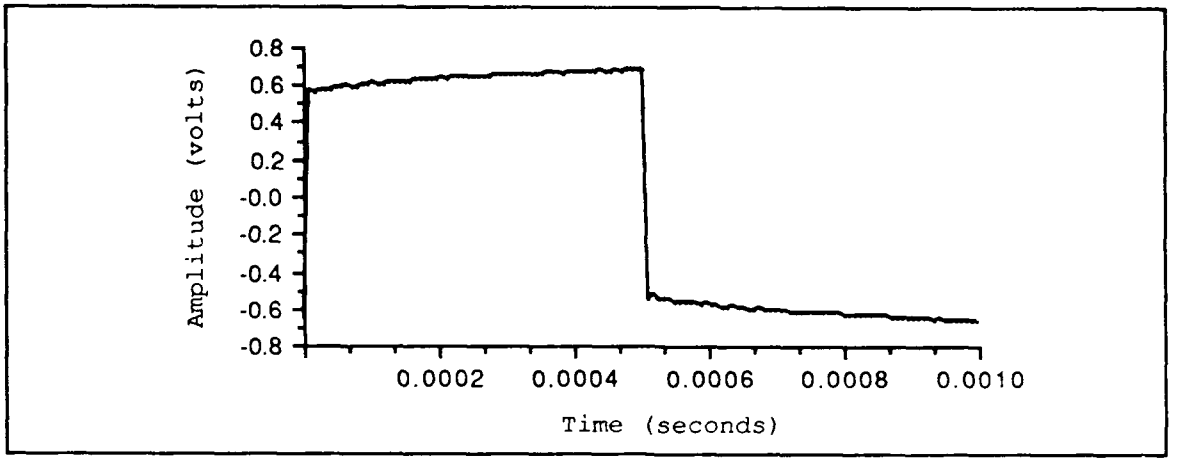

Figure V-48. Initial Pulse Response in the Time-Domain for Chem1 Exposed to Filtered Room Air.

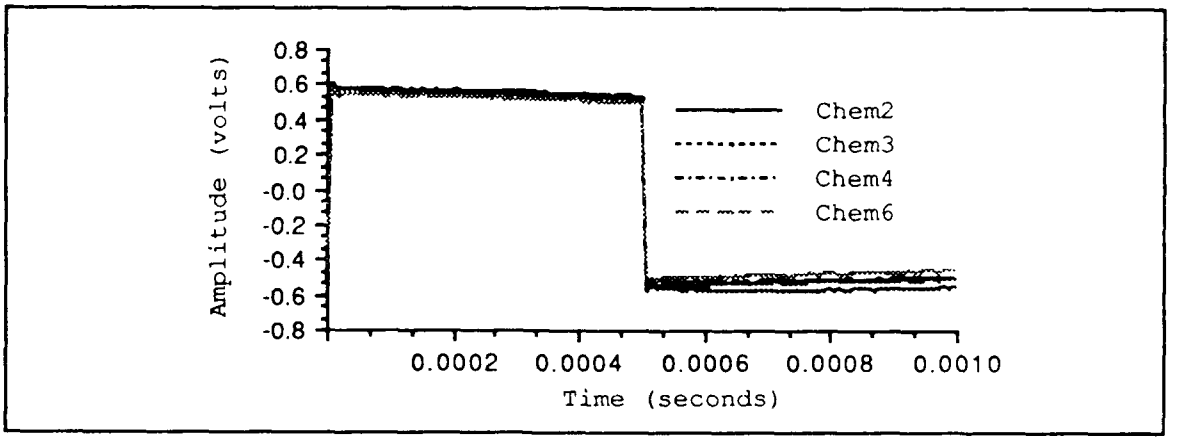

Figure V-49. Initial Pulse Response in the Time-Domain for Chem2, Chem3, Chem4, and Chem6 Exposed to Filtered Room Air.

As depicted in the Figures V-48 and V-49, the initial pulse response in the time domain is similar for the lead-doped, nickel-doped, copper-doped, and undoped phthalocyanines. The electrical

response when challenged with 20 ppb of NO_2 (3% RH; 30° C) is depicted in Figures V-50 and V-51.

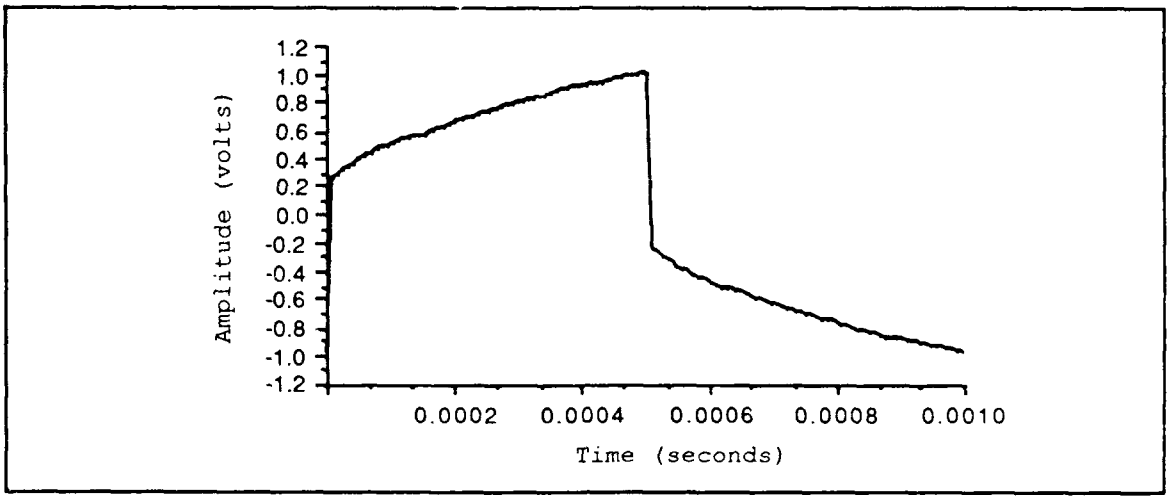

Figure V-50. Pulse Response in the Time Domain of Chem1 When Challenged with 20 ppb of NO_2 (3% RH; 30° C).

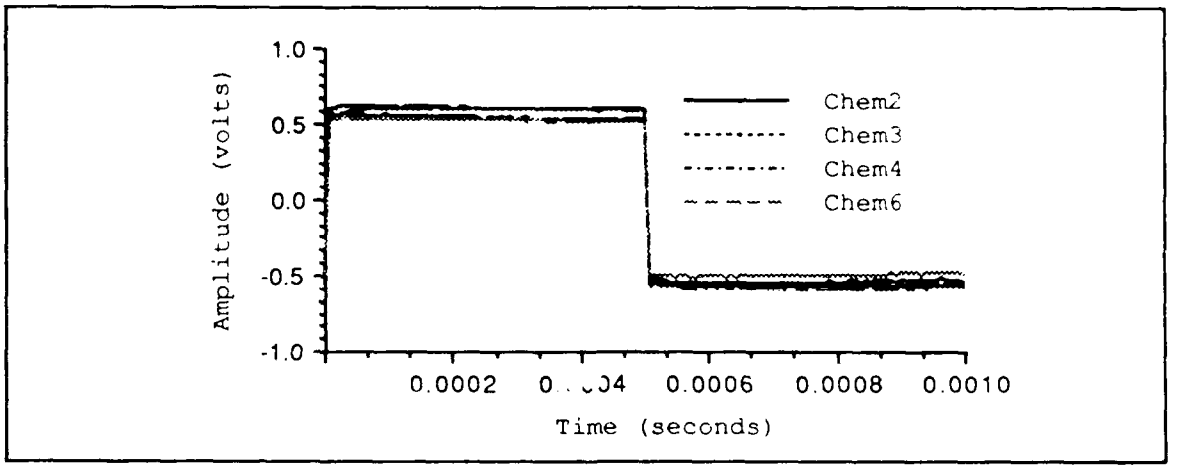

Figure V-51. Pulse Response in the Time Domain of Chem2, Chem3, Chem4, and Chem6 When Challenged with 20 ppb of NO_2 (3% RH; 30° C)

From Figures V-50 and V-51, the electrical response of the cobalt-doped phthalocyanine is evidently different from the other materials when challenged with NO_2. Specifically, the percent difference is illustrated in Figure V-52. In this figure, the percent difference between the time-domain pulse response corresponding to filtered room air and 20 ppb of NO_2 is depicted for Chem1 and Chem2. The same data for Chem3, Chem4, and Chem6 is summarized in Figure V-53 (Chem2 is depicted in both figures to facilitate the comparison).

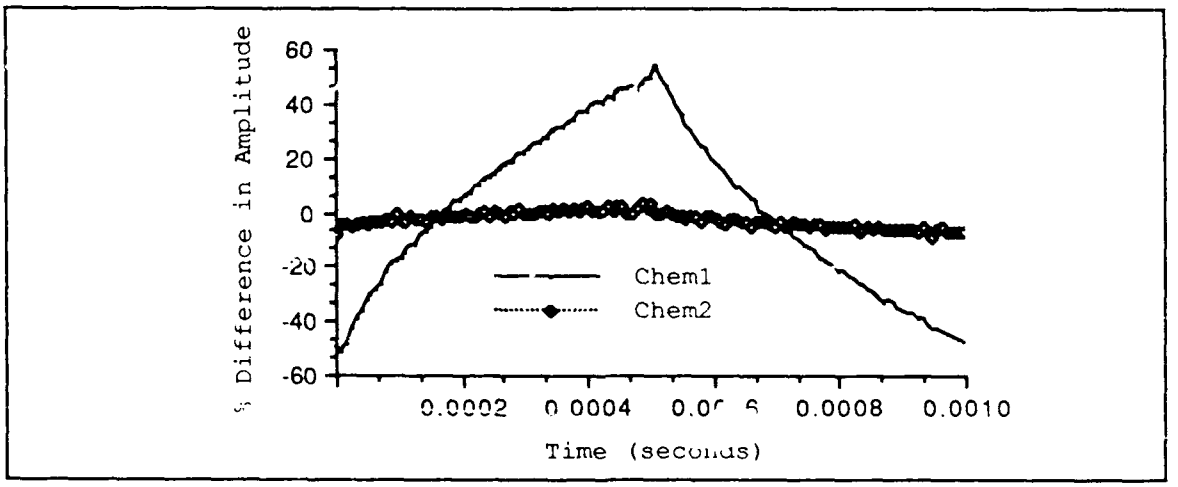

Figure V-52. Percent Difference of the Time-Domain Pulse Response for Chem1 and Chem2 with a Challenge of 20 ppb of NO_2 Using the Response to Filtered Room Air as the Reference.

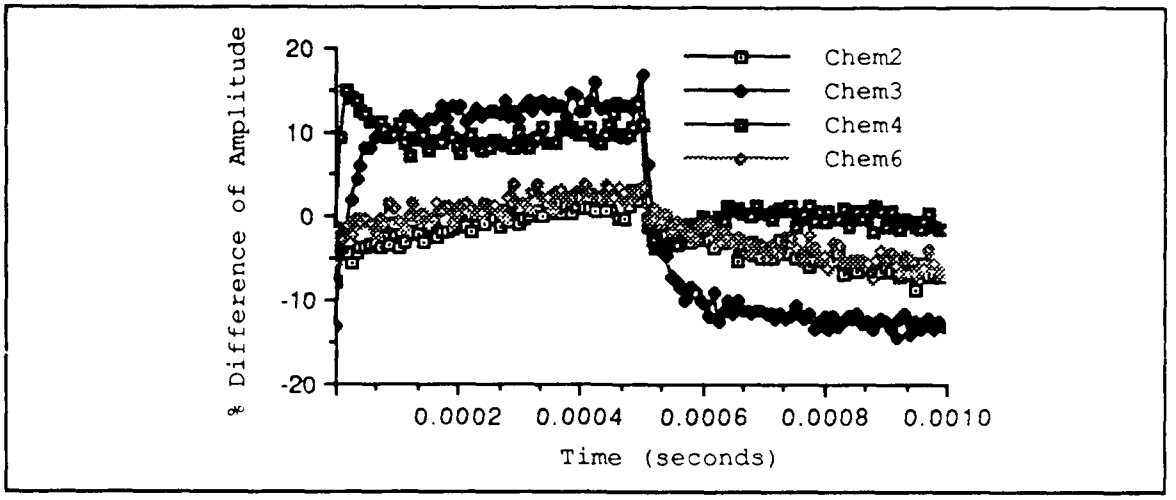

Figure V-53. Percent Difference of the Time-Domain Pulse Response for Chem2, Chem3, Chem4, and Chem6 with a Challenge of 20 ppb of NO_2 Using the Response to Filtered Room Air as the Reference.

Using Figures V-52 and V-53, the phthalocyanine thin films could be ranked by their sensitivity to NO_2. The order of the ranking from most to least sensitive is cobalt-, nickel-, copper-, and lead-doped phthalocyanine, with undoped phthalocyanine being the least sensitive.

The time-domain pulse response of Chem1 is summarized in Figure V-54 as a function of the concentration of the NO_2 (3% RH; 30° C). This data correlates with the previous DC resistance data corresponding to Chem1. As the DC resistance decreases, the magnitude of the pulse that is transmitted through the interdigitated gate electrode will be attenuated to a lessor degree.

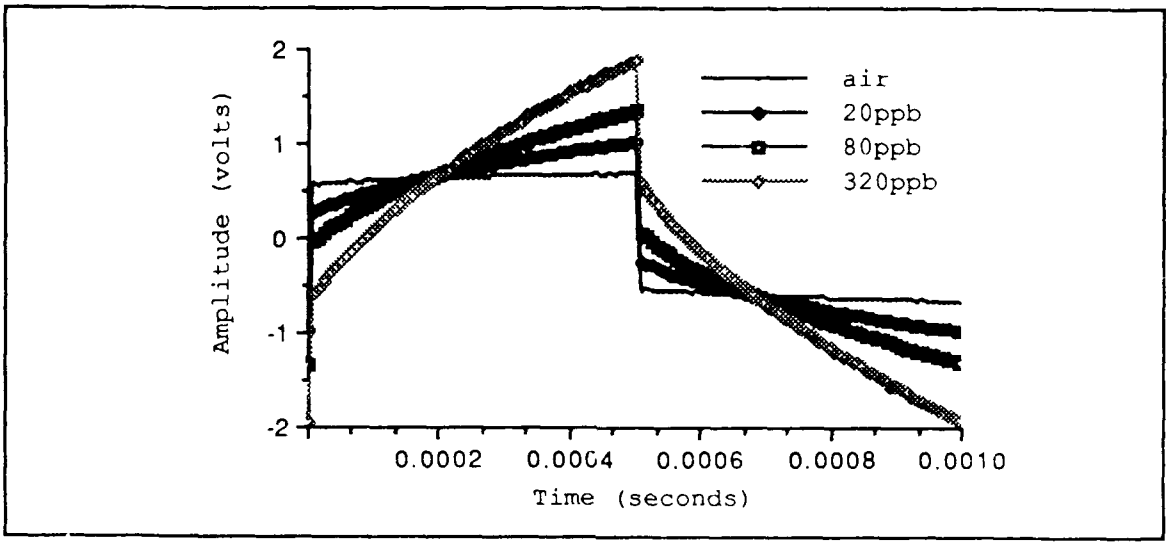

Figure V-54. Time-Domain Pulse Response of Chem1 as a Function of the Concentration of NO_2 (3% RH; 30° C).

After the standard set of measurements were completed, the test cell was purged with filtered room air. The electrical response of the microsensor was monitored to determine the reversibility of the microsensor. In Figure V-55, the reversibility of the sensing elements is depicted. The time-domain pulse response was measured before the challenge with 20 ppb of NO_2 (3% RH; 30° C), and after the purge with filtered room air. The purge measurement was made after approximately 45 minutes of purging. The percent difference of the time-domain pulse response was computed using the initial filtered room air as the reference.

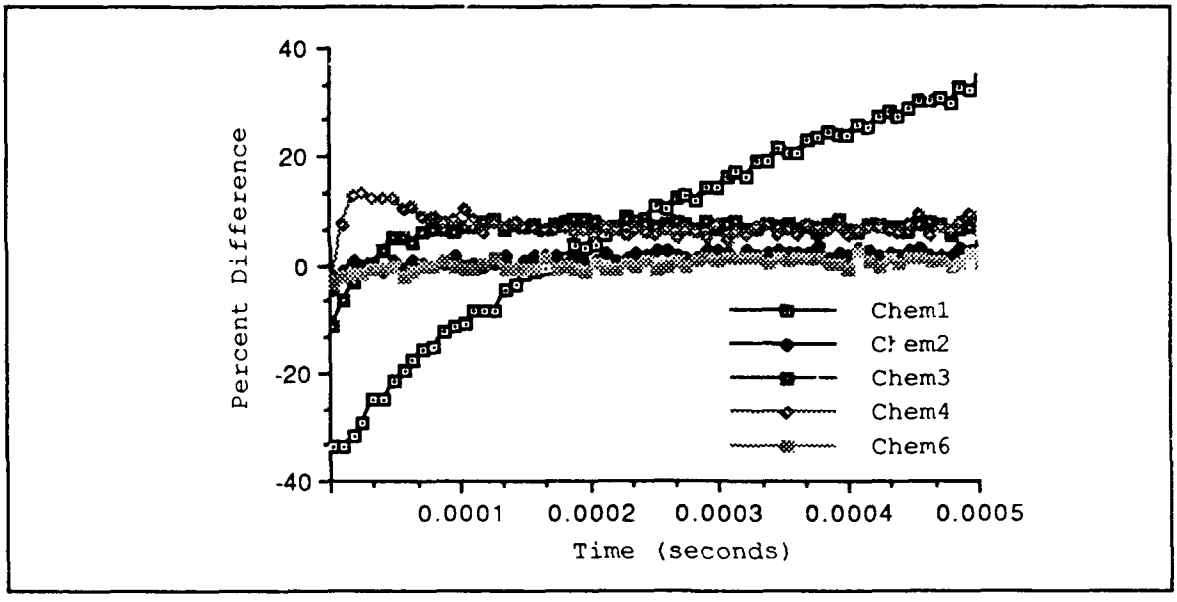

Figure V-55. A Measure of the Reversibility of the Microsensor after Approximately 45 Minutes of Purge (3% RH; 30° C).

Figure V-55 does not truly rank the reversibility for a significant reason. The method used to determine the reversibility failed to account for the lack of the sensitivity of the respective materials. The least sensitive material would appear to be the most reversible since the corresponding electrical response changed very little when challenged by the test gas. For example, if a particular material had no sensitivity, then the initial value should equal the challenged value which, in turn, should equal the purge value. Hence, the computed difference used to determine the reversibility should equal zero. However, for reversibility to be defined in a practical sense, reversibility should imply that sensitivity exists.

To ensure that the microsensor was reversed to a common initial state before each test gas challenge, a specific purge process

was developed. The process uses a heat treatment process to fully reverse the materials. In addition, this process facilitates the comparison of the electrical responses corresponding to the different test gas concentrations by ensuring a common initial state. The process is addressed in the following section concerning bake-out effects.

Bake-out Effects.

While collecting data for this research, the effects produced by changing the operating temperature of the microsensor were observed. To better quantify these effects, a specific procedure was designed. In general, the procedure involved initially challenging the microsensor with a known concentration of the challenge gas to induce a change in the pulse response with respect to time. Next, the challenge gas flow was terminated, and the test cell was purged with filtered room air. At this point, the operating temperature of the microsensor was elevated, and the microsensor's response was observed for a fixed period of time. This step was then followed by a lowering of the operating temperature to its initial value, and the pulse response with respect to time was recorded. A particular experiment is presented as a representative example.

After exposing the microsensor that was being operated at 30°C with a 20 ppb NO_2 challenge concentration at 5% relative humidity, the test cell was purged, and the microsensor temperature was elevated to 70°C for a duration of 60 minutes. This procedure was defined as the bake-out process. At the conclusion of the bake-out process, the temperature was decreased to 30°C. During the course

of the bake-out process, the pulse response of the microsensor in the initial state before gas exposure was found to be essentially realized (that is, the film's response is reversible).

In Figure V-56, the effect of the operating temperature was observed after 11 and at 60 minutes while the operating temperature was 70°C. This figure depicts how the pulse response gradually changed with respect to time during the bake-out process. Figure V-57 depicts the entire evaluation procedure.

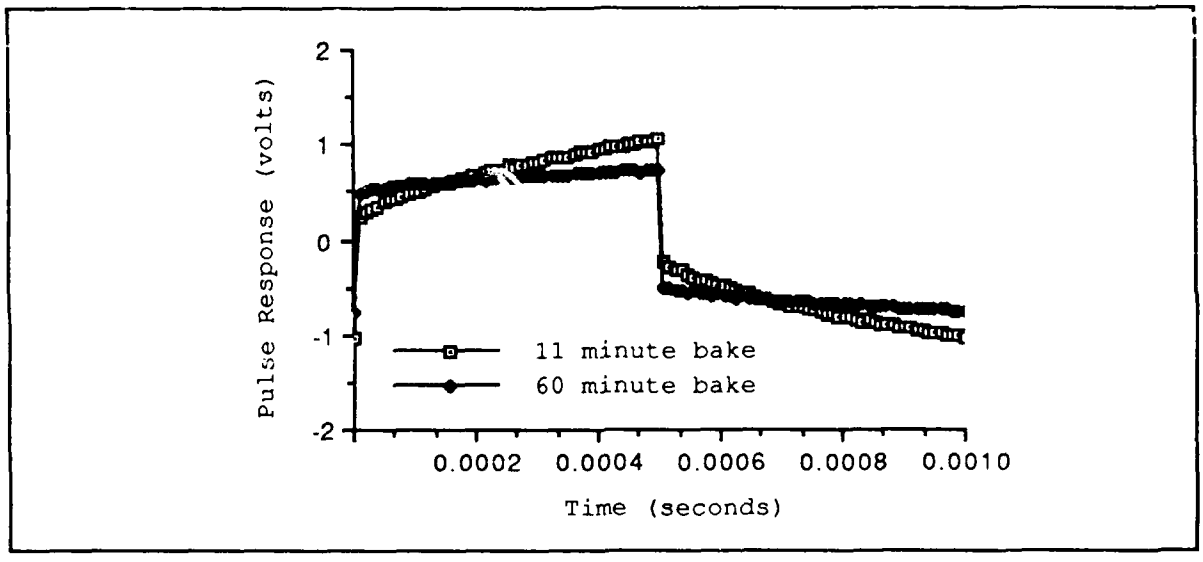

Figure V-56. Time-Domain Pulse Response after Elevating the Operating Temperature to 70°C During the Bake-Out Process.

Specifically, Figure V-57 depicts the sequence consisting of the pulse response with respect to time before challenge (before), after 5 minutes of exposure to the challenge gas (during), with 16 minutes of

purge by filtered room air after the exposure (after), and then after completion of the bake-out process (bake-out).

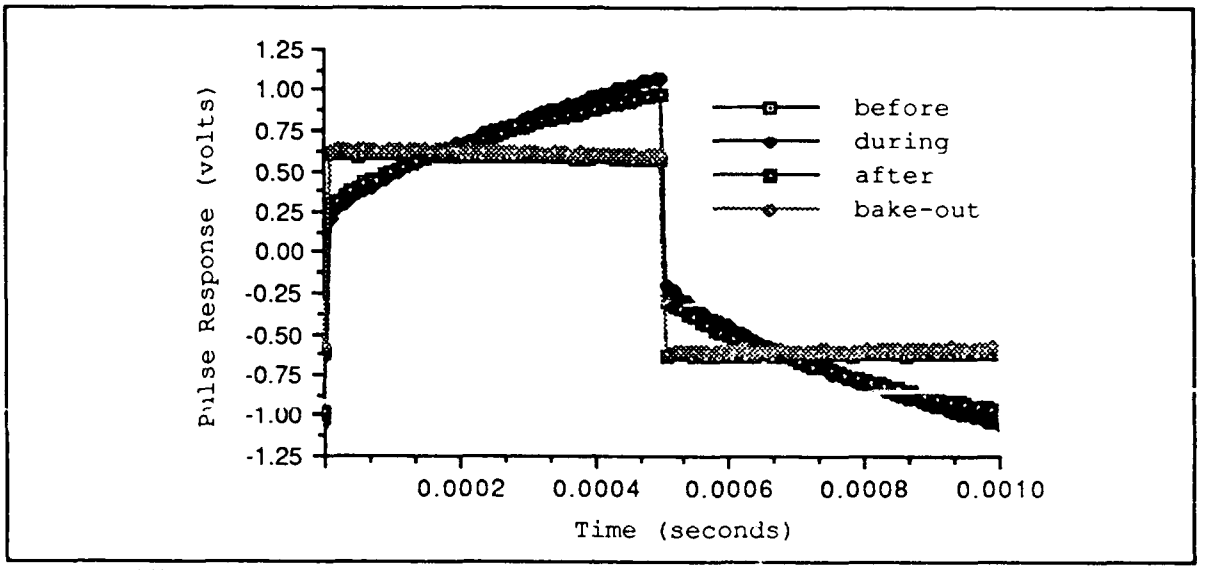

Figure V-57. Demonstration of the Reversibility of the Phthalocyanine Compounds Using the Bake-Out Process.

Elevated Operating Temperature.

The microsensor's operating temperature was elevated to 120°C to observe the effect of temperature on the microsensor's electrical response. The percent difference of the time-domain pulse response is depicted in Figures V-58 and V-59. The electrical response of the responsive microsensor element while exposed to filtered room air is used as the reference value in the percent difference calculation. The challenge gas was 20 ppb of NO_2 (3% RH; 120°C).

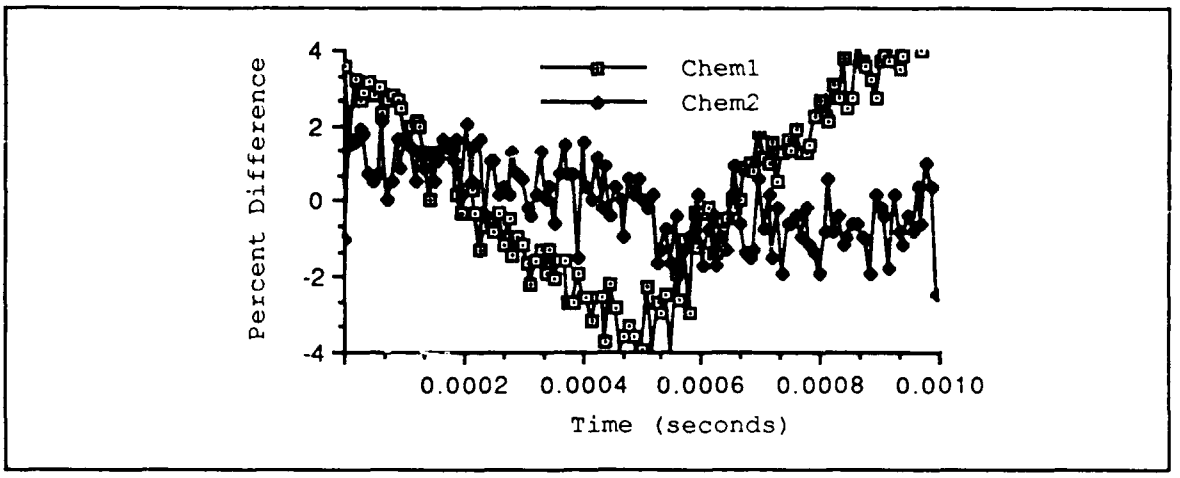

Figure V-58. Percent Difference in the Time-Domain Pulse Response for Chem1 and Chem2 When Exposed to 20 ppb of NO_2 Using Air as the Reference (3% RH; 120°C).

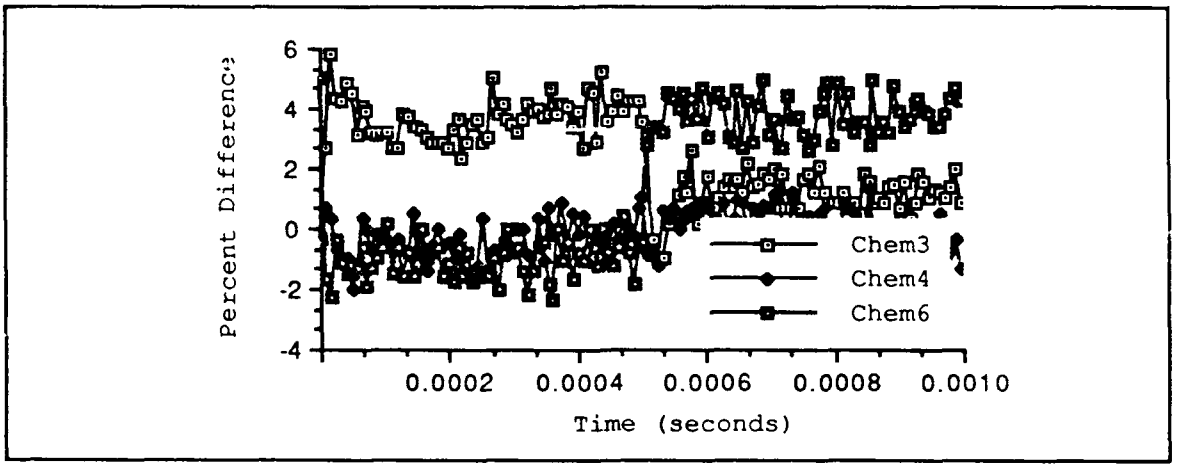

Figure V-59. Percent Difference in the Time-Domain Pulse Response for Chem3, Chem4, and Chem6 When Exposed to 20 ppb of NO_2 Using Air as the Reference (3% RH; 120°C).

Using Figures V-52, V-53, V-58, and V-59, it was apparent that the electrical response was generally degraded with the increase in operating temperature. For example, the electrical response of the cobalt-doped phthalocyanine coated sensor (Chem1) decreased from

approximately a 60% change to approximately a 4% change upon exposure to 20 ppb of NO_2.

Change of Thin Film Thickness.

The thin film thickness was decreased when depositing the phthalocyanine compounds onto Die2. In addition, the sensing element designated as Chem6 was left uncoated. The resulting change in the electrical response of the microsensor is presented in this section. Figure V-60 is a representative example of the time-domain pulse response using the cobalt-doped phthalocyanine coated interdigitated gate electrode. The challenge gas is 20 ppb of NO_2 at 1% RH. The microsensor was operated at 30°C.

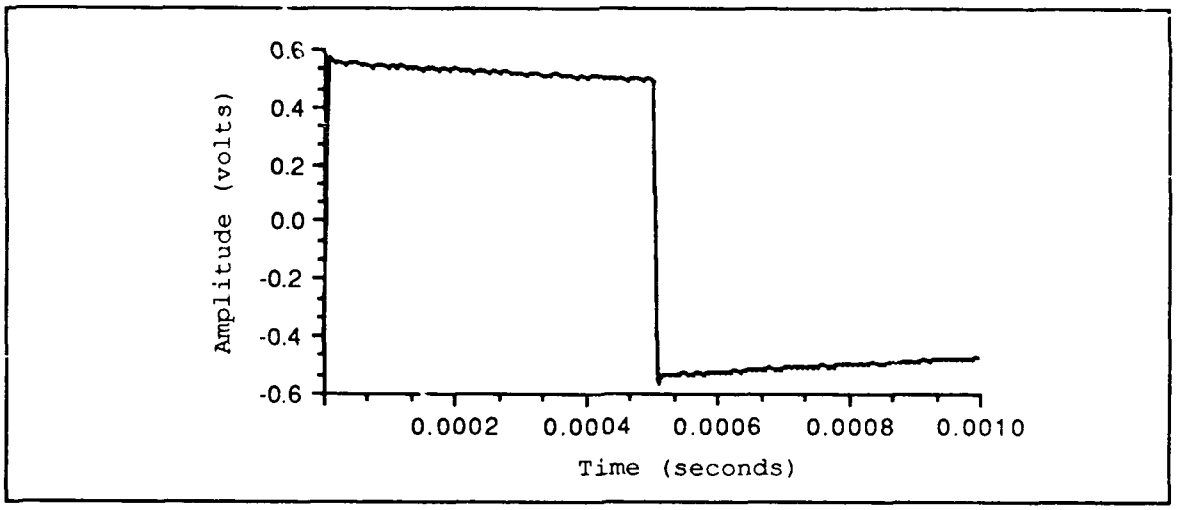

Figure V-60. Time-Domain Pulse Response of Chem1 Using Die2 When Challenged with 20 ppb of NO_2 (1% RH; 30°C).

The percent difference of the time-domain pulse response is depicted in Figures V-61 and V-62 for the microsensor. The

reference response corresponds to filtered room air, and the challenge gas was 20 ppb of NO_2 (1% RH; 30°C).

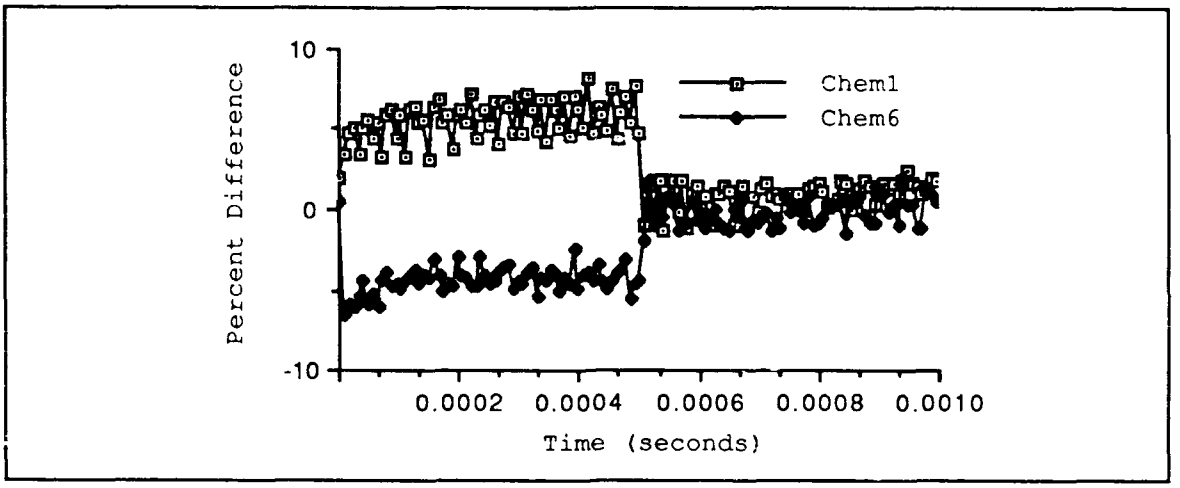

Figure V-61. Percent Difference of the Time-Domain Pulse Response for Chem1 and Chem6 Using Die2 for 20 ppb of NO_2 (1% RH; 30°C).

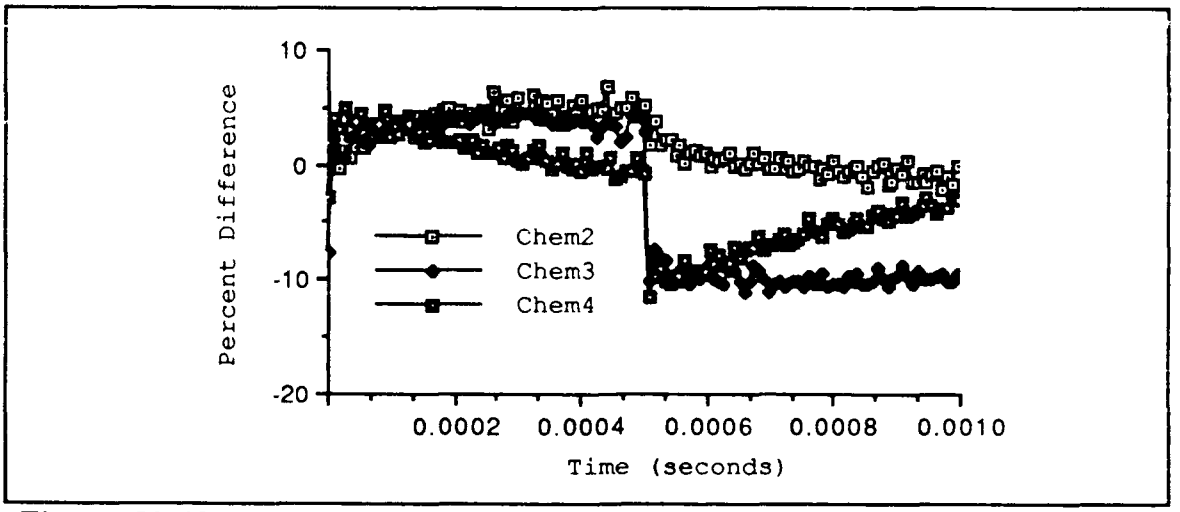

Figure V-62. Percent Difference of the Time-Domain Pulse Response for Chem2, Chem3, and Chem4 for 20 ppb of NO_2 (1% RH; 30°C).

An effect of decreasing the thin film thickness with Die2 was to decrease the superior performance of the cobalt-doped phthalocyanine. In Figure V-61, the magnitude of the change in the electrical response for Chem1 and Chem6 are essentially equivalent. However, the technique used in the data reduction scheme yields a different sign (negative for the uncoated and positive for the coated) for the positive amplitude portion of the excitation signal. This means that the measurement techniques employed could not unequivocally distinguish the electrical response between an uncoated and a coated interdigitated gate electrode. The response of Chem6 also may indicate contamination of the microsensor's surface.

The uncoated interdigitated gate electrode was further characterized. Figure V-63 depicts the DC resistance of the uncoated interdigitated gate electrode before and during exposure to 20 ppb of NO_2. This consideration provides a basis for determining the shunt resistance of the field-oxide supporting the metal fingers of the interdigitated gate electrode. The spectral response and the transfer function are illustrated in Figures V-64 and V-65, respectively.

Based upon the results depicted in Figures V-64 and V-65, the spectral peaks found in the frequency domain response are attributable to the interdigitated gate electrode structure as it is currently fabricated. However, the magnitude of the peaks appear to be larger for the uncoated interdigitated gate electrode. When comparing the DC response data and the AC response data, larger changes in the electrical responses between filtered room air and challenge test gas occur with the DC data (for example, the DC

resistance). Hence, much of the AC response information may be dominated by the structure for the film thicknesses and materials studied in this thesis.

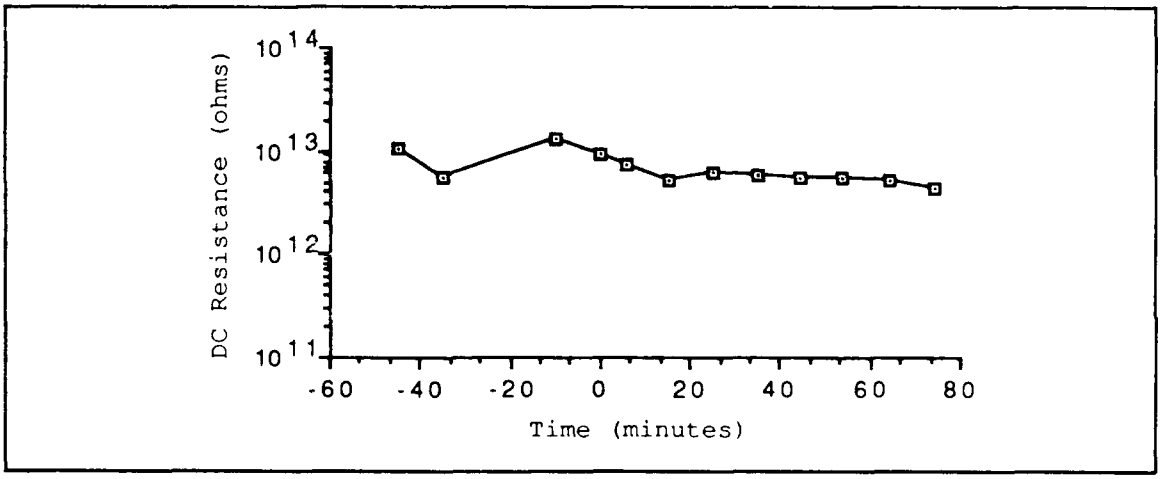

Figure V-63. DC Resistance of the Uncoated Interdigitated Gate Electrode (Chem6; Die2; 30°C).

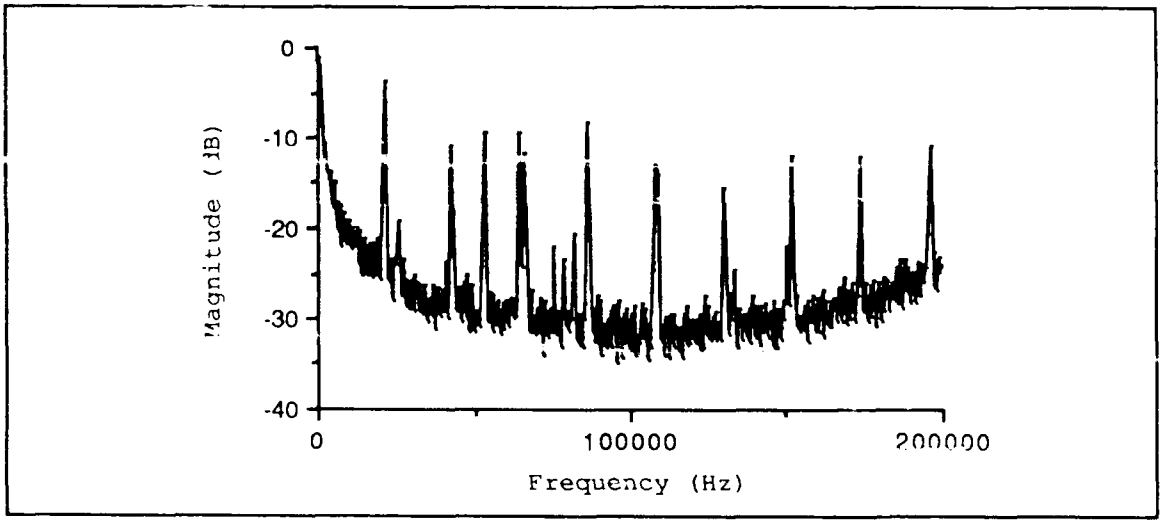

Figure V-64. Normalized Spectral Response in the Frequency Domain of the Uncoated Interdigitated Gate Electrode (Chem6; Die2; 30°C).

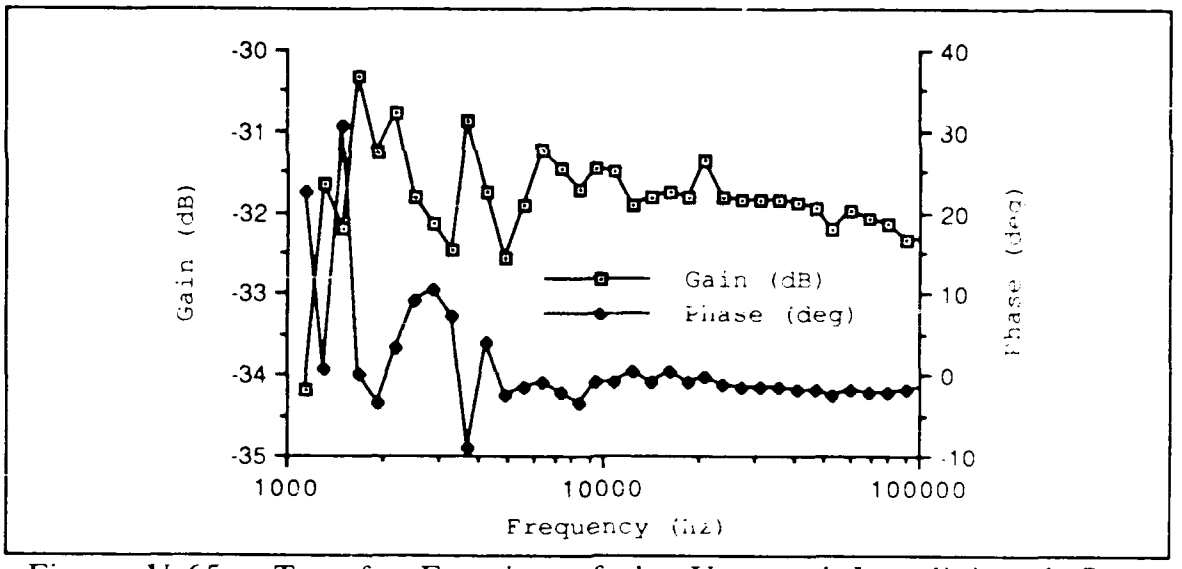

Figure V-65. Transfer Function of the Uncoated Interdigitated Gate Electrode (Chem6; Die2; 30°C).

Another potential problem was found with the thinner film thickness studied with Die2. This problem is depicted in Figure V-66. In the figure, the challenge gas (20 ppb of NO_2) begins to flow into the test cell at time equals zero. When this response is compared to the corresponding response for the thicker film (Die1) with Figures V-10 and V-11, the cobalt-doped phthalocyanine's DC resistance is nearly 4 orders of magnitude greater for the thinner film. This larger DC resistance may prove to be problematic with a practical sensor since the it is more difficult to reliably measure extremely large DC resistances.

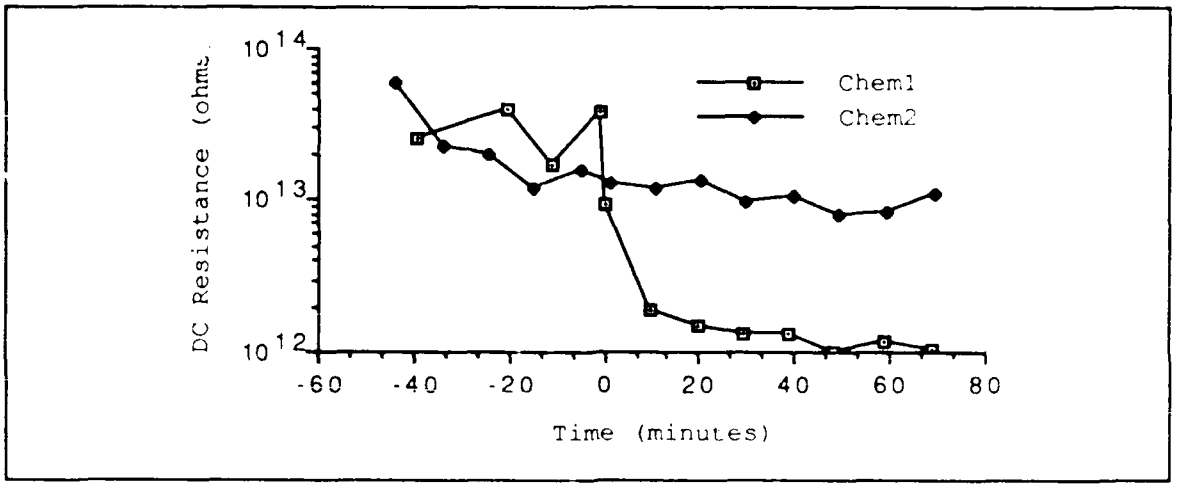

Figure V-66. DC Resistance of Chem1 and Chem2 (Die2) When Exposed to 20 ppb of NO_2 (1% RH; 30°C).

Exposure to DIMP.

The specificity of the microsensor was determined by examining the electrical response of the microsensor when exposed to equal concentrations of dissimilar test gases. The primary gas to be detected by this microsensor was NO_2. DIMP was chosen as the dissimilar test gas. The microsensor fabricated using Die1 was used in the measurements. In Figure V-67, the time-domain pulse response of Chem1 is presented. The sensing element was challenged with 20 ppb of DIMP at 1% RH. The microsensor was operated at 30°C.

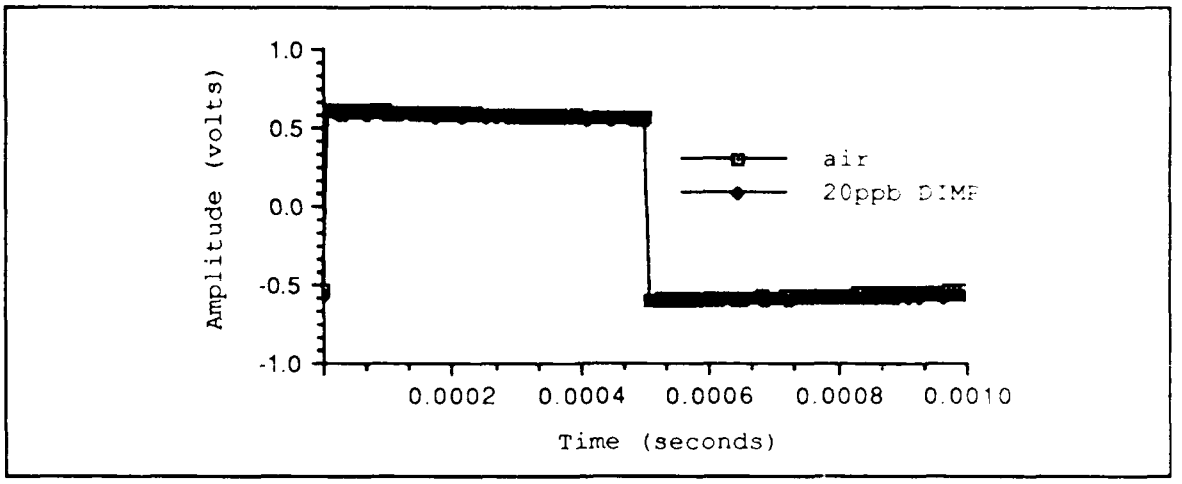

Figure V-67. Time-Domain Pulse Response of Chem1 Challenged with 20 ppb of DIMP (1% RH; 30°C).

The percent difference of the time-domain pulse response for each sensing element is given in Figures V-68 and V-69 where the reference response corresponds to the filtered room air exposure.

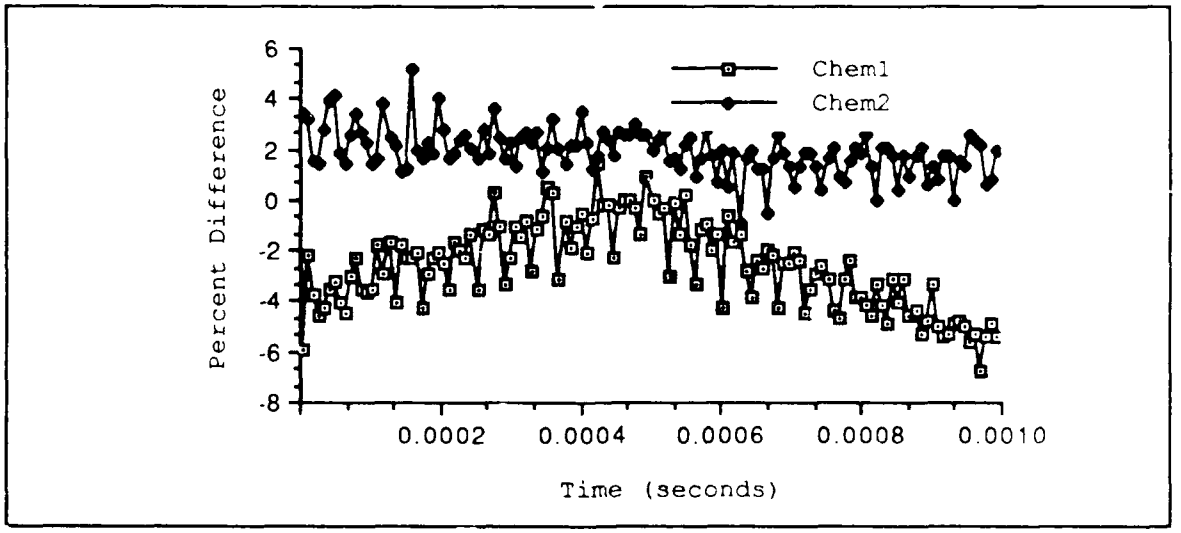

Figure V-68. Percent Difference of Time-Domain Pulse Response of Chem1 and Chem2 When Challenged with 20 ppb of DIMP Using Filtered Room Air as a Reference (1% RH; 30°C).

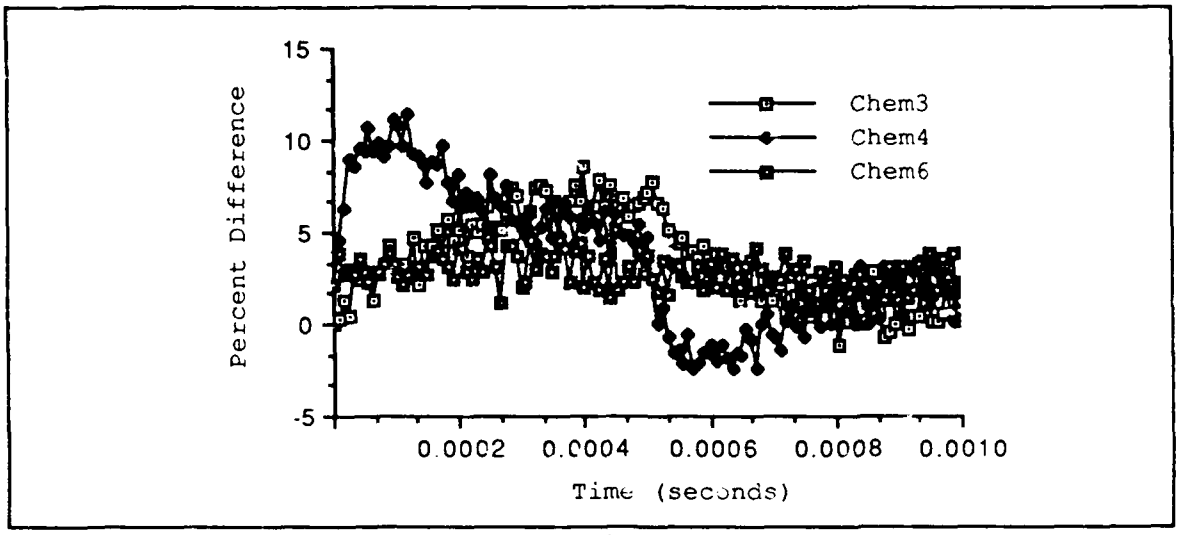

Figure V-69. Percent Difference of Time-Domain Pulse Response of Chem3, Chem4, and Chem6 When Challenged with 20 ppb of DIMP Using Filtered Room Air as a Reference (1% RH; 30°C).

Figures V-70 through V-74 compare the percent difference in the time-domain pulse response upon exposure to DIMP and NO_2 to illustrate the selectivity of the microsensor. In all the figures, the reference time-domain pulse response corresponds to exposure with filtered room air prior to challenging with the test gas as previously defined for the work presented in this chapter.

Based upon the responses depicted in Figures V-70 through V-74, the rank order of the specificity from the most to the least selective is cobalt-doped phthalocyanine, nickel-doped phthalocyanine, lead-doped phthalocyanine, undoped

phthalocyanine, and then copper-doped phthalocyanine coated sensing elements.

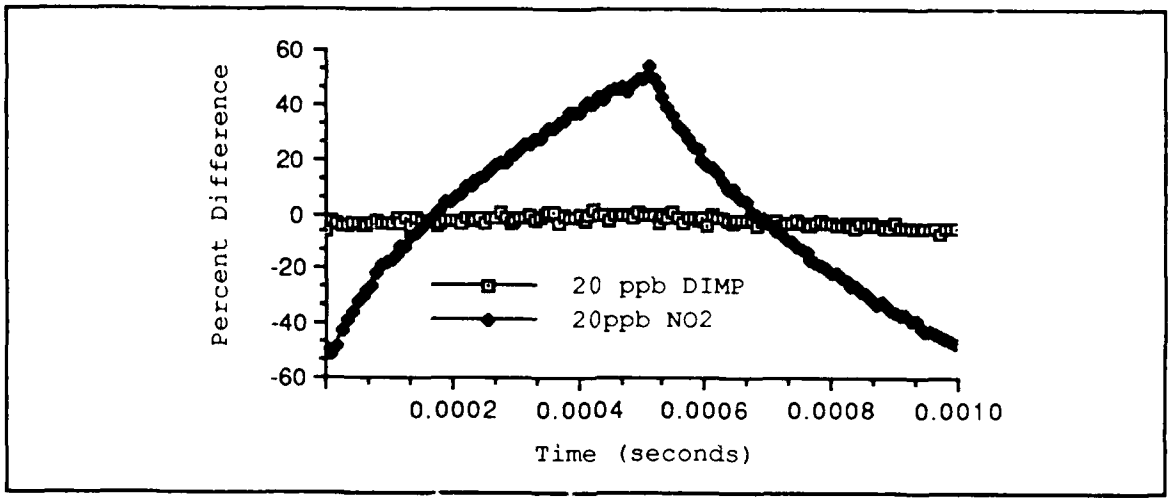

Figure V-70. Selectivity of Chem1 for Exposure to DIMP and NO_2.

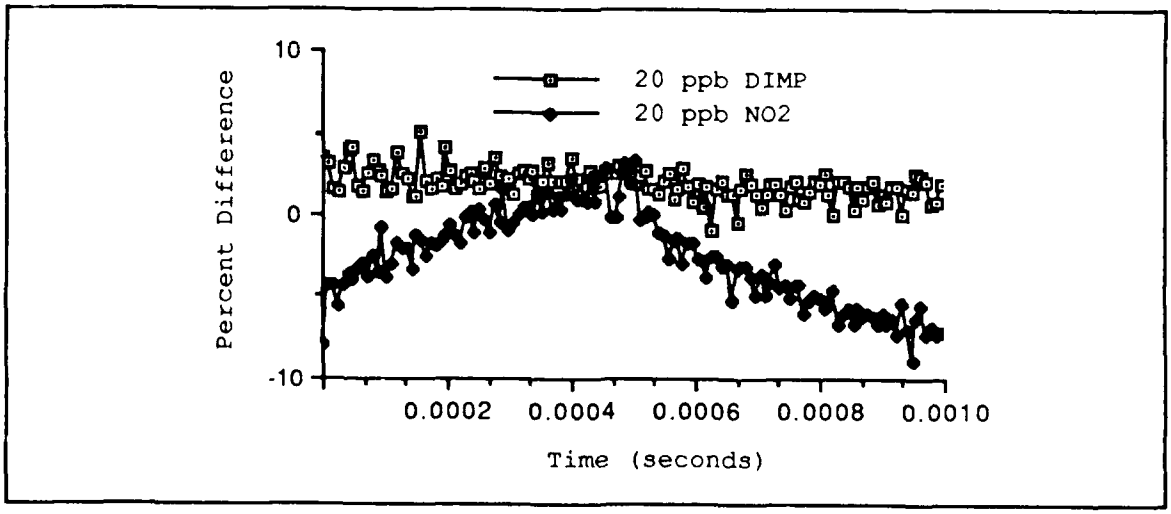

Figure V-71. Selectivity of Chem2 for Exposure to DIMP and NO_2.

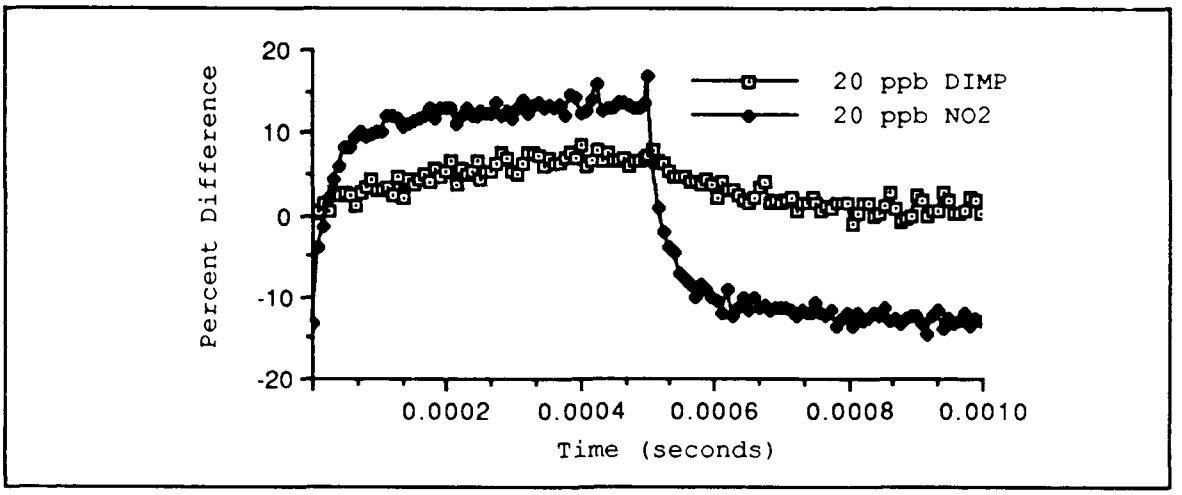

Figure V-72. Selectivity of Chem3 for Exposure to DIMP and NO_2.

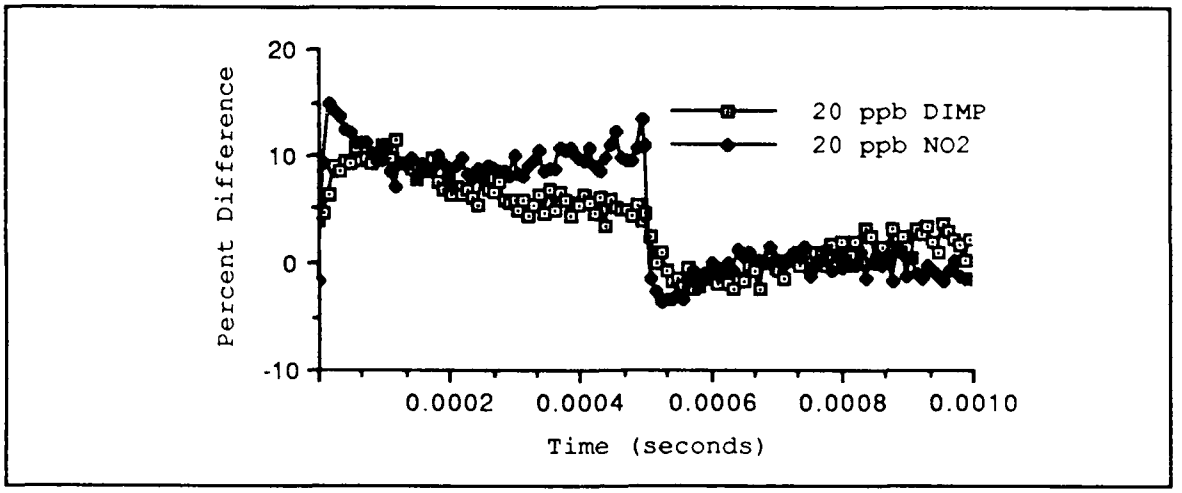

Figure V-73. Selectivity of Chem4 for Exposure to DIMP and NO_2.

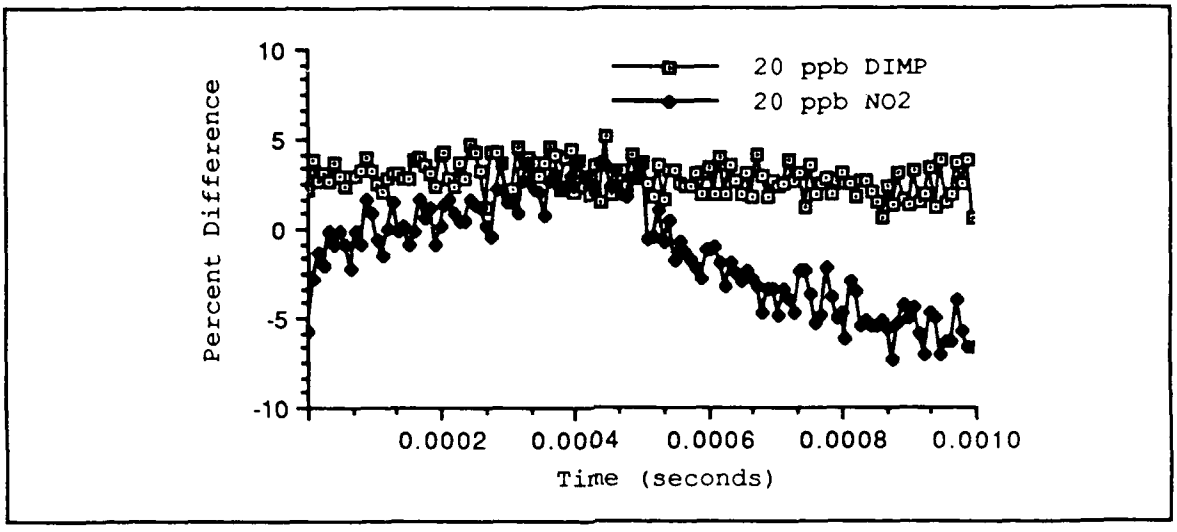

Figure V-74. Selectivity of Chem6 for Exposure to DIMP and NO_2.

The spectral response in the frequency-domain was examined. The representative responses of the cobalt-doped phthalocyanine coated interdigitated gate electrode is depicted in Figures V-75 and V-76.

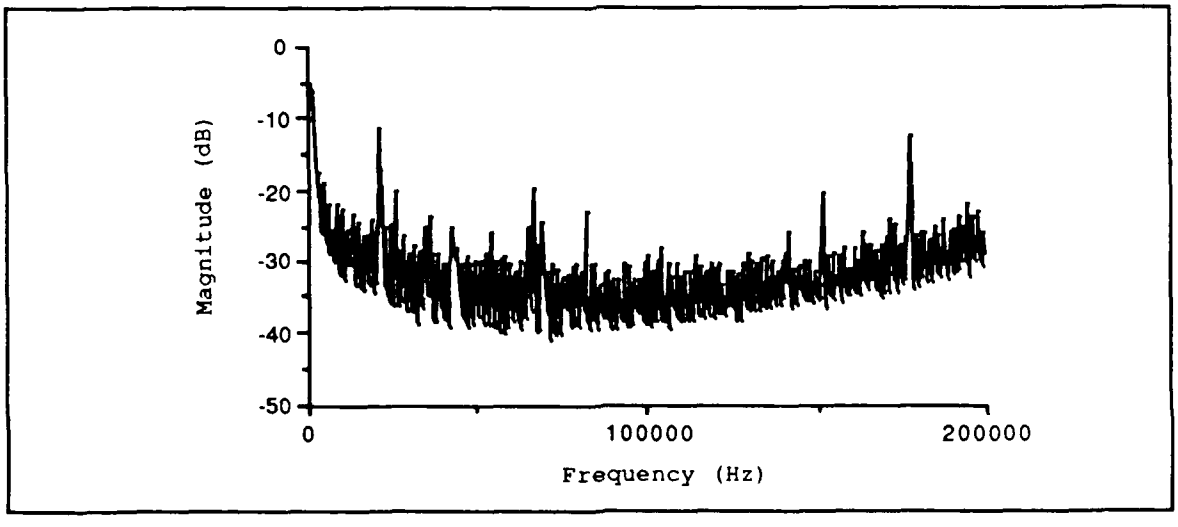

Figure V-75. Normalized Spectral Response of Chem1 to 20 ppb of DIMP.

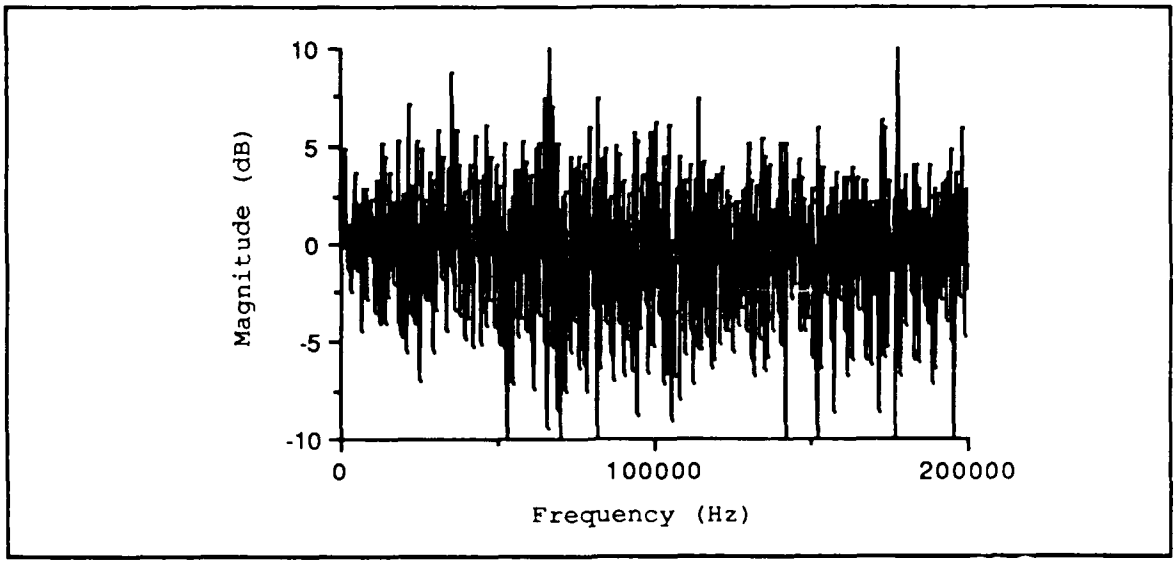

Figure V-76. Double Normalization of the Spectral Response of Chem1 to 20 ppb of DIMP.

The response of Chem1 to 20 ppb of DIMP is markedly different when comparing these responses to the equivalent response of an uncoated interdigitated gate electrode or an exposure of Chem1 to 20 ppb of nitrogen dioxide (Figures V-43, V-44, and V-64). Additional differences in the response between DIMP and nitrogen dioxide are found when comparing the AC impedance data using a simplified electrical model of the interdigitated gate electrode.

Simplified Electrical Model.

The parameter values of a simplified electrical model were extracted from the measured AC impedance data. Since all the voltage-bias connections were left open-circuited, the proposed

electrical model was further simplified. The shunt path to ground through the MOS capacitors was neglected since an electrical connection was not made to the p-well. In this simplified case, the signal path begins at the driven gate electrode and terminates at the floating gate electrode. The shunt signal paths through R_b and R_s are lumped together in an equivalent resistor. Also, the shunt signal paths through C_s, C_b, and C_a are lumped together in an equivalent capacitor. The parasitic capacitance associated with the model element C_{ox} is approximated as a shunt signal path from the driven gate electrode to the floating gate electrode, as well. Therefore, C_{ox} is lumped into the equivalent capacitor. The effect of this simplification is to reduce the network model to a two-port model with three nodes. The impedance is determined as a through-impedance. A schematic is presented in Figure V-77.

The calibration plane of the AC impedance measurement is shown in Figure V-77. This plane is depicted to emphasize an additional simplification. It was assumed that since the AC impedance analyzer was calibrated, the electrical connections external to the interdigitated gate electrode structure could be neglected. This assumption allows the network model to be simplified by neglecting the analyzer's input and output impedance.

Using this electrical model and the measured AC impedance, the equivalent resistor's value and the equivalent capacitor's value could be inferred. In terms of the electrical network, the magnitude (M) of the AC impedance is determined by:

$$M = \frac{R(\omega)}{\sqrt{1 + \omega^2 R^2(\omega) C^2(\omega)}} \qquad (5.1)$$

where $R(\omega)$ is the equivalent frequency dependent resistor's value (ohms), $C(\omega)$ is the equivalent frequency dependent capacitor's value (Farads), and ω is the frequency (radians per second). The phase (P) associated with the AC impedance is determined by:

$$P = -\tan^{-1}(\omega R(\omega) C(\omega)) \qquad (5.2)$$

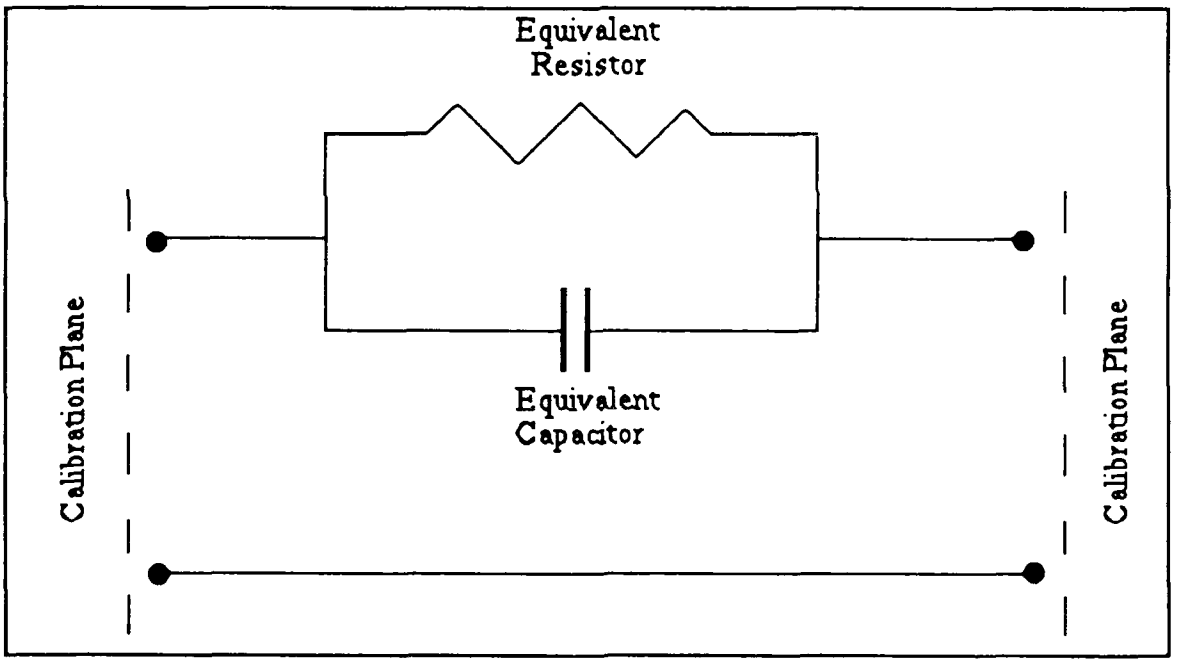

Figure V-77. Schematic of the Simplified Electrical Model.

Since the frequency, magnitude, and phase are measured, there are two unkowns ($R(\omega)$ and $C(\omega)$) defined by two equations (5.1 and 5.2). Therefore, the values of $R(\omega)$ and $C(\omega)$ were determined at

each frequency, and they are plotted in Figures V-78 and V-79. The AC impedance data associated with the 30°C exposure to NO_2 were evaluated for this purpose. The values associated with filtered room air immediately prior to the respective exposures are designated as air20, air80, and air320. The values after exposure to the various concentrations of NO_2 are designated as 20ppb, 80ppb, and 320ppb.

The results for the corresponding exposure to DIMP is plotted in Figures V-80 and V-81. In Figure V-78, the resistor values converged. However, in Figure V-80, the resistor values for 320 ppb diverged over the frequency range. Also, the capacitor values corresponding to the DIMP exposure remained relatively unchanged.

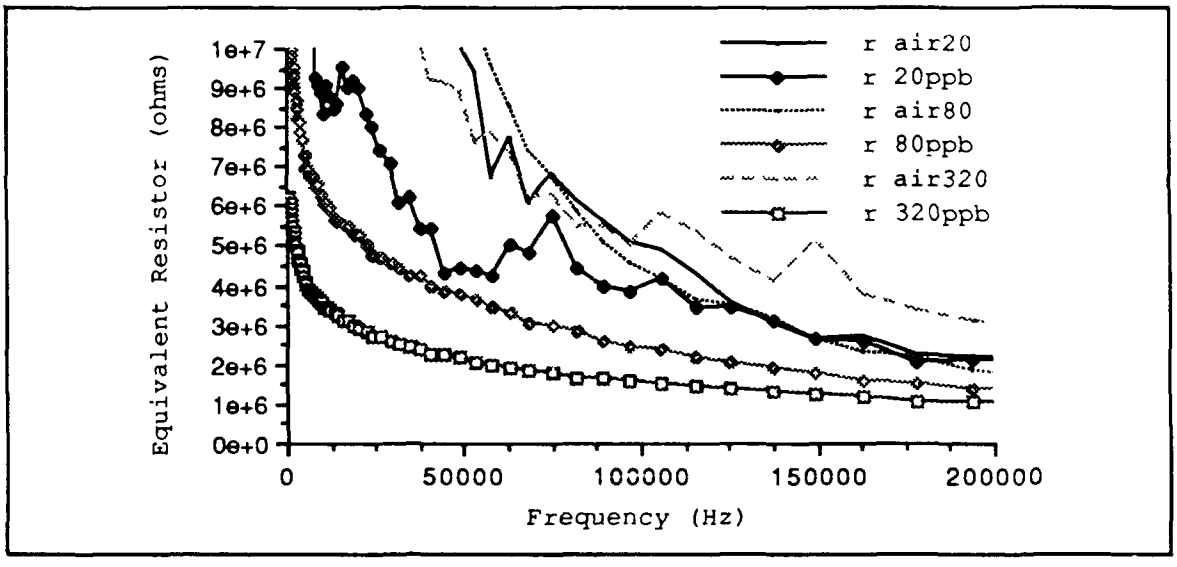

Figure V-78. Simplified Electrical Model's Equivalent Resistance Values with Exposure to NO_2.

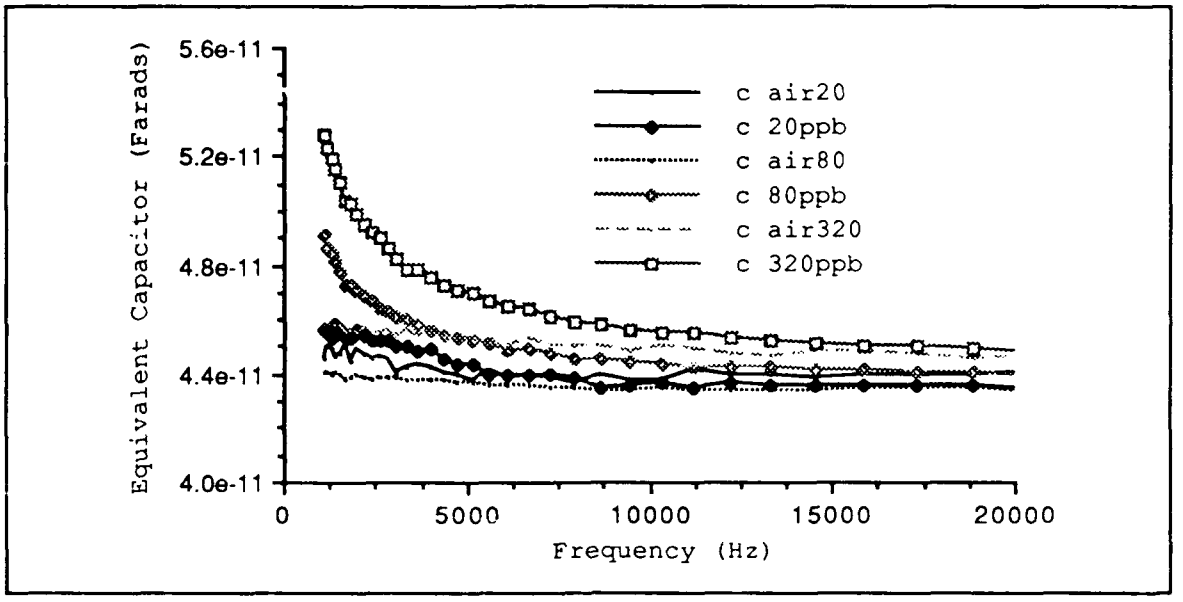

Figure V-79. Simplified Electrical Model's Equivalent Capacitor Values with Exposure to NO_2.

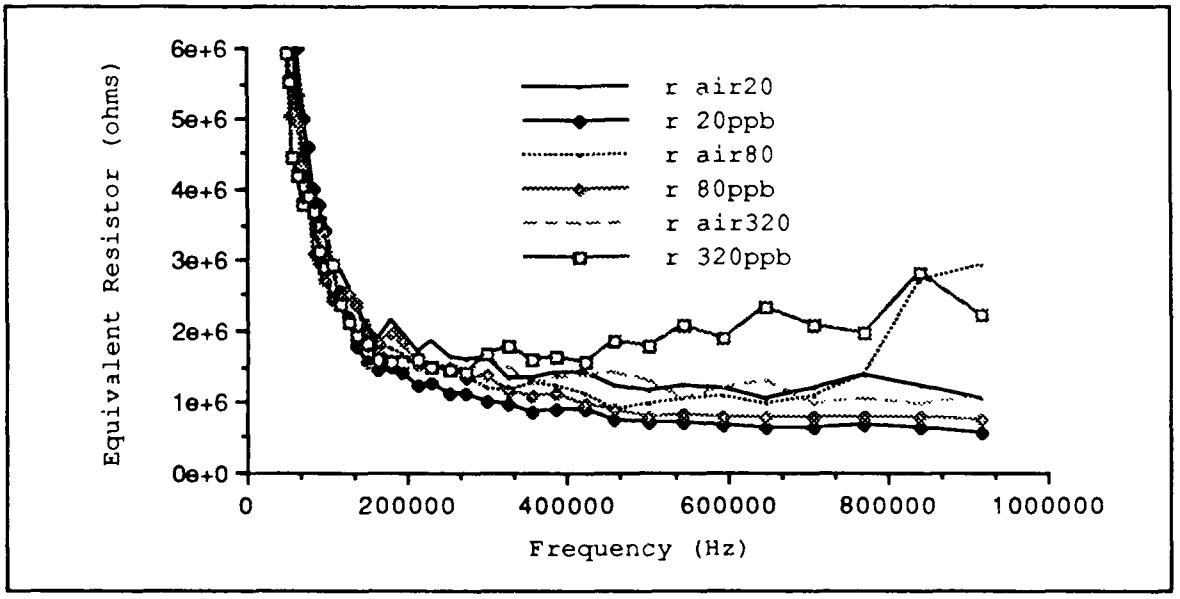

Figure V-80. Simplified Electrical Model's Equivalent Resistor Values with Exposure DIMP.

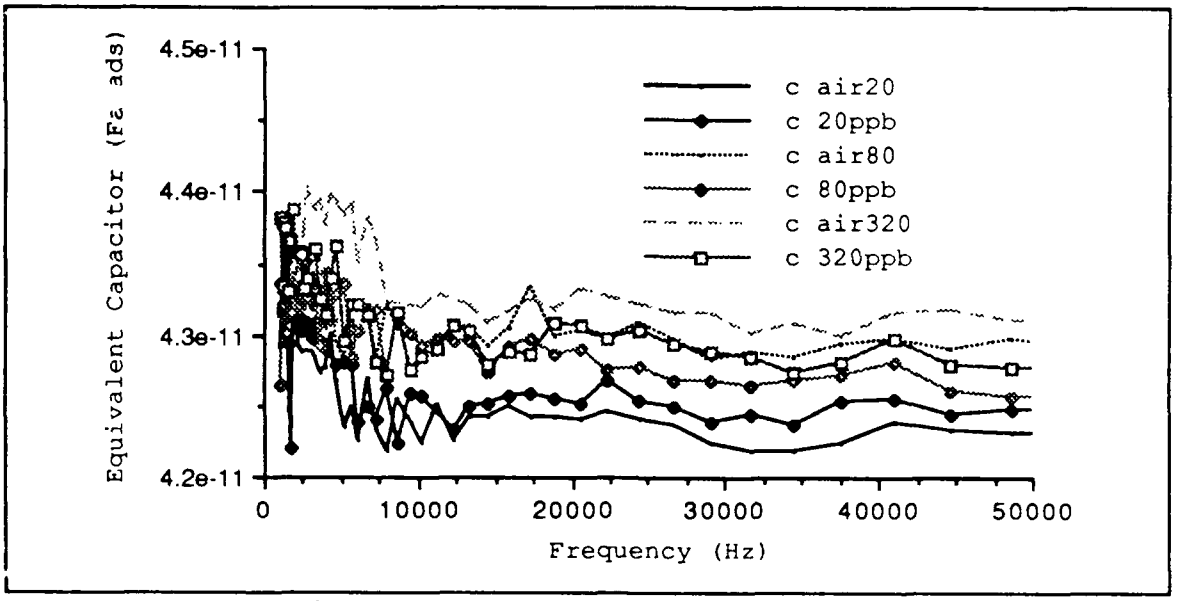

Figure V-81. Simplified Electrical Model's Equivalent Capacitor Values with Exposure to DIMP.

Summary

The design of the microsensor integrated circuit was validated, and the phthalocyanine compounds were evaluated for use with the microsensor. The design validation consisted of characterizing the frequency response of the microsensor. This was accomplished by measuring the transfer function of the sensing elements in a selected and unselected mode. A nominal voltage gain between 21 dB and 24 dB was measured with a 3-dB cut-off frequency of approximately 450 KHz. The isolation varied from -42 dB to -22 dB.

Since a possible application of the microsensor is for the detection of vapors from detonation materials, the comparisons of the phthalocyanine compounds focused upon low concentrations (20

ppb). In addition, a practical detector for this type of application may reasonably be expected to be contained within a controlled environment, such as constant relative humidity. Therefore, the comparisons of the phthalocyanine compounds were restricted to dry gas exposures (that is, less than 5% relative humidity).

With respect to the materials examined, the cobalt-doped phthalocyanine was found to be the most sensitive. Specifically, the rank ordering of the sensitivity of the materials to nitrogen dioxide from the most to the least sensitive is cobalt-doped phthalocyanine, nickel-doped phthalocyanine, copper-doped phthalocyanine, lead-doped phthalocyanine, and finally, the undoped phthalocyanine.

The rank ordering of the reversibility was determined not to be useful as defined. This was due to the fact that the less sensitive materials appeared to be the most reversible when the definition used in this research was applied. However, the materials were determined to be reversible with the application of a heat treatment procedure designated as a bake-out process. In addition, the rank ordering of the specificity was found to be (from the most to the least selective) cobalt-doped phthalocyanine, nickel-doped phthalocyanine, lead-doped phthalocyanine, undoped phthalocyanine, and then copper-doped phthalocyanine. With regards to the specificity, the potential application of the AC impedance and the frequency-domain spectral response for gas identification was found to warrant further investigation.

For the conditions applied to this research, the increase in temperature to 120°C from 30°C hindered the performance of the

microsensor based upon the time-domain pulse response data. Using the same criteria, the performance of the microsensor was also degraded with the thinner film thickness.

VI. Conclusions and Recommendations

Conclusions

A microsensor for the detection of nitrogen dioxide was designed, fabricated, and evaluated. The principal features of the design consisted of:

(1) a two-dimensional array of nine sensing elements utilizing an interdigitated gate electrode field-effect transistor (IGEFET),
(2) MOSFET amplifiers to provide signal gain,
(3) a reference element with a MOSFET amplifier to provide temperature compensation, and
(4) an electronic multiplexing circuit for interrogating specific elements in the array.

The interdigitated gate electrode structures were coated with thin films of cobalt-doped phthalocyanine, copper-doped phthalocyanine, lead-doped phthalocyanine, nickel-doped phthalocyanine, and undoped phthalocyanine. The IGEFET was used as the chemically-sensitive field-effect transistor component of the microsensor.

To fabricate the microsensor, a technique to deposit the thin films of phthalocyanine compounds was explored. The technique involved the thermal sublimation of the phthalocyanine compounds under vacuum with subsequent physical vapor deposition onto the

interdigitated gate electrode structures. The process used metal masks to pattern the coatings to minimize the occurrence of chemical reactions with the deposited phthalocyanine compounds (which might have occurred had masks been patterned with photoresist) during the deposition process. This process was found to produce conformal coatings of the phthalocyanine compounds over the metal fingers and field-oxide portions of the interdigitated gate electrode structure.

The evaluation of the fabricated microsensor was completed for two principal aspects. The first aspect of the evaluation involved the electrical characteristics of the microsensor's integrated circuit. The second aspect of the evaluation involved the electrical response of the phthalocyanine coated sensing elements when exposed to a challenge gas.

The characterization of the microsensor's integrated circuit was accomplished by measuring the transfer function of the sensing elements in a selected and unselected mode. The input stimulus was applied directly to the floating gate of the interdigitated electrode structure to avoid including the effects of the polymer. A nominal voltage gain between 21 dB and 24 dB was measured with a 3-dB cut-off frequency of approximately 450 KHz. The isolation varied from -42 dB to -22 dB.

To facilitate the evaluation of the various phthalocyanine compounds for their suitability as the chemically-sensitive membrane that coats the interdigitated gate electrode, two simplifying assumptions were made. Since a possible application of

the microsensor involves the detection of vapors from detonation materials, the comparisons of the phthalocyanine compounds focused upon low concentrations (20 ppb). In addition, a practical detector for this type of application may reasonably be expected to be contained within a controlled environment, such as constant relative humidity. Therefore, the comparisons of the phthalocyanine compounds were restricted to dry gas exposures (that is, less than 5% relative humidity).

Of the materials examined, the cobalt-doped phthalocyanine film was found to be the most sensitive. Specifically, the rank ordering of the sensitivity of the materials to nitrogen dioxide from the most to the least sensitive is cobalt-doped phthalocyanine, nickel-doped phthalocyanine, copper-doped phthalocyanine, lead-doped phthalocyanine, and finally, the undoped phthalocyanine.

The rank ordering of the reversibility was determined not to be useful as defined. This was due to the fact that the less sensitive materials appeared to be the most reversible when the definition used in this research was applied. However, the materials were determined to be reversible with the application of a heat treatment designated as a bake-out process. In addition, the rank ordering of the specificity was found to be (from the most to the least selective) cobalt-doped phthalocyanine, nickel-doped phthalocyanine, lead-doped phthalocyanine, undoped phthalocyanine, and then copper-doped phthalocyanine.

For the conditions applied to this research, the increase in temperature to 120°C from 30°C hindered the performance of the

microsensor based upon the time-domain pulse response data. Using the same criteria, the performance of the microsensor was also degraded with the thinner film thickness.

Recommendations

The results of this research have demonstrated the feasibility of fabricating a chemically-sensitive integrated circuit based upon an array of sensing elements. However, unresolved issues remain. In addition, further investigations should be made to enhance the chemically sensing performance of the device. The specific recommendations include the following:

1. The technique used to deposit the thin films of phthalocyanine needs to be fully characterized. The errors in determining the film thickness should be quantified by verifying the profilometer results with a second independent measurement. For example, a thin structure could be patterned in silicon dioxide. Then, an ellipsometer could be used to determine the structure's thickness by more conventional means. Once the thickness is determined using the ellipsometer, the thickness could be determined using the profilometer after coating the surface with gold. The comparison of the two results would then involve two measurement principles (contact profilometry and optical polarization).

2. Also involving the deposition process, the deposited phthalocyanine compounds need to be further characterized concerning the surface morphology, physical structure, and electrical

material parameters. Knowing the morphology and physical structure may facilitate understanding the conduction process. With this information, an approximate model of the carrier transport may be determined that might indicate how to enhance the electrical effects produced by vapor adsorption. For example, the frequency dependent permittivity and the loss tangent of the deposited phthalocyanine compounds need to be determined to facilitate accurate simulation of the electrical models of the coated interdigitated gate electrodes.

3. Using the data collected during this thesis research and the data collected by past research at AFIT concerning the CHEMFET, parameter values for an approximate electrical model should be extracted. This remains as an unresolved issue. For example, the current design of the microsensor allows for the measurement of the input- and output-impedance of the coated interdigitated gate electrode as a function of the applied bias to the p-well isolation. The data collected to date at AFIT concerns the through-impedance and the transfer function. Using only the through-impedance and the transfer function, it may not be possible to extract the parameter values of individual components in the approximate electrical model from the measured electrical performance.

4. Other structures for the interdigitated gate electrode should be investigated. Ideally, a structure where the metal fingers are located on the surface of the phthalocyanine film should be fabricated to enhance the detection of surface effects. The phthalocyanine compounds would be deposited before the metal

fingers in the fabrication process. The operation of the sensing element would be analogous to the operation of a four-point probe. However, the practical implementation of this structure may alter the sensing surface of the phthalocyanine rendering it useless. Another alternative is to replace the p-well isolation under the interdigitated gate electrode with a metal layer, such as metal-1 in the MOSIS fabrication process. This would eliminate the frequency and voltage bias dependent parasitic effects of the MOS capacitance. Therefore, a simpler electrical network may be produced. A simpler electrical model would facilitate the optimization of the coated interdigitated gate electrode structure.

5. Signal processing techniques should be fully implemented to generate and recognize the various response-surfaces associated with variable gas exposure (type and concentration). This could be implemented with the data already collected at AFIT, and then tested with the current and future designs of the sensing elements of a microsensor. Once validated, the technique should be extended to mixtures of the gases to determine the feasibility of constructing practical integrated circuits for the detection of chemical vapors in less constrained environments, such as a common workplace.

Appendix A

Processing Characteristics and Simulation Models

This appendix lists the processing characteristics of the integrated circuit technology used to fabricate the microsensor, as well as the simulation models used to design the microsensor. Also, the simulation models used to determine the expected performance of the microsensor electronics (after the vendor's fabrication characteristics were received) are presented in this appendix.

The SPICE3 (U. C. Berkeley, CA) input file used to initially design the microsensor was:

```
chemfet using inverting amplifiers
********************    establish subcircuit models
*********
*IGEFET and inverters
.subckt amp 1 5 4 6
*node 1=vdd
*node 5=vss
*node 4=input
*node 6=output
*apply substrate bias
vbias 9 0 dc -5v
*load bias
ramp1 1 2 6.7e3
ramp2 1 3 10e3
ramp3 1 6 7.5e3
m1 2 4 5 9 N l=3U w=9U as=81P ad=81P
```

```
m2 3 2 5 9 N l=3U w=11U as=81P ad=81P
m3 6 3 5 9 N l=3U w=12U as=108P ad=108P
*end of subcircuit for amp
.ends amp
*****************************************************
*one differential amplifier
.subckt damp 3 5 1 2 4
*node 1=vin-
*node 2=vin+
*node 3=vdd
*node 4=output
*node 5=vss
*the current mirrors consist of two pmos devices
m1 6 6 3 3 P l=6U w=36U as=324P ad=324P
m2 4 6 3 3 P l=6U w=36U as=324P ad=324P
*the positive input terminal sense
m3 6 2 7 7 N l=3U w=24U as=216P ad=216P
*the negative input terminal sense
m4 4 1 7 7 N l=3U w=24U as=216P ad=216P
*tne current source
m5 7 3 5 5 N l=3U w=12U as=108P ad=108P
*end of subcircuit for damp
.ends damp
*****************************************************
*****
*analog switch model
.subckt switch 1 2 3 4
*node 1=input
*node 2=N-switch control
*node 3=P-switch control
*node 4=output
*to turn on switch use -5 volts on P-switch and +5 on N-
switch
*to turn off switch use +5 on P-switch and -5 on N-switch
*bias the switch substrate
vsubn 5 0 dc -5v
vsubp 6 0 dc 5v
*this is the t-gate switch
m21 4 2 1 5 N l=3U w=15U as=135P ad=135P
m22 1 3 4 6 P l=3U w=15U as=135P ad=135P
.ends switch
```

```
**********          end of subcircuit models
**********

*****************************************************
*
*        set-up the simulation model of chemfet
*****************************************************
*
*apply the bias voltages
vdd 1 0 dc 5v
vss 2 0 dc -5v
*this is the signal source for ac and tran analysis
*models the chemfet electrode that was selected by MUX
vin 3 0 dc 0.0 ac .01 0 sin(0 .01 1e6 0 0)
*vin 3 0 dc 0.0 ac .0001 0 pulse(0 .0001 0 1e-6 1e-6 50e-6
100e-6)
*****************************************************
******
*instantiate the first stage of amplifier on CHEMFET element
*****************************************************
******
*this is the one that will be allowed to pass thru MUX
x1 1 2 3 4 amp
*the remaining chemfet signals are blocked by the MUX
*remaining eight chemfet elements
x11 1 2 3 41 amp
x12 1 2 3 42 amp
x13 1 2 3 43 amp
x14 1 2 3 44 amp
x15 1 2 3 45 amp
x16 1 2 3 46 amp
x17 1 2 3 47 amp
x18 1 2 3 48 amp
*reference amp
x19 1 2 3 49 amp
*****************************************************
******
*signal must pass through the transmission gate
*****************************************************
******
*turn on gate +5 on N-switch -5 on P-switch
*turn-off is opposite application of voltages
```

```
vcntrlN 5 0 dc 5v
vcntrlP 6 0 dc -5v
*this is the chemfet signal that is allowed to pass
x2 4 5 6 7 switch
*the remaining switches to block the unselected elements &
*reference amp
x21 41 6 5 7 switch
x22 42 6 5 7 switch
x23 43 6 5 7 switch
x24 44 6 5 7 switch
x25 45 6 5 7 switch
x26 46 6 5 7 switch
x27 47 6 5 7 switch
x28 48 6 5 7 switch
x29 49 6 5 7 switch
*end of the transmission gate's MUX
*****************************************************
******
*now pass the signal off chip through a voltage follower
*****************************************************
******
x3 1 2 9 7 9 damp
*put a simulated load on the output of the chip
rload 9 0 1e6
cload 9 0 2e-12
.WIDTH OUT=80
.model P pmos level=4
+ vfb = -.49449 lvfb = .0473111 wvfb = -.078748
+ phi = .711038 lphi = 0 wphi = 0
+ k1 = .549022 lk1 = -.1098 wk1 = .211133
+ k2 = .0225369 lk2 = .0133462 wk2 = .0214418
+ eta = -.011378 leta = .0599553 weta = .0109074
+ muz = 173.524 dl = .502141 dw = -.20323
+ u0 = .129663 lu0 = .0395758 wu0 = -.089559
+ u1 = .0282132 lu1 = .288861 wu1 = -.13103
+ x2mz = 7.49207 lx2mz = -3.3077 wx2mz = 4.43137
+ x2e = -.00081113 lx2e = -.0023066 wx2e = -.0029608
+ x3e = .000855699 lx3e = -.003979 wx3e = -.00061957
+ x2u0 = .00634967 lx2u0 = -.0021908 wx2u0 = .00304801
+ x2u1 = .000525933 lx2u1 = .00057697 wx2u1 = .00896684
+ mus = 187.23 lmus = 89.9055 wmus = -19.539
+ x2ms = 7.00102 lx2ms = -.47434 wx2ms = 8.73424
```

```
+ x3ms = -.14304 lx3ms = 11.6728 wx3ms = -7.9883
+ x3u1 = -.016595 lx3u1 = .00351738 wx3u1 = .00384252
+ tox = .028 temp = 27 vdd = 5
+ cgdo = 3.09624e-10 cgso = 3.09624e-10 cgbo = -2.50626e-
10
+ xpart = 1
+ n0 = 1 ln0 = 0 wn0 = 0
+ nb = 0 lnb = 0 wnb = 0
+ nd = 0 lnd = 0 wnd = 0
+ rsh = 20.58 cj = .0004015 cjsw = 5.023e-10
+ js = 1.e-08 pb = .8 pbsw = .51
+ mj = .4465 mjsw = .2705 wdf = 0
+ dell = 0
.model N nmos level=4
+ vfb = -.78837 lvfb = -.021873 wvfb = -.12029
+ phi = .801437 lphi = 0 wphi = 0
+ k1 = 1.05382 lk1 = .0864105 wk1 = .588742
+ k2 = -.0087349 lk2 = .0845206 wk2 = .0774966
+ eta = -.0025165 leta = .00946697 weta = .00706382
+ muz = 431.198 dl = .7921 dw = -.11735
+ u0 = .051871 lu0 = .0428904 wu0 = -.035902
+ u1 = .0252047 lu1 = .608867 wu1 = -.34032
+ x2mz = 11.1852 lx2mz = -22.808 wx2mz = 38.2982
+ x2e = -.00020831 lx2e = -.0062271 wx2e = -.00071188
+ x3e = .000225369 lx3e = -.000686 wx3e = -.0042937
+ x2u0 = .00301681 lx2u0 = -.014095 wx2u0 = .0297249
+ x2u1 = -.0021476 lx2u1 = .00786076 wx2u1 = .004818
+ mus = 412.323 lmus = 259.338 wmus = 37.6417
+ x2ms = 4.86473 lx2ms = -19.202 wx2ms = 69.3915
+ x3ms = -2.6586 lx3ms = 47.7003 wx3ms = -13.265
+ x3u1 = -.002006 lx3u1 = .0668089 wx3u1 = -.019504
+ tox = .028 temp = 27 vdd = 5
+ cgdo = 4.88415e-10 cgso = 4.88415e-10 cgbo = -1.44718e-
10
+ xpart = 1
+ n0 = 1 ln0 = 0 wn0 = 0
+ nb = 0 lnb = 0 wnb = 0
+ nd = 0 lnd = 0 wnd = 0
+ rsh = 20.58 cj = .0004015 cjsw = 5.023e-10
+ js = 1.e-08 pb = .8 pbsw = .51
+ mj = .4465 mjsw = .2705 wdf = 0
+ dell = 0
```

```
*
.OPTIONS DEFL=3U DEFW=6U DEFAS=45P DEFAD=45P
+ITL1=500 ABSTOL=100P VNTOL=100U CHGTOL=1E-14
+NOPAGE LIMPTS=500 RELTOL=.005 CPTIME=5000 ITL5=0
.END
```

The multiplexer logic was verified using an event driven logic-level model. The logic-level simulator used was Esim (distributed by U. C. Berkeley with permission from M.I.T.). The multiplexer logic simulation follows:

```
| units: 1    tech: cmos-pw format: UCB
e AND_INPUT'#2 AND_INPUT#2 GND 200 1999.75 30400 -7500
e B AND_INPUT'#2 GND 200 1999.75 29400 -7500
e AND_INPUT#1 GND chem1 200 3199.5 25500 -8800
e AND_INPUT#1 chem2 GND 200 3199.5 23600 -8800
e AND_INPUT'#1 chem3 GND 200 3199.5 21700 -8800
e AND_INPUT'#1 chem4 GND 200 3199.5 19800 -8800
e AND_INPUT#1 chem5 GND 200 3199.5 17900 -8800
e AND_INPUT#1 chem6 GND 200 3199.5 16000 -8800
e AND_INPUT'#1 chem7 GND 200 3199.5 14100 -8800
e AND_INPUT'#1 chem8 GND 200 3199.5 12200 -8800
e AND_INPUT#1 chem9 GND 200 3199.5 10300 -8800
e AND_INPUT#1 chem10 GND 200 3199.5 8400 -8800
e AND_INPUT'#1 AND_INPUT#1 GND 200 1999.75 30400 -9900
e C AND_INPUT'#1 GND 200 1999.75 29400 -9900
p AND_INPUT'#1 Vdd AND_INPUT#1 4500.75 359.75 34400 -
10100
p C Vdd AND_INPUT'#1 200 4199.5 35600 -10200
e AND_INPUT#0 GND chem1 200 3199.5 25500 -11200
e AND_INPUT'#0 GND chem2 200 3199.5 23600 -11200
e AND_INPUT#0 GND chem3 200 3199.5 21700 -11200
e AND_INPUT'#0 GND chem4 200 3199.5 19800 -11200
e AND_INPUT#0 GND chem5 200 3199.5 17900 -11200
e AND_INPUT'#0 GND chem6 200 3199.5 16000 -11200
e AND_INPUT#0 GND chem7 200 3199.5 14100 -11200
e AND_INPUT'#0 GND chem8 200 3199.5 12200 -11200
e AND_INPUT#0 GND chem9 200 3199.5 10300 -11200
e AND_INPUT'#0 GND chem10 200 3199.5 8400 -11200
e AND_INPUT'#0 AND_INPUT#0 GND 200 1999.75 30400 -
12300
e D AND_INPUT'#0 GND 200 1999.75 29400 -12300
p AND_INPUT'#0 Vdd AND_INPUT#0 4500.75 359.75 34400 -
12500
p D Vdd AND_INPUT'#0 200 4199.5 35600 -12600
```

```
p GND Vdd chem1 200 400 26200 600
p GND Vdd chem2 200 400 24300 600
p GND Vdd chem3 200 400 22400 600
p GND Vdd chem4 200 400 20500 600
p GND Vdd chem5 200 400 18600 600
p GND Vdd chem6 200 400 16700 600
p GND Vdd chem7 200 400 14800 600
p GND Vdd chem8 200 400 12900 600
p GND Vdd chem9 200 400 11000 600
p GND Vdd chem10 200 400 9100 600
e AND_INPUT#3 GND chem1 200 3199.5 25500 -4000
e AND_INPUT#3 chem2 GND 200 3199.5 23600 -4000
e AND_INPUT#3 chem3 GND 200 3199.5 21700 -4000
e AND_INPUT#3 chem4 GND 200 3199.5 19800 -4000
e AND_INPUT#3 chem5 GND 200 3199.5 17900 -4000
e AND_INPUT#3 chem6 GND 200 3199.5 16000 -4000
e AND_INPUT#3 chem7 GND 200 3199.5 14100 -4000
e AND_INPUT#3 chem8 GND 200 3199.5 12200 -4000
e AND_INPUT'#3 chem9 GND 200 3199.5 10300 -4000
e AND_INPUT'#3 chem10 GND 200 3199.5 8400 -4000
e AND_INPUT'#3 AND_INPUT#3 GND 200 1999.75 30400 -5100
e A AND_INPUT'#3 GND 200 1999.75 29400 -5100
p AND_INPUT'#3 Vdd AND_INPUT#3 4500.75 359.75 34400 -
5300
p A Vdd AND_INPUT'#3 200 4199.5 35600 -5400
e AND_INPUT#2 GND chem1 200 3199.5 25500 -6400
p B Vdd AND_INPUT'#2 200 4199.5 35600 -7800
p AND_INPUT'#2 Vdd AND_INPUT#2 4500.75 359.75 34400 -
7700
e AND_INPUT#2 chem10 GND 200 3199.5 8400 -6400
e AND_INPUT#2 chem9 GND 200 3199.5 10300 -6400
e AND_INPUT'#2 chem8 GND 200 3199.5 12200 -6400
e AND_INPUT'#2 chem7 GND 200 3199.5 14100 -6400
e AND_INPUT'#2 chem6 GND 200 3199.5 16000 -6400
e AND_INPUT'#2 chem5 GND 200 3199.5 17900 -6400
e AND_INPUT#2 chem4 GND 200 3199.5 19800 -6400
e AND_INPUT#2 chem3 GND 200 3199.5 21700 -6400
e AND_INPUT#2 chem2 GND 200 3199.5 23600 -6400
C Vdd GND 513
C AND_INPUT#0 GND 67
C AND_INPUT'#0 GND 81
C AND_INPUT#1 GND 74
```

```
C AND_INPUT'#1 GND 75
C AND_INPUT#2 GND 74
C AND_INPUT'#2 GND 75
C AND_INPUT#3 GND 86
C AND_INPUT'#3 GND 63
```

The input file used to exercise the previously listed logic consisted of the following data:

```
I
I
I
h Vdd
l GND
w A
w B
w C
w D
w chem1
w chem2
w chem3
w chem4
w chem5
w chem6
w chem7
w chem8
w chem9
w chem10
V A 0000000011
V B 0000111100
V C 0011001100
V D 0101010101
G
q
```

The input generated the following output file, which was verified by the proper operation of the selector logic:

```
56 transistors, 24 nodes (10 pulled up)
initialization took 36 steps
initialization took 0 steps
initialization took 0 steps
>0000000011:A
>0000111100:B
>0011001100:C
>0101010101:D
>1000000000:chem1
>0100000000:chem2
>0010000000:chem3
>0001000000:chem4
>0000100000:chem5
>0000010000:chem6
>0000001000:chem7
>0000000100:chem8
>0000000010:chem9
>0000000001:chem10
56 transistors, 24 nodes (10 pulled up)
```

The following integrated circuit processing data was supplied by MOSIS after the microsensor was fabricated:

* RUN: M95C / CECIL — VENDOR: ORBIT
* TECHNOLOGY: SCPE — FEATURE SIZE: 2.0um

PARAMETERS: W/L	N-CHANNEL	P-CHANNEL	UNITS
Vth (Vds=.05V) 3/2	1.160	-.745	V
Vth (Vds=.05V)18/2	1.055	-.721	V
Idss (Vgds=5V)18/2	2279.0	-1242.0	uA
Vpt (Id=1.0uA)18/2	16.18	-15.45	V
Vth (Vds=.05V)50/50	1.025	-.750	V
Vbkd (Ij=1.0uA)50/50	15.8	-16.5	V
Kp 50/50 (Uo*Cox/2)	24.5	10.45	uA/V^2
Gamma 50/50 (2.5v,5.0v)	1.109	.441	V^0.5
Delta Length	.513	.171	um
Delta Width (Effective=Drawn-Delta)	.046	.032	um

COMMENTS: These parameters seem normal.

III. FIELD OXIDE

TRANSISTOR PARAMETERS: GATE	SOURCE/DRAIN N + ACTIVE	SOURCE/DRAIN P + ACTIVE	UNITS
Vth (Vbs=0,I=1uA) Poly	17.3	-27.1	V
Vth (Vbs=0,I=1uA) Metal1	17.3	-20.9	V
Vth (Vbs=0,I=1uA) Metal2	17.4	-12.0	V

COMMENTS: These parameters seem normal.

IV. PROCESS PARAMETERS: UNITS	N POLY	P POLY	N DIFF	P DIFF	METAL 1	METAL 2	POLY 2
Sheet Resistance Ohm/sq	18.5	19.9	23.7	69.2	.049	.029	20.2
Width Variation um (Measured - Drawn)	-.192	-.161	.346	.254	.089	.410	.015
Contact Resist. Ohms (Metal1 to Layer)	7.52	8.93	17.97	39.35	----	.035	8.19
Gate Oxide Thickness: Angst.	----	----	----	411.	----	----	----

COMMENTS: These parameters seem normal.

V. CAPACITANCE PARAMETERS: UNITS	N POLY	P DIFF	METAL 1	METAL 2	POLY 2
Area Cap fF/um^2 (Layer to subs)	.072	.412	.216	.036	.024	----
Area Cap fF/um^2 (Layer to Poly)	----	----	----	.044	.022	.474
Area Cap fF/um^2 (Layer to Metal1)	----	----	----	----	.036	.045
Fringe Cap fF/um (Layer to subs)	----	.530	.247	----	----	----

COMMENTS: These parameters seem normal.

VI. CIRCUIT
PARAMETERS:

Vinv,	K = 1	2.32 V
Vinv,	K = 1.5	2.52 V
Vlow,	K = 2.0	0.00 V
Vhigh,	K = 2.0	5.01 V
Vinv,	K = 2.0	2.66 V
Gain,	K = 2.0	-12.29

Ring Oscillator Frequency 28.49 MHz (31 stages @ 5.0V)

COMMENTS: The ring oscillator frequency is typical.

M95C SPICE LEVEL 2 PARAMETERS

```
.MODEL CMOSN NMOS LEVEL=2 LD=0.243906U TOX=411.000000E-10
+ NSUB=2.230000E+16 VTO=1.068 KP=5.018000E-05 GAMMA=1.024
+ PHI=0.6 UO=597.303 UEXP=0.142861 UCRIT=89159.5
+ DELTA=1.38386 VMAX=71683.1 XJ=0.250000U
LAMBDA=1.953712E-02
+ NFS=7.327201E+11 NEFF=1 NSS=1.000000E+12 TPG=1.000000
+ RSH=23.600000 CGDO=3.073878E-10 CGSO=3.073878E-10
+CGBO=6.564240E-10
+ CJ=4.040000E-04 MJ=0.457000 CJSW=5.020000E-10
MJSW=0.369000 +PB=0.800000
* Weff = Wdrawn - Delta_W
* The suggested Delta_W is 0.00 um
.MODEL CMOSP PMOS LEVEL=2 LD=0.250000U TOX=411.000000E-10
+ NSUB=5.400000E+15 VTO=-0.73 KP=2.007000E-05 GAMMA=0.5039
+ PHI=0.6 UO=238.902 UEXP=0.215244 UCRIT=21917.9
+ DELTA=1.01034 VMAX=41620.5 XJ=0.250000U
LAMBDA=5.724220E-02
+ NFS=1.191843E+12 NEFF=1.001 NSS=1.000000E+12 TPG=-1.000000
+ RSH=70.100000 CGDO=3.150679E-10 CGSO=3.150679E-10
+CGBO=6.564240E-10
+ CJ=2.080000E-04 MJ=0.466000 CJSW=2.230000E-10
MJSW=0.127000 +PB=0.700000
* Weff = Wdrawn - Delta_W
* The suggested Delta_W is 0.00 um
```

M95C SPICE BSIM PARAMETERS

NM1 PM1 DU1 DU2 ML1 ML2
*
*PROCESS=orbit
*RUN=m95c
*WAFER=14
*Gate-oxide thickness= 411.0 angstroms
*Geometries (W-drawn/L-drawn, units are um/um) of transistors measured were:
* 3.0/2.0, 6.0/2.0, 18.0/2.0, 18.0/5.0, 18.0/25.0
*Bias range to perform the extraction (Vdd)=5 volts
*DATE=05-06-89
*
*NMOS PARAMETERS
*
-6.06924133903353e-01,-2.00753657388490e-02,-7.39219509734510e-01
7.70430093620283e-01, 0.00000000000000e+00, 0.00000000000000e+00
9.15146630862213e-01, 9.72185523700295e-02, 1.58624689948246e+00
-7.94143604478796e-02, 5.95061988556805e-02, 4.98731192385094e-01
1.49966373663941e-03, 2.32748677517989e-03, 2.27105335887662e-02
4.99011937635921e+02,7.46194E-001,-5.52594E-002
1.78139126897101e-02, 1.50483950931917e-01,-3.05797177995356e-01
1.06741206757391e-01, 3.19396757054450e-01, 4.98405575238045e-01
1.37447218152595e+01,-3.45601820689190e+01, 1.11580876629667e+02
-8.58537203292464e-04,-1.19779325441167e-02, 2.07361417936266e-02
-2.00969508184277e-03,-2.69070047142389e-03, 6.15703103032119e-03
1.49207414982358e-03,-4.51425120235782e-03, 1.69899233879958e-02

```
  2.96174757624600e-02,-3.22888269627443e-02,
7.23039962553305e-02
  4.67707121717506e+02,  4.12414194705069e+02,
2.95969591789634e+02
  4.32124571732670e+00,-2.17988692952133e+01,
1.32376711544400e+02
-6.97307784602596e+00,  7.93937158236720e+01,
1.58650083352690e+01
-4.60563132878969e-03,  8.17364702083216e-02,
5.91681643407255e-02
4.11000E-002,  2.70000000000000e+01,  5.00000000000000e+00
4.70203E-010,4.70203E-010,6.43058E-010
1.00000E+000,0.00000E+000,0.00000E+000
1.00000E+000,0.00000E+000,0.00000E+000
0.00000E+000,0.00000E+000,0.00000E+000
0.00000E+000,0.00000E+000,0.00000E+000
*
* Gate Oxide Thickness is 410 Angstroms
*
*
*PMOS PARAMETERS
*
-1.72569434674820e-01,-1.41443883690600e-01,-
2.96700437790582e-01
  6.68559183548914e-01,  0.00000000000000e+00,
0.00000000000000e+00
  3.20688729951411e-01,  1.25829954906707e-01,
3.90545431363996e-01
-4.61691286299804e-02,  9.69747360757807e-02,
4.76854637197827e-02
-1.15286948686628e-04,  5.79689384847231e-02,-
6.41128135553033e-03
  2.40954546027695e+02,2.77823E-001,-4.19540E-001
  1.41576752580660e-01,  4.43911924440849e-02,-
1.04315951958508e-01
-2.10608294344991e-02,  5.10019259104388e-01,
4.27170395090183e-02
  1.06341768479827e+01,-4.47387706421899e+00,
5.42635458170274e+00
  1.08203281075985e-03,-5.92602059644244e-03,-
8.91183415220471e-03
```

```
  2.49427345174033e-04,-4.88369010711971e-03,-
4.61885180465470e-03
  8.12999872629999e-03,-6.26088645129279e-03,
6.31429635495288e-03
-3.94434923923152e-03,  1.36584346258480e-02,
4.00632354728362e-02
  2.22743704745999e+02,  3.45510616946786e+02,-
5.06278565405238e+01
  6.73486293666905e+00,  1.01108847964610e+01,
2.77831917492407e+01
-2.52681265618659e+00,  3.67228508108751e+01,
4.50358458176591e+00
-9.67538237728308e-03,  1.53852180671895e-02,
2.21849471023104e-02
4.11000E-002,  2.70000000000000e+01,  5.00000000000000e+00
1.75066E-010,1.75066E-010,5.54944E-010
1.00000E+000,0.00000E+000,0.00000E+000
1.00000E+000,0.00000E+000,0.00000E+000
0.00000E+000,0.00000E+000,0.00000E+000
0.00000E+000,0.00000E+000,0.00000E+000
*
*N+ diffusion::
*
23.6,    4.040000e-04,    5.020000e-10,    1.000000e-08,    0.8
0.8,   0.457,   0.369,   0,   0
*
*P+ diffusion::
*
70.1,    2.080000e-04,    2.230000e-10,    1.000000e-08,    0.7
0.7,   0.466,   0.127,   0,   0
*
*METAL LAYER -- 1
*
4.860000e-02,    2.600000e-05,    0,    0,    0
0,   0,   0,   0,   0
*
*METAL LAYER -- 2
*
2.910000e-02,    1.300000e-05,    0,    0,    0
0,   0,   0,   0,   0
```

The Proc2mod program (U. C. Berkeley) was utilized along with the previous MOSIS process data to extract the following level-four SPICE3 (U. C. Berkeley) models:

```
.model orbit_pm1_du2 pmos level=4
+ vfb = -.172569 lvfb = -.141444 wvfb = -.2967
+ phi = .668559 lphi = 0 wphi = 0
+ k1 = .320689 lk1 = .12583 wk1 = .390545
+ k2 = -.0461691 lk2 = .0969747 wk2 = .0476855
+ eta = -.000115287 leta = .0579689 weta = -.00641128
+ muz = 240.955 dl = .277823 dw = -.41954
+ u0 = .141577 lu0 = .0443912 wu0 = -.104316
+ u1 = -.0210608 lu1 = .510019 wu1 = .042717
+ x2mz = 10.6342 lx2mz = -4.47388 wx2mz = 5.42635
+ x2e = .00108203 lx2e = -.00592602 wx2e = -.00891183
+ x3e = .000249427 lx3e = -.00488369 wx3e = -.00461885
+ x2u0 = .00813 lx2u0 = -.00626089 wx2u0 = .0063143
+ x2u1 = -.00394435 lx2u1 = .0136584 wx2u1 = .0400632
+ mus = 222.744 lmus = 345.511 wmus = -50.6279
+ x2ms = 6.73486 lx2ms = 10.1109 wx2ms = 27.7832
+ x3ms = -2.52681 lx3ms = 36.7229 wx3ms = 4.50358
+ x3u1 = -.00967538 lx3u1 = .0153852 wx3u1 = .0221849
+ tox = .0411 temp = 27 vdd = 5
+ cgdo = 1.75066e-10 cgso = 1.75066e-10 cgbo = 5.54944e-10
+ xpart = 1
+ n0 = 1 ln0 = 0 wn0 = 0
+ nb = 0 lnb = 0 wnb = 0
+ nd = 0 lnd = 0 wnd = 0
+ rsh = 70.1 cj = .000208 cjsw = 2.23e-10
+ js = 1.e-08 pb = .7 pbsw = .7
+ mj = .466 mjsw = .127 wdf = 0
+ dell = 0
.model orbit_pm1_du1 pmos level=4
+ vfb = -.172569 lvfb = -.141444 wvfb = -.2967
+ phi = .668559 lphi = 0 wphi = 0
+ k1 = .320689 lk1 = .12583 wk1 = .390545
+ k2 = -.0461691 lk2 = .0969747 wk2 = .0476855
+ eta = -.000115287 leta = .0579689 weta = -.00641128
+ muz = 240.955 dl = .277823 dw = -.41954
```

```
+ u0 = .141577 lu0 = .0443912 wu0 = -.104316
+ u1 = -.0210608 lu1 = .510019 wu1 = .042717
+ x2mz = 10.6342 lx2mz = -4.47388 wx2mz = 5.42635
+ x2e = .00108203 lx2e = -.00592602 wx2e = -.00891183
+ x3e = .000249427 lx3e = -.00488369 wx3e = -.00461885
+ x2u0 = .00813 lx2u0 = -.00626089 wx2u0 = .0063143
+ x2u1 = -.00394435 lx2u1 = .0136584 wx2u1 = .0400632
+ mus = 222.744 lmus = 345.511 wmus = -50.6279
+ x2ms = 6.73486 lx2ms = 10.1109 wx2ms = 27.7832
+ x3ms = -2.52681 lx3ms = 36.7229 wx3ms = 4.50358
+ x3u1 = -.00967538 lx3u1 = .0153852 wx3u1 = .0221849
+ tox = .0411 temp = 27 vdd = 5
+ cgdo = 1.75066e-10 cgso = 1.75066e-10 cgbo = 5.54944e-10
+ xpart = 1
+ n0 = 1 ln0 = 0 wn0 = 0
+ nb = 0 lnb = 0 wnb = 0
+ nd = 0 lnd = 0 wnd = 0
+ rsh = 23.6 cj = .000404 cjsw = 5.02e-10
+ js = 1.e-08 pb = .8 pbsw = .8
+ mj = .457 mjsw = .369 wdf = 0
+ dell = 0
.model orbit_nm1_du2 nmos level=4
+ vfb = -.606924 lvfb = -.0200754 wvfb = -.73922
+ phi = .77043 lphi = 0 wphi = 0
+ k1 = .915147 lk1 = .0972186 wk1 = 1.58625
+ k2 = -.0794144 lk2 = .0595062 wk2 = .498731
+ eta = .00149966 leta = .00232749 weta = .0227105
+ muz = 499.012 dl = .746194 dw = -.0552594
+ u0 = .0178139 lu0 = .150484 wu0 = -.305797
+ u1 = .106741 lu1 = .319397 wu1 = .498406
+ x2mz = 13.7447 lx2mz = -34.5602 wx2mz = 111.581
+ x2e = -.000858537 lx2e = -.0119779 wx2e = .0207361
+ x3e = -.0020097 lx3e = -.0026907 wx3e = .00615703
+ x2u0 = .00149207 lx2u0 = -.00451425 wx2u0 = .0169899
+ x2u1 = .0296175 lx2u1 = -.0322888 wx2u1 = .072304
+ mus = 467.707 lmus = 412.414 wmus = 295.97
+ x2ms = 4.32125 lx2ms = -21.7989 wx2ms = 132.377
+ x3ms = -6.97308 lx3ms = 79.3937 wx3ms = 15.865
+ x3u1 = -.00460563 lx3u1 = .0817365 wx3u1 = .0591682
+ tox = .0411 temp = 27 vdd = 5
+ cgdo = 4.70203e-10 cgso = 4.70203e-10 cgbo = 6.43058e-10
+ xpart = 1
```

```
+ n0 = 1 ln0 = 0 wn0 = 0
+ nb = 0 lnb = 0 wnb = 0
+ nd = 0 lnd = 0 wnd = 0
+ rsh = 70.1 cj = .000208 cjsw = 2.23e-10
+ js = 1.e-08 pb = .7 pbsw = .7
+ mj = .466 mjsw = .127 wdf = 0
+ dell = 0
.model orbit_nm1_du1 nmos level=4
+ vfb = -.606924 lvfb = -.0200754 wvfb = -.73922
+ phi = .77043 lphi = 0 wphi = 0
+ k1 = .915147 lk1 = .0972186 wk1 = 1.58625
+ k2 = -.0794144 lk2 = .0595062 wk2 = .498731
+ eta = .00149966 leta = .00232749 weta = .0227105
+ muz = 499.012 dl = .746194 dw = -.0552594
+ u0 = .0178139 lu0 = .150484 wu0 = -.305797
+ u1 = .106741 lu1 = .319397 wu1 = .498406
+ x2mz = 13.7447 lx2mz = -34.5602 wx2mz = 111.581
+ x2e = -.000858537 lx2e = -.0119779 wx2e = .0207361
+ x3e = -.0020097 lx3e = -.0026907 wx3e = .00615703
+ x2u0 = .00149207 lx2u0 = .00451425 wx2u0 = .0169899
+ x2u1 = .0296175 lx2u1 = -.0322888 wx2u1 = .072304
+ mus = 467.707 lmus = 412.414 wmus = 295.97
+ x2ms = 4.32125 lx2ms = -21.7989 wx2ms = 132.377
+ x3ms = -6.97308 lx3ms = 79.3937 wx3ms = 15.865
+ x3u1 = -.00460563 lx3u1 = .0817365 wx3u1 = .0591682
+ tox = .0411 temp = 27 vdd = 5
+ cgdo = 4.70203e-10 cgso = 4.70203e-10 cgbo = 6.43058e-10
+ xpart = 1
+ n0 = 1 ln0 = 0 wn0 = 0
+ nb = 0 lnb = 0 wnb = 0
+ nd = 0 lnd = 0 wnd = 0
+ rsh = 23.6 cj = .000404 cjsw = 5.02e-10
+ js = 1.e-08 pb = .8 pbsw = .8
+ mj = .457 mjsw = .369 wdf = 0
+ dell = 0
```

Using the extracted level-four models and the MOSIS processing data, a new simulation model was assembled. The main features other than the modified MOS transistor parameters are the shortened gate lengths, the estimate of the input capacitance ("capara" in the network model), and the modified lumped resistor values due to processing variables. The simulation input file consisted of the following data:

```
expected chemfet performance
**********      establish  subcircuit  models
**********
*IGEFET and inverters
.subckt amp 1 5 4 6
*node 1=vdd
*node 5=vss
*node 4=input
*node 6=output
*apply substrate bias
vbias 9 0 dc -5v
*load bias
ramp1 1 2 7.68e3
ramp2 1 3 11.47e3
ramp3 1 6 8.6e3
m1 2 4 5 9 N l=2.5U w=9U as=81P ad=81P
m2 3 2 5 9 N l=2.5U w=11U as=81P ad=81P
m3 6 3 5 9 N l=2.5U w=12U as=108P ad=108P
capara 4 0 43e-12
*end of subcircuit for amp
.ends amp
**********
*one differential amplifier
.subckt damp 3 5 1 2 4
*node 1=vin-
*node 2=vin+
*node 3=vdd
*node 4=output
*node 5=vss
```

```
*the current mirrors consist of two pmos devices
m1 6 6 3 3 P l=5.83U w=36U as=324P ad=324P
m2 4 6 3 3 P l=5.83U w=36U as=324P ad=324P
*the positive input terminal sense
m3 6 2 7 7 N l=2.5U w=24U as=216P ad=216P
*the negative input terminal sense
m4 4 1 7 7 N l=2.5U w=24U as=216P ad=216P
*the current source
m5 7 3 5 5 N l=2.5U w=12U as=108P ad=108P
*end of subcircuit for damp
.ends damp
*****************************************************************
*analog switch model approximation
.subckt switch 1 2 3 4
*node 1=input
*node 2=N-switch control
*node 3=P-switch control
*node 4=output
*to turn on switch use -5 volts on P-switch and +5 on N-switch
*to turn off wsitch use +5 on P-switch and -5 on N-switch
*bias the switch substrate
vsubn 5 0 dc -5v
vsubp 6 0 dc 5v
*this is the t-gate switch
m21 4 2 1 5 N l=2.5U w=15U as=135P ad=135P
m22 1 3 4 6 P l=2.83U w=15U as=135P ad=135P
.ends switch
*******************    end of subcircuit models
*******************
*****************************************************************
*        set-up the simulation model of chemfet
*****************************************************************
*apply the bias voltages
vdd 1 0 dc 5v
vss 2 0 dc -5v
*this is the signal source for ac and tran analysis
*models the chemfet electrode that was selected by MUX
vin 3 99 dc 0.0 ac .01 0 sin(0 .01 1e3 0 0)
voffset 99 0 dc -0.2v
*vin 3 0 dc 0.0 ac .01 0 pulse(0 .01 0 1e-4 1e-4 50e-3 100e-3)
*****************************************************************
******
```

```
*instantiate the first stage of amplifier on CHEMFET element
*********************************************************
******
*this is the one that will be allowed to pass thru MUX
x1 1 2 3 4 amp
*the remaining chemfet signals are blocked by the MUX
*remaining eight chemfet elements
x11 1 2 0 41 amp
x12 1 2 0 42 amp
x13 1 2 0 43 amp
x14 1 2 0 44 amp
x15 1 2 0 45 amp
x16 1 2 0 46 amp
x17 1 2 0 47 amp
x18 1 2 0 48 amp
*reference amp
x19 1 2 0 49 amp
*********************************************************
******
*signal must pass through the transmission gate
*********************************************************
******
*turn on gate +5 on N-switch -5 on P-switch
*turn-off is opposite application of voltages
vcntrlN 5 0 dc 5v
vcntrlP 6 0 dc -5v
*this is the chemfet signal that is allowed to pass
x2 4 5 6 7 switch
*the remaining switches to block the unselected elements &
reference
x21 41 6 5 7 switch
x22 42 6 5 7 switch
x23 43 6 5 7 switch
x24 44 6 5 7 switch
x25 45 6 5 7 switch
x26 46 6 5 7 switch
x27 47 6 5 7 switch
x28 48 6 5 7 switch
x29 49 6 5 7 switch
*end of the transmission gate's MUX
*********************************************************
******
```

```
*now pass the signal off chip through a voltage follower
*********************************************************
******
x3 1 2 9 7 9 damp
*put a simulated load on the output of the chip
rload 9 0 1e6
cload 9 0 28e-12
.WIDTH OUT=80
.model P pmos level=4
+ vfb = -.172569 lvfb = -.141444 wvfb = -.2967
+ phi = .668559 lphi = 0 wphi = 0
+ k1 = .320689 lk1 = .12583 wk1 = .390545
+ k2 = -.0461691 lk2 = .0969747 wk2 = .0476855
+ eta = -.000115287 leta = .0579689 weta = -.00641128
+ muz = 240.955 dl = .277823 dw = -.41954
+ u0 = .141577 lu0 = .0443912 wu0 = -.104316
+ u1 = -.0210608 lu1 = .510019 wu1 = .042717
+ x2mz = 10.6342 lx2mz = -4.47388 wx2mz = 5.42635
+ x2e = .00108203 lx2e = -.00592602 wx2e = -.00891183
+ x3e = .000249427 lx3e = -.00488369 wx3e = -.00461885
+ x2u0 = .00813 lx2u0 = -.00626089 wx2u0 = .0063143
+ x2u1 = -.00394435 lx2u1 = .0136584 wx2u1 = .0400632
+ mus = 222.744 lmus = 345.511 wmus = -50.6279
+ x2ms = 6.73486 lx2ms = 10.1109 wx2ms = 27.7832
+ x3ms = -2.52681 lx3ms = 36.7229 wx3ms = 4.50358
+ x3u1 = -.00967538 lx3u1 = .0153852 wx3u1 = .0221849
+ tox = .0411 temp = 27 vdd = 5
+ cgdo = 1.75066e-10 cgso = 1.75066e-10 cgbo = 5.54944e-10
+ xpart = 1
+ n0 = 1 ln0 = 0 wn0 = 0
+ nb = 0 lnb = 0 wnb = 0
+ nd = 0 lnd = 0 wnd = 0
+ rsh = 70.1 cj = .000208 cjsw = 2.23e-10
+ js = 1.e-08 pb = .7 pbsw = .7
+ mj = .466 mjsw = .127 wdf = 0
+ dell = 0
.model N nmos level=4
+ vfb = -.606924 lvfb = -.0200754 wvfb = -.73922
+ phi = .77043 lphi = 0 wphi = 0
+ k1 = .915147 lk1 = .0972186 wk1 = 1.58625
+ k2 = -.0794144 lk2 = .0595062 wk2 = .498731
+ eta = .00149966 leta = .00232749 weta = .0227105
```

```
+ muz = 499.012 dl = .746194 dw = -.0552594
+ u0 = .0178139 lu0 = .150484 wu0 = -.305797
+ u1 = .106741 lu1 = .319397 wu1 = .498406
+ x2mz = 13.7447 lx2mz = -34.5602 wx2mz = 111.581
+ x2e = -.000858537 lx2e = -.0119779 wx2e = .0207361
+ x3e = -.0020097 lx3e = -.0026907 wx3e = .00615703
+ x2u0 = .00149207 lx2u0 = -.00451425 wx2u0 = .0169899
+ x2u1 = .0296175 lx2u1 = -.0322888 wx2u1 = .072304
+ mus = 467.707 lmus = 412.414 wmus = 295.97
+ x2ms = 4.32125 lx2ms = -21.7989 wx2ms = 132.377
+ x3ms = -6.97308 lx3ms = 79.3937 wx3ms = 15.865
+ x3u1 = -.00460563 lx3u1 = .0817365 wx3u1 = .0591682
+ tox = .0411 temp = 27 vdd = 5
+ cgdo = 4.70203e-10 cgso = 4.70203e-10 cgbo = 6.43058e-10
+ xpart = 1
+ n0 = 1 ln0 = 0 wn0 = 0
+ nb = 0 lnb = 0 wnb = 0
+ nd = 0 lnd = 0 wnd = 0
+ rsh = 23.6 cj = .000404 cjsw = 5.02e-10
+ js = 1.e-08 pb = .8 pbsw = .8
+ mj = .457 mjsw = .369 wdf = 0
+ dell = 0


*
.OPTIONS DEFL=3U DEFW=6U DEFAS=45P DEFAD=45P
+ITL1=500 ABSTOL=100P VNTOL=100U CHGTOL=1E-14
+NOPAGE LIMPTS=500 RELTOL=.005 CPTIME=5000 ITL5=0
.END
```

Appendix B

Bond Pad Diagram

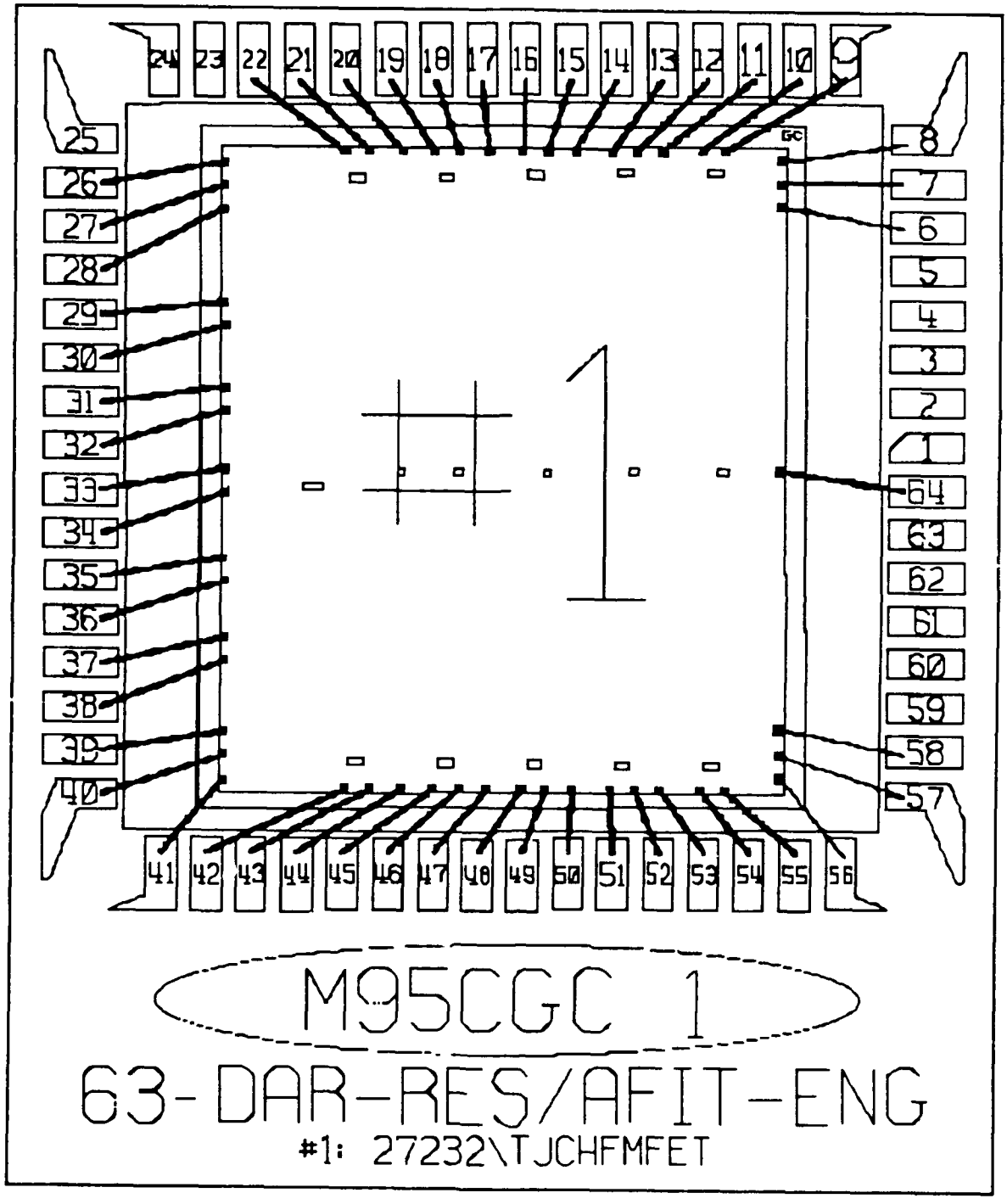

Figure B-1. Bond Pad Diagram.

Appendix C

Phthalocyanine Thin Film Deposition Process

This appendix describes the technique developed to deposit the phthalocyanine compounds using the equipment available in the AFIT Cooperative Electronics and Materials Processing Laboratory. This technique includes a procedure for determining the deposited film's thickness. The deposition of the phthalocyanine compounds onto the interdigitated gate electrode structure was evaluated, as well. Die3 was used to make this evaluation.

Deposition Process

In general, the deposition process can be characterized as a physical vapor deposition process that was similar to the one used in the previous research of Wiseman (7). However, unlike Wiseman's effort, thermal sublimation under a vacuum was used as the vapor source. The deposition procedure in this research was a multi-step process. The major steps were mask fabrication, material deposition, and thickness determination.

Mask Fabrication.

Initially, three masks were fabricated to pattern the various thin films of the phthalocyanine compounds. The schematics of the rubylith patterns used to fabricate the masks are given in Figures C-1, C-2, and C-3. The rubylith patterns were cut to dimensions 50

times larger than the intended mask. The reference numbers given within the figures correspond to the coordinates of the corners in inches. These coordinates were used to cut the rubylith on the plotting table (Xynetics, Inc., Model 1100, Canoga Park, CA). These patterns were printed on high resolution photolithographic plates using a camera platform for mask generation (HLC Engineering Co., Model 6720P DEKACON III, Oreland, PA). The photographic images were then printed onto copper-beryllium (CuBe) foil (NGK Metals Corp., Berylco 25 alloy with XHM temper, Elkhart, IN).

The process used to print the images on the CuBe foil involved several steps. The foil was cut into circular pieces approximately three inches in diameter, and it then was cleaned and polished on a slurry table for one minute. The cleaning solution consisted of a 1:10 sodium hydroxide and deionized water mixture.

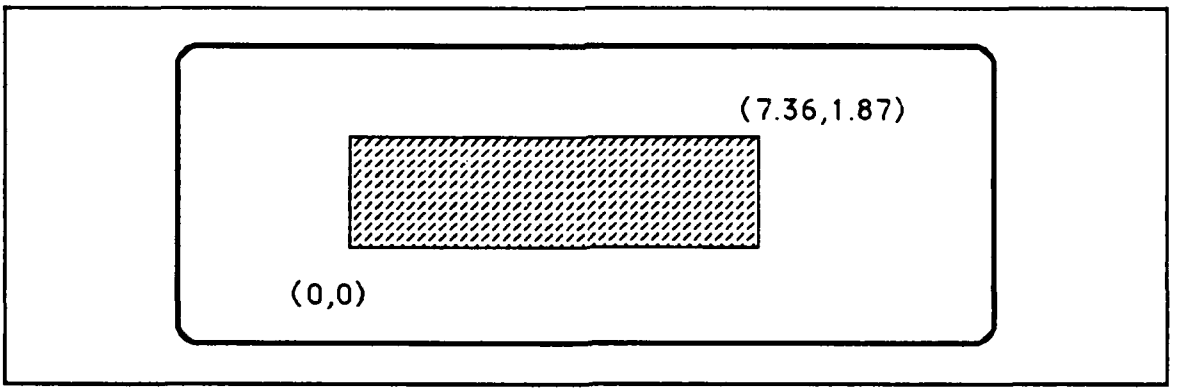

Figure C-1. Mask Used to Coat One Interdigitated Gate Electrode Structure.

After cleaning the foil, two coats of negative photoresist (Olin Hunt Specialty Products, Inc., Waycoat, Type 3, 28cps, West Paterson, NJ) were hard baked on one side of the foil in a photoresist oven (Lab-Line Instruments, Inc., Model Imperial IV, Melrose Park, IL) after spinning at 2000 rpm for 15 seconds (Headway Research Inc., Photoresist Spinner, Model 1-EC101D-R485, Garland, TX).

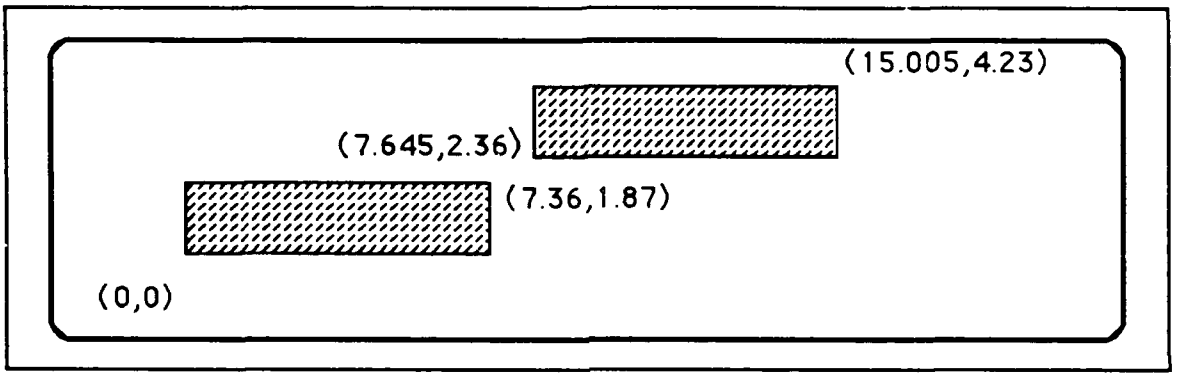

Figure C-2. Mask Used to Coat Two Interdigitated Gate Electrode Structures.

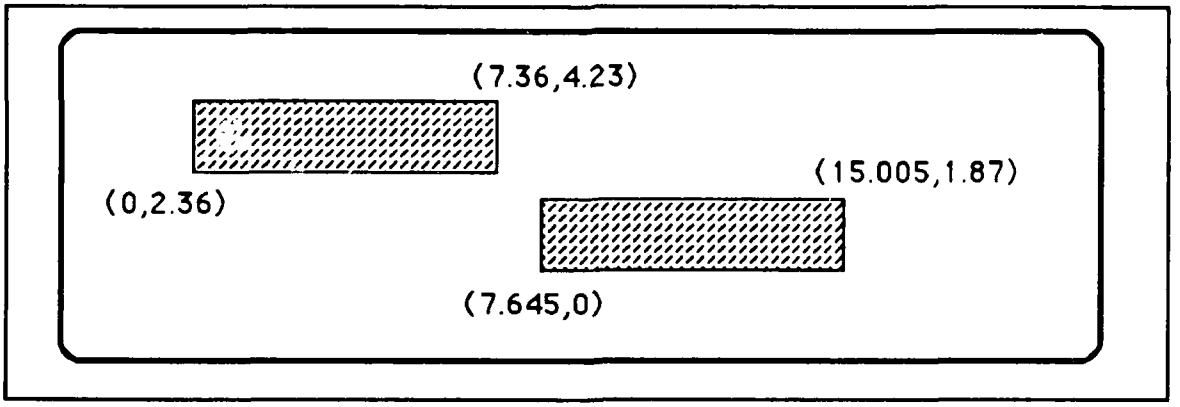

Figure C-3. Second Mask Used to Coat Two Interdigitated Gate Electrode Structures.

After hard baking one side of the foil to protect that side during the etch process, the other side of the foil was coated with hexamethyldisilazane and one coat of negative photoresist. The photographic plates were then printed onto this side of the foil using a mask aligner (Karl Suss, Model MJB3UV300, Waterbury Center, VT). The photoresist was then developed and rinsed by spinning the mask at 2000 rpm for 30 seconds with xylene, and for 30 seconds with butyl acetate.

After hard baking the photographic image on the foil, the CuBe was etched with ferric chloride. After etching, the foil was rinsed with deionized water. The mask was then visually inspected for obvious defects such as incomplete patterns. This step concluded the mask fabrication process.

Material Deposition.

The procedure used to deposit the phthalocyanine compounds involved thermal sublimation of the material under vacuum. To accomplish this process, the appropriate mask was aligned over the interdigitated gate electrodes. This was accomplished by first soft-baking a negative photoresist film on the side of the mask that would be oriented towards the die. The mask was secured such that it was in contact with the die using the procedure developed by Wiseman (7).

The die with the mask was then positioned inside the vacuum system of the thermal evaporation system (Denton Vacuum Corp., Model DV-602, Cherry Hill, NJ). The particular phthalocyanine compound to be deposited was loaded into the thermal evaporation

boat. Next, the vacuum chamber was evacuated to a pressure of 10^{-5} torr.

The phthalocyanine compounds were heated with an AC current of approximately 150 amperes supplied from the 2 KVA power supply of the deposition system. The deposition process was monitored with a quartz crystal microbalance (QCM). The QCM's electronics were established for an average material density of 1.63 g/cm^3, and an acoustic impedance of 25.04 g/cm-sec. The empirical tooling factor used during the deposition process was determined by a previous calibration process for the particular phthalocyanine compound. The calibration is discussed in the next section. The deposition process was halted when the microbalance indicated a predetermined thickness value.

This deposition process was repeated for each of the phthalocyanine materials. The phthalocyanine materials used included:

(1) Copper Phthalocyanine (Fluka Chemical Corp., Stock 61215, Ronkonkoma, NY),

(2) Nickel (II) Phthalocyanine (Fluka Chemical Corp., Stock 72265, Ronkonkoma, NY),

(3) Phthalocyanine (Pfaltz & Bauer, Inc., Stock P18140, Waterbury, CT),

(4) Lead Phthalocyanine (Pfaltz & Bauer, Inc., Stock L02080, Waterbury, CT), and

(5) Cobalt (II) Phthalocyanine (Fluka Chemical Corp., Stock 60855, Ronkonkoma, NY).

After the deposition process was completed for each die, Die1 and Die2 were mounted into 64-pin dual-in-line (DIP) packages supplied from MOSIS. The process associated with packaging the microsensor was accomplished using the resources of the Electronics Device Research Division, Wright Research and Development Laboratory, Wright-Patterson Air Force Base, OH.

Thickness Determination.

A process to determine the thickness of the phthalocyanine thin films was developed during this research. In general, the process involved depositing a pattern of the various phthalocyanine compounds onto oxidized silicon wafers. The thickness was determined by contact profilometry, and the corresponding microbalance measurement that was recorded during the deposition process. Hence, the actual film thickness was determined by the profilometer rather than the microbalance. That is, the microbalance only provides a real-time indication of when to stop the deposition process.

There were several problems encountered attempting to measure the thickness of the phthalocyanine thin films (7). For example, a major problem arises when using contact profilometry. In this technique, a stylus (with a tip radius of about 5 microns) is transported across a sample to be measured. The stylus tracks the changes in the sample's profile as it travels across the sample. When using this technique with phthalocyanine compounds, the stylus scratches their surface. This effect is shown in the photomicrograph in Figure C-4.

In Figure C-4, the result of using a profilometer (Sloan Technology Corp., Model Dek-Tak 900051, Santa Barbara, CA) on a nickel-doped phthalocyanine film, whose thickness was 2000 Å, on an oxidized silicon wafer is shown at a 30° tilt. The same sample is shown in Figure C-5 with a close-up view of the scratch on the right in Figure C-4.

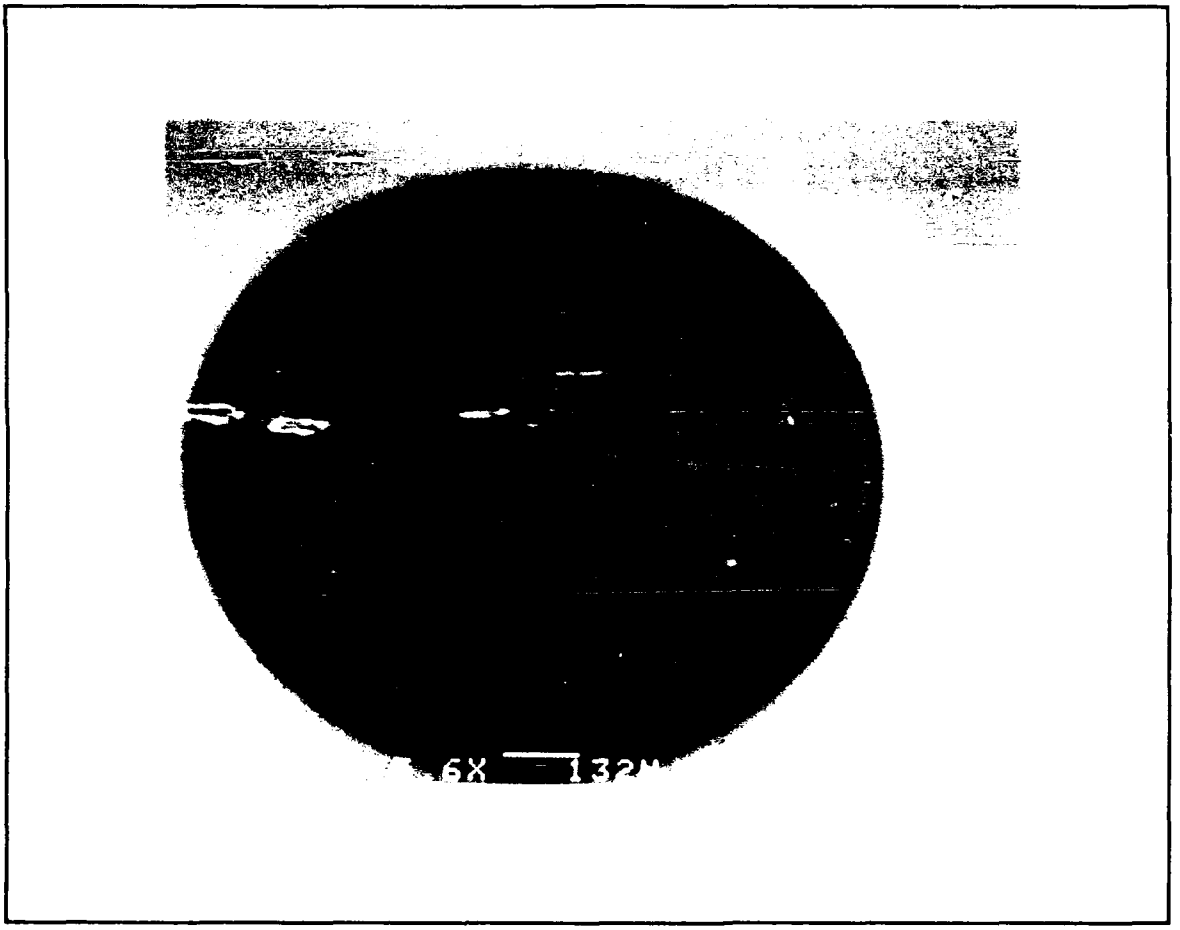

Figure C-4. Photomicrograph of a Scratch in Nickel (II) Phthalocyanine.

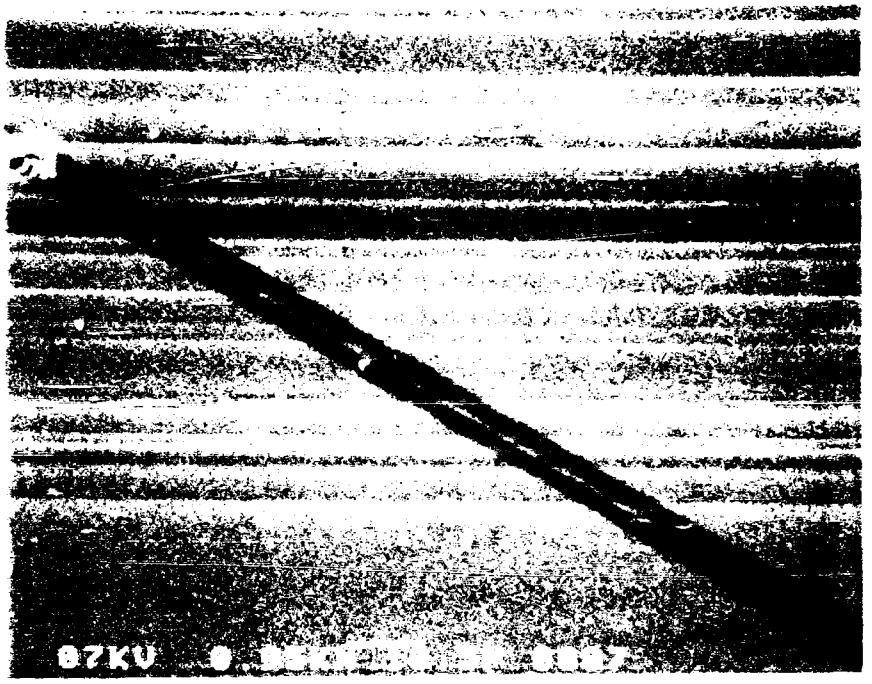

Figure C-5. Close-up View of a Scratch in the Nickel (II) Phthalocyanine Film.

Scratching the film's surface introduces an error in the thickness measurement. As the material thickness decreases, the margin of error will increase, if the scratch characteristic is uniform for different film thicknesses. As is evident in Figures C-4 and C-5, the actual change in height of the profilometer stylus does not correspond to the profile of the material. Instead, it tracks with the extent of the depth of the channel, and the debris that accumulates

in the channel is due to material displacement. This effect is reflected in the jagged trace from the profilometer depicted in Figure C-6. The trace in Figure C-6 is associated with a copper-doped phthalocyanine film whose thickness is approximately 4000 Å. The scale for the trace is 2000 Å per major division.

In this research, it was found that coating the phthalocyanine with a thin layer of gold would prevent scratching. The gold was applied using conventional sputtering equipment (Structure Probe Inc., SPI Sputterer, Model 13131, West Chester, PA) already developed for treating biological samples for scanning electron microscope analysis. After sputtering the gold over the sample to be measured, the sample thickness was determined using the profilometer.

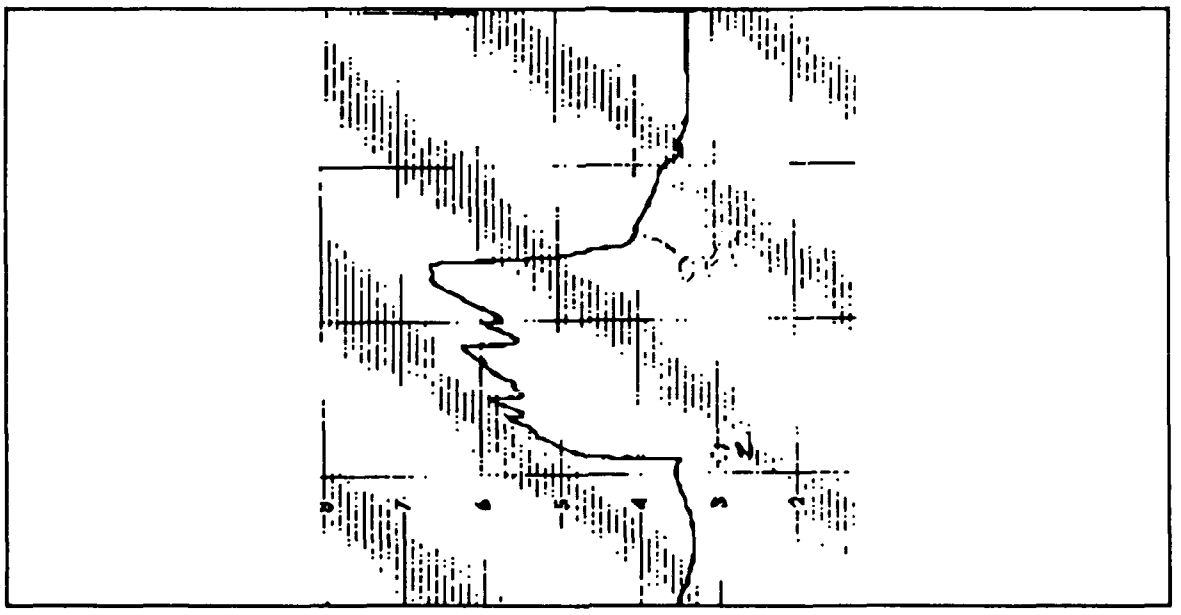

Figure C-6. Profilometer Trace of a Copper-Doped Phthalocyanine Film.

A principal assumption is that the gold coating is uniformly distributed over the profile of the sample. Therefore, any change in the profile that is detected by the profilometer is assumed to be due to the phthalocyanine material. For this research, it was determined that a gold layer whose thickness was 500-750 Å was sufficient to prevent scratching.

As an example of this process, the sample depicted in the previous figures was subsequently coated with gold. After applying the gold film, the sample's profile was checked again with the profilometer. In Figure C-7, a photomicrograph of the previous scratch that is now coated with gold is shown. From this picture, it could be inferred that the gold deposition does not adversely affect the profile since the surface appears to be unaffected (the scratch was not obliterated).

Figure C-8 is a photomicrograph of the same nickel-doped phthalocyanine sample that has been placed on the profilometer after being coated with gold. Scratching is not evident. The image is viewed at a 30^{o} tilt, as well.

The result of the gold deposition over the phthalocyanine compounds produced a "cleaner" trace when the Dek-Tak profilometer was used. As an example, the profile of a copper-doped phthalocyanine sample is shown in Figure C-9, before depositing gold. The trace of Figure C-9 was repeated after coating the sample with gold. The resulting trace using the same height scale (2000 Å per major division) is shown in Figure C-10.

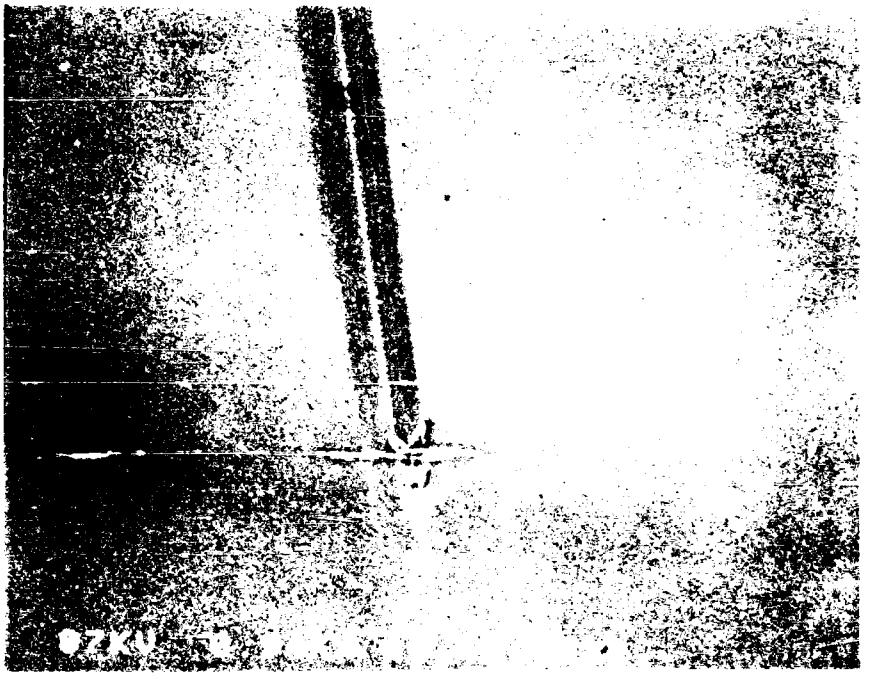

Figure C-7. Profilometer Scratch With Gold Coating (30° Tilt).

Therefore, a deposition process was implemented to take advantage of the effect of the gold coating over the phthalocyanine compounds. Before each material was deposited over an interdigitated gate electrode, several depositions were made of the phthalocyanine compound onto quarter-sections of oxidized silicon wafers. The deposition pattern was made by using one of the

stainless steel grids supplied with the quartz crystal microbalance in the thermal evaporation system.

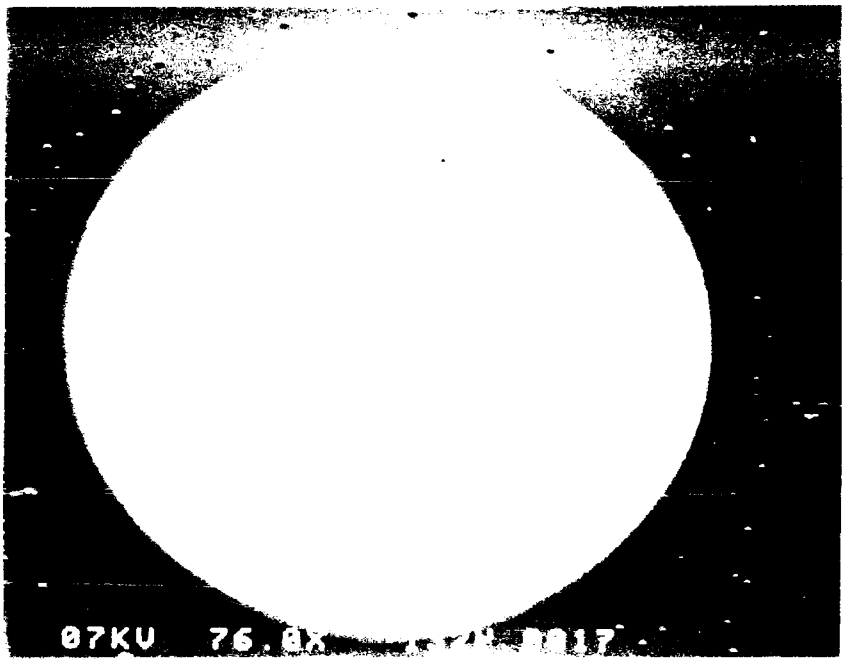

Figure C-8. Photomicrograph of a Profile Examined Using the Dek-Tak Profilometer After Being Coated with Gold.

After each deposition, the film thickness was measured using the revised profilometer procedure. The deposition time was varied until the desired film thickness was found. At this point, the microbalance thickness monitor was adjusted by changing the tooling

factor. It was adjusted until the microbalance indicated a convenient value (the desired film thickness was used).

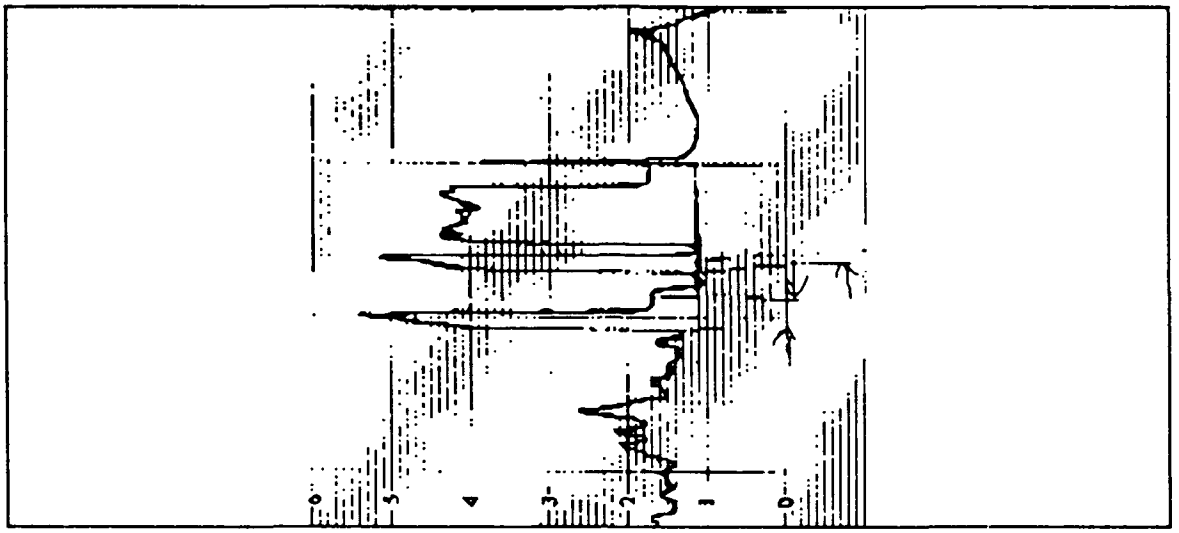

Figure C-9. Dek-Tak Profilometer Trace Before Coating the Sample with Gold.

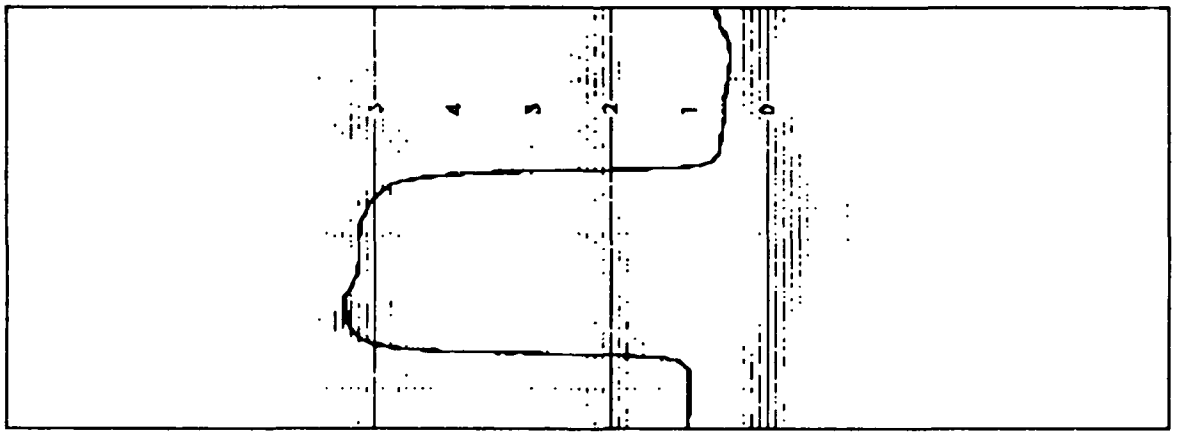

Figure C-10. Dek-Tak Profilometer Trace After Coating the Sample with Gold.

The die and its appropriate mask were placed in the vacuum chamber along with another masked oxidized quartered wafer section. The deposition process was reaccomplished until the microbalance indicated the desired thickness. During this step, a calibration check was accomplished using the profilometer on the oxidized wafer section rather than the microsensor's interdigitated gate electrode.

Deposition onto the Interdigitated Electrode

The deposition of the phthalocyanine compounds onto the interdigitated gate electrode structure was evaluated in this thesis research. Die3 was used to make this evaluation with a scanning electron microscope (International Scientific Instruments, Model WB-6, Milpitas, CA).

The evaluation procedure involved depositing the cobalt-, copper-, lead-, and nickel-doped phthalocyanines using a configuration similar to that used for Die2 (depicted in Figure C-11). The same deposition technique that was used for Die1 and Die2 was used as well.

In Figure C-12, an overall view of the interdigitated gate electrodes on Die3 is shown at a 30^{o} tilt. The structure in the photomicrograph that runs diagonally across the lower left quadrant of the view is an image of the conductive tape used to prevent charge accumulation on the die.

Of particular interest, is the stark contrast between the images of the lead-doped phthalocyanine and the other materials. This observation is interesting because, during the deposition of the lead-doped phthalocyanine, the material remaining in the thermal evaporation boat became "spongy" in appearance. This effect was not observed during the deposition of the other materials.

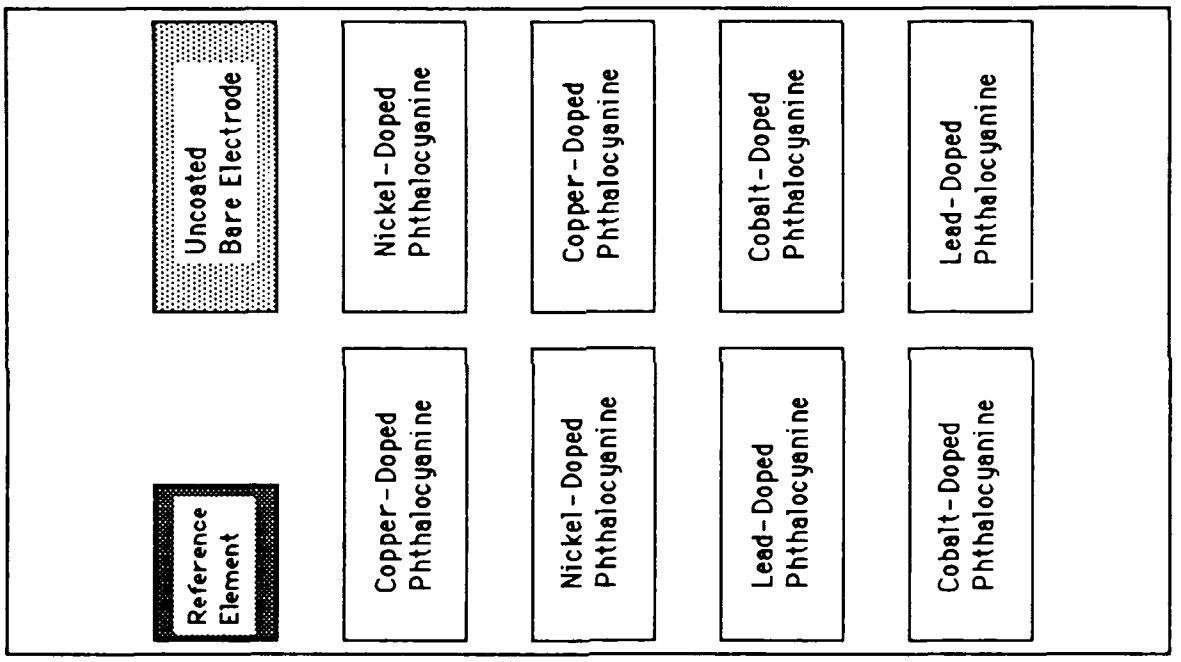

Figure C-11. Schematic of Die3's Polymer Configuration.

Other factors are the differences in atomic numbers of materials and the different charging rates of those materials within the SEM. The atomic number of the central metal atom in the , cobalt-, copper-, and nickel-doped phthalocyanines is similar (27, 29,

and 28, respectively). However, the atomic number of the central metal atom in the lead-doped phthalocyanine is significantly different (82). Additionally, as the different materials are scanned by the electron beam, charge may accumulate. The charge accumulation consequently alters the electron scattering. The effect can produce brighter images with the SEM. Therefore, the electron scattering from the lead-doped phthalocyanine should differ by some degree when compared to the other materials.

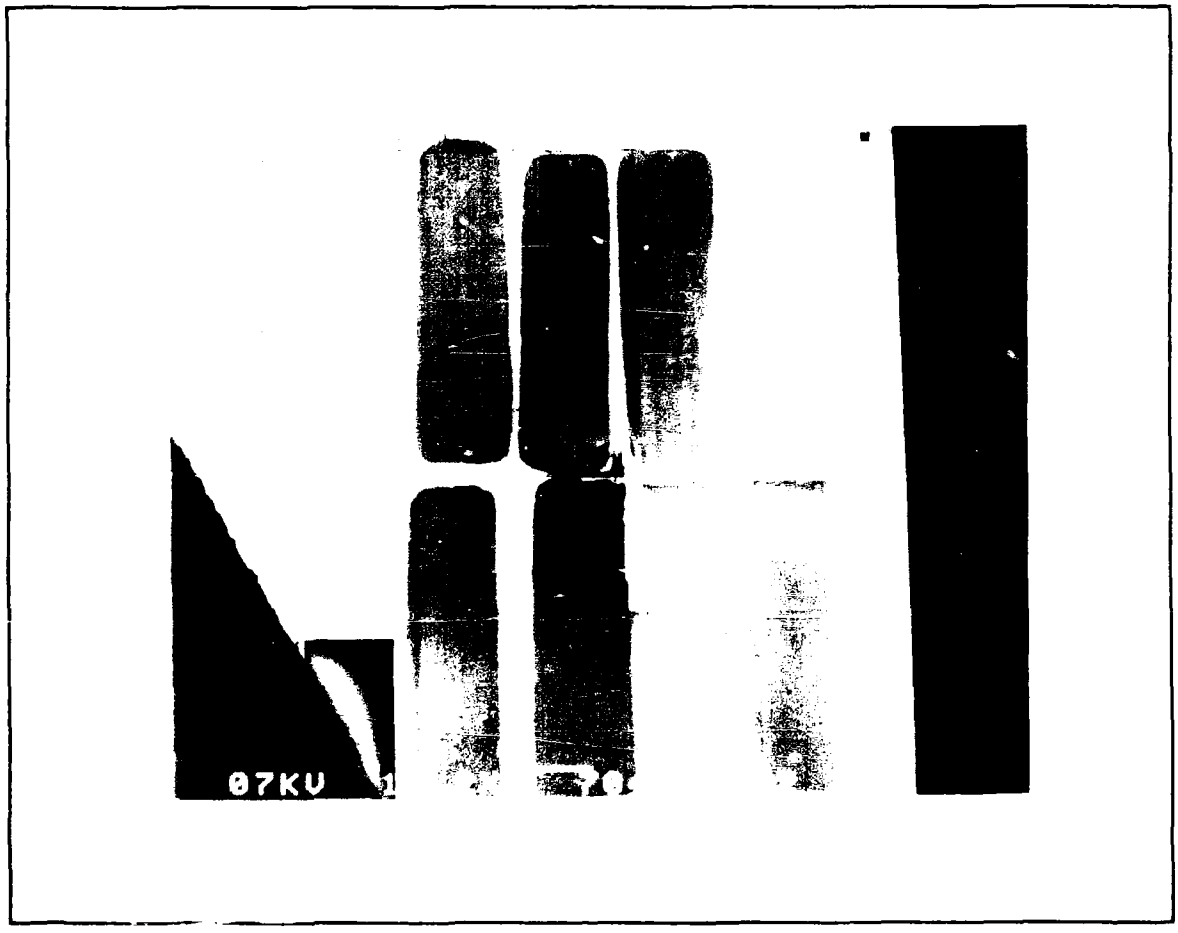

Figure C-12. Photomicrograph of Die3.

In Figure C-13, an image of the uncoated interdigitated gate electrode finger of Chem7 is shown at a 60° tilt. In this photomicrograph, the initial relative roughness of the metal surface of the finger structure is apparent.

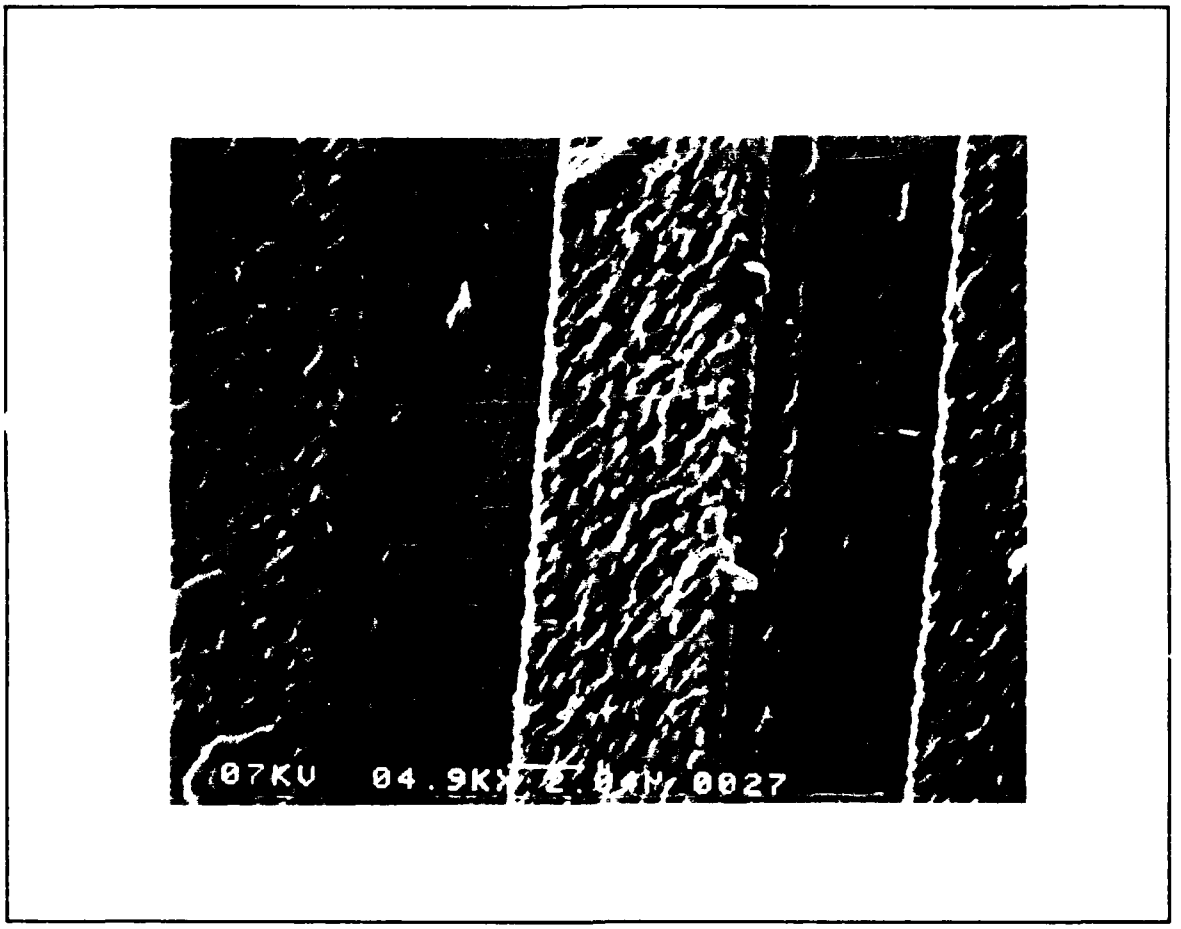

Figure C-13. Uncoated Interdigitated Gate Electrode of Chem7.

In Figure C-14, an image of the boundary of the nickel-doped phthalocyanine on the interdigitated gate electrode of Chem7 is shown at a 60° tilt. The boundary of the material is imaged as a

change in contrast that runs diagonally through the photomicrograph. It is evident from the image that the phthalocyanine compound continuously coats the interdigitated gate electrode through the gap, along the side of the metal finger, and across the top of the metal finger. This observation was inferred by noting how the contrast differs between the coated and uncoated region of the interdigitated gate electrode structure.

Figure C-14. Edge of Phthalocyanine Thin Film Across Chem7.

The image depicted in Figure C-15 involves a cobalt-doped phthalocyanine film within the gap of the interdigitated gate electrode of Chem1. It is viewed with a 60° tilt, as well. Using Figure C-14 and Figure C-15, it can be inferred that the effective surface area of the phthalocyanine compounds is larger than that implied by just a simple planar calculation using the interdigitated gate electrode dimensions.

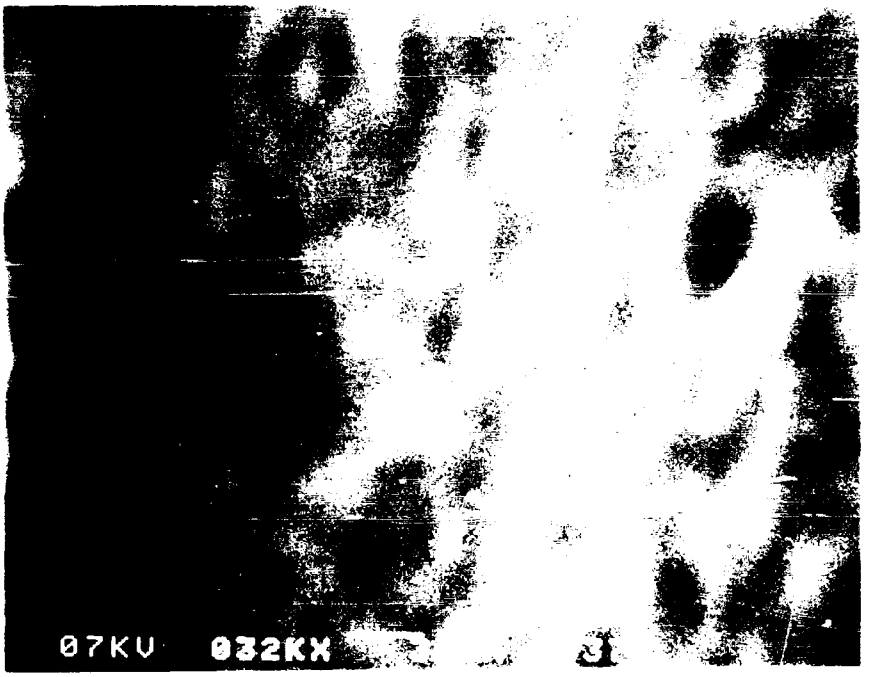

Figure C-15. Gap Region of Coated Interdigitated Gate Electrode of Chem1.

Summary

In this thesis research, a technique was developed for depositing thin films of phthalocyanine compounds using the resources available in the AFIT Cooperative Electronics and Materials Processing Laboratory. The technique used thermally sublimed phthalocyanines under vacuum with subsequent physical vapor deposition onto the interdigitated gate electrodes. The development of the process principally involved determining a method to evaluate the film thickness of the phthalocyanine compounds. As time permits, the procedure should be fully characterized. However, the developed technique was applied for the purposes of this thesis research.

Appendix D

Determination of Gas Concentration

To facilitate the calculation of the challenge gas concentration, a computer program was written to determine its concentration. The manual procedure for calculating the challenge gas concentation was a multi-step process. First, the flowmeter setting (Gilmont Instruments) was read. This value was then located on the appropriate calibration nomograph for that flowmeter, and the approximate gas flow (volume per unit time) was identified. Next, the permeation tube's rate was determined. This was determined by reading the permeation rate (mass per unit time) from an isothermal calibration plot provided by the vendor (G-Cal Industries, Chatsworth, CA). By dividing the permeation rate by the flow rate and multiplying by an appropriate empirical factor, the concentration of the challenge gas was then determined. The manufacturer of the permeation tube supplied the empirical scaling factor. Each time this manual procedure was repeated, there was the potential to misread the calibration nomograph. Therefore, a computer program was written to improve the reliability of this process.

The permeation tube vendor provided relatively precise data on the permeation rates at two temperatures. Therefore, it was a simple matter to determine the logarithmic formula that yielded the permeation rate as a function of temperature in degrees Celcius. The flow rate formula was found by constructing a new nomograph of the flowmeter using linear scaling. Next, a fifth-degree polynomial was

least-squares fitted to the nomograph. The nomograph of the flowmeter used during DIMP challenges is depicted in Figure D-1.

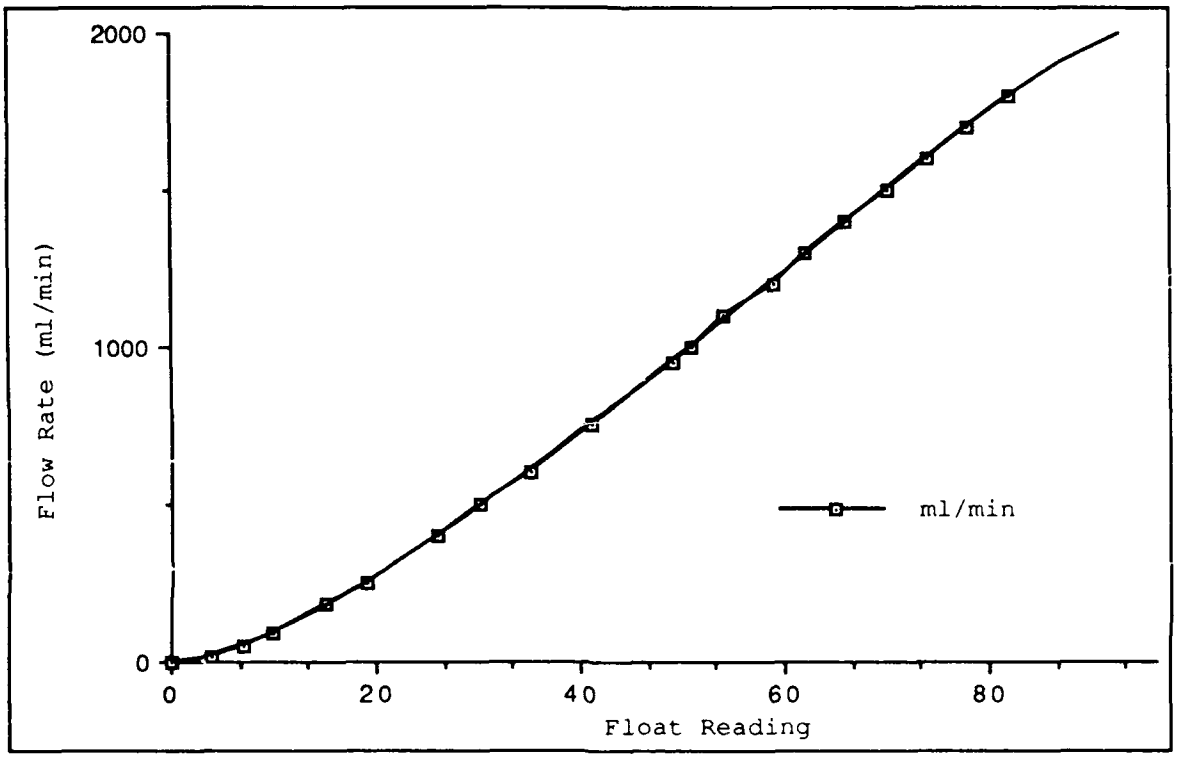

Figure D-1. Nomograph of the Gilmont Industries Flowmeter 25083 with a Glass Float.

The formula for the permeation rate, flow rate, and concentration of DIMP are found in lines 90-100, 120-130, and 140-150, respectively, in the following BASIC computer program:

```
10 CLS
15 PRINT "DIMP CONCENTRATION USING FLOW METER 25083 & GLASS
FLOAT"
17 PRINT "SELECT THE PERMEATION TUBE:"
18 PRINT "        (1) S/N G-5645"
19 PRINT "        (2) S/N G-4942"
20 PRINT ""
21 INPUT "TUBE NUMBER:  ",TUBE
25 PRINT "SELECTED PERMEATION TUBE #";TUBE
30 PRINT ""
40 PRINT ""
50 INPUT "BATH TEMPERATURE:  ",BATH
55 'ENTER TEMP IN CELSIUS
58 IF BATH < -10 OR BATH > 50 THEN PRINT "OUT OF RANGE":GOTO 50
60 INPUT "FLOAT READING:  ",F
65 IF F < 0 OR F > 85 THEN PRINT "OUT OF RANGE":GOTO 60
70 PRINT ""

90 IF TUBE=1 THEN P=10^(9.77658E-3 * BATH + 2.4088)
92 IF TUBE=2 THEN P=10^(9.89381E-3 * BATH + 3.38612)
100 PRINT "PERMEATION RATE = ";P;" NANOGRAMS/MINUTE"

120  FLOW=-2.7204 + 3.3626*F + 0.74862*F^2 - 1.4349E-2*F^3
121  FLOW=FLOW + 1.4982E-4*F^4 - 6.3991E-7*F^5
125 'USE A 5TH DEGREE POLYNOMIAL FIT TO FLOW CURVES

130 PRINT "FLOW RATE FOR METER 25083 = ";FLOW;" ML/MIN"
135 PRINT ""
137 IF TUBE=1 THEN K=0.136
138 IF TUBE=2 THEN K=0.136
140 C=K*P/FLOW 'THIS IS CONCENTRATION IN PPM
145 C=C*1000    'SCALE CONCENTRATION TO PPB
150 PRINT "DIMP CONCENTRATION = ";C;" ppb"
155 PRINT ""
160 INPUT "CALCULATE ANOTHER POINT [Y/N]?  ",ANS$
165 IF ANS$="Y" OR ANS$="y" THEN GOTO 30
170 SYSTEM
180 END
```

The new nomograph found for the flowmeter used during NO_2 challenges is depicted in Figure D-2.

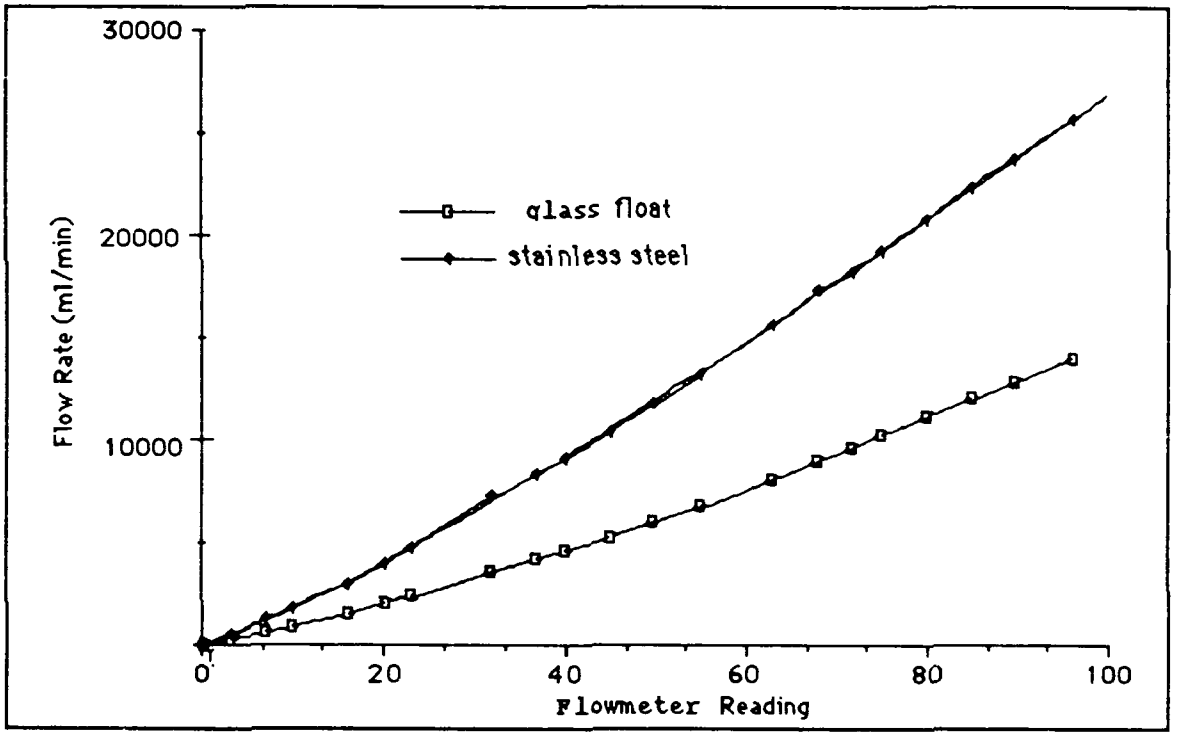

Figure D-2. Nomograph of the Gilmont Industries Flowmeter C8753.

The formula for permeation rate, flow rate, and concentration of NO_2 are found in lines 90-100, 120-130, and 140-150, respectively, in the following BASIC computer program:

```
10 CLS
15 PRINT "NO2 CONCENTRATION USING FLOW METER C8753 & SS
FLOAT"
17 PRINT "SELECT THE PERMEATION TUBE:"
```

```
18 PRINT "       (1) S/N G-5361"
19 PRINT "       (2) S/N G-4766"
20 PRINT ""
21 INPUT "TUBE NUMBER:  ",TUBE
25 PRINT "SELECTED PERMEATION TUBE #";TUBE
30 PRINT ""
40 PRINT ""
50 INPUT "BATH TEMPERATURE:  ",BATH
55 'ENTER TEMP IN CELSIUS
58 IF BATH < -10 OR BATH > 50 THEN PRINT "OUT OF RANGE":GOTO 50
60 INPUT "FLOAT READING:  ",F
65 IF F < 0 OR F > 96 THEN PRINT "OUT OF RANGE":GOTO 60
70 PRINT ""

90 IF TUBE=1 THEN P=10^(7.832E-3 * BATH + 3.398)
92 IF TUBE=2 THEN P=10^(8.6754E-3 * BATH + 2.7276)
100 PRINT "PERMEATION RATE = ";P;" NANOGRAMS/MINUTE"

120  FLOW=2.9058 + 147.21*F + 3.7911*F^2 - 6.6126E-2*F^3
121  FLOW=FLOW + 6.5797E-4*F^4 - 2.5609E-6*F^5
125 'USE A 5TH DEGREE POLYNOMIAL FIT TO FLOW CURVES

130 PRINT "FLOW RATE FOR SS BALL = ";FLOW;" ML/MIN"
135  PRINT ""
137 IF TUBE=1 THEN K=0.532
138 IF TUBE=2 THEN K=0.532
140 C=K*P/FLOW 'THIS IS CONCENTRATION IN PPM
145 C=C*1000    'SCALE CONCENTRATION TO PPB
150 PRINT "NO2 CONCENTRATION = ";C;" ppb"
155  PRINT ""
160 INPUT "CALCULATE ANOTHER POINT [Y/N]?  ",ANS$
165 IF ANS$="Y" OR ANS$="y" THEN GOTO 30
170 SYSTEM
180 END
```

Appendix E

Data Acquisition Software

The following programs were used to acquire the DC resistance with respect to time, DC resistance with respect to applied bias, AC impedance, gain/phase, spectral data, and time-domain oscilloscope data.

DC resistance with respect to time for the microsensor:

```
100 CLS
200 '
300 '
400 PRINT," EVALUATION OF DC RESISTANCE WRT TIME"
500 PRINT ""
600 '
700 '
1100 DEF SEG=&HC400            ' ADDRESS OF GP-IB INTERFACE
1200 INIT%=0                 ' OFFSET OF INITIALIZE ROUTINE
1300 TRANSMIT%=3               ' OFFSET OF TRANSMIT ROUTINE
1400 RECIEVE%=6                ' OFFSET OF RECIEVE ROUTINE
1500 SEND%=9                  ' OFFSET OF SEND ROUTINE
1600 SPOLL%=12                 ' OFFSET OF SERIAL POLL ROUTINE
1700 ENTER%=21                 ' OFFSET OF ENTER ROUTINE
1800 '
1900 '
2000 '
2100 ' GP-IB ADDRESSES OF INSTRUMENTS
2200 '
2300 HP4194%=17: HP4192%=9: PRINTER%=1: MY.ADDR%=21: K617%=27
2400 HP8566%=18: SWITCH%=28
2500 '
2600 SYSCON%=0                 'PC488 ACTS AS CONTROLLER
2700 '
2800 CALL INIT%(MY.ADDR%,SYSCON%)
2900 '
3300 HOURS =0
3400 MINUTES = 0
3500 SECONDS = 0
3600 '
3700 INPUT "EXPERIMENT INFORMATION: ", EXPERIMENT$
3710 INPUT "NAME OF DC IMPEDANCE DATA FILE: ", IMPFILE$
3720 INPUT "GAS: ",GAS$
3730 INPUT "BATH TEMPERATURE: ",BATH$
3735 INPUT "FLOW RATE: ",FLOWR$
3740 INPUT "CHIP TEMPERATURE: ",CHIPTEMP$
```

```
3750 INPUT "VESSEL HUMIDTY:  ",VHUMD$
4600 OPEN "O",#1, IMPFILE$
4700 PRINT#1, EXPERIMENT$;" ";DATE$;" ";TIME$
4710 PRINT#1, "GAS=";GAS$;" BATH=";BATH$;" FLOW=";FLOWR$;
4720 PRINT#1, " T=";CHIPTEMP$;" H=";VHUMD$
4800 PRINT#1, "MINUTES";CHR$(9);"ELECTRODE";CHR$(9);"VOLTAGE",
4810 PRINT#1, CHR$(9);"RESISTANCE"
5000 '
5300 '
5400 '
5500 '          SET-UP ELECTROMETER FOR MEASUREMENT
5600 PRINT " "
5650 PRINT "SET-UP THE ELECTROMETER FOR ZERO CORRECT"
5660 INPUT "ENTER RETURN WHEN READY", NULL$
5700 S$="F1"              'SET TO MEASURE AMPS
5800 CALL SEND%(K617%,S$,STATUS%)
5900 S$="R0X"             'SET TO AUTO RANGE
6000 CALL SEND%(K617%,S$,STATUS%)
6100 S$="Z1X"             'PERFORM ZERO CORRECT
6200 CALL SEND%(K617%,S$,STATUS%)
6300 S$="T0X"
6400 CALL SEND%(K617%,S$,STATUS%)
6500 '
6600 S$="F5X"             'SET TO V/I OHMS MODE
6700 CALL SEND%(K617%,S$,STATUS%)
6800 S$="V00X"            'SET INTERNAL VOLTAGE SOURCE TO 00V
6900 CALL SEND%(K617%,S$,STATUS%)
7000 '
7100 '
7200 '
7300 'ESTABLISH OUTER LOOP COUNTER
7400 BIGC=0
17300 '
17310 '
17320 PRINT "INITIAL ELECTROMETER SET-UP COMPLETE"
17330 PRINT " "
17350 INPUT "CONNECT DUT, HIT RETURN WHEN READY", NULL$
17400 'TURN ON ELAPSE TIMER
17500 CLS
17600 BEGIN.TIME$=TIME$
17700 BEGIN.HRS= VAL(LEFT$(BEGIN.TIME$,2))
17800 BEGIN.MIN= VAL(MID$(BEGIN.TIME$,4,2))
17900 BEGIN.SEC= VAL(RIGHT$(BEGIN.TIME$,2))
18000 ON TIMER (1) GOSUB 47400
18100 TIMER ON
18200 '
18600 '
18650 INPUT "NUMBER OF ELECTRODES TO BE SAMPLED  ",NELECT
18652 INPUT "BIAS VOLTAGE:  ",VINIT
18660 CLS
18670 PRINT "MINUTES";CHR$(9);"ELECTRODE";CHR$(9);"VOLTAGE",
18680 PRINT CHR$(9);"RESISTANCE
18690 S$="V"+STR$(VINIT)+"X"  'SET THE INTERNAL VOLTAGE SOURCE
18695 CALL SEND%(K617%,S$,STATUS%)

18700 '                   'DATA INPUT LOOP

18800 FOR N=1 TO NELECT     'SELECT THE ELECTRODE
18805 PRINT "CONNECT ELECTRODE ";N,
18806 INPUT "RETURN WHEN READY",NULL$
19100 S$="C0X"                'ENABLE READING
19200 CALL SEND%(K617%,S$,STATUS%)
19250 S$="O1X"              'TURN ON VOLTAGE SOURCE
```

```
19260 CALL SEND%(K617%,S$,STATUS%)
19300 TEMP$=SPACE$(16)
19400 FOR I=1 TO 40000: NEXT I    'LET ELECTROMETER SETTLE
19500 CALL ENTER%(TEMP$,LENGTH%,K617%,STATUS%)
19600 DC.RESIST= VAL(RIGHT$(TEMP$,12))
19700 PRINT#1, TOTALT;CHR$(9);N;CHR$(9);VINIT,
19705 PRINT#1, CHR$(9);DC.RESIST
19710 PRINT TOTALT;CHR$(9);N;CHR$(9);VINIT,
19805 PRINT CHR$(9);DC.RESIST
19810 BIGC=BIGC+1
19900 S$="O0X"                    'TURN OFF VOLTAGE SOURCE
20000 CALL SEND%(K617%,S$,STATUS%)
20005 NEXT N
20006 IF BIGC > 7*NELECT THEN BIGC=0 :GOTO 20010
20007 FOR BIGL=1 TO 300000: NEXT BIGL :GOTO 18700
20010 S$="V0X"                    'SET VOLTAGE TO ZERO
20020 CALL SEND%(K617%,S$,STATUS%)
20100 S$="C1X"                    'DISABLE READING
20200 CALL SEND%(K617%,S$,STATUS%)
20300 '
27400 '
27500 '
27600 '
27700 INPUT "COLLECT MORE DATA, Y OR N:", MOREDATA$
27800 IF MOREDATA$="N" THEN 28100
27900 GOTO 18690
28000 '
28100 CLOSE #1
28800 SYSTEM
28900 '
29000 '
29100 '
29200 '
47400 '              TIMER ROUTINE
47500 '
47800 TIME.NOW$=TIME$
47900 NOW.HRS= VAL(LEFT$(TIME.NOW$,2))
48000 NOW.MIN= VAL(MID$(TIME.NOW$,4,2))
48100 NOW.SEC= VAL(RIGHT$(TIME.NOW$,2))
48200 SECONDS= NOW.SEC-BEGIN.SEC
48300 IF SECONDS >= 0 THEN 48500
48400 SECONDS=SECONDS+60: NOW.MIN=NOW.MIN-1
48500 MINUTES=NOW.MIN-BEGIN.MIN
48600 IF MINUTES >= 0 THEN 48800
48700 MINUTES=MINUTES+60: NOW.HRS=NOW.HRS-1
48800 IF NOW.HRS<BEGIN.HRS THEN NOW.HRS=NOW.HRS+24
48900 HOURS=NOW.HRS-BEGIN.HRS
48905 'TOTAL TIME IN MINUTES
48910 TOTALT=SECONDS/60.0 + MINUTES + 60.0*HOURS
49700 RETURN
```

DC resistance with respect to time taken with respect to one microsensor element at a time:

```
100 CLS
200 '
300 '
400 PRINT," EVALUATION OF NONLINEAR RESISTANCE OVER TIME"
500 PRINT ""
600 '
700 '
800 DIM REAL.REF(406), IMAG.REF(406), DATA1#(405)
810 DIM DATA2#(405), FREQ(405)
900 DIM FFT.TEST(800), FFT.REF(800), DATA3(800)
910 DIM GAIN(400), PHS(400)
1000 DIM GFREQ(400), FFT.FREQ(800)
1100 DEF SEG=&HC400              ' ADDRESS OF GP-IB INTERFACE
1200 INIT%=0                   ' OFFSET OF INITIALIZE ROUTINE
1300 TRANSMIT%=3                 ' OFFSET OF TRANSMIT ROUTINE
1400 RECIEVE%=6                  ' OFFSET OF RECIEVE ROUTINE
1500 SEND%=9                   ' OFFSET OF SEND ROUTINE
1600 SPOLL%=12                   ' OFFSET OF SERIAL POLL ROUTINE
1700 ENTER%=21                   ' OFFSET OF ENTER ROUTINE
1800 '
1900 '
2000 '
2100 ' GP-IB ADDRESSES OF INSTRUMENTS
2200 '
2300 HP4194%=17: HP4192%=9: PRINTER%=1: MY.ADDR%=21: K617%=27
2400 HP8566%=18: SWITCH%=28
2500 '
2600 SYSCON%=0                   'PC488 ACTS AS CONTROLLER
2700 '
2800 CALL INIT%(MY.ADDR%,SYSCON%)
2900 '
3000 EX$="EX"
3100 FREQ(0)=5
3200 ELAPSE.TIME$="00:00:00"
3300 HOURS =0
3400 MINUTES = 0
3500 SECONDS = 0
3600 '
3700 INPUT "EXPERIMENT INFORMATION: ", EXPERIMENT$
3800 INPUT "NAME OF IMPEDANCE DATA FILE: ", IMPFILE$
4600 OPEN "O",#1, IMPFILE$
4700 PRINT#1, EXPERIMENT$;" ";DATE$;" ";TIME$
4800 PRINT#1, "TIME";CHR$(9);"ELECTRODE";CHR$(9);"VOLTAGE",
4810 PRINT#1, CHR$(9);"RESISTANCE"
5000 '
5300 '
5400 '
5500 '          SET-UP ELECTROMETER FOR MEASUREMENT
5600 PRINT " "
5650 PRINT "SET-UP THE ELECTROMETER FOR ZERO CORRECT"
5660 INPUT "ENTER RETURN WHEN READY", NULL$
5700 S$="F1"                 'SET TO MEASURE AMPS
5800 CALL SEND%(K617%,S$,STATUS%)
5900 S$="R0X"                'SET TO AUTO RANGE
6000 CALL SEND%(K617%,S$,STATUS%)
6100 S$="Z1X"                'PERFORM ZERO CORRECT
6200 CALL SEND%(K617%,S$,STATUS%)
```

```
6300 S$="T0X"
6400 CALL SEND%(K617%,S$,STATUS%)
6500 '
6600 S$="F5X"              'SET TO V/I OHMS MODE
6700 CALL SEND%(K617%,S$,STATUS%)
6800 S$="V00X"             'SET INTERNAL VOLTAGE SOURCE TO 00V
6900 CALL SEND%(K617%,S$,STATUS%)
7000 '
7100 '
7200 '
17300 '
17310 CLS
17320 PRINT "INITIAL ELECTROMETER SET-UP COMPLETE"
17330 PRINT " "
17350 INPUT "CONNECT DUT, HIT RETURN WHEN READY", NULL$
17400 'TURN ON ELAPSE TIMER
17500 CLS
17600 BEGIN.TIME$=TIME$
17700 BEGIN.HRS= VAL(LEFT$(BEGIN.TIME$,2))
17800 BEGIN.MIN= VAL(MID$(BEGIN.TIME$,4,2))
17900 BEGIN.SEC= VAL(RIGHT$(BEGIN.TIME$,2))
18000 ON TIMER (1) GOSUB 47400
18100 TIMER ON
18200 '
18600 '
18650 INPUT "ELECTRODE NUMBER TO BE SAMPLED:  ",NELECT
18652 INPUT "BIAS VOLTAGE:  ",VBIAS
18660 CLS
18670 PRINT "TIME";CHR$(9);"ELECTRODE";CHR$(9);"VOLTAGE",
18680 PRINT CHR$(9);"RESISTANCE
18700 '                    'DATA INPUT LOOP
18800 N=NELECT     'SELECT THE ELECTRODE
19100 S$="C0X"               'ENABLE READING
19200 CALL SEND%(K617%,S$,STATUS%)
19250 S$="O1X"               'TURN ON VOLTAGE SOURCE
19260 CALL SEND%(K617%,S$,STATUS%)
19270 VN=VBIAS   'SET THE VOLTAGE
19275 S$="V"+STR$(VN)+"X"  'SET THE INTERNAL VOLTAGE SOURCE
19280 CALL SEND%(K617%,S$,STATUS%)
19290 FOR COUNT=1 TO 10   'LOOP THROUGH SEVERAL MEASUREMENTS
19300 TEMP$=SPACE$(16)
19400 FOR I=1 TO 20000: NEXT I    'LET ELECTROMETER SETTLE
19500 CALL ENTER%(TEMP$,LENGTH%,K617%,STATUS%)
19600 DC.RESIST= VAL(RIGHT$(TEMP$,12))
19700 PRINT#1, ELAPSE.TIME;CHR$(9);N;CHR$(9);VN,
19705 PRINT#1, CHR$(9);DC.RESIST
19800 PRINT ELAPSE.TIME;CHR$(9);N;CHR$(9);VN,
19805 PRINT CHR$(9);DC.RESIST
19850 NEXT COUNT
19900 S$="O0X"               'TURN OFF VOLTAGE SOURCE
20000 CALL SEND%(K617%,S$,STATUS%)
20010 S$="V0X"               'SET VOLTAGE TO ZERO
20020 CALL SEND%(K617%,S$,STATUS%)
20100 S$="C1X"               'DISABLE READING
20200 CALL SEND%(K617%,S$,STATUS%)
20300 '
27400 '
27500 '
27600 '
27700 INPUT "COLLECT MORE DATA, Y OR N:", MOREDATA$
27800 IF MOREDATA$="N" THEN 28100
27900 GOTO 17350
28000 '
```

```
28100 CLOSE #1
28800 STOP
28900 '
29000 '
29100 '
29200 '
47400 '              TIMER ROUTINE
47500 '
47600 'Y=CSRLIN
47700 'X=POS(0)
47800 TIME.NOW$=TIME$
47900 NOW.HRS= VAL(LEFT$(TIME.NOW$,2))
48000 NOW.MIN= VAL(MID$(TIME.NOW$,4,2))
48100 NOW.SEC= VAL(RIGHT$(TIME.NOW$,2))
48200 SECONDS= NOW.SEC-BEGIN.SEC
48300 IF SECONDS >= 0 THEN 48500
48400 SECONDS=SECONDS+60: NOW.MIN=NOW.MIN-1
48500 MINUTES=NOW.MIN-BEGIN.MIN
48600 IF MINUTES >= 0 THEN 48800
48700 MINUTES=MINUTES+60: NOW.HRS=NOW.HRS-1
48800 IF NOW.HRS<BEGIN.HRS THEN NOW.HRS=NOW.HRS+24
48900 HOURS=NOW.HRS-BEGIN.HRS
49000 IF SECONDS<10 THEN SECONDS$="0" + RIGHT$(STR$(SECONDS),1)
49100 IF SECONDS >= 10 THEN SECONDS$=RIGHT$(STR$(SECONDS),2)
49200 IF MINUTES<10 THEN MINUTES$="0" + RIGHT$(STR$(MINUTES),1)
49300 IF MINUTES >= 10 THEN MINUTES$=RIGHT$(STR$(MINUTES),2)
49400 'ELAPSE.TIME$= STR$(HOURS) + ":" + MINUTES$ +":" + SECONDS$
49500 'THE FOLLOWING ELAPSE.TIME IS IN MINUTES
49600 ELAPSE.TIME=HOURS*60 + MINUTES + SECONDS/60
49700 RETURN
```

DC resistance with respect to the applied bias:

```
100 CLS
200 '
300 '
400 PRINT," EVALUATION OF NONLINEAR RESISTANCE"
500 PRINT ""
600 '
700 '
800 DIM REAL.REF(406), IMAG.REF(406), DATA1#(405)
810 DIM DATA2#(405), FREQ(405)
900 DIM FFT.TEST(800), FFT.REF(800), DATA3(800)
910 DIM GAIN(400), PHS(400)
1000 DIM GFREQ(400), FFT.FREQ(800)
1100 DEF SEG=&HC400              ' ADDRESS OF GP-IB INTERFACE
1200 INIT%=0                   ' OFFSET OF INITIALIZE ROUTINE
1300 TRANSMIT%=3                 ' OFFSET OF TRANSMIT ROUTINE
1400 RECIEVE%=6                  ' OFFSET OF RECIEVE ROUTINE
1500 SEND%=9                   ' OFFSET OF SEND ROUTINE
1600 SPOLL%=12                   ' OFFSET OF SERIAL POLL ROUTINE
1700 ENTER%=21                   ' OFFSET OF ENTER ROUTINE
1800 '
1900 '
2000 '
2100 ' GP-IB ADDRESSES OF INSTRUMENTS
2200 '
2300 HP4194%=17: HP4192%=9: PRINTER%=1: MY.ADDR%=21: K617%=27
2400 HP8566%=18: SWITCH%=28
2500 '
2600 SYSCON%=0                   'PC488 ACTS AS CONTROLLER
2700 '
2800 CALL INIT%(MY.ADDR%,SYSCON%)
2900 '
3000 EX$="EX"
3100 FREQ(0)=5
3200 ELAPSE.TIME$="00:00:00"
3300 HOURS =0
3400 MINUTES = 0
3500 SECONDS = 0
3600 '
3700 INPUT "EXPERIMENT INFORMATION: ", EXPERIMENT$
3720 INPUT "GAS: ",GAS$
3730 INPUT "BATH TEMPERATURE: ",BATH$
3735 INPUT "FLOW RATE: ",FLOWR$
3740 INPUT "CHIP TEMPERATURE: ",CHIPTEMP$
3750 INPUT "VESSEL HUMIDTY: ",VHUMD$
3800 INPUT "NAME OF IMPEDANCE DATA FILE: ", IMPFILE$
4600 OPEN "O",#1, IMPFILE$
4700 PRINT#1, EXPERIMENT$;" ";DATE$;" ";TIME$
4710 PRINT#1, "GAS=";GAS$;" BATH=";BATH$;" FLOW=";FLOWR$;
4720 PRINT#1, " T=";CHIPTEMP$;" H=";VHUMD$
4800 PRINT#1, "TIME";CHR$(9);"ELECTRODE";CHR$(9);"VOLTAGE",
4810 PRINT#1, CHR$(9);"RESISTANCE"
5000 '
5300 '
5400 '
5500 '          SET-UP ELECTROMETER FOR MEASUREMENT
5600 PRINT " "
5650 PRINT "SET-UP THE ELECTROMETER FOR ZERO CORRECT"
5660 INPUT "ENTER RETURN WHEN READY", NULL$
```

```
5700 S$="F1"                'SET TO MEASURE AMPS
5800 CALL SEND%(K617%,S$,STATUS%)
5900 S$="R0X"               'SET TO AUTO RANGE
6000 CALL SEND%(K617%,S$,STATUS%)
6100 S$="Z1X"               'PERFORM ZERO CORRECT
6200 CALL SEND%(K617%,S$,STATUS%)
6300 S$="T0X"
6400 CALL SEND%(K617%,S$,STATUS%)
6500 '
6600 S$="F5X"               'SET TO V/I OHMS MODE
6700 CALL SEND%(K617%,S$,STATUS%)
6800 S$="V00X"              'SET INTERNAL VOLTAGE SOURCE TO 00V
6900 CALL SEND%(K617%,S$,STATUS%)
7000 '
7100 '
7200 '
17300 '
17310 CLS
17320 PRINT "INITIAL ELECTROMETER SET-UP COMPLETE"
17330 PRINT " "
17350 INPUT "CONNECT DUT, HIT RETURN WHEN READY", NULL$
17400 'TURN ON ELAPSE TIMER
17500 CLS
17600 BEGIN.TIME$=TIME$
17700 BEGIN.HRS= VAL(LEFT$(BEGIN.TIME$,2))
17800 BEGIN.MIN= VAL(MID$(BEGIN.TIME$,4,2))
17900 BEGIN.SEC= VAL(RIGHT$(BEGIN.TIME$,2))
18000 ON TIMER (1) GOSUB 47400
18100 TIMER ON
18200 '
18600 '
18650 INPUT "ELECTRODE NUMBER TO BE SAMPLED:  ",NELECT
18652 INPUT "INITIAL BIAS VOLTAGE:  ",VINIT
18654 INPUT "FINAL BIAS VOLTAGE:  ",VFINAL
18656 INPUT "BIAS VOLTAGE STEP SIZE:  ",VSTEP
18660 CLS
18670 PRINT "TIME";CHR$(9);"ELECTRODE";CHR$(9);"VOLTAGE",
18680 PRINT CHR$(9);"RESISTANCE
18700 '                     'DATA INPUT LOOP
18800  N=NELECT     'SELECT THE ELECTRODE
19100 S$="C0X"                'ENABLE READING
19200 CALL SEND%(K617%,S$,STATUS%)
19250 S$="O1X"                'TURN ON VOLTAGE SOURCE
19260 CALL SEND%(K617%,S$,STATUS%)
19270 FOR VN=VINIT TO VFINAL STEP VSTEP  'SWEEP THE VOLTAGE
19275 S$="V"+STR$(VN)+"X"  'SET THE INTERNAL VOLTAGE SOURCE
19280 CALL SEND%(K617%,S$,STATUS%)
19300 TEMP$=SPACE$(16)
19400 FOR I=1 TO 40000: NEXT I    'LET ELECTROMETER SETTLE
19500 CALL ENTER%(TEMP$,LENGTH%,K617%,STATUS%)
19600 DC.RESIST= VAL(RIGHT$(TEMP$,12))
19700 PRINT#1, ELAPSE.TIME$;CHR$(9);N;CHR$(9);VN,
19705 PRINT#1, CHR$(9);DC.RESIST
19800 PRINT ELAPSE.TIME$;CHR$(9);N;CHR$(9);VN,
19805 PRINT CHR$(9);DC.RESIST
19850 NEXT VN
19900 S$="O0X"                'TURN OFF VOLTAGE SOURCE
20000 CALL SEND%(K617%,S$,STATUS%)
20010 S$="V0X"                'SET VOLTAGE TO ZERO
20020 CALL SEND%(K617%,S$,STATUS%)
20100 S$="C1X"                'DISABLE READING
20200 CALL SEND%(K617%,S$,STATUS%)
20300 '
```

```
27400 '
27500 '
27600 '
27700 INPUT "COLLECT MORE DATA, Y OR N:", MOREDATA$
27800 IF MOREDATA$="N" THEN 28100
27900 GOTO 18650
28000 '
28100 CLOSE #1
28800 SYSTEM
28900 '
29000 '
29100 '
29200 '
47400 '              TIMER ROUTINE
47500 '
47600 'Y=CSRLIN
47700 'X=POS(0)
47800 TIME.NOW$=TIME$
47900 NOW.HRS= VAL(LEFT$(TIME.NOW$,2))
48000 NOW.MIN= VAL(MID$(TIME.NOW$,4,2))
48100 NOW.SEC= VAL(RIGHT$(TIME.NOW$,2))
48200 SECONDS= NOW.SEC-BEGIN.SEC
48300 IF SECONDS >= 0 THEN 48500
48400 SECONDS=SECONDS+60: NOW.MIN=NOW.MIN-1
48500 MINUTES=NOW.MIN-BEGIN.MIN
48600 IF MINUTES >= 0 THEN 48800
48700 MINUTES=MINUTES+60: NOW.HRS=NOW.HRS-1
48800 IF NOW.HRS<BEGIN.HRS THEN NOW.HRS=NOW.HRS+24
48900 HOURS=NOW.HRS-BEGIN.HRS
49000 IF SECONDS<10 THEN SECONDS$="0" + RIGHT$(STR$(SECONDS),1)
49100 IF SECONDS >= 10 THEN SECONDS$=RIGHT$(STR$(SECONDS),2)
49200 IF MINUTES<10 THEN MINUTES$="0" + RIGHT$(STR$(MINUTES),1)
49300 IF MINUTES >= 10 THEN MINUTES$=RIGHT$(STR$(MINUTES),2)
49400 ELAPSE.TIME$= STR$(HOURS) + ":" + MINUTES$ +":" + SECONDS$
49700 RETURN
```

AC impedance with respect to frequency:

```
100 CLS
200 '
300 '
400 PRINT," HP4194A IMPEDANCE DATA TRANSFER "
500 '
600 '
700 '
900 DIM MAG(400), PHS(400)
1000 DIM GFREQ(400)
1100 DEF SEG=&HC400          ' ADDRESS OF GP-IB INTERFACE
1200 INIT%=0                 ' OFFSET OF INITIALIZE ROUTINE
1300 TRANSMIT%=3             ' OFFSET OF TRANSMIT ROUTINE
1400 RECIEVE%=6              ' OFFSET OF RECIEVE ROUTINE
1500 SEND%=9                 ' OFFSET OF SEND ROUTINE
1600 SPOLL%=12               ' OFFSET OF SERIAL POLL ROUTINE
1700 ENTER%=21               ' OFFSET OF ENTER ROUTINE
1800 '
1900 '
2000 '
2100 ' GP-IB ADDRESSES OF INSTRUMENTS
2200 '
2300 HP4194%=17: HP4192%=9: PRINTER%=1: MY.ADDR%=21: K617%=27
2400 SWITCH%=28
2500 '
2600 SYSCON%=0                    'PC488 ACTS AS CONTROLLER
2700 '
2800 CALL INIT%(MY.ADDR%,SYSCON%)
2900 '
3600 PRINT " "
8600 PRINT "SET-UP 4194 FOR IMPEDANCE MEASUREMENTS"
8700 '
8800 '
8900 S$="RST"          'INITIALIZE 4194 TO POWER ON SETTING
9000 CALL SEND%(HP4194%,S$,STATUS%)
9100 S$="RQS2"         'UNMASK AND ENABLE BIT1 FOR SRQ
9200 CALL SEND%(HP4194%,S$,STATUS%)
9300 S$="FNC1"                    'SET 4194 TO IMPEDANCE MODE
9400 CALL SEND%(HP4194%,S$,STATUS%)
9500 S$="PHS2"              'SET PHASE SCALE TO EXPANSION MODE
9600 CALL SEND%(HP4194%,S$,STATUS%)
9700 S$="SWM2"                    'SET SWEEP MODE TO SINGLE
9800 CALL SEND%(HP4194%,S$,STATUS%)
9900 S$="SWT2"                   'SET TO LOG SWEEP
10000 CALL SEND%(HP4194%,S$,STATUS%)
10100 S$="OSC=1V"          'SET SWEEP OSCILLATOR TO 1VOLT
10200 CALL SEND%(HP4194%,S$,STATUS%)
10300 S$="MCF0"                   'TURN MARKERS OFF
10400 CALL SEND%(HP4194%,S$,STATUS%)
10900 S$="ITM1"            'SET INTEGRATION TIME TO 1mSEC
11000 CALL SEND%(HP4194%,S$,STATUS%)
11050 S$="START=1000HZ"  'STRT SWEEP AT 1KHZ
11060 CALL SEND%(HP4194%,S$,STATUS%)
11100 S$="STOP=1000000HZ"          'SWEEP TO 1MHz
11200 CALL SEND%(HP4194%,S$,STATUS%)
11300 '
11400 INPUT "PERFORM THE OFFSET REF STORE, THEN RETURN", NULL$
11500 '
12700 '
12710 S$="BIAS=2V"        'SET BIAS VOLTAGE TO 2VOLT
```

```
12720 CALL SEND%(HP4194%,S$,STATUS%)
12800 S$="X?"                    'READ IN FREQUENCY POINTS
12900 CALL SEND%(HP4194%,S$,STATUS%)
13000 S$="MLA TALK 17"           '4194 TO OUTPUT
13100 CALL TRANSMIT%(S$,STATUS%)
13200 TEMP$=SPACE$(15)
13300 FOR I=0 TO 400
13400 CALL RECIEVE%(TEMP$,LENGTH%,STATUS%)
13500 GFREQ(I)=VAL(LEFT$(TEMP$,12))
13600 NEXT I
13700 '
13820 '
17500 CLS
18200 '
18300 INPUT "EXPERIMENT INFORMATION:  ",EXPERIMENT$
18310 INPUT "GAS:  ",GAS$
18320 INPUT "BATH TEMPERATURE:  ",BATH$
18330 INPUT "FLOW RATE:  ",FLOWR$
18340 INPUT "CHIP TEMPERATURE:  ",CHIPTEMP$
18350 INPUT "VESSEL HUMIDTY:  ",VHUMD$
18400 INPUT "NAME OF IMPEDANCE DATA FILE:", GATEGP.FILE$
18510 INPUT "NUMBER OF ELECTRODES TO BE SAMPLED:  ",NELECT
18520 OPEN "O",#2, GATEGP.FILE$
18530 '
18535 PRINT#2, EXPERIMENT$;" ";DATE$;" ";TIME$
18540 PRINT#2, "GAS=";GAS$;" BATH=";BATH$;" FLOW=";FLOWR$;
18545 PRINT#2, " T=";CHIPTEMP$;" H=";VHUMD$
18547 PRINT#2, "ELECTRODE","FREQUENCY","Z-MAG","PHASE"
18550 CLS
18610 ' SET UP THE WAVETEK SWITCH
18611 'S$="SF1"    'SET SINGLE AND MAKE-BEFORE BREAK
18612 'CALL SEND%(SWITCH%,S$,STATUS%)
18700 '                    'DATA INPUT LOOP
18800 FOR N=1 TO NELECT      'LOOP THROUGH THE NUMBER OF ELECTRODES
18805 PRINT "CONNECT ELECTRODE ";N,
18807 INPUT "HIT RETURN WHEN READY",NULL$
18810 'IF N=1 THEN GOTO 18830
18815 'IF N=5 THEN GOTO 18835
18820 'S$="K"+STR$(N)+"CI" : GOTO 18840
18830 'S$="K8OK1CI":GOTO 18840
18835 'S$="K4OK5CI":GOTO 18840
18840 'CALL SEND%(SWITCH%,S$,STATUS%)  'SELECT ELECTRODE
19000 '
21700 GOSUB 42100    ' GO GET DATA
21800 '
21850 FOR I= 0 TO 400
21900 PRINT#2,  N;CHR$(9);GFREQ(I);CHR$(9);MAG(I);CHR$(9);PHS(I)
21910 IF (I MOD 100) = 0 THEN PRINT N,GFREQ(I),MAG(I),PHS(I)
22000 NEXT I
22100 NEXT N   ' LOOP THROUGH THE ELECTRODE
27400 'S$="K"+STR$(N)+"OI"    'SHUT-OFF THE SWITCH
27440 'CALL SEND%(SWITCH%,S$,STATUS%)
27480 CLOSE #2
27500 '
27600 '
27700 INPUT "COLLECT MORE DATA, Y OR N:", MOREDATA$
27800 IF MOREDATA$="N" THEN 28200
27900 GOTO 18300
28000 '
28200 '
28800 STOP
42100 '
42200 '
```

```
42300 '                    HP4194 DATA INPUT ROUTINE
42400 '
42500 '
42600 CALL SPOLL%(HP4194%,POLL%,STATUS%)  'MAKE SURE SRQ IS NOT SET
42700 S$="SWTRG"                          'PERFORM SINGLE SWEEP
42800 CALL SEND%(HP4194%,S$,STATUS%)
42900 CALL SPOLL%(HP4194%,POLL%,STATUS%)  'IS SWEEP COMPLETE?
43000 IF ((POLL% AND 64) <> 64) THEN 42900  'IF NOT CONTINUE POLL
43100 '
43200 S$="AUTOA"                          'AUTOSCALE DISPLAY A
43300 CALL SEND%(HP4194%,S$,STATUS%)
43400 S$="AUTOB"                          'AUTOSCALE DISPLAY B
43500 CALL SEND%(HP4194%,S$,STATUS%)
43600 S$="A?"                             'READ IN MAG VALUE
43700 CALL SEND%(HP4194%,S$,STATUS%)      'FROM THE ARRAY REG A
45300 '
45400 S$= "MLA TALK 17"
45500 CALL TRANSMIT%(S$,STATUS%)
45600 TEMP$= SPACE$(13)
45700 FOR I = 0 TO 400
45800 CALL RECIEVE%(TEMP$,LENGTH%,STATUS%)
45900 MAG(I)=VAL(LEFT$(TEMP$,12))         'EXTRACT MAG VALUE
46000 NEXT I
46100 '
46200 S$="B?"                 'READ IN PHASE FROM ARRAY REGISTER B
46300 CALL SEND%(HP4194%,S$,STATUS%)
46400 S$= "MLA TALK 17"
46500 CALL TRANSMIT%(S$,STATUS%)
46600 FOR I= 0 TO 400
46700 CALL RECIEVE%(TEMP$,LENGTH%,STATUS%)
46800 PHS(I)= VAL(LEFT$(TEMP$,12))        'EXTRACT PHASE VALUE
46900 NEXT I
47000 '
47100 '
47200 CALL SPOLL%(HP4194%,POLL%,STATUS%)   'MAKE SURE SRQ NOT SET
47300 RETURN
```

Gain and phase measurements with respect to frequency:

```
100 CLS
200 '
300 '
400 PRINT," HP4194A GAIN/PHASE SOFTWARE"
500 '
600 '
700 '
900 DIM GAIN(400), PHS(400)
1000 DIM GFREQ(400)
1100 DEF SEG=&HC400              ' ADDRESS OF GP-IB INTERFACE
1200 INIT%=0                   ' OFFSET OF INITIALIZE ROUTINE
1300 TRANSMIT%=3                 ' OFFSET OF TRANSMIT ROUTINE
1400 RECIEVE%=6                  ' OFFSET OF RECIEVE ROUTINE
1500 SEND%=9                   ' OFFSET OF SEND ROUTINE
1600 SPOLL%=12                   ' OFFSET OF SERIAL POLL ROUTINE
1700 ENTER%=21                   ' OFFSET OF ENTER ROUTINE
1800 '
1900 '
2000 '
2100 ' GP-IB ADDRESSES OF INSTRUMENTS
2200 '
2300 HP4194%=17: HP4192%=9: PRINTER%=1: MY.ADDR%=21: K617%=27
2310 SWITCH%=28
2400 '
2500 '
2600 SYSCON%=0                        'PC488 ACTS AS CONTROLLER
2700 '
2800 CALL INIT%(MY.ADDR%,SYSCON%)
2900 '
3600 '                SET-UP WAVETEK SWITCH
3610 'S$="SFI"    'SET SINGLE AND MAKE BEFORE BREAK
3620 'CALL SEND%(SWITCH%,S$,STATUS%)
8600 '                 SET-UP 4194 FOR G/P MEASUREMENTS
8700 '
8800 '
8900 S$="RST"        'INIT.  . 4194 TO POWER ON SETTING
9000 CALL SEND%(HP4194%,S$,STATUS%)
9100 S$="RQS2"       'UNMASK AND ENABLE BIT1 FOR SRQ
9200 CALL SEND%(HP4194%,S$,STATUS%)
9300 S$="FNC2"       'SET 4194 TO GAIN PHASE MODE
9400 CALL SEND%(HP4194%,S$,STATUS%)
9500 S$="PHS2"       'SET PHASE SCALE TO EXPANSION MODE
9600 CALL SEND%(HP4194%,S$,STATUS%)
9700 S$="SWM2"       'SET SWEEP MODE TO SINGLE
9800 CALL SEND%(HP4194%,S$,STATUS%)
9900 S$="SWT2"       'SET TO LOG SWEEP
10000 CALL SEND%(HP4194%,S$,STATUS%)
10010 INPUT "ENTER THE OSCILLATOR LEVEL IN VOLTS: ",OSCV
10100 S$="OSC="+STR$(OSCV)+"V"  'SET SWEEP OSCILLATOR IN VOLTS
10200 CALL SEND%(HP4194%,S$,STATUS%)
10300 S$="MCF0"                      'TURN MARKERS OFF
10400 CALL SEND%(HP4194%,S$,STATUS%)
10500 S$="ZIR2"       'SET REF CHANNEL INPUT IMP.=50 ohm
10600 CALL SEND%(HP4194%,S$,STATUS%)
10700 S$="ZIT2"       'SET TEST CHANNEL INPUT IMP=50 ohm
10800 CALL SEND%(HP4194%,S$,STATUS%)
10810 S$="ATR2"       'SET REF CHANNEL INPUT 20DB
10820 CALL SEND%(HP4194%,S$,STATUS%)
10830 S$="ATT2"       'SET TEST CHANNEL INPUT IMP=20DB
```

```
10840 CALL SEND%(HP4194%,S$,STATUS%)
10900 S$="ITM1"          'SET INTEGRATION TIME TO 1mSEC
11000 CALL SEND%(HP4194%,S$,STATUS%)
11050 S$="START=1000HZ" 'START SWEEP AT 1KHZ
11060 CALL SEND%(HP4194%,S$,STATUS%)
11100 S$="STOP=200000HZ"       'SWEEP TO 200KHz
11200 CALL SEND%(HP4194%,S$,STATUS%)
11300 PRINT "BYPASS THE AMPLIFIER AND SHORT THE TEST CELL"
11400 INPUT "OFFSET REF STORE, RETURN WHEN READY", NULL$
11500 '
11600 '
11700 S$="SWTRG"                    'PERFORM SINGLE SWEEP
11800 CALL SEND%(HP4194%,S$,STATUS%)
11900 CALL SPOLL%(HP4194%,POLL%,STATUS%)
12000 IF ((POLL% AND 64) <> 64) THEN 11900
12100 S$="OFSTR"                    'STORE OFFSET DATA
12200 CALL SEND%(HP4194%,S$,STATUS%)
12300 S$="AOF1"                     'OFFSET A ON
12400 CALL SEND%(HP4194%,S$,STATUS%)
12500 S$="BOF1"                     'OFFSET B ON
12600 CALL SEND%(HP4194%,S$,STATUS%)
12700 '
12800 S$="X?"                       'READ IN FREQUENCY POINTS
12900 CALL SEND%(HP4194%,S$,STATUS%)
13000 S$="MLA TALK 17"                '4194 TO OUTPUT
13100 CALL TRANSMIT%(S$,STATUS%)
13200 TEMP$=SPACE$(15)
13300 FOR I=0 TO 400
13400 CALL RECIEVE%(TEMP$,LENGTH%,STATUS%)
13500 GFREQ(I)=VAL(LEFT$(TEMP$,12))
13600 NEXT I
13700 '
13820 '
17500 CLS
18200 '
18300 INPUT "EXPERIMENT INFORMATION:",EXPERIMENT$
18800 INPUT "NAME OF GAIN/PHASE DATA FILE:", GATEGP.FILE$
18810 INPUT "GAS:  ",GAS$
18815 INPUT "BATH TEMPERATURE:  ",BATH$
18820 INPUT "FLOW RATE:  ",FLOWR$
18825 INPUT "CHIP TEMPERATURE:  ",CHIPTEMP$
18830 INPUT "VESSEL HUMIDTY:  ",VHUMD$
18835 INPUT "NUMBER OF ELECTRODES TO BE SAMPLED:", NELECT
18840 OPEN "O",#2, GATEGP.FILE$
18850 PRINT#2, EXPERIMENT$;" ";DATE$;" ";TIME$
18855 PRINT#2, "GAS=";GAS$;" BATH=";BATH$;" FLOW=";FLOWR$;
18860 PRINT#2, " T=";CHIPTEMP$;" H=";VHUMD$
21200 '
21300 CLS
21400 INPUT "CONNECT DUT TO 4194, RETURN WHEN READY", NULL$
21510 PRINT#2, "OSCILLATOR LEVEL = ";OSCV;" VOLTS"
21520 PRINT "OSCILLATOR LEVEL = ";OSCV;" VOLTS"
21550 PRINT#2,  "ELECTRODE","FREQUENCY","GAIN","PHASE"
21600 FOR N= 1 TO NELECT
21603 PRINT "CONNECT ELECTRODE ";N;
21604 INPUT "HIT RETURN WHEN READY",NULL$
21605 '
21610 '
21615 'IF N=1 THEN GOTO 21630
21620 'IF N=5 THEN GOTO 21635
21625 'S$="K"+STR$(N)+"CI" :GOTO 21640
21630 'S$="K8OK1CI":GOTO 21640
21635 'S$="K4OK5CI"
```

```
21640 'CALL SEND%(SWITCH%,S$,STATUS%) 'SELECT ELECTRODE
21700 GOSUB 42100    'GET 4194 DATA
21750 PRINT "ELECTRODE","FREQ";CHR$(9);"GAIN";CHR$(9);"PHS"
21800 FOR I= 0 TO 400
21900 PRINT#2, N;CHR$(9);GFREQ(I);CHR$(9);GAIN(I);CHR$(9);PHS(I)
22000 IF (I MOD 100) = 0 THEN PRINT N,GFREQ(I),GAIN(I),PHS(I)
22050 NEXT I
22100 'LOOP BACK AND SCAN REST OF THE ELECTRODES
22200 NEXT N
27400 CLOSE #2
27405 'SHUT-OFF THE SWITCH
27410 'S$="K"+STR$(N)+"OI"
27415 'CALL SEND%(SWITCH%,S$,STATUS%)
27500 '
27600 '
27700 INPUT "COLLECT MORE DATA, Y OR N:", MOREDATA$
27800 IF MOREDATA$="N" THEN 28200
27900 GOTO 18300
28000 '
28200 '
28800 SYSTEM
42100 '
42200 '
42300 '                    HP4194 DATA INPUT ROUTINE
42400 '
42500 '
42600 CALL SPOLL%(HP4194%,POLL%,STATUS%)  'MAKE SURE SRQ IS NOT SET
42700 S$="SWTRG"                          'PERFORM SINGLE SWEEP
42800 CALL SEND%(HP4194%,S$,STATUS%)
42900 CALL SPOLL%(HP4194%,POLL%,STATUS%)        'IS SWEEP COMPLETE?
43000 IF ((POLL% AND 64) <> 64) THEN 42900   'IF NOT CONTINUE POLL
43100 '
43200 S$="AUTOA"                          'AUTOSCALE DISPLAY A
43300 CALL SEND%(HP4194%,S$,STATUS%)
43400 S$="AUTOB"                          'AUTOSCALE DISPLAY B
43500 CALL SEND%(HP4194%,S$,STATUS%)
44600 '
44700 S$="A?"            'READ IN GAIN FROM ARRAY REGISTER A
44800 CALL SEND%(HP4194%,S$,STATUS%)
44900 '
45300 '
45400 S$= "MLA TALK 17"
45500 CALL TRANSMIT%(S$,STATUS%)
45600 TEMP$= SPACE$(13)
45700 FOR I = 0 TO 400
45800 CALL RECIEVE%(TEMP$,LENGTH%,STATUS%)
45900 GAIN(I)=VAL(LEFT$(TEMP$,12))            'EXTRACT GAIN VALUE
46000 NEXT I
46100 '
46200 S$="B?"            'READ IN PHASE FROM ARRAY REGISTER B
46300 CALL SEND%(HP4194%,S$,STATUS%)
46400 S$= "MLA TALK 17"
46500 CALL TRANSMIT%(S$,STATUS%)
46600 FOR I= 0 TO 400
46700 CALL RECIEVE%(TEMP$,LENGTH%,STATUS%)
46800 PHS(I)= VAL(LEFT$(TEMP$,12))     'EXTRACT PHASE VALUE
46900 NEXT I
47000 '
47100 '
47200 CALL SPOLL%(HP4194%,POLL%,STATUS%)  'MAKE SURE SRQ NOT SET
47300 RETURN
```

Spectrum magnitude versus frequency:

```
10  REM PROGRAM TO DUMP SPECTRUM FROM HP8566 TO PC FILE
20 REM ---------- Initialization & Setup ----------
30 DEF SEG=&HC400                ' PC-488 memory address
40 INIT=0 : XMIT=3 : RECV=6 : SEND=9 : SPOLL=12 ' PC-488 routines
50 PPOLL=15 : ENTER=21 : TARRAY=200 : RARRAY=203 : DMA2=206
60 DIM D%(2048)
70 MY.ADDR%=0 : SYS.CONTROL%=0    ' initialize as system ctrlr
80 CALL INIT (MY.ADDR%,SYS.CONTROL%)
90 REM ---------- Transmit ----------
100 S$="UNL UNT"
110 CALL XMIT (S$,STATUS%)
120 IF STATUS%<>0 THEN GOTO 1200
130 CLS : PRINT " "
140 PRINT "         HP8566 (SPECTRUM ANALYZER) Control Software"
150 PRINT " "
160 PRINT "          (1)  SET-UP OPERATION"
170 PRINT "          (2)  X-FER DATA TO PC FILE"
180 PRINT "          (3)  EXIT TO DOS"
190 PRINT "" :INPUT "ENTER CHOICE:  ",MENU
200 IF MENU=1 THEN GOSUB 240
210 IF MENU=2 THEN GOSUB 710
220 IF MENU=3 THEN GOTO 1150
230 GOTO 130
240 REM  SET UP HP8566 TO INITIAL STATE
241 CLS: INPUT "CALIBRATE THE SPECTRUM ANALYZER? [Y/N] ",ANS$
242 IF ANS$="n" OR ANS$="N" THEN GOTO 250
243 IF ANS$="Y" OR ANS$="y" THEN GOTO 245
244 GOTO 241
245 GOSUB 1300
250 CLS: INPUT "RECALL A SAVED INSTRUMENT STATE? [Y/N] ",ANS$
260 IF ANS$="n" OR ANS$="N" THEN GOTO 341
270 IF ANS$="Y" OR ANS$="y" THEN GOTO 290
280 GOTO 250
290 INPUT "ENTER THE REGISTER NUMBER:  ",S$
300 S$="RC "+S$
310 REM ---------- Send ----------
320 ADDR%=18                     ' device address
330 CALL SEND (ADDR%,S$,STATUS%)
340 IF STATUS%<>0 THEN GOTO 1200
341 REM  determine if calibrated data will be used
342 CLS: INPUT "USE CALIBRATED DATA? [Y/N] ",ANS$
343 IF ANS$="n" OR ANS$="N" THEN CORR=0:GOTO 350
344 IF ANS$="Y" OR ANS$="y" THEN GOTO 346
345 GOTO 342
346 GOSUB 1400
350 REM  ESTABLISH FREQUENCY DATA POINTS TO STORE IN FILE
360 S$="FA OA"
370 ADDR%=18                     ' device address
380 CALL SEND (ADDR%,S$,STATUS%)
390 IF STATUS%<>0 THEN GOTO 1200
400 R$=SPACE$(80)          'allocate receive buffer
410 CALL ENTER (R$,LENGTH%,ADDR%,STATUS%)
420 IF STATUS%<>0 THEN GOTO 1200
430 ST=VAL(LEFT$(R$,LENGTH%))
440 S$="FB OA"
450 CALL SEND (ADDR%,S$,STATUS%)
460 IF STATUS%<>0 THEN GOTO 1200
470 R$=SPACE$(80)          'allocate receive buffer
480 CALL ENTER (R$,LENGTH%,ADDR%,STATUS%)
```

```
490 IF STATUS%<>0 THEN GOTO 1200
500 FINAL=VAL(LEFT$(R$,LENGTH%))
510 REM
520 REM DETERMINE FREQ STEP SIZES
530 STP=INT((FINAL - ST)/1000)
535 'STP=FINAL/1000
540 REM SET END OF TEXT AND WRITE TITLE
550 S$="DT@ KSE TJCHEMFET " + DATE$ +"@ HD"
560 CALL SEND (ADDR%,S$,STATUS%)
570 IF STATUS%<>0 THEN GOTO 1200
580 REM CHECK SWEEP TIME SINCE LONG SWEEPS WILL CAUSE TIME-OUT
590 REM CONDITION WHEN CAPTURING DATA
600 S$="ST OA"
610 CALL SEND (ADDR%,S$,STATUS%)
620 IF STATUS%<>0 THEN GOTO 1200
630 R$=SPACE$(80)          'allocate receive buffer
640 CALL ENTER (R$,LENGTH%,ADDR%,STATUS%)
650 IF STATUS%<>0 THEN GOTO 1200
660 SWEEP=VAL(LEFT$(R$,LENGTH%))
670 S$="HD"
680 CALL SEND (ADDR%,S$,STATUS%)
690 IF STATUS%<>0 THEN GOTO 1200
700 RETURN
710 REM CAPTURE DATA AND X-FER TO PC
720 REM TAKE A SWEEP AND FORMAT DATA FOR TRANSFER
730 CLS:PRINT "CAPTURING DATA..."
740 S$="S2 TS O3 TA"
750 ADDR%=18
760 CALL SEND (ADDR%,S$,STATUS%)
770 IF STATUS%=0 THEN GOTO 820
780 REM COULD BE A LONG SWEEP TIME IS HOLDING UP SYSTEM
790 IF STATUS%<>8 OR (STATUS%=8 AND SWEEP < 10) THEN GOTO 1200
800 CALL SPOLL (ADDR%,POLL%,STATUS%)
810 GOTO 770
820 CLS:PRINT "DATA CAPTURED ON HP8566"
830 INPUT "ENTER FILE NAME TO STORE DATA:  ", N$
835 INPUT "FILE INFORMATION:  ",EXPERIMENT$
837 INPUT "GAS:  ",GAS$
838 INPUT "BATH TEMPERATURE:  ",BATH$
839 INPUT "FLOW RATE:  ",FLOWR$
840 INPUT "CHIP TEMPERATURE:  ",CHIPTEMP$
841 INPUT "VESSEL HUMIDTY:  ",VHUMD$
842 OPEN "O",#1, N$
843 PRINT#1, EXPERIMENT$;" ";DATE$;" ";TIME$
844 PRINT#1, "GAS=";GAS$;" BATH=";BATH$;" FLOW=";FLOWR$;
845 PRINT#1, " T=";CHIPTEMP$;" H=";VHUMD$
860 PRINT#1, "FREQ";CHR$(9);"AMPLITUDE"
870 REM ---------- Transmit ----------
880 S$="MLA TALK 18"
890 CALL XMIT (S$,STATUS%)
900 IF STATUS%<>0 THEN GOTO 1200
910 REM ---------- Receive ----------
920 REM DRESS-UP THE PC SCREEN OUTPUT
930 CLS:PRINT "POINT#       FREQ          VALUE"
940 R$=SPACE$(32)          ' allocate receive buffer
950 FOR I=0 TO 1000
960             CALL RECV (R$,LENGTH%,STATUS%)
970             IF STATUS%<>0 THEN GOTO 1200
980             A=VAL(R$) + CORR
990             FREQ=ST + (I*STP)
1000            PRINT#1, FREQ;CHR$(9);A
1010            IF (I MOD 100)=0 THEN PRINT I,FREQ,A
1020 NEXT I
```

```
1030 CLOSE #1:PRINT "":PRINT "X-FER COMPLETED TO ";N$
1040 INPUT "RETURN TO CONTINUE", DUMMY
1050 REM ---------- Transmit ----------
1060 S$="UNL UNT"
1070 CALL XMIT (S$,STATUS%)
1080 IF STATUS%<>0 THEN GOTO 1200
1090 REM PUT HP8566 BACK INTO CONTINUOUS SWEEP
1100 S$="S1"
1110 ADDR%=18
1120 CALL SEND (ADDR%,S$,STATUS%)
1130 IF STATUS%<>0 THEN GOTO 1200
1140 RETURN
1150 REM MAKE SURE HP8566 IS LISTENING- Serial Poll
1160 ADDR%=18                          ' device address
1170 CALL SPOLL (ADDR%,POLL%,STATUS%)
1180 IF STATUS%<>0 THEN PRINT "SPOLL": GOTO 1200
1190 CLS: SYSTEM
1200 PRINT "COMM PROBLEM -- CHECK SET-UP AND RESTART PROGRAM"
1210 STOP
1300 REM THIS IS THE CALIBRATION ROUTINE
1310 CLS:PRINT "CONNECT THE CAL OUTPUT TO THE INPUT CONNECTOR"
1305 PRINT "":
1320 INPUT "ENTER RETURN WHEN CONNECTED",DUMMY
1330 S$="KSW"
1340 ADDR%=18
1345 CALL SEND (ADDR%,S$,STATUS%)
1350 IF STATUS%=0 THEN GOTO 1375
1355 REM CAL TAKES A LONG TIME WHICH CAUSES TIME OUT ON STATUS
1357 PRINT "CALIBRATION IN PROGRESS..."
1360 IF STATUS%<>6  THEN GOTO 1200
1365 CALL SPOLL (ADDR%,POLL%,STATUS%)
1370 GOTO 1350
1375 CLS:PRINT "CALIBRATION IS COMPLETE"
1380 PRINT "CONNECT DUT":PRINT "":PRINT ""
1385 INPUT "ENTER RETURN WHEN CONNECTED",DUMMY
1390 RETURN
1400 REM TURN ON THE CALIBRATION
1405 S$="KSX"
1410 ADDR%=18
1420 CALL SEND (ADDR%,S$,STATUS%)
1430 IF STATUS%<>0 THEN GOTO 1200
1435 S$="KS[":ADDR%=18          'GET THE AMPLITUDE CORRECTION
1436 CALL SEND (ADDR%,S$,STATUS%)
1437 IF STATUS%<>0 THEN GOTO 1200
1440 R$=SPACE$(80)              'allocate receive buffer
1450 CALL ENTER (R$,LENGTH%,ADDR%,STATUS%)
1460 IF STATUS%<>0 THEN GOTO 1200
1470 CORR=VAL(LEFT$(R$,LENGTH%)) 'CORRECTION TO ADD IN DB AMPLITUDE
1440 RETURN
1500 END
```

Time-domain oscilloscope data:

```
10 REM PROGRAM TO CAPTURE SCOPE DISPLAY IN PC FILE
20 '
30 '
40 '
50 ' OPTIONS (BYPASS IF VERB="NO")
60 '
160 PRINT"(1) FOR CHAN1, (2) FOR CHAN2, OR ANY OTHER KEY--BOTH"
161 GOSUB 1520: IF A$="1" THEN CHOPT=1
162 IF A$="2" THEN CHOPT=2
180 K=1 : 'CHANNEL 1
185 IF CHOPT <>0 THEN K= CHOPT
190  OPTION BASE 1
200 REM ------------ Initialization & Setup ----------
210 DEF SEG=&HC400              ' PC-488 memory address
220 INIT=0 : XMIT=3 : RECV=6 : SEND=9 : SPOLL=12 ' PC-488 routines
230 PPOLL=15 : ENTER=21 : TARRAY=200 : RARRAY=203 : DMA2=206
240  DIM D%(2048),VPOINT(1300)
250 MY.ADDR%=21: SYS.CONTROL%=0    ' initialize as system ctrlr
260 CALL INIT (MY.ADDR%,SYS.CONTROL%)
270 '
280 '
290 '
300 REM ---------------- Send --------------------
310 CLS:LOCATE 1,1
320 PRINT"SCOPE GRABBER NOW GRABBING CHANNEL ";K
330 S$="CLEAR;HEADER OFF"
340 ADDR%=15                            ' device address
350 CALL SEND (ADDR%,S$,STATUS%)
360 IF STATUS%<>0 THEN 1500
370 REM ---------------- Send --------------------
380 N$=RIGHT$(STR$(K),1)
390 S$="CHANNEL "+N$+";DISPLAY FORMAT 2"
400 ADDR%=15                            ' device address
410 CALL SEND (ADDR%,S$,STATUS%)
420 IF STATUS%<>0 THEN 1500
430 REM ---------------- Send --------------------
440 S$="ACQUIRE TYPE AVERAGE COUNT 32 COMPLETE 90 POINTS 1000;"
450 CALL SEND (ADDR%,S$,STATUS%)
455 FOR SCOPEW=1 TO 10000: NEXT SCOPEW 'WAIT FOR SCOPE TO SETTLE
460 IF STATUS%<>0 THEN 1500
470 REM ---------------- Send --------------------
480 S$="DIGITIZE CHANNEL"+N$+";
490 ADDR%=15                            ' device address
500 CALL SEND (ADDR%,S$,STATUS%)
510 IF STATUS%<>0 THEN 1500
520 REM ---------------- Send --------------------
530 ADDR%=15                            ' device address
540 S$="WAVEFORM POINTS?"
550 CALL SEND (ADDR%,S$,STATUS%)
560 IF STATUS%<>0 THEN 1500
570 REM ---------------- Enter -------------------
580 R$=SPACE$(13)           'allocate receive buffer
590 ADDR%=15                            ' device address
600 CALL ENTER (R$,LENGTH%,ADDR%,STATUS%)
610 IF STATUS%<>0 THEN 1500
620 POINTS=VAL(R$):PRINT "THE NUMBER OF WAVE POINTS=";POINTS,
630 IF POINTS>1300 THEN PRINT"WARNING: EXCESS POINTS (MAX 1300)"
640 REM ---------------- Send --------------------
```

```
650 ADDR%=15                        ' device address
660 S$="WAVEFORM XINC?"
670 CALL SEND (ADDR%,S$,STATUS%)
680 IF STATUS%<>0 THEN 1500
690 R$=SPACE$(30)           'allocate receive buffer
700 ADDR%=15                        ' device address
710 CALL ENTER (R$,LENGTH%,ADDR%,STATUS%)
720 IF STATUS%<>0 THEN 1500
730 XINC=VAL(R$):'--------- Send ------------------------
740 ADDR%=15                        ' device address
750 S$="WAVEFORM XOR?"
760 CALL SEND (ADDR%,S$,STATUS%)
770 IF STATUS%<>0 THEN 1500
780 R$=SPACE$(30)           'allocate receive buffer
790 ADDR%=15                        ' device address
800 CALL ENTER (R$,LENGTH%,ADDR%,STATUS%)
810 IF STATUS%<>0 THEN 1500
820 XORG=VAL(R$):'--------- Send ------------------------
830 ADDR%=15                        ' device address
840 S$="WAVEFORM YREF?"
850 CALL SEND (ADDR%,S$,STATUS%)
860 IF STATUS%<>0 THEN 1500
870 R$=SPACE$(13)           'allocate receive buffer
880 ADDR%=15                        ' device address
890 CALL ENTER (R$,LENGTH%,ADDR%,STATUS%)
900 IF STATUS%<>0 THEN 1500
910 YREF=VAL(R$):'---------- Send ------------------------
920 ADDR%=15                        ' device address
930 S$="WAVEFORM YINC?"
940 CALL SEND (ADDR%,S$,STATUS%)
950 IF STATUS%<>0 THEN 1500
960 R$=SPACE$(13)           'allocate receive buffer
970 ADDR%=15                        ' device address
980 CALL ENTER (R$,LENGTH%,ADDR%,STATUS%)
990 IF STATUS%<>0 THEN 1500
1000 YINC=VAL(R$):'---------- Send ------------------------
1010 ADDR%=15                       ' device address
1020 S$="WAVEFORM YOR?"
1030 CALL SEND (ADDR%,S$,STATUS%)
1040 IF STATUS%<>0 THEN 1500
1050 REM ---------- Enter ----------
1060 R$=SPACE$(13)          'allocate receive buffer
1070 ADDR%=15                       ' device address
1080 CALL ENTER (R$,LENGTH%,ADDR%,STATUS%)
1090 IF STATUS%<>0 THEN 1500
1100 YOR=VAL(R$)
1120 S$="WAVEFORM FORMAT ASCII;WAVEFORM DATA? "
1130 ADDR%=15                       ' device address
1140 CALL SEND (ADDR%,S$,STATUS%)
1150 IF STATUS%<>0 THEN 1500
1160 REM ---------- Transmit ----------
1170 S$="MLA TALK 15"
1180 CALL XMIT (S$,STATUS%)
1190 IF STATUS%<>0 THEN 1500
1200 INPUT "SCOPE FILE NAME:  ",TRACE$
1205 INPUT "EXPERIMENT INFORMATION:  ",EXPERIMENT$
1207 INPUT "GAS:  ",GAS$
1210 INPUT "BATH TEMPERATURE:  ",BATH$
1211 INPUT "FLOW RATE:  ",FLOWR$
1212 INPUT "CHIP TEMPERATURE:  ",CHIPTEMP$
1213 INPUT "VESSEL HUMIDTY:  ",VHUMD$
1214 OPEN "O",#1, TRACE$
1215 PRINT#1, EXPERIMENT$;" ";DATE$;" ";TIME$
```

```
1216 PRINT#1, "GAS=";GAS$;" BATH=";BATH$;" FLOW=";FLOWR$;
1217 PRINT#1, " T=";CHIPTEMP$;" H=";VHUMD$
1227 PRINT#1, "TIME";CHR$(9);"VOLTAGE"
1230 PRINT " "
1240 PRINT "(INDEX)    TIME      VOLTAGE"
1250 PRINT "------------------------------"
1260 FOR I=1 TO POINTS
1270 REM ---------- Receive ----------
1280 R1$=SPACE$(32)            ' allocate receive buffer
1290 IF STATUS%<>0 THEN 1500
1300 TPOINT=XINC*I+XORG
1310 CALL RECV (R1$,LENGTH%,STATUS%)
1320 IF STATUS%<>0 THEN 1500
1330 VPOINT(I)=((VAL(R1$)-YREF)*YINC)+YOR
1350 IF (I MOD 100)=0 THEN PRINT "(";I;")",TPOINT;",",VPOINT(I)
1360 PRINT#1,TPOINT;CHR$(9);VPOINT(I)
1370 NEXT I
1430 CLOSE #1
1440 K=K+1 : IF CHOPT<>0 THEN K=3
1470 IF K<3 THEN 300
1471 '
1472 ' RETURN CONTROL OF SCOPE TO OPERATOR
1480 S$="LOCAL"
1490 CALL SEND (ADDR%,S$,STATUS%)
1491 S$="UNL UNT"
1492 CALL XMIT (S$,STATUS%)
1493 IF STATUS%<>0 THEN 1500
1494 PRINT:PRINT"FINISHED":STOP
1500 PRINT "CHECK EQUIPMENT SET-UP AND RE-EXECUTE":STOP
1520 REM KEY POLL
1540 A$=INKEY$:IF A$="" THEN 1540
1550 RETURN
1560 END
```

The following program was written to capture the amplifiers' DC characteristics from the Hewlett Packard Model HP 4145 Semiconductor Parameter Analyzer:

```
5 REM THIS PROGRAM WILL "CAPTURE" THE SCREEN ON THE HP4145
10 REM INITIALIZE THE 488 VARIABLES
15 DEF SEG=&HC400
20 INIT%=0
30 TRANSMIT%=3
40 RECIEVE%=6
50 SEND%=9
60 SPOLL%=12
70 ENTER%=21
80 HP4145%=2: MYADDR%=21
90 SYSCON%=0
99 REM initialize the card
100 CALL INIT%(MYADDR%,SYSCON%)
105 REM GET THE DRAIN VOLTAGE DATA
110 PRINT " "
115 INPUT "ENTER THE INITIAL VIN VOLTAGE: ",VD1
120 INPUT "ENTER THE VIN VOLTAGE STEP SIZE: ",VDS
125 INPUT "ENTER THE NUMBER OF STEPS: ",VDNS
130 PRINT " "
135 REM GET THE GATE VOLTAGE DATA
140 INPUT "ENTER THE INITIAL BIAS VOLTAGE: ",VG1
145 INPUT "ENTER THE BIAS VOLTAGE STEP SIZE: ",VGS
150 INPUT "ENTER THE NUMBER OF STEPS: ",VGNS
155 PRINT " "
160 REM GET THE VOUT DATA
165 REM DETERMINE THE NUMBER OF CURRENT POINTS TO FETCH
170 POINTS=VDNS*VGNS
172 OPTION BASE 1
173 REM DIMENSION THE ARRAY TO HOLD THE DATA
175 DIM A(POINTS)
180 PRINT "RETRIEVING THE VOUT VOLTAGE VALUES FROM HP4145"
185 PRINT " "
190 GOSUB 500
260 REM COMBINE THE THREE SETS OF DATA INTO THE FINAL OUTPUT
265 INPUT "ENTER THE NAME OF FILE TO STORE DATA: ", N$
270 OPEN "O", #1, N$
275 VD=VD1
276 VG=VG1
280 DIM OUTDATA(VDNS,VGNS)
282 FOR K=1 TO VGNS
285         FOR J=1 TO VDNS
287             OUTDATA(J,K)=A(J +(K-1)*VDNS)
290         NEXT J
292 NEXT K
293 REM WRITE THE OUTPUT FILE
294 PRINT#1,VD1,
295 FOR K=1 TO VGNS
296     IF K>1 THEN VG=VG+VGS
297     PRINT#1,CHR$(9);VG,
298     NEXT K
299     PRINT#1,""
300 FOR J=1 TO VDNS
301         IF J>1 THEN VD=VD+VDS
```

```
302              PRINT#1,VD,
303         FOR K=1 TO VGNS
310                                  PRINT#1,CHR$(9);OUTDATA(J,K),
320         NEXT K
321      PRINT#1,""
325  NEXT J
330 CLOSE #1
335 PRINT "ALL DONE" :SYSTEM
340 STOP
500 REM SUBROUTINE TO TRANSFER DATA FROM HP4145 TO PC
501  CALL SPOLL%(HP4145%,POLL%,STATUS%)
506 S$="UNL UNT"
507 CALL TRANSMIT(S$,STATUS%)
508 S$="BC"
509  CALL SEND%(HP4145%,S$,STATUS%)
510 S$="DO 'VOUT"
520  CALL SEND%(HP4145%,S$,STATUS%)
530 S$="MLA TALK 2"
540 CALL TRANSMIT%(S$,STATUS%)
545 TEMP$=SPACE$(13)
550 FOR I=1 TO POINTS
560 CALL RECIEVE%(TEMP$,LENGTH%,STATUS%)
571  A(I)=VAL(RIGHT$(TEMP$,12))
580 NEXT I
585 S$="UNL UNT"
586 CALL TRANSMIT%(S$,STATUS%)
590 RETURN
600 END
```

Appendix F

Data Reduction Software

The following BASIC computer programs were written to facilitate the data reduction process. The first BASIC computer program reformats the gain and phase data of the microsensor to simplify the generation of response plots. The second BASIC computer program normalizes the spectrum response data stored in one file relative to a reference file of spectrum response data. Both computer programs yield the envelope of three sets of data points by discarding the median value. The additional BASIC computer programs facilitate the other aspects of data reduction, such as reducing the time-domain data, AC impedance data, and the transfer function data.

Gain and Phase BASIC Computer Program

```
REM program will reduce gain/phase data
REM computes a smoothing average over 5 points
REM keeps every 10 points
REM  and discard last unprintable DOS file character

DEFINT n
DIM freqa(401),maga(401),phasea(401),freqg(401),magg(401),phaseg(401)

LET ans$="n"


INPUT "file with refamp data: ",air$
INPUT "file with gain/phase data: ",gas$
getname:
INPUT "name of file to store data: ",normal$

INPUT "electrode number to extract: ",elect
```

```
PRINT ""
PRINT ""

PRINT "file with refamp data:            ";air$
PRINT "file with gain/phase data:     ";gas$
PRINT "store data in file :  ";normal$
PRINT "extracting electrode number:  ";elect

OPEN "O",#3,normal$
OPEN "I",#2,air$
OPEN "I",#1,gas$


    LINE INPUT#2,firstline$
    PRINT firstline$
    LINE INPUT#1,firstline$
    LINE INPUT #1,secondline$
     LINE INPUT #1,thirdline$
     LINE INPUT #1,fourthline$
    PRINT firstline$
   PRINT secondline$
    PRINT thirdline$
    PRINT fourthline$

PRINT #3, "" Frequency (Hz)";CHR$(9);"Gain (dB)";CHR$(9),"Phase (deg)"

LET n=0
REM read refamp data
WHILE NOT EOF(2)
    INPUT #2, freqin,magin,phasein
    freqa(n)=freqin: maga(n)=magin: phasea(n)=phasein
    n=n+1
    IF n=401 THEN bustout1
skipit: REM continue

WEND
bustout1:

PRINT n;" points read from file ";air$

LET n=0
REM read in gain/phase data for an electrode
WHILE NOT EOF(1)

    LINE INPUT #1, linein$
    t=LEN(linein$)
    start=1
    counter=1

    FOR position=2 TO t

     IF MID$(linein$,position,1)<>CHR$(9) AND position <> t THEN smallskip
     lenchr=position-start
     tempin=VAL(MID$(linein$,start,lenchr))
    IF counter=1 THEN electin=tempin
   IF electin <>elect THEN skipit1

    IF counter=2 THEN freqg(n)=tempin
    IF counter=3 THEN magg(n)=tempin
    IF counter=4 THEN phaseg(n)=tempin
     counter=counter+1:start=position

 smallskip:
```

```
   NEXT position

   n=n+1
   IF n=401 THEN bustout
skipit1: REM continue

WEND
bustout:

PRINT n;" points read from file ";gas$

REM smooth the data by averaging over 5 points and print every 10
last=n-3
FOR n=2 TO last

avmaga=(maga(n-2) + maga(n-1) + maga(n) + maga(n+1) + maga(n+2))/5
avphasea=(phasea(n-2) + phasea(n-1) + phasea(n) + phasea(n+1) + phasea(n+2))/5


avmagg=(magg(n-2) + magg(n-1) + magg(n) + magg(n+1) + magg(n+2))/5
avphaseg=(phaseg(n-2) + phaseg(n-1) + phaseg(n) + phaseg(n+1) + phaseg(n+2))/5

REM remove the refamp data from the gain/phase data
difmag=avmagg-avmaga : difphase=avphaseg-avphasea

IF (n MOD 10)=0 THEN PRINT #3, freqa(n);CHR$(9);difmag;CHR$(9);difphase
NEXT n

CLOSE #1 : CLOSE #2 : CLOSE #3

INPUT "extract more data?:",ans$
IF ans$="y" OR ans$="Y" THEN getname
END
```

Spectrum Normalizing BASIC Computer Program

```
REM program that normalizes spectral data
REM and yields envelope of every three points

DEFINT n,last,keepers,t,posit,posht
DIM frequ(1009),ampu(1009),freqn(1009),ampn(1009)


INPUT "file of spectral data to be normalized: ",unnormal$
INPUT "file containing reference data: ",ref$
INPUT "name of file to store normalized data: ",normal$
PRINT ""
PRINT ""
PRINT "file of spectral data to be normalized: ";unnormal$
PRINT "file containing reference data: ";ref$
PRINT "name of file to store normalized data: ";normal$

OPEN "I", #1,unnormal$
OPEN "I",#2,ref$
OPEN "O",#3,normal$

FOR n=2 TO 1 STEP -1
   LINE INPUT#n,firstline$
   LINE INPUT #n,secondline$
   LINE INPUT #n, thirdline$
   PRINT firstline$
   PRINT secondline$
NEXT n

PRINT #3, "normalized spectral data from file ";unnormal$
PRINT #3, secondline$

LET n=0

WHILE NOT EOF(1)
   LINE INPUT #1, linein$
REM now parse the string for values and ignore the last null character
   t=LEN(linein$)
   IF t<3 THEN skipit
   FOR posit=1 TO t
      character$=RIGHT$( LEFT$(linein$,posit),1 )
      IF character$=CHR$(9) THEN posht=posit
   NEXT posit
   frequ(n)=VAL(LEFT$(linein$,posht))
   ampu(n)=VAL(RIGHT$(linein$,t-posht))
  n=n+1
skipit: REM continue
WEND
PRINT n;" points read from file ";unnormal$

LET n=0
WHILE NOT EOF(2)
   LINE INPUT #2, linein$
REM now parse the string for values and ignore the last null character
   t=LEN(linein$)
   IF t<3 THEN skipit2
   FOR posit=1 TO t
      character$=RIGHT$( LEFT$(linein$,posit),1 )
      IF character$=CHR$(9) THEN posht=posit
```

```
   NEXT posit
    freqr=VAL(LEFT$(linein$,posht))
    ampr=VAL(RIGHT$(linein$,t-posht))

   IF freqr<>frequ(n) THEN GOTO badfile
    freqn(n)=freqr
   ampn(n)=ampu(n)-ampr
   n=n+1
skipit2: REM continue

WEND
last =n-1

REM  want to reduce the number of data points in the file
REM   so will discard each 2,4,6,... point if the amplitude is between
REM    the two adjacent points

LET keepers=2
PRINT  #3,freqn(0);CHR$(9);ampn(0)
FOR n=1 TO (last-1)
   IF ampn(n-1) < ampn(n) AND ampn(n) < ampn(n+1) THEN GOTO continue
   IF ampn(n-1) > ampn(n) AND ampn(n) > ampn(n+1) THEN GOTO continue
    PRINT #3,freqn(n);CHR$(9);ampn(n)
  keepers=keepers+1
continue: NEXT n
PRINT #3,freqn(last);CHR$(9);ampn(last)

PRINT keepers;" points kept in file ";normal$
PRINT ""
PRINT ""

GOTO finished

badfile:
   PRINT "the frequency points do not match between files at point ";n

finished:

   CLOSE #1 : CLOSE #2 : CLOSE #3
END
```

Time-Domain (Oscilloscope) Data Reduction BASIC Computer Program

```
REM program will find %difference in time domain data
REM discard anything before t=0
REM keeps every fourth point
REM  and discard last unprintable EOS file character

DEFINT n,last,keepers,t
DEFDBL tempin
DIM scopetime(1100),amp(1100), otime(1100), oamp(1100)

INPUT "file of td data to be reduced:  ",ref$
INPUT "file of reference td data:   ",diffile$
INPUT "name of file to store data:  ",normal$
PRINT ""
PRINT ""
PRINT "file to be read:            ";ref$
PRINT "file of reference td data:   ";diffile$
PRINT "name of file to store data:  ";normal$

OPEN "I",#1,diffile$
OPEN "I",#2,ref$
OPEN "O",#3,normal$

   LINE INPUT#1,firstline$
   LINE INPUT #1,secondline$
    LINE INPUT #1,thirdline$
   PRINT firstline$
   PRINT secondline$
   PRINT thirdline$
    LINE INPUT#2,firstline$
   LINE INPUT #2,secondline$
    LINE INPUT #2,thirdline$
   PRINT firstline$
   PRINT secondline$
   PRINT thirdline$
PRINT #3, "" Time (seconds)";CHR$(9);"% Difference"
LET n=0
REM read in data
WHILE NOT EOF(2)

   LINE INPUT #2, linein$
   t=LEN(linein$)

   IF t<3 THEN bustout
   start=1
   counter=1

   FOR position=2 TO t

    IF MID$(linein$,position,1)<>CHR$(9) AND position <> t THEN smallskip
    lenchr=position-start
    tempin=VAL(MID$(linein$,start,lenchr))
   IF counter=1 THEN scopetime(n)=tempin
  IF scopetime(n) < 0 THEN skipit1
   IF counter=2 THEN amp(n)=tempin
    counter=counter+1:start=position
smallskip:
   NEXT position
   n=n+1
```

```
skipit1: REM continue

WEND
bustout:

PRINT n;" points read from file ";ref$
last =n-1

PRINT "reading file:  ";diffile$

LET n=0
REM read in data
WHILE NOT EOF(1)

   LINE INPUT #1, linein$
   t=LEN(linein$)

   IF t<3 THEN bustout2
   start=1
   counter=1

   FOR position=2 TO t

    IF MID$(linein$,position,1)<>CHR$(9) AND position <> t THEN smallskip2

    lenchr=position-start

    tempin=VAL(MID$(linein$,start,lenchr))
   IF counter=1 THEN otime(n)=tempin
  IF otime(n) < 0 THEN skipit2

   IF counter=2 THEN oamp(n)=tempin
    counter=counter+1:start=position

smallskip2:
   NEXT position

   n=n+1

skipit2: REM continue

WEND
bustout2:

PRINT n;" points read from file ";diffile$

olast=n-1

FOR n=0 TO last
   IF (n MOD 4) <> 0 THEN skipit3
    PRINT #3, scopetime(n);CHR$(9);100*(amp(n)-oamp(n))/ABS(oamp(n))

   skipit3:
   REM print only every 4
   NEXT n
finished:
FOR n=1 TO 5
PRINT CHR$(7)
NEXT n

   CLOSE #2 : CLOSE #3
END
```

BASIC Computer Program to Reduce the AC Impedance Data

```
REM program will reduce impedance data
REM computes the average values and compares between files
REM keeps every tenth point
REM  and discard last unprintable DOS file character

DEFINT n
DIM freqa(401),maga(401),phasea(401),freqg(401),magg(401),phaseg(401)

REM conversion factor to convert degrees to radians
deg2rad=3.14159/180
getname:
INPUT "file with air impedance data to be reduced: ",air$
INPUT "file with gas impedance data: ",gas$
INPUT "name of file to store data: ",normal$
INPUT "electrode number to extract: ",elect
PRINT ""
PRINT ""
PRINT "file to be read air:          ";air$
PRINT "file with gas data:    ";gas$
PRINT "store data in file :  ";normal$
PRINT "extracting electrode number:  ";elect

OPEN "I",#2,air$
OPEN "I",#1,gas$
OPEN "O",#3,normal$
   LINE INPUT#2,firstline$
   LINE INPUT #2,secondline$
    LINE INPUT #2,thirdline$
   PRINT firstline$
   PRINT secondline$
   PRINT thirdline$
    LINE INPUT#1,firstline$
   LINE INPUT #1,secondline$
    LINE INPUT #1,thirdline$
   PRINT firstline$
   PRINT secondline$
   PRINT thirdline$
PRINT #3, "" Frequency (Hz)";CHR$(9);"Magnitude (ohms)";CHR$(9);"Phase
(deg)";CHR$(9);"real";CHR$(9);"imag"

LET n=0

WHILE NOT EOF(2)
   INPUT #2, electin,dummy,freqin,dummy,magin,phasein
   IF electin <>elect THEN skipit
   freqa(n)=freqin: maga(n)=magin: phasea(n)=phasein
   n=n+1
    IF n=401 THEN bustout1
skipit: REM continue

WEND
bustout1:

PRINT n;" points read from file ";air$

LET n=0
WHILE NOT EOF(1)
   INPUT #1, electin,dummy,freqin,dummy,magin,phasein
   IF electin <>elect THEN skipit1
   freqg(n)=freqin: magg(n)=magin: phaseg(n)=phasein
```

```
   n=n+1
   IF n=401 THEN bustout
skipit1: REM continue

WEND
bustout:

PRINT n;" points read from file ";gas$

REM smooth the data by averaging over 5 points and print every 10
last=n-3
FOR n=2 TO last

avmaga=(maga(n-2) + maga(n-1) + maga(n) + maga(n+1) + maga(n+2))/5
avphasea=(phasea(n-2) + phasea(n-1) + phasea(n) + phasea(n+1) + phasea(n+2))/5
realpa=avmaga*COS(deg2rad*avphasea):imagpa=avmaga*SIN(deg2rad*avphasea)

avmagg=(magg(n-2) + magg(n-1) + magg(n) + magg(n+1) + magg(n+2))/5
avphaseg=(phaseg(n-2) + phaseg(n-1) + phaseg(n) + phaseg(n+1) + phaseg(n+2))/5
realpg=avmagg*COS(deg2rad*avphaseg):imagpg=avmagg*SIN(deg2rad*avphaseg)


difmag=100*(avmagg-avmaga)/avmaga :difphase=100*(avphaseg-avphasea)/avphasea
difrealp=100*(realpg-realpa)/realpa : difimagp=100*(imagpg-imagpa)/imagpa
IF (n MOD 10)=0 THEN PRINT #3,
freqa(n);CHR$(9);difmag;CHR$(9);difphase;CHR$(9);difrealp;CHR$(9);difimagp
NEXT n


CLOSE #1 : CLOSE #2 : CLOSE #3

INPUT "extract more data?:",ans$
IF ans$="y" OR ans$="Y" THEN getname
END
```

BASIC Computer Program Used to Reduce Transfer Function Data

```
REM program will reduce gain/phase data
REM
REM keeps every 10 points
REM  and discard last unprintable DOS file character

DEFINT n
DIM freqa(401),maga(401),phasea(401),freqg(401),magg(401),phaseg(401)

LET ans$="n"
INPUT "file with refamp data:  ",air$
INPUT "file with gain/phase data:  ",gas$
getname:
INPUT "name of file to store data:  ",normal$
INPUT "electrode number to extract:  ",elect
PRINT ""
PRINT ""
PRINT "file with refamp data:            ";air$
PRINT "file with gain/phase data:     ";gas$
PRINT "store data in file :  ";normal$
PRINT "extracting electrode number:  ";elect

OPEN "O",#3,normal$
OPEN "I",#2,air$
OPEN "I",#1,gas$
    LINE INPUT#2,firstline$
    PRINT firstline$
    LINE INPUT#1,firstline$
    LINE INPUT #1,secondline$
     LINE INPUT #1,thirdline$
     LINE INPUT #1,fourthline$
    PRINT firstline$
   PRINT secondline$
    PRINT thirdline$
    PRINT fourthline$
PRINT #3, "" Frequency (Hz)";CHR$(9);"Gain (dB)";CHR$(9);"Phase (deg)"
LET n=0
REM read refamp data
WHILE NOT EOF(2)
   INPUT #2, freqin,magin,phasein
   freqa(n)=freqin: maga(n)=magin: phasea(n)=phasein
   n=n+1
    IF n=401 THEN bustout1
skipit: REM continue

WEND
bustout1:

PRINT n;" points read from file ";air$

LET n=0
REM read in gain/phase data for an electrode
WHILE NOT EOF(1)

   LINE INPUT #1, linein$
   t=LEN(linein$)
   start=1
   counter=1
   FOR position=2 TO t
```

```
    IF MID$(linein$,position,1)<>CHR$(9) AND position <> t THEN smallskip
    lenchr=position-start
     tempin=VAL(MID$(linein$,start,lenchr))
   IF counter=1 THEN electin=tempin
  IF electin <>elect THEN skipit1
    IF counter=2 THEN freqg(n)=tempin
    IF counter=3 THEN magg(n)=tempin
    IF counter=4 THEN phaseg(n)=tempin
     counter=counter+1:start=position
smallskip:
    NEXT position
    n=n+1
    IF n=401 THEN bustout
skipit1: REM continue

WEND
bustout:
PRINT n;" points read from file ";gas$
REM smooth the data by averaging over 5 points and print every 10
last=n-3
FOR n=2 TO last
avmaga=(maga(n-2) + maga(n-1) + maga(n) + maga(n+1) + maga(n+2))/5
avphasea=(phasea(n-2) + phasea(n-1) + phasea(n) + phasea(n+1) + phasea(n+2))/5
avmagg=(magg(n-2) + magg(n-1) + magg(n) + magg(n+1) + magg(n+2))/5
avphaseg=(phaseg(n-2) + phaseg(n-1) + phaseg(n) + phaseg(n+1) + phaseg(n+2))/5
REM remove the refamp data from the gain/phase data
difmag=avmagg-avmaga : difphase=avphaseg-avphasea

IF (n MOD 10)=0 THEN PRINT #3, freqa(n);CHR$(9);difmag;CHR$(9);difphase
NEXT n


CLOSE #1 : CLOSE #2 : CLOSE #3

INPUT "extract more data?:",ans$
IF ans$="y" OR ans$="Y" THEN getname

END
```

Appendix G

Additional Results of the Characterization of the Microsensor's Frequency Response

This appendix contains the additional microsensor's frequency responses that are described in detail within the first section of Chapter V.

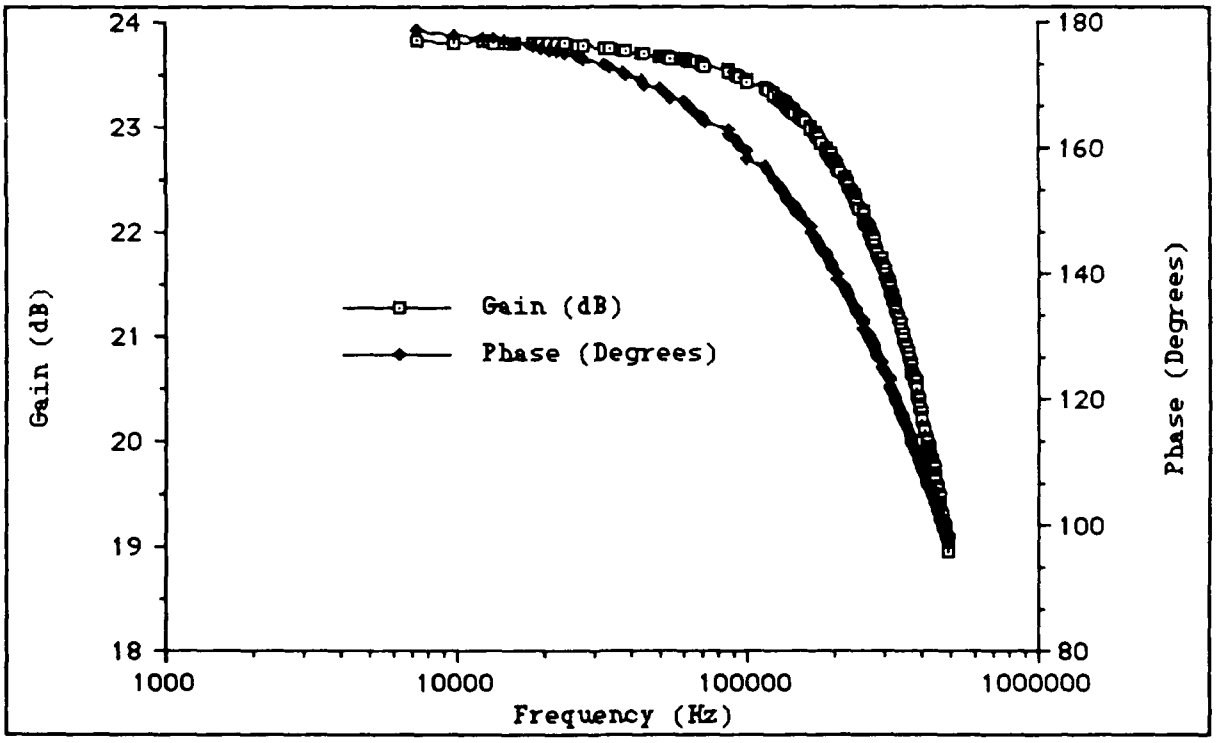

Figure G-1. Sensing Element Chem3 Selected.

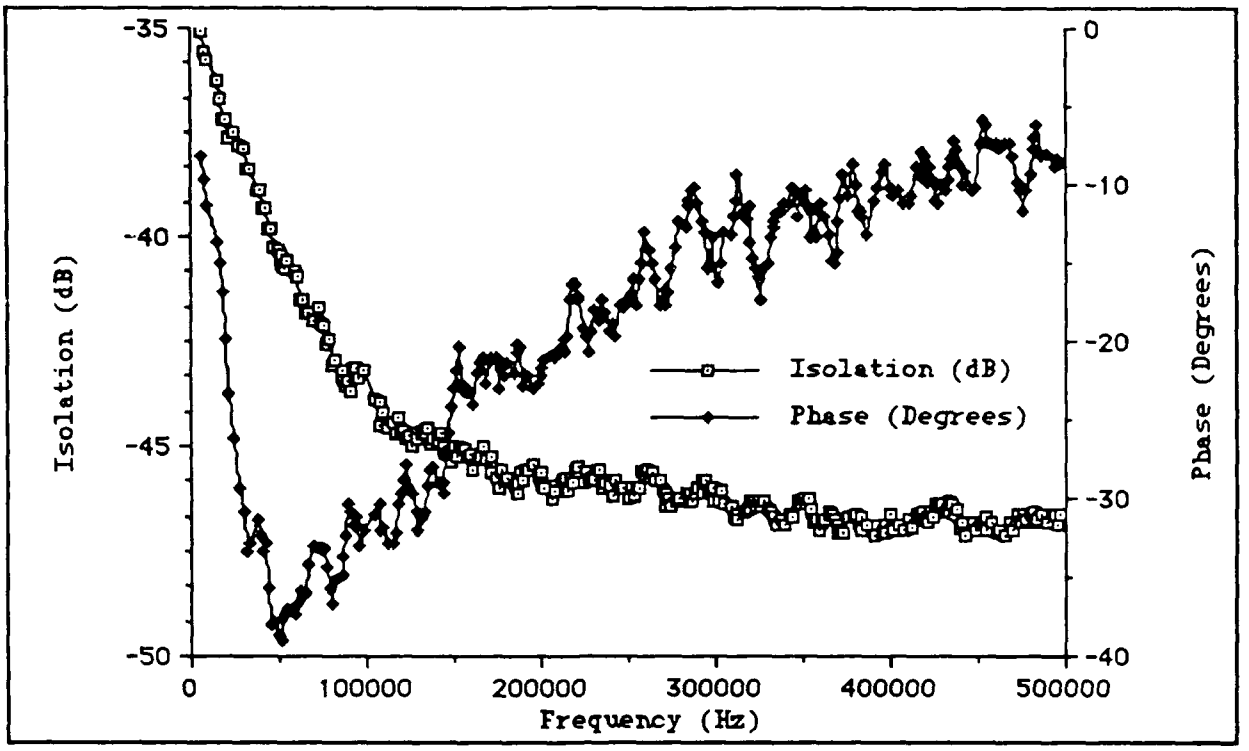

Figure G-2. Sensing Element Chem3 Unselected.

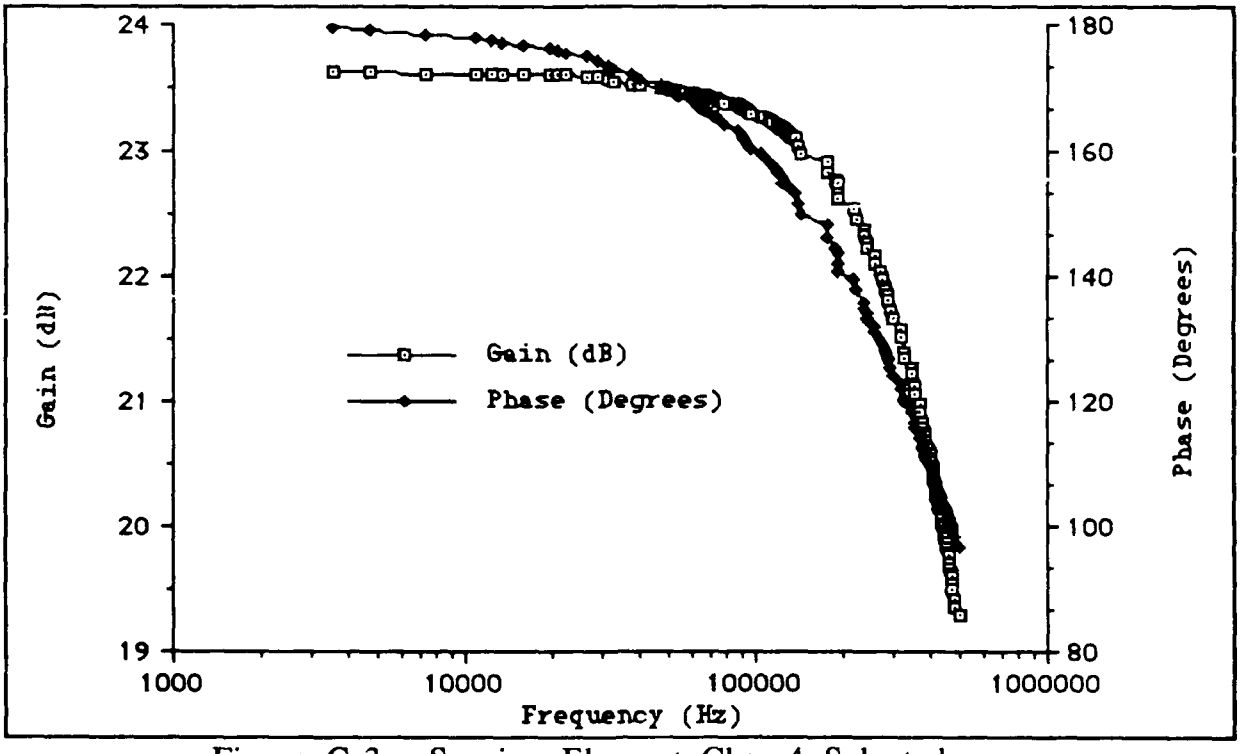

Figure G-3. Sensing Element Chem4 Selected.

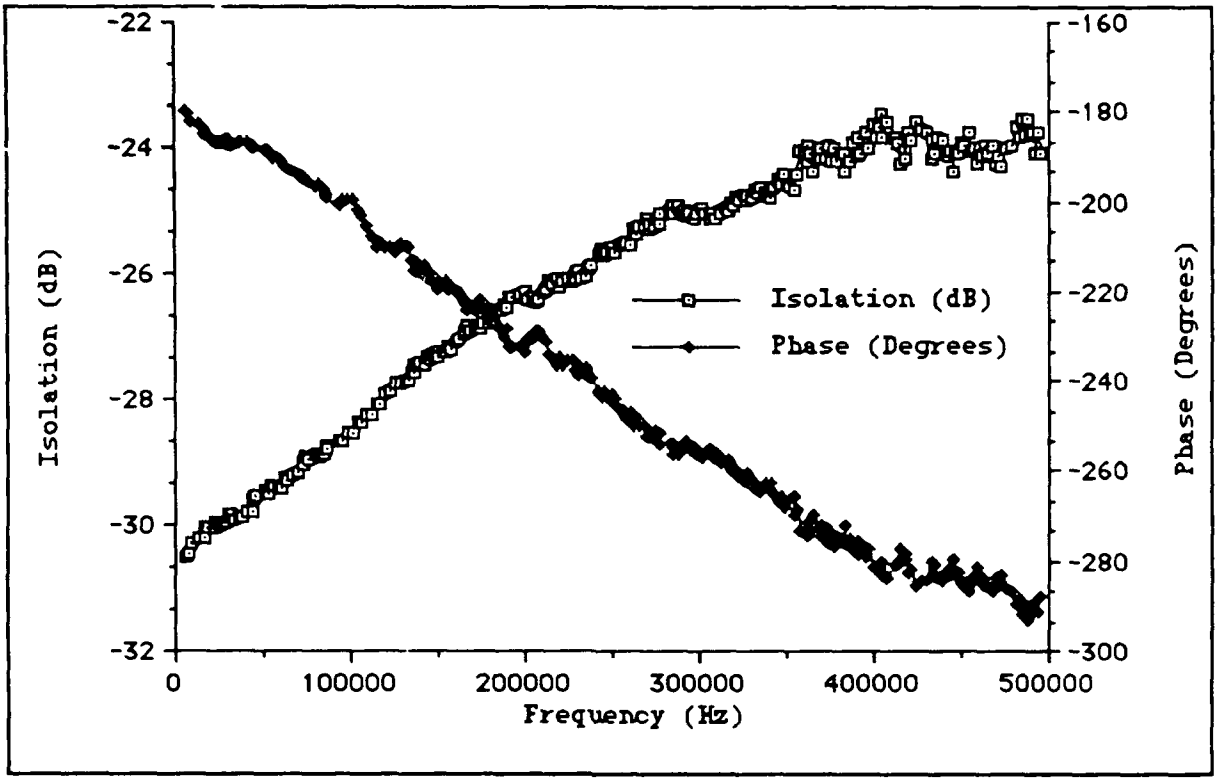

Figure G-4. Sensing Element Chem4 Unselected.

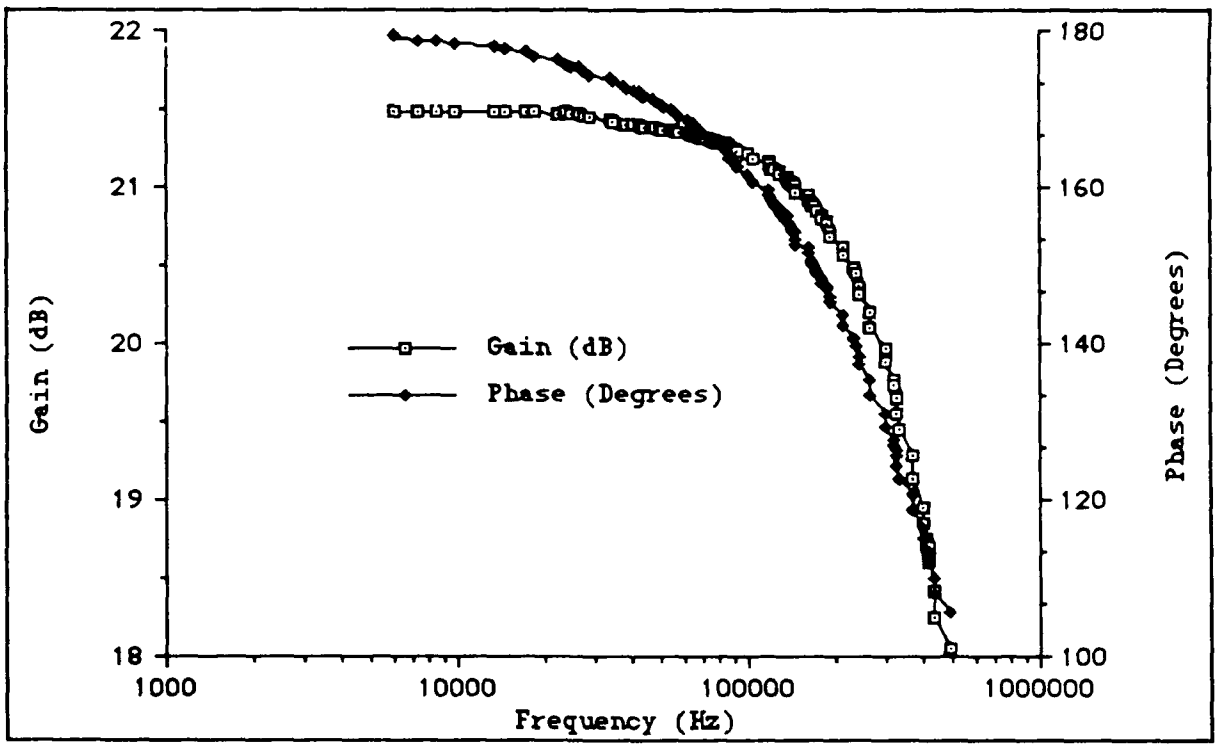

Figure G-5. Sensing Element Chem6 Selected.

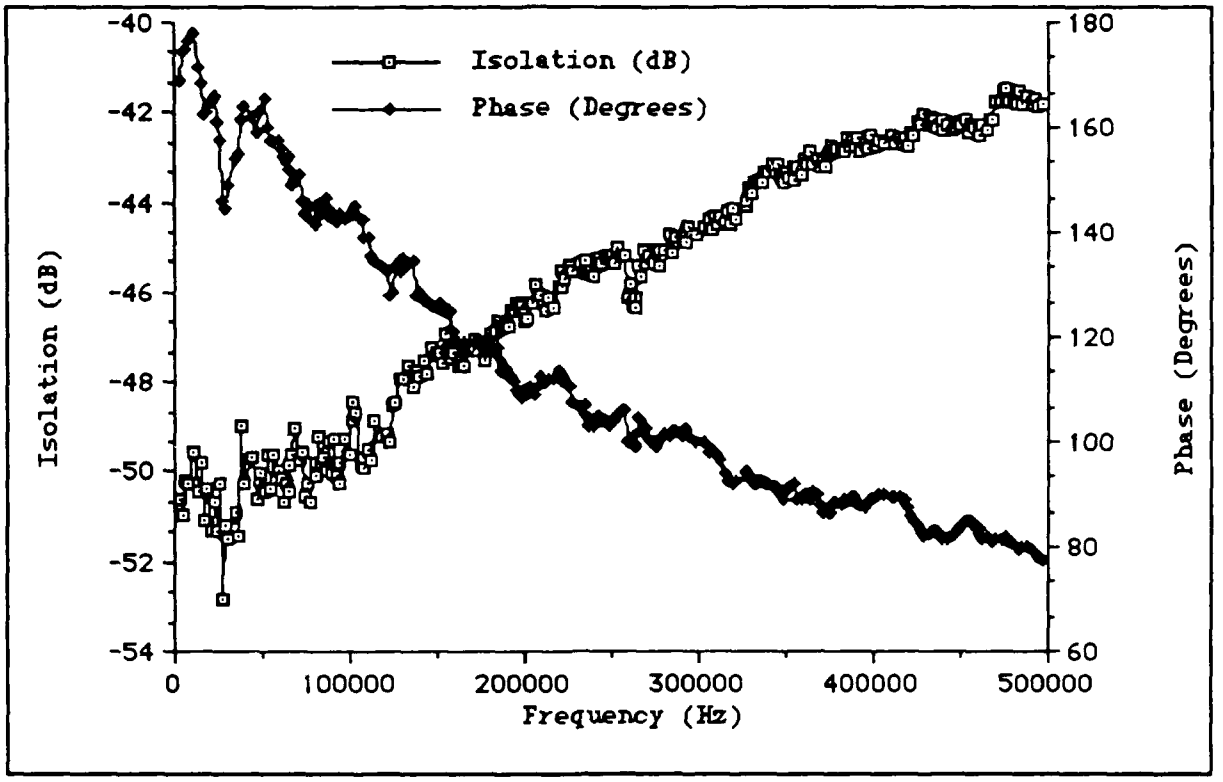

Figure G-6. Sensing Element Chem6 Unselected.

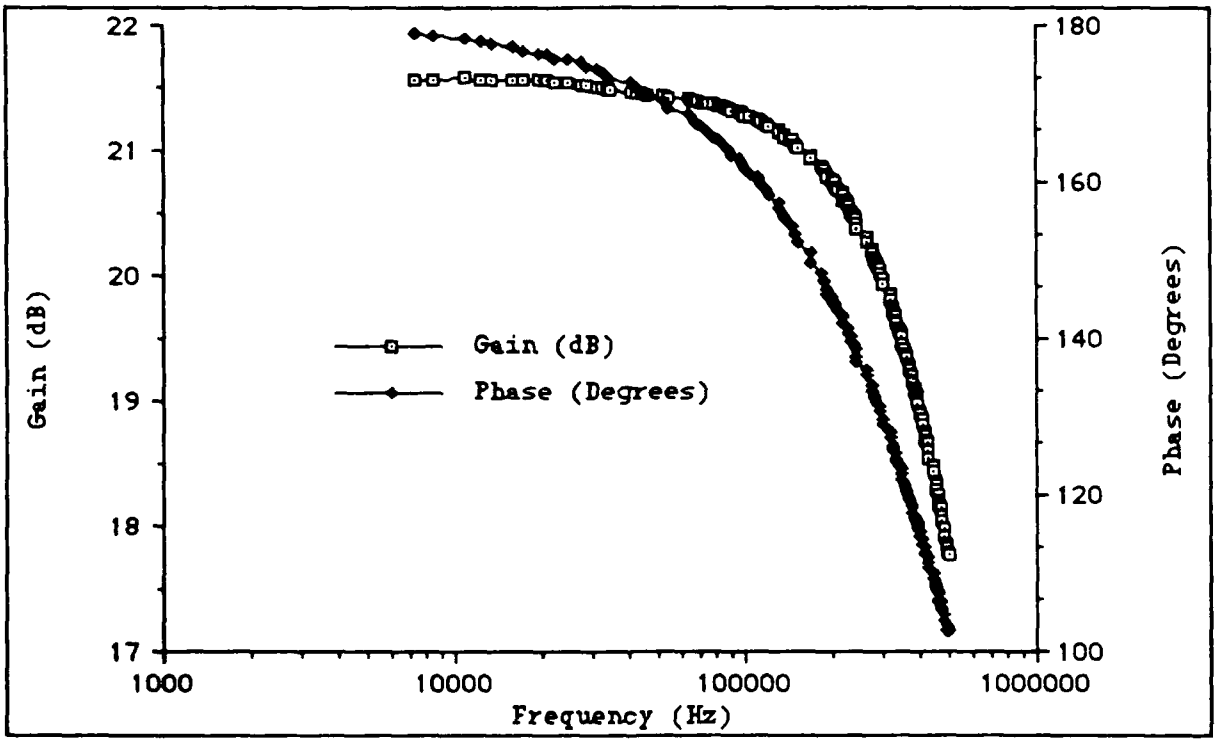

Figure G-7. Sensing Element Chem7 Selected.

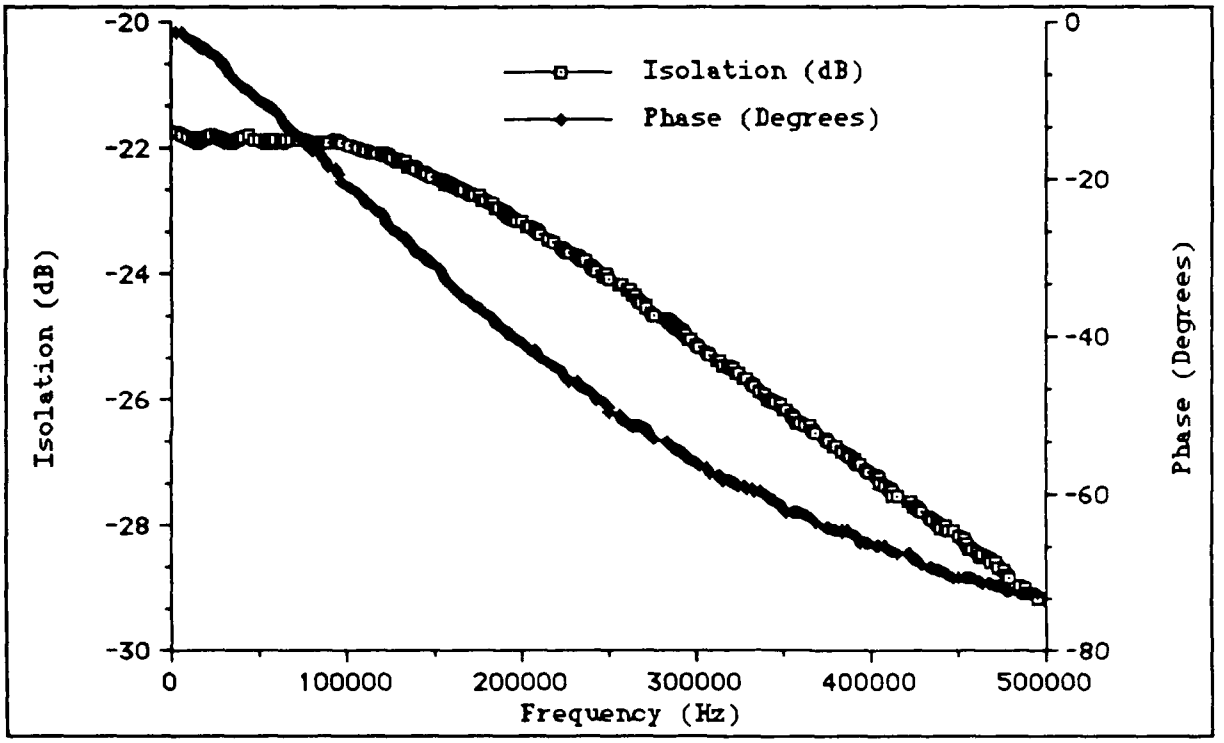

Figure G-8. Sensing Element Chem7 Unselected.

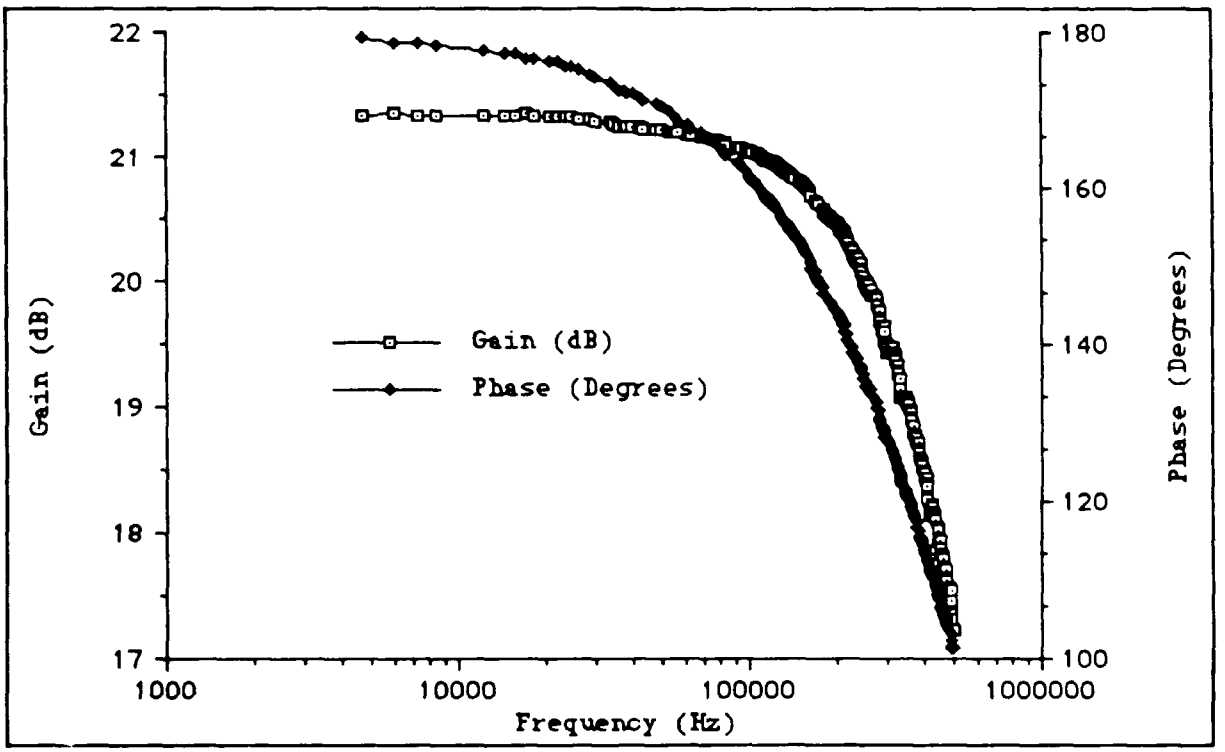

Figure G-9. Sensing Element Chem8 Selected.

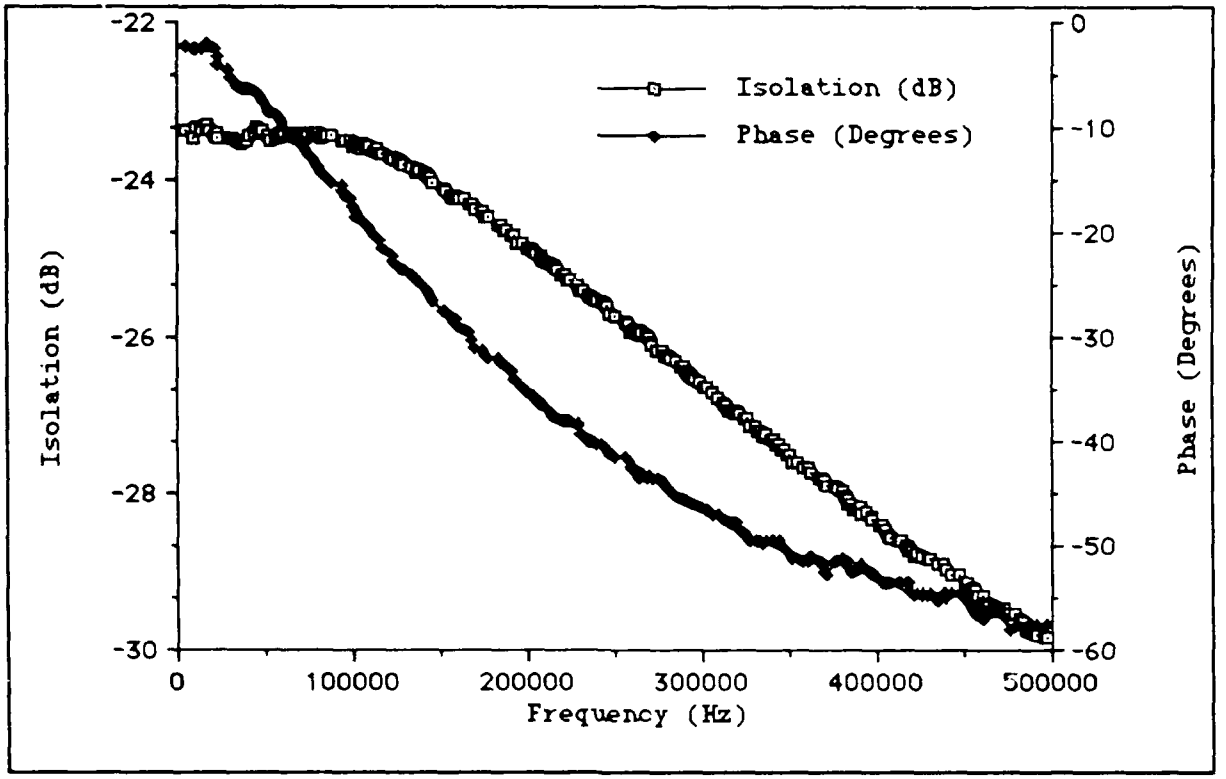

Figure G-10. Sensing Element Chem8 Unselected.

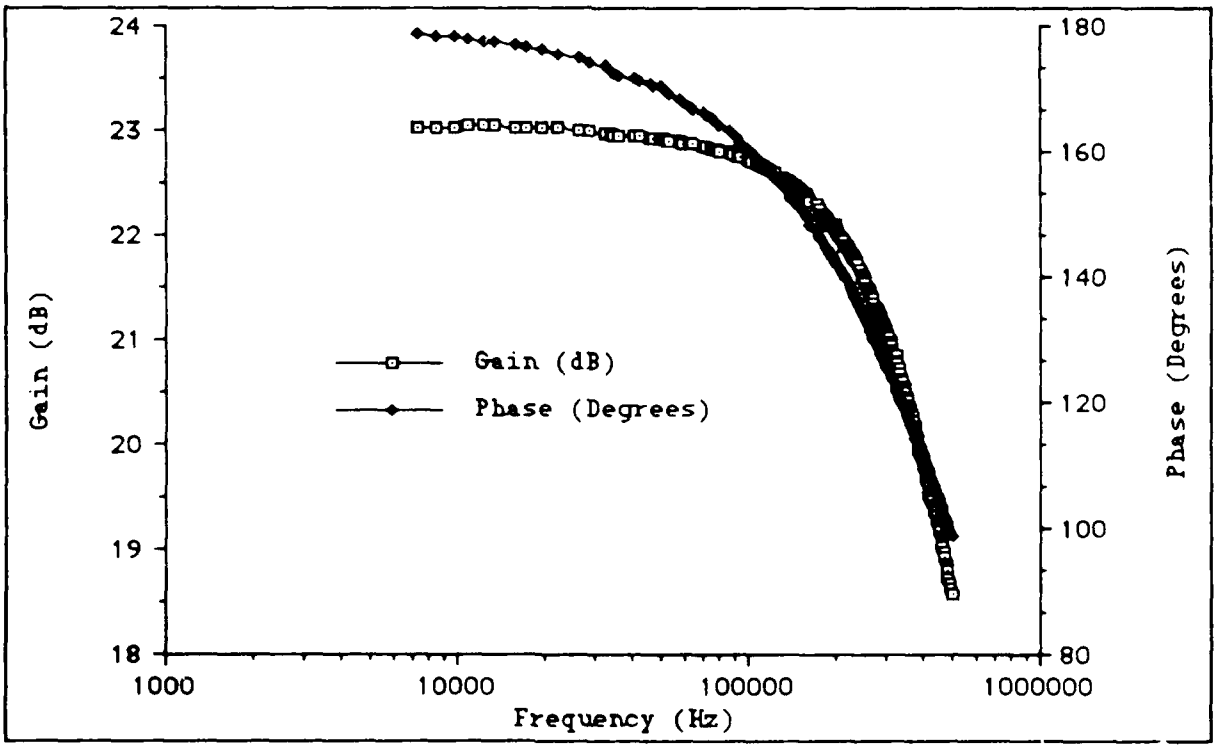

Figure G-11. Sensing Element Chem9 Selected.

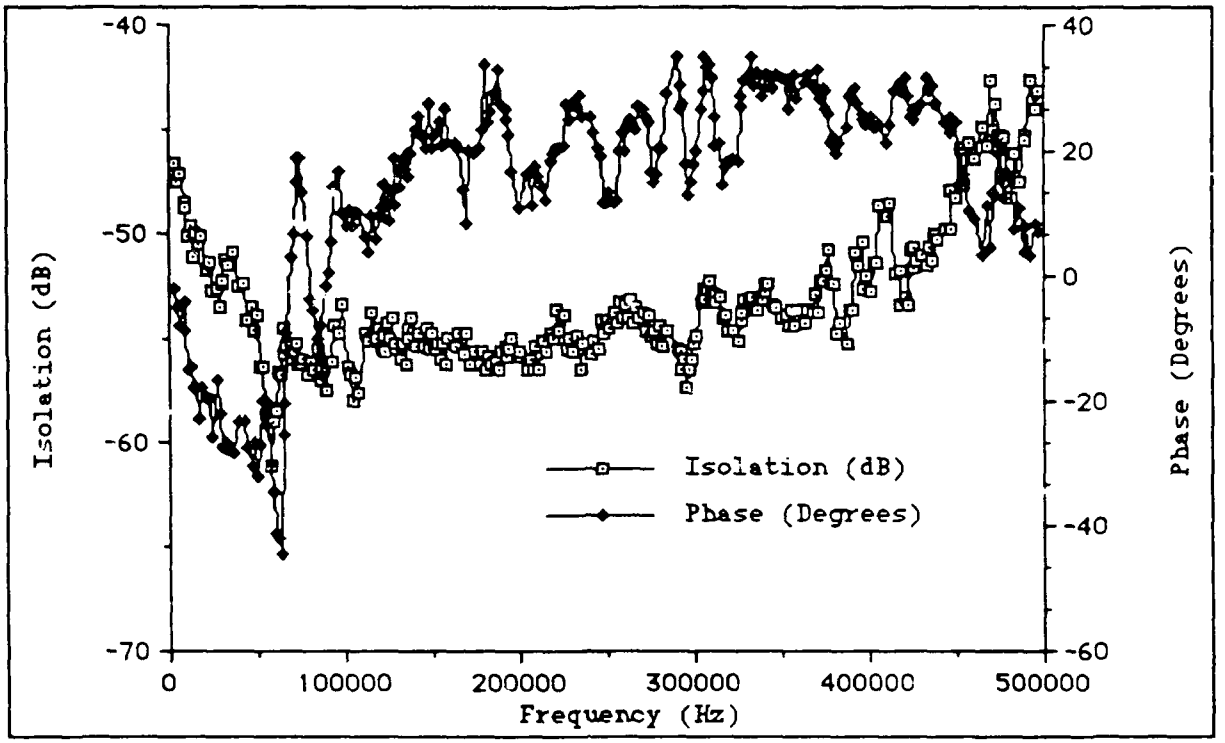

Figure G-12. Sensing Element Chem9 Unselected.

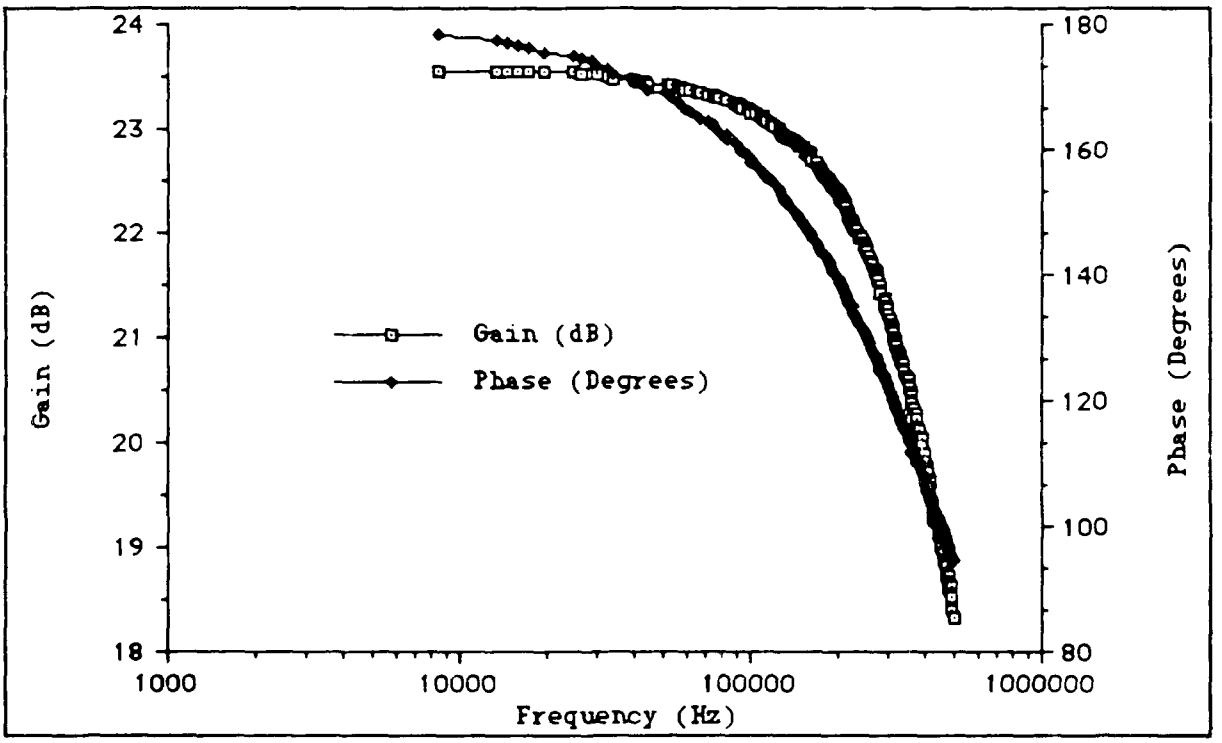

Figure G-13. Sensing Element Chem10 Selected

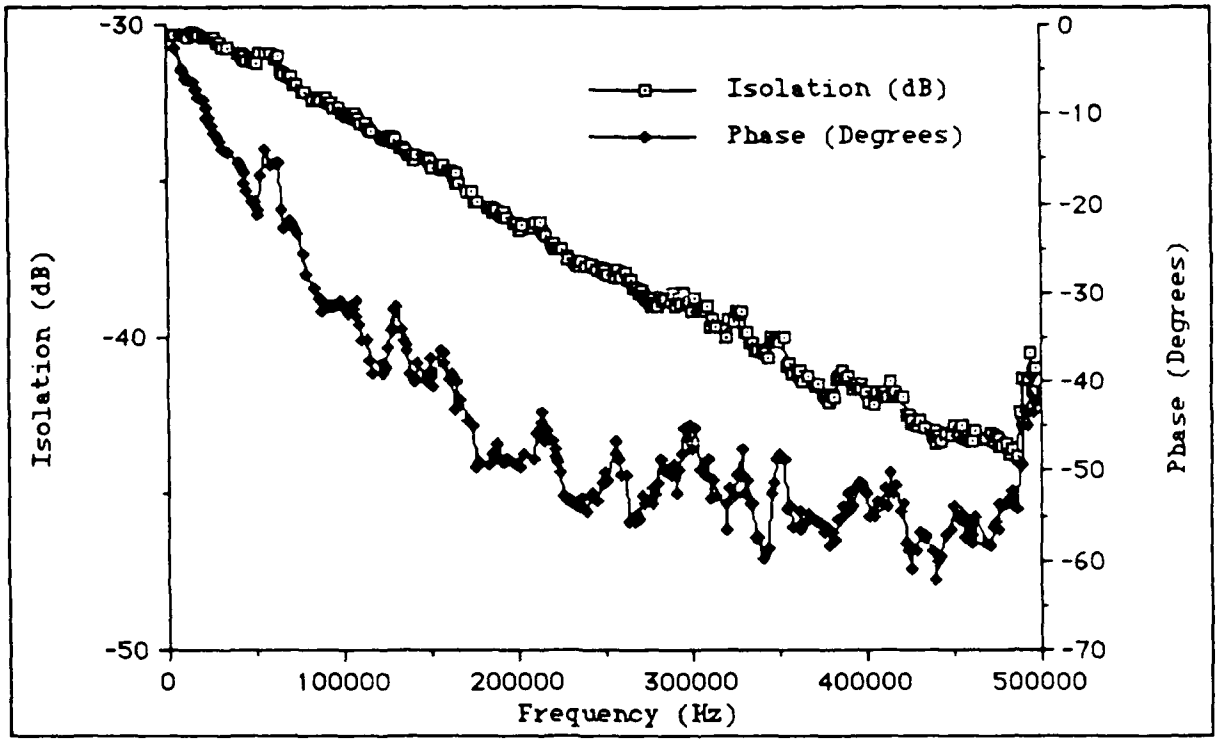

Figure G-14. Sensing Element Chem10 Unselected.

Appendix H

Response of the Phthalocyanine Thin Film Coatings to Dry Laboratory Nitrogen Gas and Filtered Room Air at Various Humidities

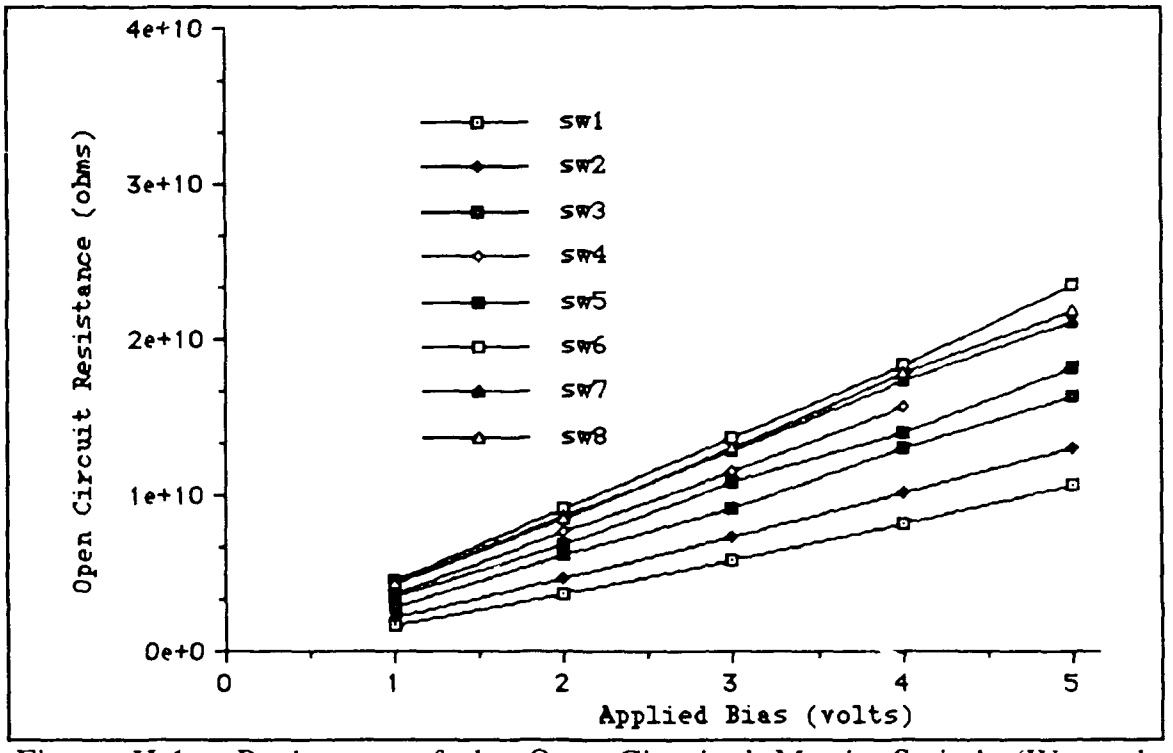

Figure H-1. Resistance of the Open-Circuited Matrix Switch (Wavetek Corp., Model 604, San Diego, CA).

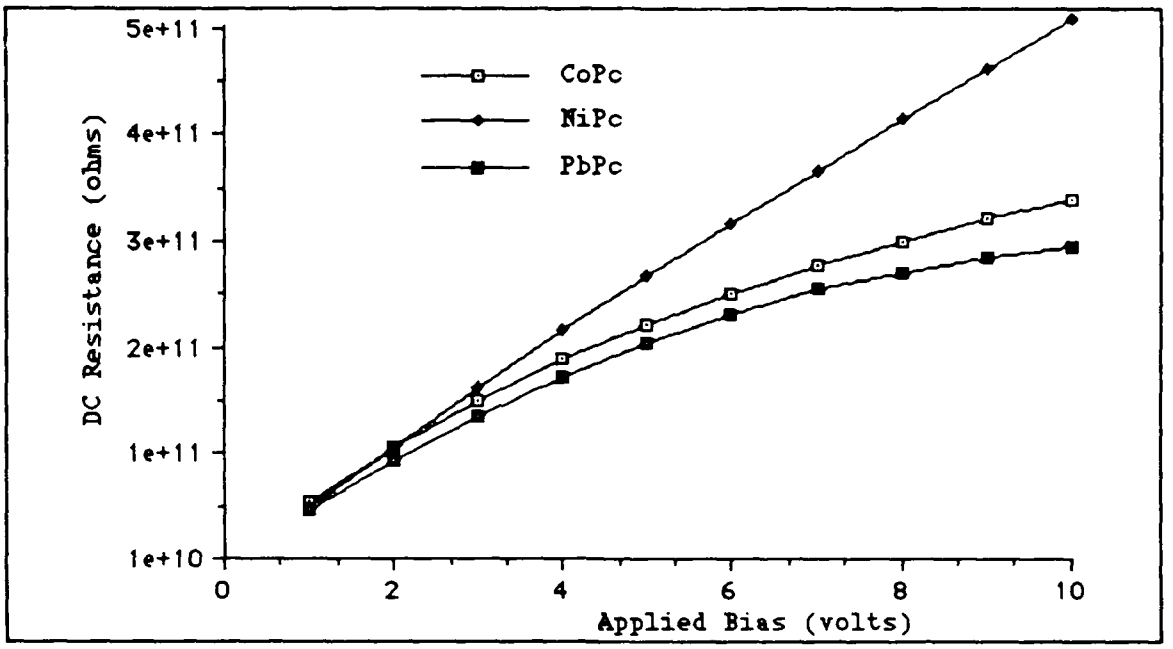

Figure H-2. DC Resistance of the Phthalocyanine Films Exposed to N_2 at 26°C and 3% Relative Humidity.

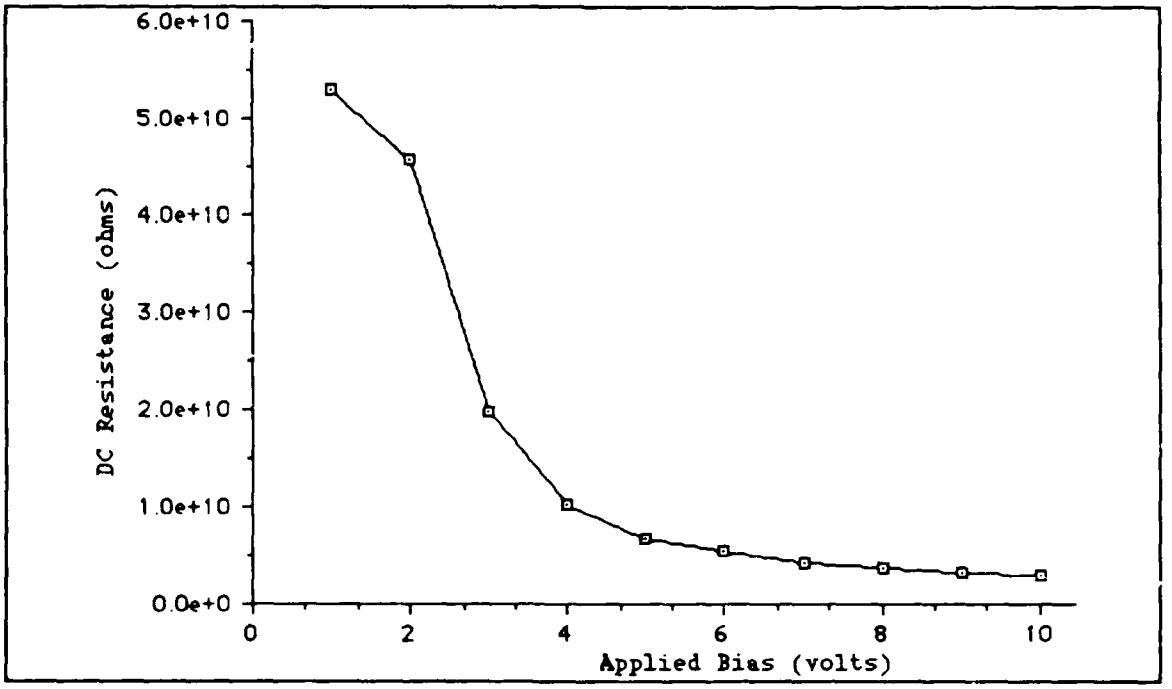

Figure H-3. DC Resistance of the Copper-Doped Phthalocyanine Film Exposed to N_2 at 26°C and 3% Relative Humidity.

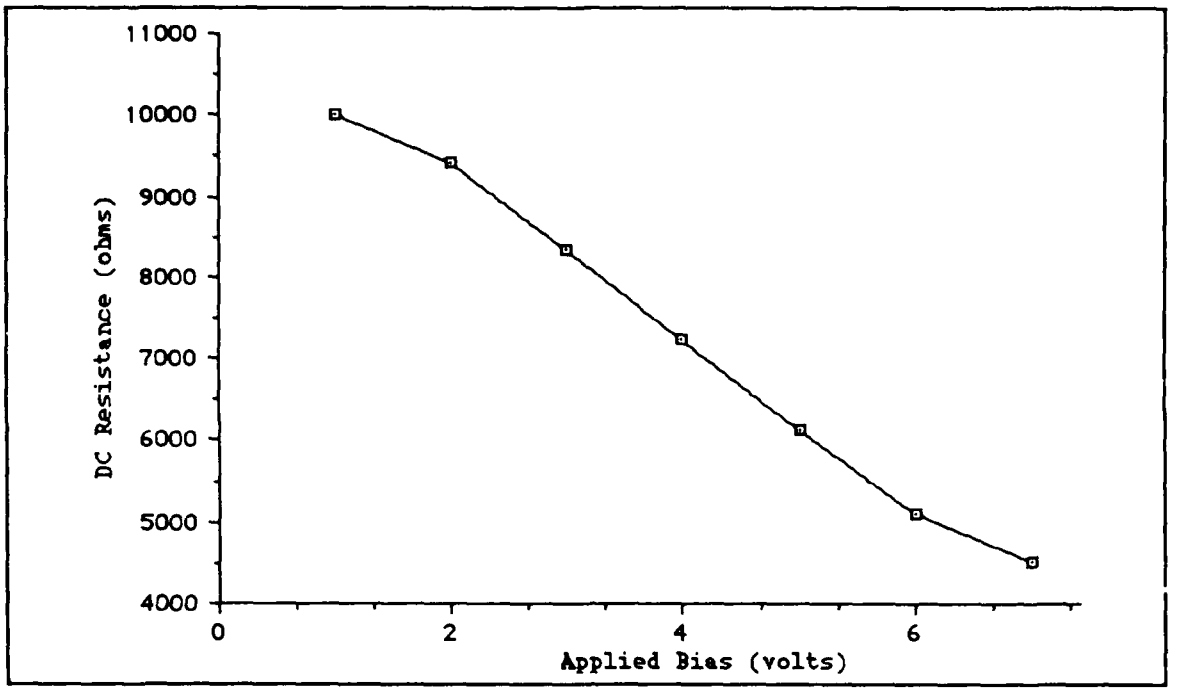

Figure H-4. DC Resistance of the Undoped Phthalocyanine Film Exposed to N_2 at 26°C and 3% Relative Humidity.

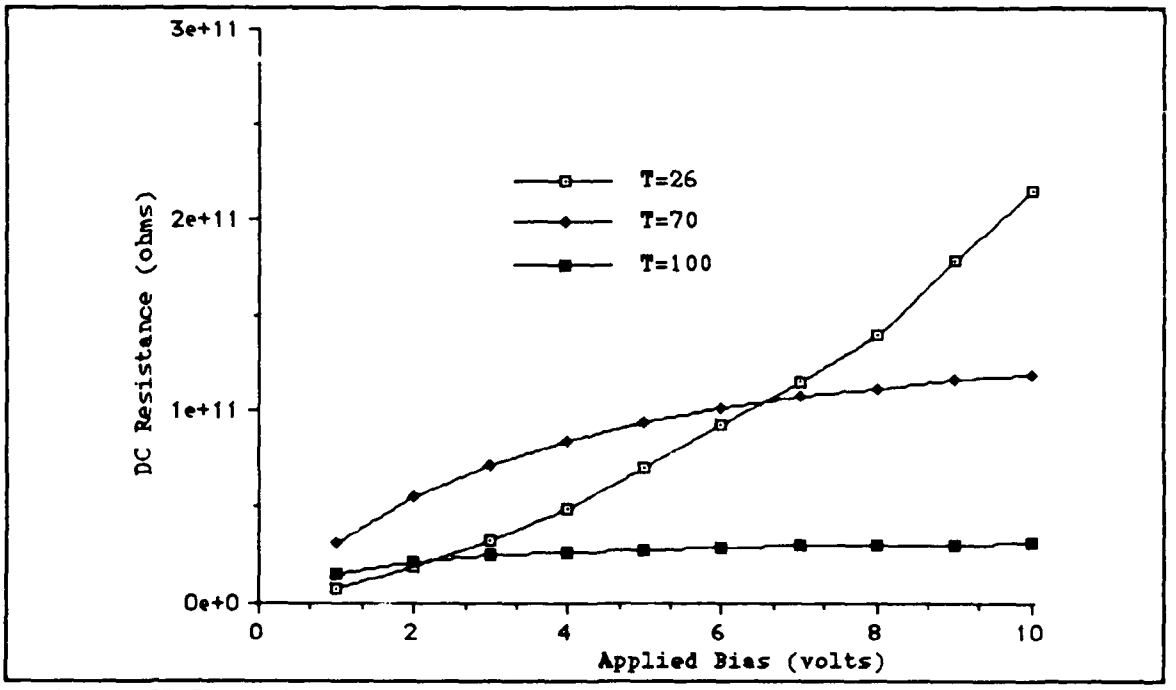

Figure H-5. DC Resistance of the Cobalt-Doped Phthalocyanine Film Exposed to Filtered Room Air at 10% Relative Humidity (Temperature (T) in degrees Celsius).

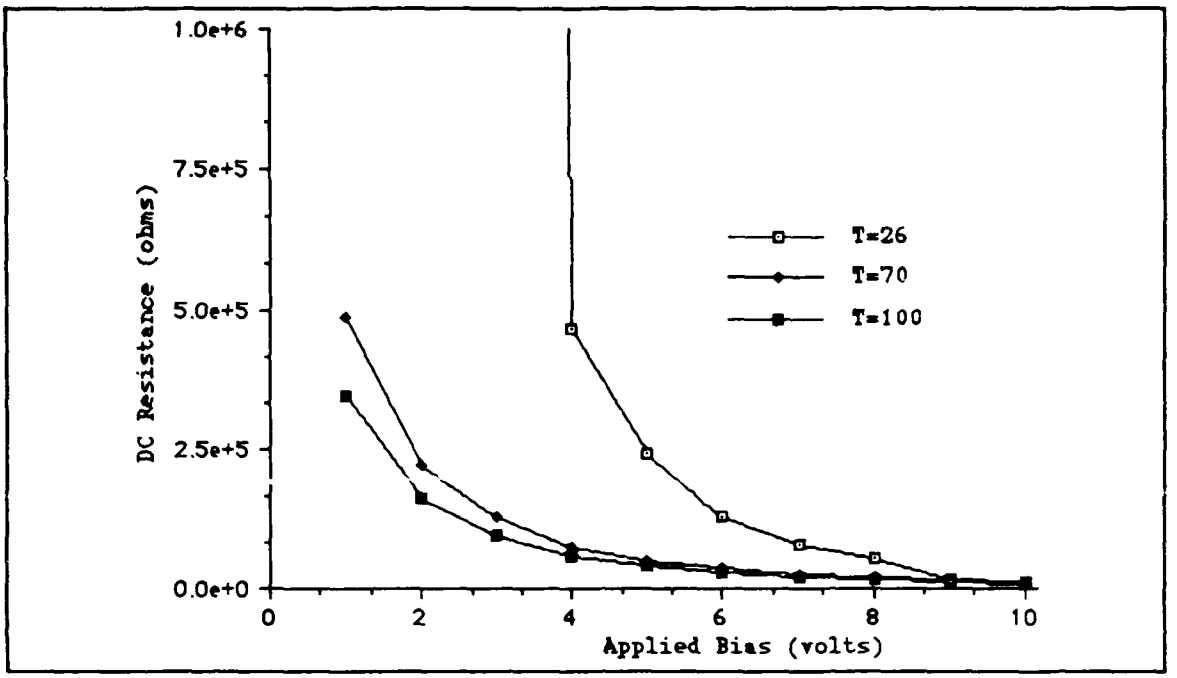

Figure H-6. DC Resistance of the Copper-Doped Phthalocyanine Film Exposed to Filtered Room Air at 10% Relative Humidity (Temperature (T) in degrees Celsius).

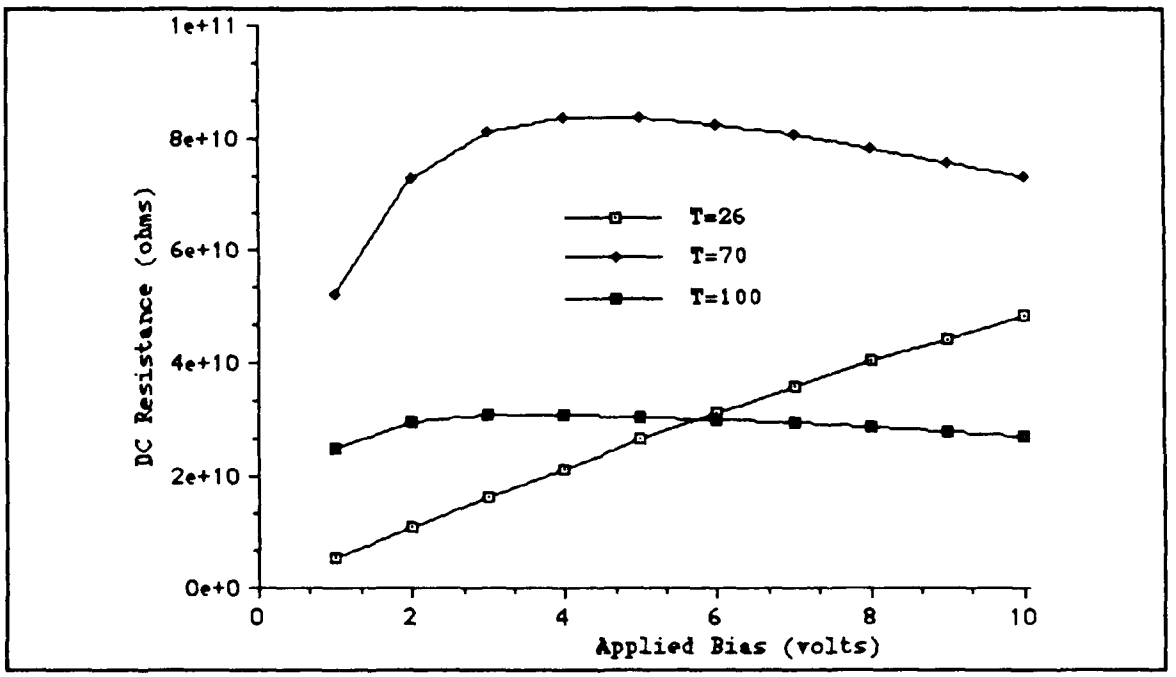

Figure H-7. DC Resistance of the Lead-Doped Phthalocyanine Film Exposed to Filtered Room Air at 10% Relative Humidity (Temperature (T) in degrees Celsius).

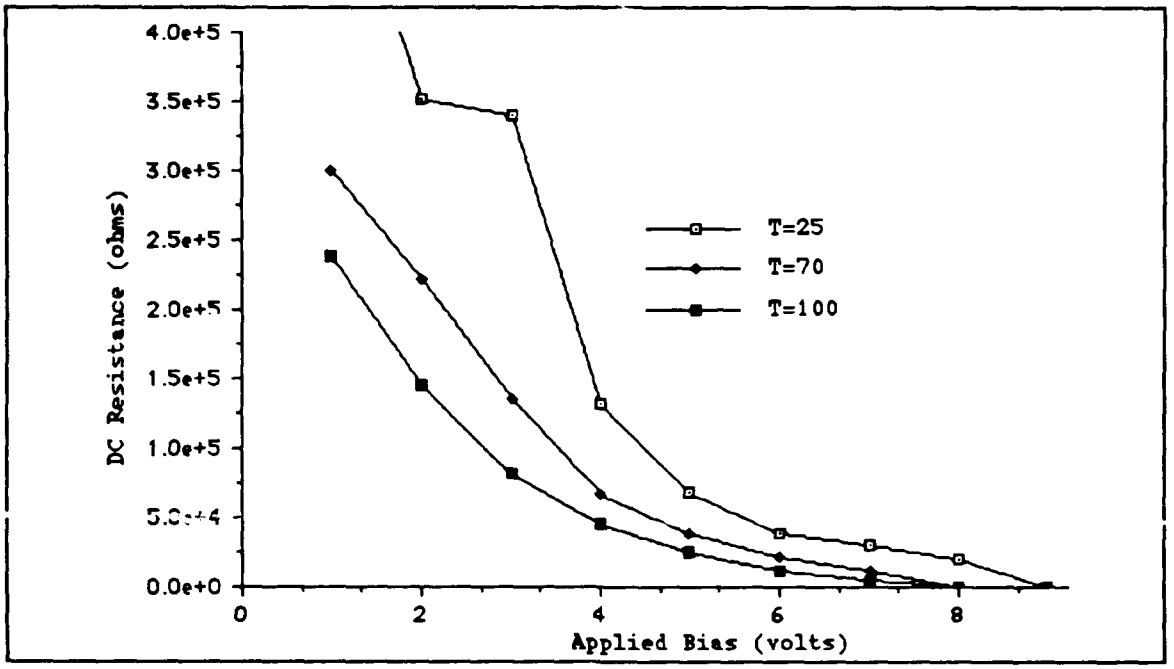

Figure H-8. DC Resistance of the Nickel-Doped Phthalocyanine Film Exposed to Filtered Room Air at 10% Relative Humidity (Temperature (T) in degrees Celsius).

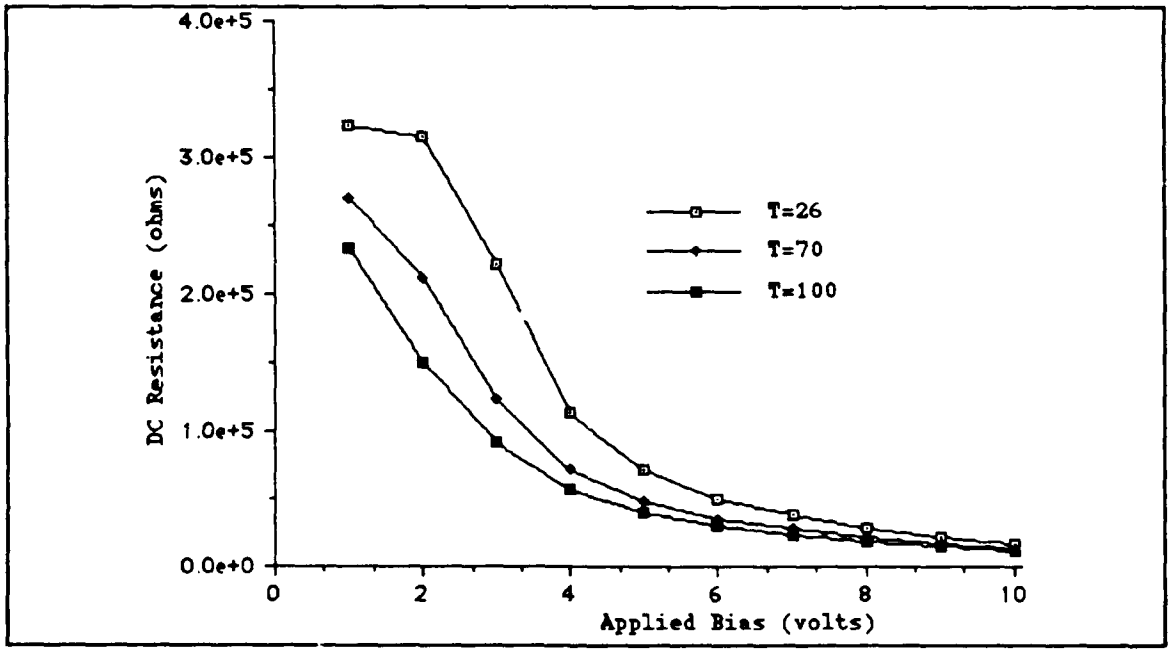

Figure H-9. DC Resistance of the Undoped Phthalocyanine Film Exposed to Filtered Room Air at 10% Relative Humidity (Temperature (T) in degrees Celsius).

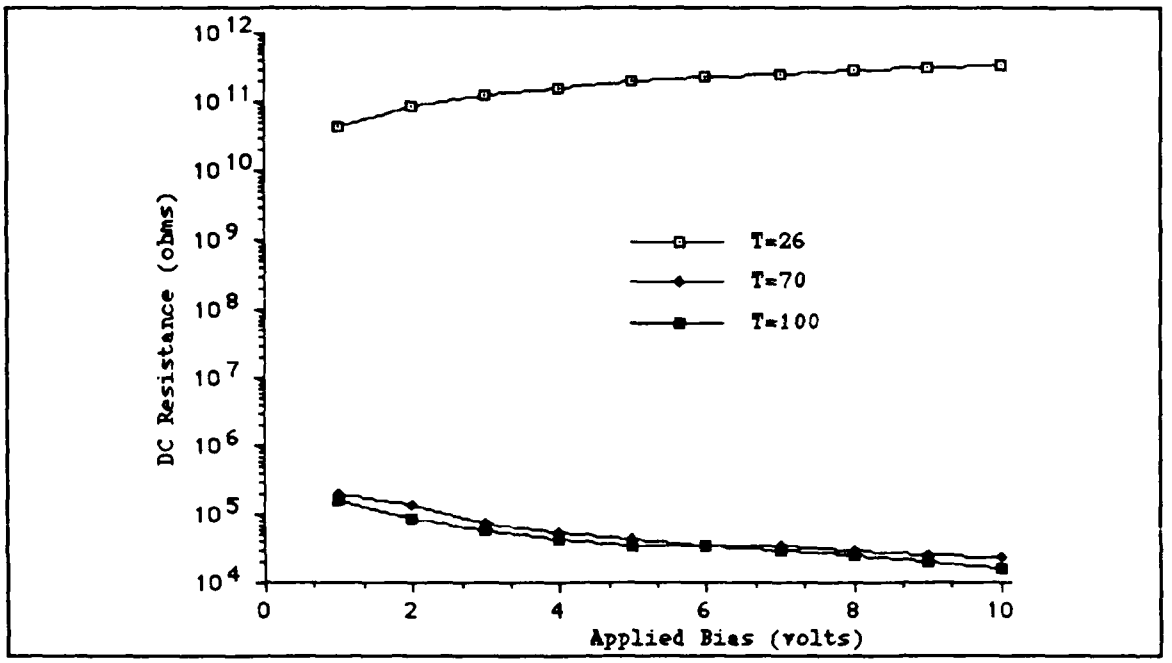

Figure H-10. DC Resistance of the Cobalt-Doped Phthalocyanine Film Exposed to Filtered Room Air at 50% Relative Humidity (Temperature (T) in degrees Celsius).

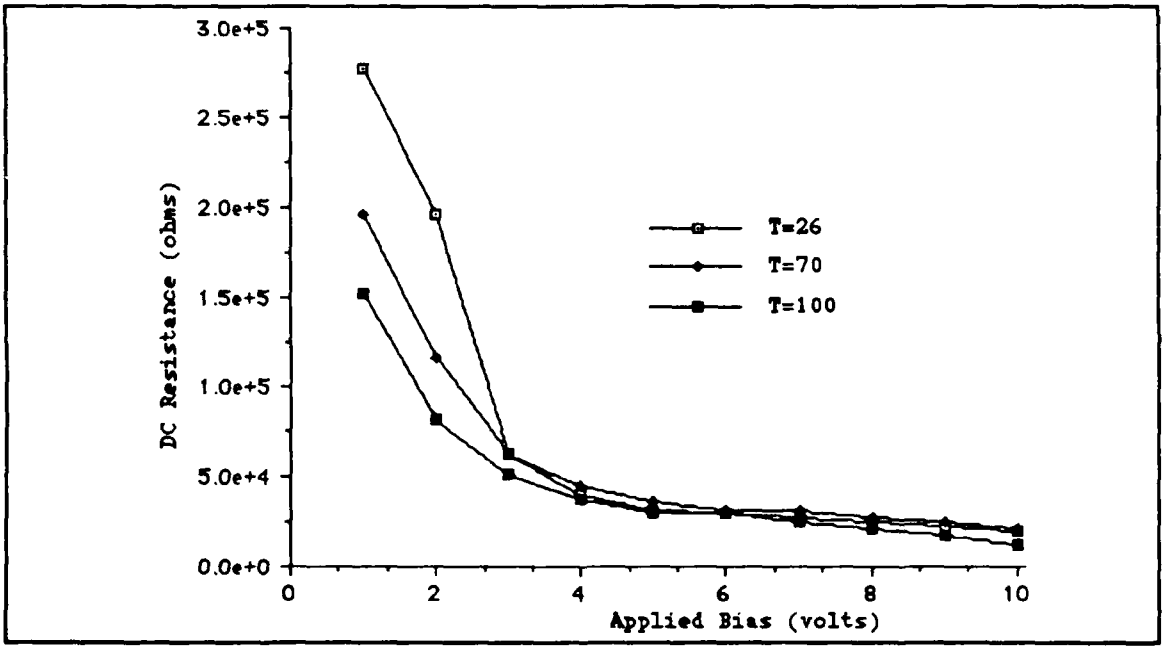

Figure H-11. DC Resistance of the Copper-Doped Phthalocyanine Film Exposed to Filtered Room Air at 50% Relative Humidity (Temperature (T) in degrees Celsius).

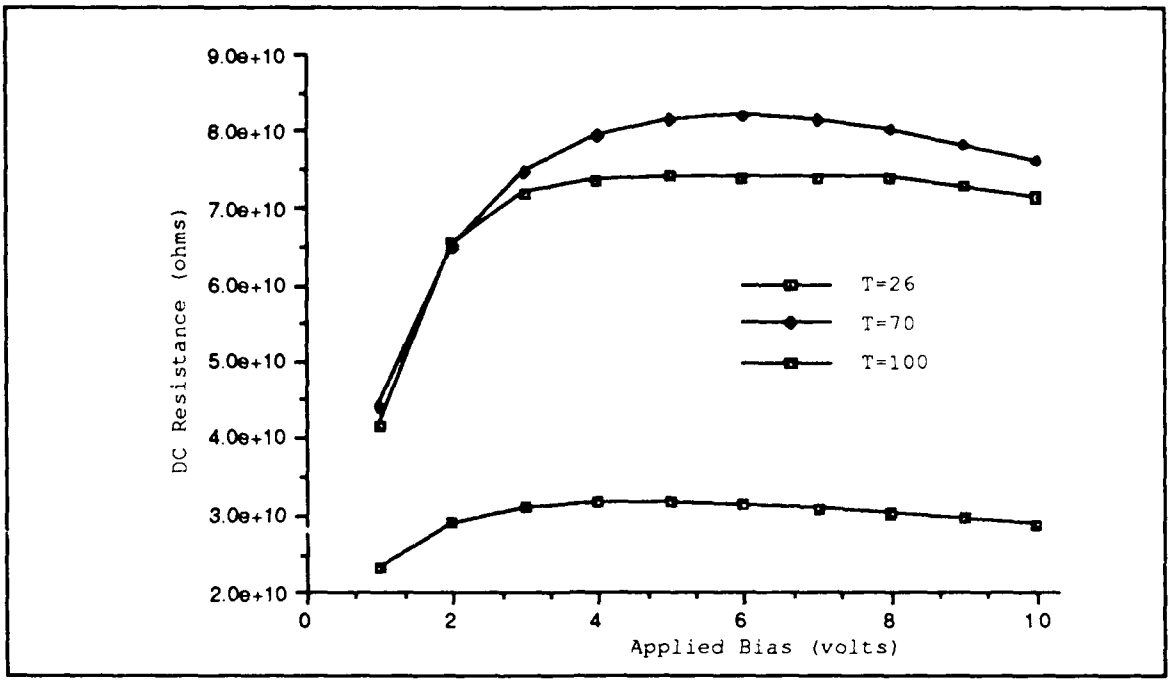

Figure H-12. DC Resistance of the Lead-Doped Phthalocyanine Film Exposed to Filtered Room Air at 50% Relative Humidity (Temperature (T) in degrees Celsius).

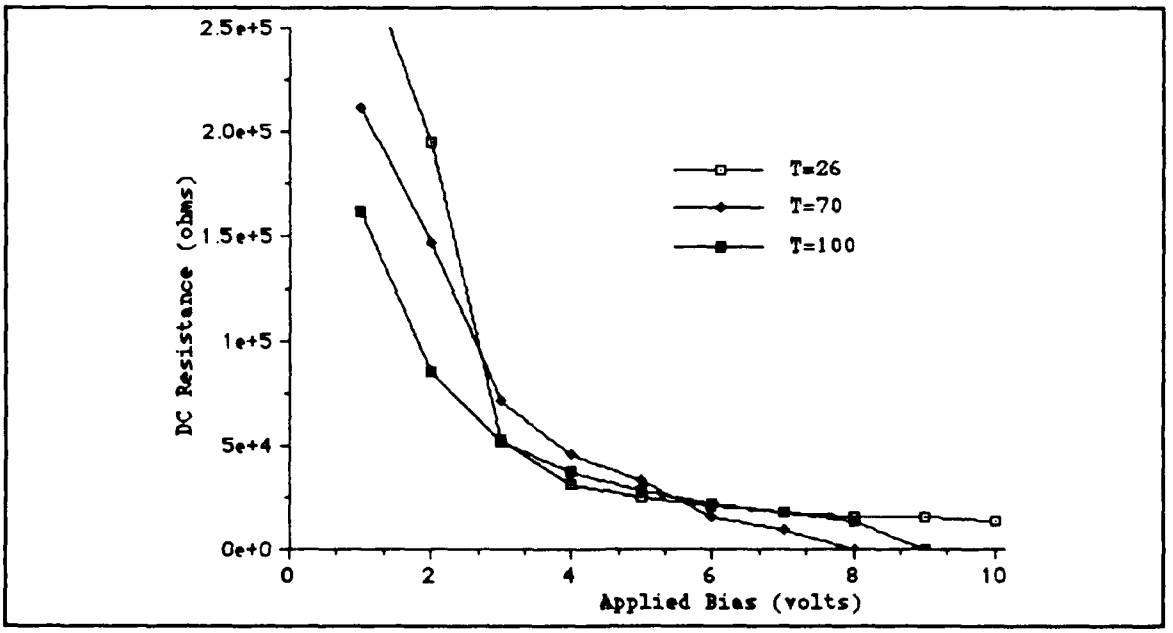

Figure H-13. DC Resistance of the Nickel-Doped Phthalocyanine Film Exposed to Filtered Room Air at 50% Relative Humidity (Temperature (T) in degrees Celsius).

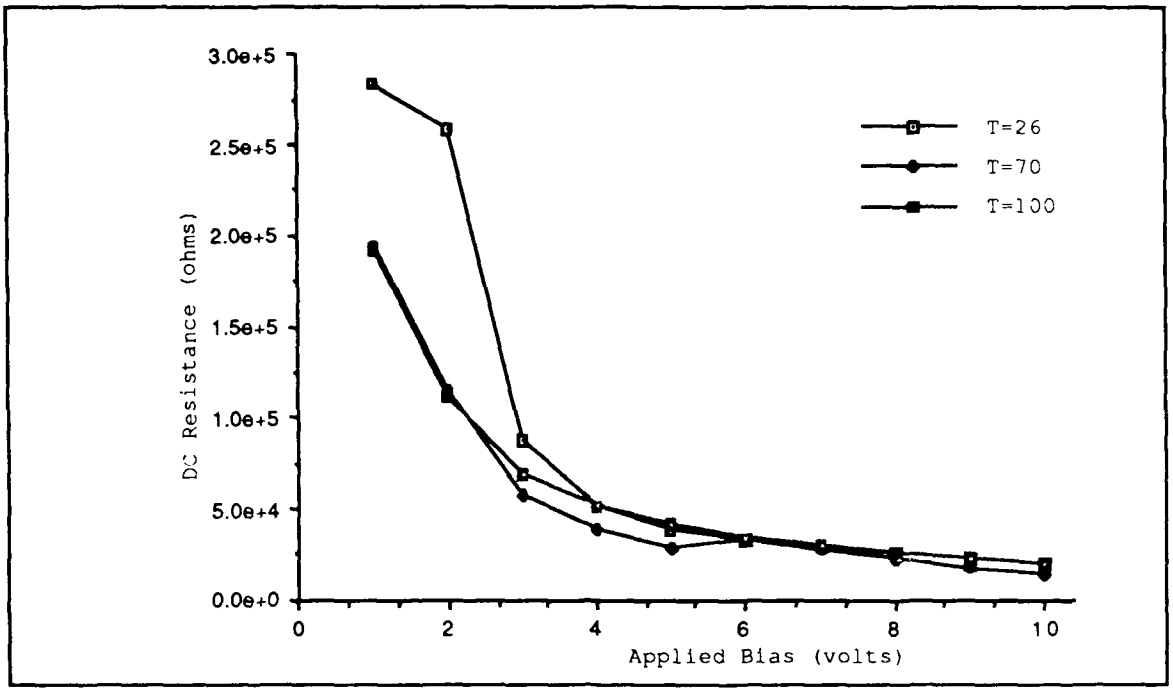

Figure H-14. DC Resistance of the Undoped Phthalocyanine Film Exposed to Filtered Room Air at 50% Relative Humidity (Temperature (T) in degrees Celsius).

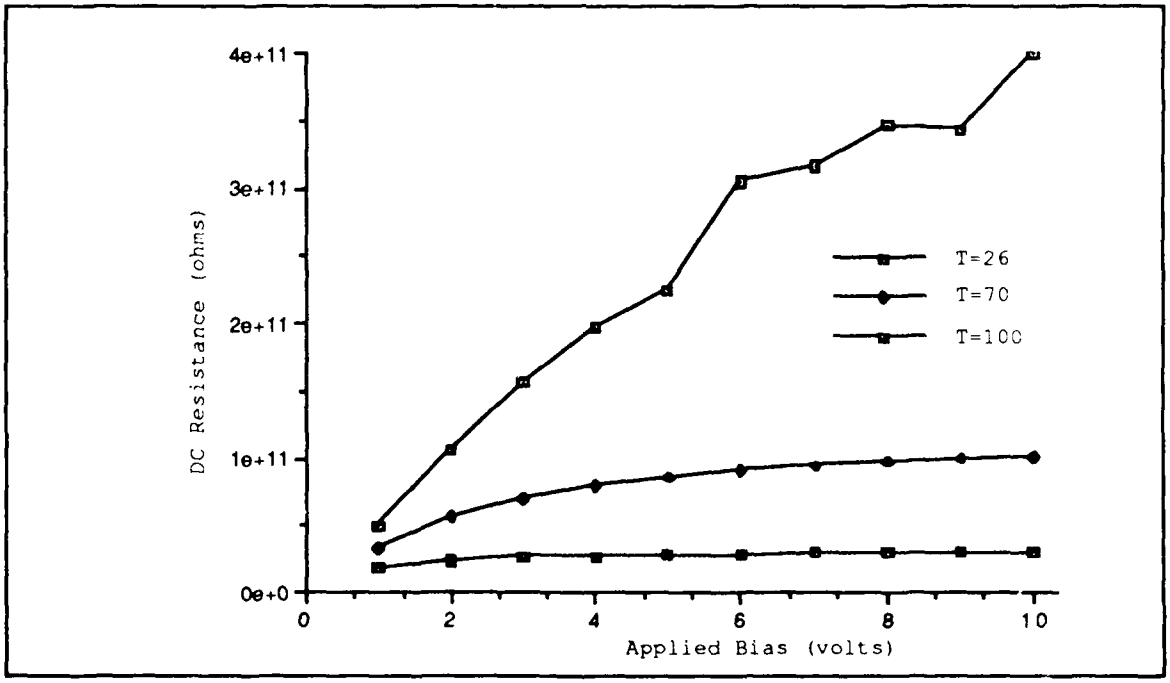

Figure H-15. DC Resistance of the Cobalt-Doped Phthalocyanine Film Exposed to Filtered Room Air at 100% Relative Humidity (Temperature (T) in degrees Celsius).

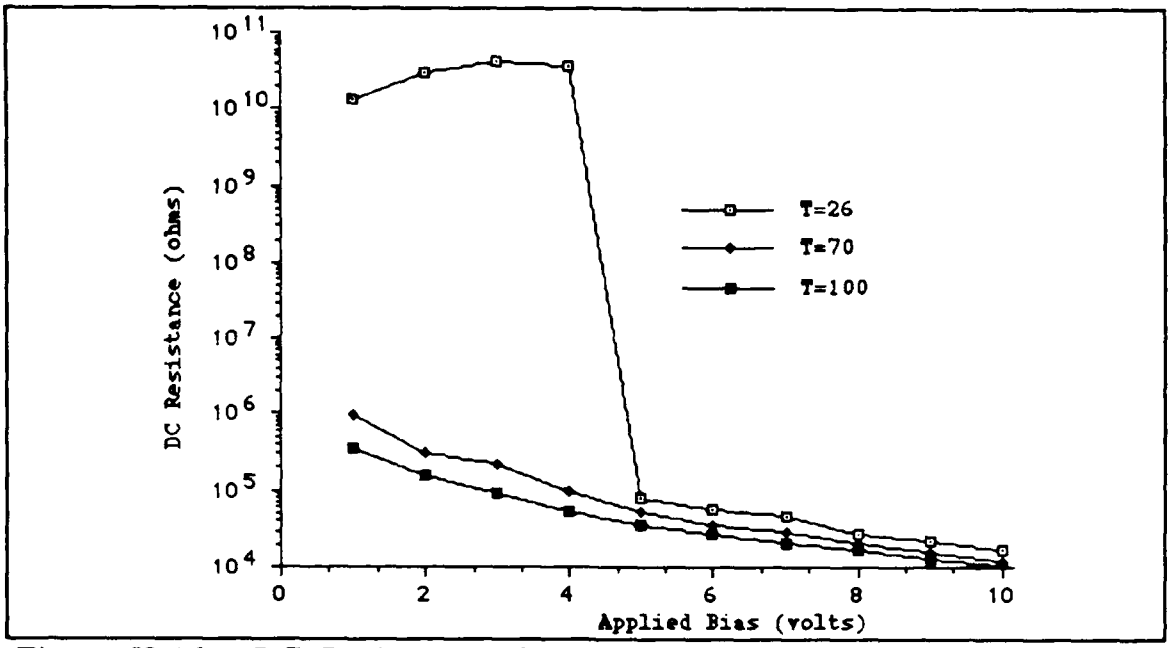

Figure H-16. DC Resistance of the Copper-Doped Phthalocyanine Film Exposed to Filtered Room Air at 100% Relative Humidity (Temperature (T) in degrees Celsius).

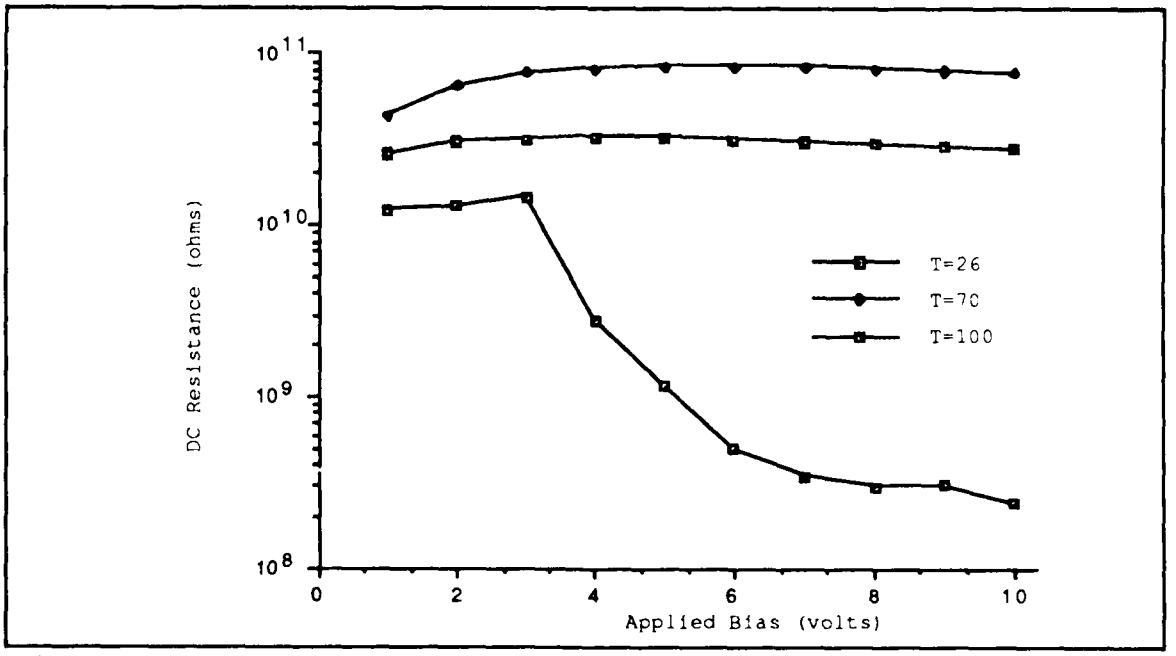

Figure H-17. DC Resistance of the Lead-Doped Phthalocyanine Film Exposed to Filtered Room Air at 100% Relative Humidity (Temperature (T) in degrees Celsius).

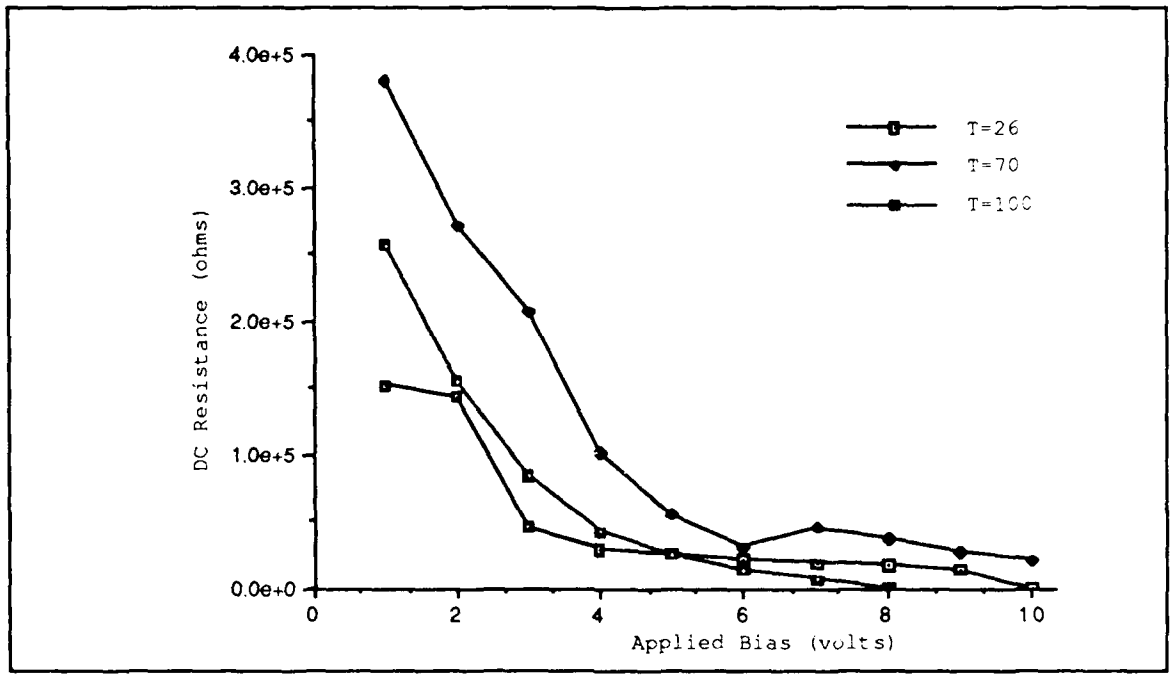

Figure H-18. DC Resistance of the Nickel-Doped Phthalocyanine Film Exposed to Filtered Room Air at 100% Relative Humidity (Temperature (T) in degrees Celsius).

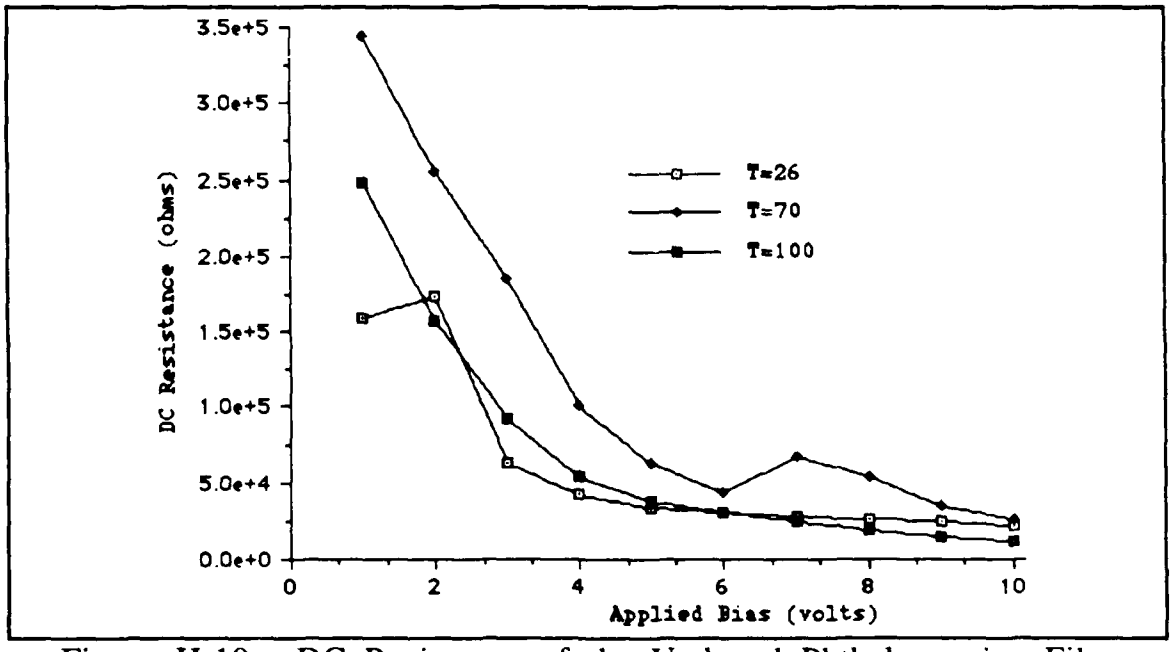

Figure H-19. DC Resistance of the Undoped Phthalocyanine Film Exposed to Filtered Room Air at 100% Relative Humidity (Temperature (T) in degrees Celsius).

Bibliography

1. Johnston, A. "Trends in Biosensor Research and Development," *Proceedings of the International Electron Devices Meeting*. 654-657. New York: IEEE Press, December 1988.

2. Wong, H. and M. H. White. "A Self-Contained CMOS Integrated pH Sensor," *Proceedings of the International Electron Devices Meeting*. 658-661. New York: IEEE Press, December 1988.

3. Johnson, C. L. , K. D. Wise, and J. W. Schwan. "A Thin-Film Gas Detector For Semiconductor Process Gases," *Proceedings of the International Electron Devices Meeting*. 662-665. New York: IEEE Press, December 1988.

4. Baumgartner, W. and T. Ricker. "Computer Assisted Dielectric Cure Monitoring in Material Quality and Cure Process Control," *SAMPE, 14*: 6-16 (July/August 1983).

5. Wohltjen, H. *et al.* "Chemical Microsensors for Vapor Detection," *Proceedings of the I.E.E.E. Solid State Sensor Conference*. 42-43. New York: IEEE Press, 1984.

6. Kolesar, E. *Chemically-Sensitive Field-Effect Transisto.* Thesis Proposal No. VI.13. Department of Electrical and Computer Engineering, Air Force Institute of Technology, Wright-Patterson AFB, OH, October 1988.

7. Kolesar, E. and J. Wiseman. "Interdigitated Gate Electrode Field Effect Transistor for the Selective Detection of Nitrogen Dioxide and Diisopropyl Methylphosphonate," *Analytical Chemistry, 61*: 2355-2361 (November 1989).

8. Khanna, S. *et al. Thin-Film Chemical Sensors Based on Electron Tunneling*. JPL Publication 85-85. Jet Propulsion Laboratory, Pasadena, California, 15 November 1985.

9. Jones, T. A. and B. Bott. "Gas-Induced Electrical Conductivity in Metal Phthalocyanines," *Sensors and Actuators, 9*: 27-37 (1986).

10. Lee, H. *Optimization of a Resin Cure.* MS thesis, Massachusetts Institute of Technology, Cambridge Massachusetts, 1982.

11. Halliday, D. and R. Resnick. *Fundamentals of Physics* (Revised Printing). New York: John Wiley & Sons, Inc., 1974.

12. Schiede E. and G. Guilbault. "Piezoelectric Detectors for Organophosphorus Compounds and Pesticides," *Analytical Chemistry, 44*: 1764-1768 (September 1972).

13. Guilbault, G. *et al.* "Piezoelectric Crystal Coating for Detection of Organophosphorus Compounds," *Analytical Chemistry, 53*: 2057-2060 (1981).

14. Wohltjen H. and A. Snow. "The Selective Detection of Vapors Using Surface Acoustic Wave Devices," *Proceedings of The Third International Conference on Solid-State Sensors and Actuators Digest of Technical Papers.* 66-70. Piscataway, New Jersey: IEEE, 1985.

15. Kolesar, E. *Electronic Detection of Low Concentrations of Organophosphorus Compounds with a Solid State Device Utilizing Supported Copper and Cuprous Oxide Island Films.* PhD Dissertation. University of Texas, Austin, Texas, May 1985 (AD-A158181).

16. Wohltjen, H. *et al.* "A Vapor-Sensitive Chemiresistor Fabricated with Planar Microelectrodes and a Langmuir-Blodgett Organic Semiconductor Film," *I.E.E.E. Transactions On Electron Devices ED-32*: 1170-1174 (July 1985).

17. Chang, S. and D. Hicks. *Tin Oxide Microsensors*, General Motors Research Report GMR-4954. Electronics Department, General Motors Research Laboratories, Warren Michigan, 19 February 1985.

18. Sberveglieri, G. *et al.* "Radio Frequency Magnetron Sputtering Growth and Characterization of Indium-Tin Oxide (ITO) Thin Films for NO_2 Gas Sensors," *Sensors and Actuators, 15*: 235-242 (1988).

19. Bergveld, P. "The Impact of MOSFET-Based Sensors," *Proceedings of The Third International Conference on Solid-State Sensors and Actuators Digest of Technical Papers.* 142-143. Piscataway New Jersey: IEEE, 1985.

20. Uyemura, J. P. *Fundamentals of MOS Digital Integrated Circuits.* Reading, Massachusetts: Addison-Wesley Publishing Company, 1988.

21. Bott, B. and T. A. Jones. "The Use of Multisensor Systems in Monitoring Hazardous Atmospheres," *Proceedings of The Third International Conference on Solid-State Sensors and Actuators Digest of Technical Papers.* 81-84. Piscataway, New Jersey: IEEE, 1985.

22. Muller, R. *et al.* "Multidimensional Sensors for Gas Analysis," *Proceedings of The Third International Conference on Solid-State Sensors and Actuators Digest of Technical Papers.* 81-84. Piscataway, New Jersey: IEEE, 1985.

23. Stetter, J. *et al. Sensor Array For Toxic Gas Detection,* United States Patent Number 4670405. Washington, D.C.: United States Patent Office, 2 June 1987.

24. Rose-Pehrsson, S. *et al.* "Data Analysis of Surface Acoustic Wave Device Coating Responses Using Pattern Recognition Methods," *Proceedings of the 1986 U. S. Army Chemical Research, Development and Engineering Center Scientific Conference on Chemical Defense Research.* 421-428. Aberdeen Proving Grounds, Maryland: U. S. Army Armament, Munitions & Chemical Command, June 1987.

25. Bolto, B. "Semiconducting Organic Polymers Containing Metal Groups," *Organic Semiconducting Polymers,* edited by J. Katon. New York: Marcel Dekker, Inc., 1968.

26. Roberts, G. *et al.* "Electronic Devices Incorporating Stable Phthalocyanine Langmuir-Blodgett Films," *Electronics and Optics*: 113-123 (July 1985).

27. Maeda, S. "Activities of the Research and Development Association for Future Electron Devices," *Proceedings of the IEEE, 77*: 1420-1429 (September 1989).

28. Syrkin, Y. and M. Dyatkina. *Structure of Molecules and the Chemical Bond.* Translated and revised by M. Partridge and D. Jordan. New York: Dover Publications, 1964.

29. Hanack, M. *et al.* "Synthesis and Properties of Conducting Bridged Macrocyclic Metal Complexes," *Handbook of Conducting Polymers*, Volume 1, edited by T. Skotheim. New York: Marcel Dekker, Inc., 1986.

30. Kanda, S. and H. Pohl. "Recent Experimental Aspects of the Electronic Behavior of Organic Macromolecular Solids," *Organic Semiconducting Polymers,* edited by J. Katon. New York: Marcel Dekker, Inc., 1968.

31. Nebergall, W. *et al. College Chemistry with Qualitative Analysis* (Fifth Edition). Lexington Massachusetts: D. C. Heath and Company, 1976.

32. Raven, P. and G. Johnson. *Understanding Biology.* St. Louis: Times Mirror/Mosby College Publishing, 1988.

33. Cotts, D. and Z. Reyes. *Electrically Conductive Organic Polymers for Advanced Applications.* Park Ridge, New Jersery: Noyes Data Corporation, 1986.

34. Mockert, H. *et al.* "Lead Phthalocyanine (PbPc) as a Prototype Organic Material for Gas Sensors: Comparative Electrical and Spectroscopic Studies to Optimize O_2 and NO_2 Sensing," *Sensors and Actuators, 19*: 159-176 (1989).

35. Jones, T. *et al.* "Fast Response Metal Phthalocyanine-Based Gas Sensors," *Sensors and Actuators, 17*: 467-474 (May1989).

36. Baker, S. *et al.* "Phthalocyanine Langmuir Blodgett-Film Gas Detector," *IEE Proceedings, 130*: 260-263 (October 1983).

37. Barger, W. *et al.* "Chemiresistor Transducers Coated With Phthalocyanine Derivatives by the Langmuir-Blodgett

Technique," *Proceedings of The Third International Conference on Solid-State Sensors and Actuators Digest of Technical Papers.* 410-413. Piscataway, New Jersey: IEEE, 1985.

38. Kaner, R. and A. MacDiarmid. "Plastics That Conduct Electricity," *Scientific American, 258*: 106-111 (February 1988).

39. Bott, D. "Structural Basis for Semiconducting and Metallic Polymers," *Handbook of Conducting Polymers*, Volume 2, edited by T. Skotheim. New York: Marcel Dekker, Inc., 1986.

40. Minami, T. and A. Kinoshita. "Preparation of Noncrystalline Solids," *Noncrystalline Semiconductors*, Volume 1, edited by Michael Pollak. Boca Raton, Florida: CRC Press, Inc., 1987.

41. Pollak, M. "Other Transport Properties," *Noncrystalline Semiconductors*, Volume 1, edited by M. Pollak. Boca Raton, Florida: CRC Press, Inc., 1987.

42. Pohl, Herbert. "Theoretical Aspects of The Electronic Behavior of Organic Macromolecular Solids," *Organic Semiconducting Polymers*, edited by J. Katon. New York: Marcel Dekker, Inc., 1968.

43. Nagels, P. "Electronic Transport in Amorphous Semiconductors," *Amorphous Semiconductors*, edited by M. Brodsky. New York: Springer-Verlag, 1985.

44. Weaire, D. and E. O'Reilly. "Electronic Properties of Amorphous Semiconductors," *Noncrystalline Semiconductors*, Volume 1, edited by M. Pollak. Boca Raton, Florida: CRC Press, Inc., 1987.

45. Pizzini, S. *et al.* "Influence of the Structure and Morphology on the Sensitivity to Nitrogen Oxides of Phthalocyanine Thin-Film Resistivity Sensors," *Sensors and Actuators, 17*: 481-491 (May1989).

46. Nieuwenhuizen, M. *et al.* "Metallophthalocyanines as Chemical Interfaces on a Surface Acoustic Wave Gas Sensor for Nitrogen Dioxide," *Analytical Chemistry, 60*: 230-235 (Februray1988).

47. Van Ewyk, R. *et al.* "Electron Donor-Acceptor Interactions and Surface Semiconductivity in Molecular Crystals as a Function of Ambient Gas," *Journal of The Chemical Society, Faraday Transactions I, 76*: 2194-2205 (October 1980).

48. Fan, F. and L. Faulkner. "Photovoltaic Effects of Metalfree and Zinc Phthalocyanines. I. Dark Electrical Properties of Rectifying Cells," *Journal of Chemical Physics, 69*: 3334-3340 (October 1978).

49. Gopel, W. *et al.* "Prototype Chemical Sensors for the Selective Detection of O_2 and NO_2 in Gases," *Sensors and Actuators, 17*: 377-384 (May 1989).

50. Archer, P. *et al.* "Kinetic Factors in the Response of Organometallic Semiconductor Gas Sensors," *Sensors and Actuators, 16*: 379-392 (1989).

51. Yoshino, K. *et al.* "Photoconduction and Emission of Phthalocyanine in the Near Infrared," *Energy and Charge Transfer in Organic Semiconductors,* edited by K. Masuda and M. Silver. New York: Plenum Press, 1974.

52. Fielding, P. "Growth and Purification of Phthalocyanine Polymorphs," *Energy and Charge Transfer in Organic Semiconductors,* edited by K. Masuda and M. Silver. New York: Plenum Press, 1974.

53. Alley, G. "Interdigital Capacitors and Their Applications to Lumped-Element Microwave Integrated Circuits," *IEEE Transactions on Microwave Theory and Techniques, MTT-18*: 1028-1033 (December 1970).

54. Sze, S. *Physics of Semiconductor Devices* (Second Edition). New York: John Wiley & Sons, Inc., 1981.

55. Kolesar, E. and R. Walser. "Organophosphorus Compound Detection with a Supported Copper + Cuprous Oxide Island Film. 1. Gas-Sensitive Film Physical Characteristics and Direct Current Studies," *Analytical Chemistry, 60*: 1731-1736 (September 1988).

56. Kiethley Instruments, Incorporated. *Instruction Manual, Model 617 Programmable Electrometer.* Cleveland, OH, 1984.

57. Hewlett Packard, Incorporated. *Operation Manual: Model 4194A Impedance/Gain-Phase Analyzer.* Palo Alto, CA, 1986.

58. Cheng, D. *Analysis of Linear Systems.* Reading, Massachusetts: Addison-Wesley Publishing Company, 1959.

Vita

Captain Thomas J. Jenkins [redacted]. He graduated from East Washington High School, Pekin, Indiana in 1975. [redacted] Indiana in 1975. [redacted]. Upon enlisting in the United States Air Force on July 29, 1979, he was assigned to the Freeman Mathematical Laboratory, Eglin Air Force Base, Florida as a computer operator. [redacted]. In 1984, he received his Bachelor of Science in Electrical Engineering and his commission in the United States Air Force after being selected for the Airman Education and Commissioning Program. Subsequently, he was assigned to the Logistics Management Center, Headquarters, Air Force Logistics Command as a computer engineer. Then, in 1987, he was assigned to the Avionics Laboratory, Wright-Patterson Air Force Base, Ohio as a microwave project engineer. In May of 1988, he entered the School of Engineering, Air Force Institute of Technology.

[redacted]

REPORT DOCUMENTATION PAGE

Form Approved
OMB No. 0704-0188

1a. REPORT SECURITY CLASSIFICATION UNCLASSIFIED	1b. RESTRICTIVE MARKINGS
2a. SECURITY CLASSIFICATION AUTHORITY	3. DISTRIBUTION/AVAILABILITY OF REPORT Approved for public release; distribution unlimited
2b. DECLASSIFICATION/DOWNGRADING SCHEDULE	
4. PERFORMING ORGANIZATION REPORT NUMBER(S) AFIT/GE/ENG/89D-18	5. MONITORING ORGANIZATION REPORT NUMBER(S)
6a. NAME OF PERFORMING ORGANIZATION School of Engineering 6b. OFFICE SYMBOL (*If applicable*) AFIT/ENG	7a. NAME OF MONITORING ORGANIZATION
6c. ADDRESS (*City, State, and ZIP Code*) Air Force Institute of Technology Wright-Patterson AFB, OH 45433-6583	7b. ADDRESS (*City, State, and ZIP Code*)
8a. NAME OF FUNDING/SPONSORING ORGANIZATION Dr. John Lavoie 8b. OFFICE SYMBOL (*If applicable*)	9. PROCUREMENT INSTRUMENT IDENTIFICATION NUMBER
8c. ADDRESS (*City, State, and ZIP Code*) Mound Research Laboratories Miamisburg, OH 45342	10. SOURCE OF FUNDING NUMBERS PROGRAM ELEMENT NO. / PROJECT NO. / TASK NO / WORK UNIT ACCESSION NO.
11. TITLE (*Include Security Classification*) See Block 19	
12. PERSONAL AUTHOR(S) Thomas J. Jenkins, B.S.E.E., Captain, USAF	
13a. TYPE OF REPORT MS Thesis 13b. TIME COVERED FROM _____ TO _____ 14. DATE OF REPORT (*Year, Month, Day*) 1989 December 4 15. PAGE COUNT 332	
16. SUPPLEMENTARY NOTATION	

17. COSATI CODES			18. SUBJECT TERMS (*Continue on reverse if necessary and identify by block number*)
FIELD	GROUP	SUB-GROUP	Chemically-Sensitive Field-Effect Transistor, CHEMFET, Sensors, Integrated Sensors, Nitrogen Dioxide, Phthalocyanine
09	01		

19. ABSTRACT (*Continue on reverse if necessary and identify by block number*)

Title: EVALUATION OF DOPED PHTHALOCYANINES AND A CHEMICALLY-SENSITIVE FIELD-EFFECT TRANSISTOR FOR DETECTING NITROGEN DIOXIDE

Thesis Chairman: Edward S. Kolesar, Jr. Major, USAF
Associate Professor of Electrical Engineering

20. DISTRIBUTION/AVAILABILITY OF ABSTRACT ☐ UNCLASSIFIED/UNLIMITED ☒ SAME AS RPT ☐ DTIC USERS	21. ABSTRACT SECURITY CLASSIFICATION UNCLASSIFIED
22a. NAME OF RESPONSIBLE INDIVIDUAL Edward S. Kolesar, Jr., Major, USAF	22b. TELEPHONE (*Include Area Code*) (513) 255-3576 22c. OFFICE SYMBOL AFIT/ENG

DD Form 1473, JUN 86 *Previous editions are obsolete.*

Abstract (block 19): This study involved the design and fabrication of an integrated circuit microsensor for the detection of nitrogen dioxide; metal-doped phthalocyanine compounds were evaluated as a candidate chemically-sensitive membrane, and their performance was compared with respect to sensitivity, reversibility, and specificity. The microsensor consisted of the integration of an array of nine sensing elements with amplifiers, a reference amplifier, and an analog multiplexer. The nine individual sensing elements used an interdigitated gate electrode field-effect transistor (IGEFET) coupled to a serially-connected pair of inverting amplifiers using metal-oxide-semiconductor field-effect transistors (MOSFETs). The interdigitated gate electrodes were coated with thin films of cobalt (II) phthalocyanine (CoPc), copper phthalocyanine (CuPc), lead phthalocyanine (PbPc), nickel (II) phthalocyanine (NiPc), and (undoped) phthalocyanine (Pc). An excitation signal was applied to the integrated circuit, and the multiplexed electrical response was measured in the time-domain and the frequency-domain. The electrical response was evaluated upon exposure to 20-, 80-, and 320-ppb of nitrogen dioxide (NO_2) and diisopropyl methylphosphonate (DIMP) using filtered room air (less than 5% relative humidity) as the diluent. The electrical response was evaluated for film thicknesses of approximately 1500 Å and 500 Å. The microsensor's operating temperature was thermostatically controlled at 30°C and 120°C for the evaluation. The rank ordering of the sensitivity of the materials to nitrogen dioxide from most to least sensitive was: CoPc, NiPc, CuPc, PbPc, and then (undoped) Pc. The materials were found to be reversible by heating the microsensor to 70°C while purging with the diluent gas. The rank ordering of the specificity towards NO_2 was (from most to least selective): CoPc, NiPc, PbPc, (undoped) Pc, and then CuPc. For the test parameters studied, the 1500 Å film thickness and the 30°C operating temperature yielded optimum microsensor electrical response.